UNIVERSITÀ DEGLI STUDI DI TRIESTE
e
UNIVERSITÀ CA' FOSCARI DI VENEZIA

XXXII CICLO DEL DOTTORATO DI RICERCA IN

_____CHIMICA_____

STRUCTURAL STUDIES OF ENZYMES: A BACTERIAL FLIPPASE AND A HUMAN KINASE

Settore scientifico-disciplinare: ____**CHIM/03**_____

DOTTORANDO / A
IRENE MARCOVICH

COORDINATORE
PROF. BARBARA MILANI

SUPERVISORE DI TESI
PROF. RITA DE ZORZI

CO-SUPERVISORE
DR. PAOLA STORICI

ANNO ACCADEMICO 2018/2019

ABSTRACT

This PhD thesis includes research work on two different projects, involving expression, purification and characterization of two enzymes.

The first project was performed at University of Trieste under the supervision of Prof. Rita De Zorzi and was aimed at the structural characterization of Wzx, an O-antigen flippase, from *Pseudomonas aeruginosa*. Wzx is an integral membrane protein located in the inner membrane of gram-negative bacteria and involved in Lipopolysaccharide (LPS) biosynthesis. *P. aeruginosa* is an opportunistic pathogen and one of the main causes of nosocomial infections, particularly difficult to eradicate due to the bacterium resistance to antibiotics. Multi drug-resistant *P. aeruginosa* strains are becoming one of the most common causes of morbidity and mortality in immune-compromised patients, pressing for the development of new drugs. As Wzx is a fundamental enzyme for the assembly of the cell wall, this protein may be a promising target for a new class of antibiotics and antibiotic co-adjuvants, specifically aimed at a single bacterial strain due to the high sequence variability of this protein. Inhibiting the proper LPS biosynthesis could result in the disruption of the bacterial outer membrane, leading to higher antibiotic permeation.

The flippase Wzx was cloned in an overexpression vector and subsequently expressed in *E. coli.* The overexpressed protein was extracted from the lipid bilayer by detergent solubilization and purified through different chromatographic techniques. Expression and purification procedures were optimized, leading to a considerable yield of the membrane protein Wzx, suitable for crystallographic studies. Unfortunately, experiments led to the crystallization of a contaminant, the Cytochrome o Ubiquinol Oxidase. However, smaller crystals grown in different conditions were obtained and, considering the differences in the unit cell parameters, the study continued with the optimization of these conditions. So far, the quality of the crystals did not allow structure determination. In parallel, protein folding and stability were investigated with circular dichroism and fluorescence spectroscopy. IR and Raman spectroscopies yielded information on the unfolding process of Wzx. The oligomeric state of the protein was investigated by negative staining EM.

The second project was performed at the Structural Biology Laboratory of the Elettra Synchrotron (Trieste), under the supervision of Dr. Paola Storici. This project was aimed at the structural determination of the complex between the human Glycogen Synthase Kinase 3β (GSK3-β) and its inhibitor SR90, synthesized by the laboratory of Dr. Stephanie Federico at University of Trieste. GSK3-β catalyzes the addition of a phosphate group to specific protein targets and is part of the regulation mechanisms of multiple metabolic pathways, including signaling cascades involved in neurodegenerative disorders. In particular, GSK3-β is implicated in the formation of β-amyloid

aggregates, in the hyperphosphorylation of protein tau and in the accumulation of α-Synuclein – molecular processes that are thought to lead to Alzheimer and Parkinson diseases. Since an inhibition of this kinase may be beneficial for the treatment of these pathologies, SR90 inhibitor was designed to covalently bind GSK3-β. In addition, SR90 is able to inhibit another kinase, the Casein Kinase1 δ (CK1-δ), by competing for ATP binding. CK1-δ is also involved in neurodegenerative pathologies and phosphorylates GSK3-β substrates, acting as a priming kinase.

Three constructs of GSK3-β were cloned and expressed in insect cells: the full length and two truncated constructs, corresponding to residues 25-393 and 35-386, respectively. In the latter, the N- and C-termini were removed due to their flexibility that may hamper the crystallization. The shorter construct (residues 35-386) was efficiently expressed and purified to a high purity grade. The inhibitor activity towards the kinase was investigated by Thermal Shift Assays to determine the binding effect on protein stability. Since the compound seemed to greatly stabilize protein folding, co-crystallization trials between GSK3-$\beta_{35\text{-}386}$ and SR90 were set up, in addition to crystallization tests for the apo protein. Conditions were initially screened using commercially available kits and subsequently optimized. The X-ray diffraction patterns of the crystals were collected at the Elettra Synchrotron obtaining data at 2.6 Å resolution for the apo kinase, at 2.4 Å resolution for the apo crystal soaked in the inhibitor solution, and at 2.3 Å for the co-crystal of GSK3-β and the inhibitor. The analysis of the electron density maps of both the co-crystallized structure and that obtained from soaking experiments demonstrated the formation of a covalent protein-inhibitor bond involving the residue Cys199 of GSK3-β, confirming previous computational modelling simulations. Activity assays were performed to assess SR90 potency, obtaining an IC_{50} value of 0.49 μM.

RIASSUNTO

Questa tesi di dottorato include il lavoro di ricerca su due progetti diversi riguardanti l'espressione, la purificazione e la caratterizzazione di due enzimi.

Il primo progetto è stato svolto all'Università di Trieste sotto la supervisione della professoressa Rita De Zorzi ed era volto alla caratterizzazione strutturale della O-antigen flippasi Wzx da *Pseudomonas aeruginosa.* Wzx è una proteina integrale di membrana che si trova nella membrana interna dei batteri gram-negativi ed è coinvolta nella biosintesi del lipopolisaccaride (LPS). *P. aeruginosa* è un patogeno opportunista e una delle principali cause delle infezioni nosocomiali, è inoltre particolarmente difficile da eradicare a causa della sua resistenza agli antibiotici. Ceppi di *Pseudomonas* multi-resistenti stanno diventando una delle cause più comuni di morbilità e mortalità nei pazienti immunocompromessi, rendendo necessario lo sviluppo di nuovi farmaci. Essendo Wzx un enzima fondamentale per la formazione della parete cellulare, questa proteina potrebbe essere un promettente bersaglio per una nuova classe di antibiotici e di adiuvanti degli antibiotici. Vista l'alta variabilità di sequenza della flippasi, questi farmaci sarebbero specificamente diretti verso un singolo ceppo batterico. L'inibizione della biosintesi dell'LPS può causare il disassemblaggio della membrana esterna del batterio portando a una maggiore permeazione degli antibiotici all'interno della cellula.

La flippasi Wzx è stata clonata in un vettore di overespressione e successivamente trasformata in *E. coli*. La proteina overespressa è stata estratta dal doppio strato fosfolipidico solubilizzandola in detergente e purificata attraverso diverse tecniche cromatografiche. Le procedure di espressione e purificazione sono state ottimizzate portando a una considerevole resa della proteina di membrana utilizzabile per gli studi cristallografici. Sfortunatamente, gli esperimenti hanno portato alla cristallizzazione di un contaminante, il Citocromo o Ubichinolo Ossidasi. Comunque, sono stati ottenuti dei piccoli cristalli in condizioni differenti che, considerando la differenza dei parametri di cella unitaria, sono stati ottimizzati. Finora la qualità dei cristalli non ha permesso la determinazione della struttura. Parallelamente, il folding e la stabilità della proteina sono stati investigati con il dicroismo circolare e la spettroscopia di fluorescenza. Inoltre, le spettroscopie IR e Raman hanno fornito informazioni sul processo di degradazione di Wzx. Lo stato oligomerico della proteina è stato investigato con il microscopio elettronico utilizzando la tecnica del *negative-staining*.

Il secondo progetto è stato svolto nel Laboratorio di Biologia Strutturale di Elettra Sincrotrone (Trieste) sotto la supervisione della dottoressa Paola Storici. Questo progetto era volto alla determinazione strutturale del complesso tra la Glicogeno Sintasi Chinasi 3β (GSK3-β) e il suo inibitore SR90, sintetizzato nel laboratorio della dottoressa Stephanie Federico all'Università di Trieste. GSK3-β catalizza l'addizione di un gruppo fosfato a specifiche proteine bersaglio e fa parte dei meccanismi di regolazione di molteplici vie metaboliche tra cui le cascate di segnale associate ai

disordini neurodegenerativi. In particolare, GSK3-β è implicata della formazione degli aggregati di β-amiloide, nell'iperfosforilazione della proteina tau e nell'accumulo di α-sinucleina che sono processi molecolari che sembrano portare alle malattie di Alzheimer e Parkinson. Visto che un'inibizione di questa chinasi può essere benefica per il trattamento di queste patologie, l'inibitore SR90 è stato progettato per legarsi covalentemente con GSK3-β. Inoltre, SR90 è in grado di inibire un'altra chinasi, la casein chinasi1 δ (CK1-δ), competendo con il legame dell'ATP. Anche CK1-δ è coinvolta nelle patologie neurodegenerative e fosforila i substrati di GSK3-β agendo come chinasi iniziatrice.

Tre costrutti sono stati clonati ed espressi in cellule d'insetto: la proteina intera e due costrutti troncati, corrispondenti ai residui 25-393 e 35-386 rispettivamente, in cui i terminali sono stati rimossi a causa della loro flessibilità che può pregiudicare la cristallizzazione. Il costrutto più corto (35-386) è stato efficientemente espresso e purificato ottenendo un alto grado di purezza. L'attività dell'inibitore sulla chinasi è stata investigata con il Thermal Shift Assay per determinare l'effetto del legame sulla stabilità della proteina. Visto che il composto si è dimostrato in grado di stabilizzare in modo considerevole la conformazione proteica, sono state effettuate delle prove di cristallizzazione su GSK3-β $_{35\text{-}386}$ complessato con SR90 e la forma apo della chinasi. Le condizioni sono state inizialmente testate usando dei kit commerciali contenenti un ampio set di condizioni di cristallizzazione e successivamente ottimizzate. I dati di diffrazione dei raggi X sono stati raccolti al Sincrotrone di Elettra ottenendo dati a una risoluzione di 2.6 Å per la forma apo, di 2.4 Å per il cristallo apo incubato in una soluzione contenente l'inibitore e a 2.3 Å per GSK3-β co-cristallizzata con SR90. L'analisi della mappa di densità elettronica sia del co-cristallo sia della forma apo incubata con l'inibitore ha dimostrato la formazione di un legame covalente tra la proteina e l'inibitore. Questo legame coinvolge la cisteina 199 di GSK3-β come predetto dai modelli computazionali. Sono stati inoltre effettuati dei saggi di attività determinando un valore di IC_{50} di 0.49 μM.

LIST OF ABBREVIATIONS

6-OHDA: 6-hydroxy dopamine

Aβ: β amyloid

Abl: Abelson Tyrosine kinase

AD: Alzheimer disease

AEBSF: 4-(2-aminoethyl)benzenesulfonyl fluoride hydrochloride

ALS: Amyotropic lateral sclerosis

BBB: Blood Brain Barrier

BCA: Bicinconinic acid

bp: base pair

$C_{12}E_8$: Octaethylene Glycol Monododecyl Ether

CD: circular dichroism

CDKL: cyclin dependent kinase like

CHAPS: 3-[(3-Cholamidopropyl)dimetilammonio]-1-propanesulfonate

CK1-δ: Casein kinase 1δ

CMC: Critical Micellar Concentration

CUO: Cytochrome o Ubiquinol Oxidase

CV: column volume

DDM: n-dodecyl-β-D-maltoside

DFG: Asp- Phe- Gly motif

DM: n-decyl-β-D-maltoside

DTT: DL-Dithiothreitol

E: eluate

FBS: Foetal Bovine Serum

FDA: Food and Drug Administration

FL: full-length

FT: flow through

GFP: Green Fluorescent Protein

Gli: Glioma-associated oncogene

GOI: gene of interest

GS: glycogen synthase

GS2: Phospho Glycogen-Syntase Peptide-2

GSK3-β: Glycogen Synthase Kinase 3β

H5: *Trichoplusia ni* High 5

List of abbreviations

Hh: Hedgehog

I: induced

IEX: Ion Exchange Chromatography

IMAC: Immobilized Metal Affinity Chromatography

IPTG: isopropyl β-D-1-thiogalactopyranoside

IR: infrared

KI: kinase inhibitor

L-DOPA: levo DOPA

LDAO: lauryldimethylamine-N-oxide

LIC: ligation independent cloning

MAPK: mitogen activated protein kinase

MOI: Multiplicity Of Infection

NFT: neurofibrillary tangles

NI: not induced

OD_{600} : optical density at 600mn

OG: n-octyl-β-D-glycoside

P: pellet

PAMPA: parallel artificial membrane permeability assay

PAO1: *Pseudomonas Aeruginosa*

PD: Parkinson disease

pFB-Bse: pFastBac-Bse

pFB-ZB: pFastBac-ZetaBasic

PHF: paired helical filaments

PK: protein kinase

PKA: cAMP-dependent protein kinase

PKB: protein kinase B

PKC: calcium dependent protein kinase

PKG: cGMP-dependent protein kinase

PMSF: phenylmethylsulfonyl fluoride

RF: Restriction enzyme Free cloning

RLU: Relative Light Unit

SDS-PAGE: sodium dodecyl sulfate polyacrylamide gel electrophoresis

SDS: sodium dodecyl sulfate

SEC: Size Exclusion Chromatography

List of abbreviations

Sf9: *Spodoptera frugiperda* 9

SMKI: small molecule kinase inhibitor

SN: supernatant

ss: single strand

TE: total extract

TEM/EM: transmission electron microscopy

TEV: Tobacco Etch Virus

TSA: Thermal Stability Assay or Thermal Shift Assay

W: wash

WB: western Blot

Wnt: Wingless and Int

SUMMARY

1. Structural characterization of proteins
    1.1. X-rays Crystallography
    1.2. Electron Microscopy
    1.3. Nuclear Magnetic Resonance
    1.4. Complementary techniques
2. The translocase Wzx: Introduction
    2.1. Pseudomonas aeruginosa
        2.1.1. Virulence Factors
        2.1.2. Resistance
    2.2. Bacterial cell wall and Plasma membrane
        2.2.1. Cell wall from gram-positive bacteria
        2.2.2. Cell wall from gram-negative bacteria
    2.3. Lipopolysaccharide
        2.3.1. Lipid A
        2.3.2. The core oligosaccharide
        2.3.3. O antigen
            2.3.3.1. O antigen biosynthesis
    2.4. Wzy pathway
        2.4.1. Wzx
        2.4.2. Wzy
        2.4.3. Wzz
    2.5. Membrane proteins
        2.5.1. Membrane proteins expression, solubilization and crystallization
3. Wzx: Aim of the work
4. Results and Discussion
    4.1. Cloning
    4.2. Overexpression of O antigen flippase
    4.3. Protein solubilization
    4.4. Protein purification: first affinity chromatography tests
    4.5. Protein purification: Size Exclusion Chromatography
    4.6. Protein purification: further Affinity Chromatography
    4.7. Protein purification: Ion Exchange Chromatography
    4.8. Anti-GFP resin affinity purification

4.9. Protein purification: detergent exchange from LDAO to $C_{12}E_8$
4.10. Protein solubilization and purification in DDM
4.11. Crystallization experiment of LDAO-solubilized Wzx protein
4.12. Optimization of Size Exclusion Chromatography step
4.13. UV visible spectroscopy analysis
4.14. Protein stability: Fluorescence intensity measurements in temperature gradient
4.15. Protein stability: Circular Dichroism measurements in temperature gradient
4.16. Protein stability: InfraRed spectroscopy analysis in temperature gradient
4.17. Protein stability: Raman spectroscopy analysis in temperature gradient
4.18. Analysis of multimeric state: TEM
5. Conclusions
6. The kinase GSK3-β: Introduction
6.1. Protein kinases
6.1.1. Protein kinases classification
6.1.2. Protein kinases structures
6.2. Glycogen synthase kinase 3 β
6.2.1. GSK3-β structure
6.2.2. GSK3-β regulation
6.2.3. GSK3-β targets and related pathologies
6.3. Casein Kinase 1δ
6.4. Protein kinase inhibitors
6.4.1. GSK3-β inhibitors
6.5. SR90 inhibitor
7. GSK3-β: Aim of the study
8. Results and discussion GSK3-β
8.1. DNA manipulations
8.1.1. Ligation Independent Cloning
8.1.2. Bacmid generation
8.1.3. Insect cells transfection
8.2. Small scale test expression
8.3. Large scale test expression and purification
8.3.1. pFB-Bse GSK3-β 35-386
8.3.2. pFB-ZB GSK3-β full length
8.4. characterization of SR90 binding

8.4.1. TSA on GSK3-β 35-386
8.4.2. SR90 activity and reversibility assays
8.5. Crystallization of GSK3-β 35-386
8.6. Data collection
8.7. Structure analysis
8.7.1. GSK3-β co-crystal
8.7.2. GSK3-β soaked and apo crystals
8.7.3. SR90 inhibitor
8.7.4. Structure comparison: Co-crystal vs Soak
8.7.5. Structure comparison: Co-crystal vs apo
8.7.6. Structure comparison: apo vs Soak
8.8. New inhibitors
9. Conclusions
10. Materials and methods
10.1. Generic specifications
10.2. Buffers
10.2.1. Wzx buffers
10.2.2. GSK3-β buffers
10.3. Bacterial growth media
10.4. Bacterial strains
10.5. Insect cells
10.6. DNA manipulations
10.6.1. Wzx
10.6.2. GSK3-β
10.6.2.1. Ligation independent cloning
10.6.2.2. Baculovirus generation
10.7. Bacterial transformation
10.8. Insect cells transfection
10.9. Small scale protein expression
10.9.1. Wzx
10.9.2. GSK3-β
10.10. Large scale expression
10.10.1. Wzx
10.10.2. GSK3-β

10.11. Solubilization in detergents
10.12. Protein purification
10.12.1. Immobilized metal affinity chromatography
10.12.1.1. Wzx
10.12.1.2. GSK3-β
10.12.2. Ion Exchange chromatography
10.12.2.1. Wzx
10.12.2.2. GSK3-β
10.12.3. Size exclusion chromatography
10.12.3.1. Wzx
10.13. Protein characterization
10.13.1. Fluorescence spectroscopy
10.13.2. Thermal stability assay
10.13.3. Kinase activity assay
10.13.4. Circular Dichroism
10.13.5. Electron Microscopy
10.13.6. InfraRed
10.13.7. Raman
10.14. Crystallization
10.14.1. Wzx
10.14.2. GSK3-β
10.15. X-ray diffraction and structure determination
10.15.1. GSK3-β
10.16. Generic procedures
11. Acknowledgements
12. Bibliography

1. STRUCTURAL CHARACTERIZATION OF PROTEINS

Detailed knowledge of protein structures is crucial for the understanding of all biological processes, from enzymes activity, to ligand-receptor interaction, to immune system evasion and signal transduction. Moreover, the determination of the target protein exact structure is essential for structure-based drug design studies, aimed at the discovery of new drugs, or at the improvement of known pharmaceutical compounds, based on the structure of their targets.

To be a promising candidate for drug design, a protein must be linked to a human disease through its specific activity and interact with known substrates within a well-defined binding pocket. Drugs targeted against human proteins modulate their activity to re-establish the homeostasis, to promote patients' recovery or to alleviate diseases symptoms. On the other hand, antimicrobial drugs are targeted towards the essential elements of a pathogen. In this case the compound interferes with pathways exclusively present in the pathogen, leading to its death (Anderson 2010).

In both cases the determination of the target structure is essential for the design of a library of potential interactors and for the following compound optimization processes, once a new lead compound has been identified. In fact, the initial design of inhibitor libraries is performed considering crystallographic or NMR (Nuclear Magnetic Resonance) data regarding the protein. When a new compound displays a promising inhibitory activity in biochemical assays, the structure of the compound-target complex is determined to further optimize the interactions and the selectivity of the inhibitor (Anderson 2010). Thus, the structural knowledge is pivotal in every step of this process, from the initial design to the optimization of the drug, to increase selectivity or inhibitory potency.

1.1. X-ray crystallography

Since the 1960's and to this day, the leading technique for determining the atomic structures of proteins is X-ray crystallography. Until few decades ago, this was the only technique that yielded structural details of biological macromolecules at the atomic level, with the well-defined parameters of resolution and R factor to assess the reliability of the experimental result. However, the use of X-ray crystallography for structural characterization of a biological assembly depends on the possibility to obtain crystals of the macromolecule, or of the macromolecular complex, of sufficient size and quality to allow the measurement of accurate diffraction intensities (Figure 1.1).

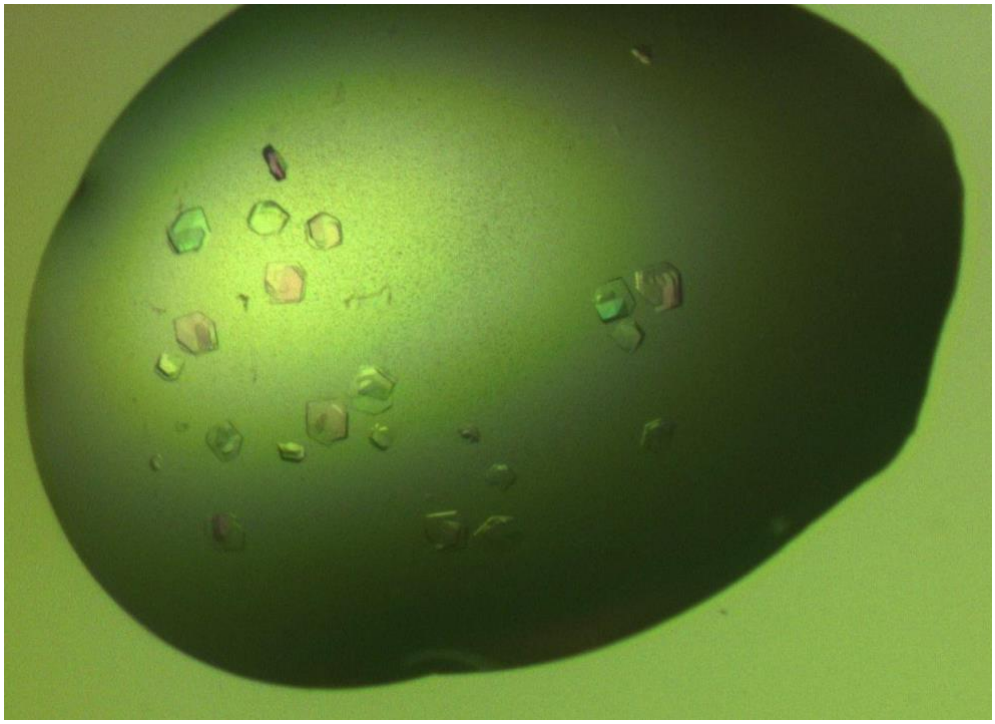

Figure 1.1: Protein crystals grown in a drop using the vapor diffusion method

In a typical diffraction experiment, a single protein crystal is fished with a loop, cryoprotected to avoid formation of ice crystals, frozen and mounted on the goniometer of a diffractometer to allow its rotation under the X-ray beam. The X-rays interact with the electron density present in the crystal originating diffracted beams that are recorded by the detector as diffraction spots. Diffracted beams, and hence diffraction spots, are different for each orientation of the protein crystal, and the rotation of the crystal allows the collection of images from different directions, yielding a complete dataset. The analysis of the position and the intensity of the spots allows the reconstruction of the electron density map from which atoms of the protein can be located. The level of detail at which protein features are observed in the electron density map depends on the resolution of the diffraction data recorded, ranging from the observation only of the polypeptide chain to the determination of the positions of single atoms of the side chains. The resolution of the data is related to the maximum scattering angle: increasing the angle allows the resolution of objects close to each other, due to the decrease in separation between the reflecting planes that generated the diffracted spots. As a result, high resolution information is obtained from diffraction spots recorded close to the external perimeter of the detector, far away from the position of the beam (Parker 2003). The high resolution that can be obtained in crystal structures is a major aid for the design of inhibitors, as bond distances and angles of the protein groups as well as position of the water molecules in the structure may suggest optimal modifications of the structure of the lead compound.

The quality of the final structure is determined by the quality of the diffraction data, that, in turn, depend on the size and physical properties of the crystalline specimen (McPherson, 1989) and on the X-ray source. The use of synchrotron radiation greatly improved the quality of the diffraction data, increasing the resolution and allowing data collection even on small protein crystals (Parker 2003). At the same time, improvements in protein crystallization techniques made available good quality crystals for a larger number of proteins and protein complexes. Nevertheless, crystallization remains a challenging step of the structural determination of biological macromolecules through X-ray diffraction techniques.

Serial femtosecond crystallography is an innovative technique that recently emerged thanks to the development of X-ray free electron lasers (XFELs), able to produce brilliant and microfocused X-rays pulses. Using this technique, diffraction data can be obtained from nanocrystals that are usually not suitable for the data collection on conventional synchrotron sources. However, these crystals are perfect for serial femtosecond crystallography due to their higher long-range order compared to bigger crystals. Due to the small dimensions of the crystals and the high intensity of the X-ray source, the radiation damage on the nanocrystals is so intense that the crystalline sample is lost just after the acquisition of the first image. Datasets obtained with this technique are very large collections of diffraction images from crystals in random orientations, requiring a significant computational effort to extract the structural information. Time resolved serial femtosecond crystallography allows the visualization of transient reaction intermediates giving a unique understanding of biological reaction mechanisms (Martin-Garcia et al. 2016).

1.2. Electron microscopy techniques

In the last decade, Electron Microscopy (EM) emerged as a mainstream technique for the determination of protein structures at high resolution. Thanks to significant improvements in the technical equipment as well as in the theoretical approaches to data analysis, it is now possible to obtain near-atomic resolution for samples embedded in vitreous ice (cryo-EM). In all electron microscopy techniques, the sample is deposited on a small metal grid that is later introduced in the high-vacuum column of the electron microscope. The interaction of the electron beam with the electric field of the sample generates the electron microscopy image on the detector of the microscope.

Negative staining EM allows the collection of two-dimensional images of proteins embedded in a thin film of a heavy-atom salt, such as uranyl acetate. This technique is based on the stronger scattering interaction of the electron beam with the heavy atoms compared to the protein, creating a dark background in which the protein appears as a white particle. Besides the improvement of

the image contrast, the stain has other important functions: the heavy atom film protects the biological specimen from the high vacuum of the microscope that could destroy its structure and decreases the radiation damage. On the other hand, the stain may cause unwanted effects on the protein, such as flattening of the protein structure on the EM grid. In addition, this technique allows the detection of large molecules only at low resolution (around 15 Å), due to the stain grain size. However, negative staining EM is an ideal preliminary technique to evaluate the monodispersity of the sample and to obtain a low-resolution model of the target protein, and is often used prior to the cryo-EM analysis (Nogales 2016).

Cryo-EM is the EM technique that experienced the greatest advantages from the technical and computational advancements of the last years. Cryo-EM is now a widely used technique in structural biology, able to analyze proteins in solution, with up-to-atomic resolution. This technique is particularly important for proteins and protein assemblies that are difficult to crystallize because it does not require well-ordered crystals. The sample is vitrified in its own buffer solution by dipping the microscopy grid in liquid ethane to create a thin layer of amorphous ice that protects the specimen from the vacuum of the microscope column and reduces the radiation damage induced by the electron beam, without hampering the resolution of the images (Cheng et al. 2015). However, since electrons have a strong interaction with the biological sample during imaging, the radiation damage appears quickly, allowing to collect only a single high-resolution image before the sample is too damaged. To obtain the 3D structure, high-resolution images of the protein in different orientations are collected. In fact, contrary to the negative staining in which proteins usually adopt a preferential orientation, in vitrified samples proteins orient randomly on the microscopy grid allowing the complete mapping of the three-dimensional structure of the protein (Lengyel et al. 2014) (Figure 1.2).

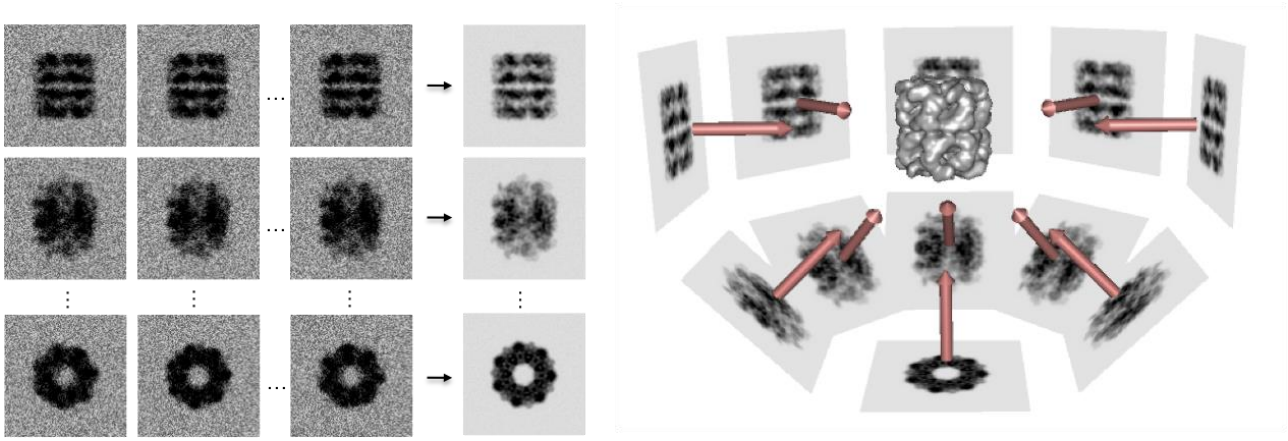

Figure 1.2: Schematic description of the Cryo-EM image analysis that leads to 3D structure determination: images of the protein are first classified according to the orientation (left) and then the 3D model is determined from the images (right). From Greg Pintillie web page

The impressive breakthrough in cryo-EM came with the development of a new class of detectors, the direct detection cameras. Previously, in CCD cameras (Charged-Coupled Device) the electrons were converted into photons via a scintillator and the photon intensity was measured, with a significant noise added to the image. Instead, in Direct Detectors electrons are measured without their conversion to photons, improving the signal-to-noise ratio of the images and, thus, increasing the image resolution. In addition, the low intensity of the electron beam required to detect a signal and the fast readout of detectors made it practical to collect subframes of a single image with a very low dose. The analysis of the subframes allows to correct sample motions, further improving the resolution of the final image (Nogales 2016). Prior to the development of Direct Detectors, cryo-EM techniques were limited to large proteins, easy to detect even in the noisy images: the size limit was about 300 kDa. Today, after the recent great improvements, molecules around 100 kDa can be visualized with a resolution of up to 2 Å (Cheng et al. 2015).
Due to the high impact that this technique had in recent years for the structural biology field, Jacques Dubochet, Joachim Frank and Richard Henderson won the Nobel prize in 2017 for their contribute to the development of Cryo-EM techniques.

Electron crystallography developed first as a technique particularly beneficial for membrane proteins, as it allowed to determine the structure of this particular class of proteins in the context of the lipid bilayer formed in the 2D crystals of the protein. The visualization of the protein surrounded by lipids allowed to determine its structure in the natural environment and to reveal its interaction with proximal lipids. Compared to crystallography, this technique requires a low amount of protein (De Zorzi et al. 2016).

More recently, new efforts in the field of electron microscopy were devoted to the structural characterization of proteins forming small three-dimensional crystals. The Micro Electron Diffraction (MicroED) approach allows the structure determination using microcrystals and decreasing the intensity of the electron source. With a lower electron dose, it is possible to collect a higher number of diffraction patterns from a single crystal allowing the high-resolution structure determination without the necessity to process data from many different crystals. In addition, the crystals used in this experiments are six orders of magnitude smaller compared to those commonly required for X-ray crystallography (Shi et al. 2013).

1.3. NMR

Compared to X-ray crystallography, Nuclear Magnetic Resonance (NMR) (Wüthrich 1989) does not require to go through the difficult process of crystallization and analyzes the protein in a more native environment at atomic resolution. Using this technique, dynamic processes such as

conformational changes promoted by ligand binding can be detected. On the other hand, to allow structure determination by NMR methods the protein has to be labelled with one or more isotopes. Therefore, to perform NMR analysis proteins should be expressed in enriched media in order to incorporate the isotopes within their amino acid residues. In addition, NMR can only determine structures of peptides or small proteins since the signal obtained by larger and more complex structures would be too difficult to analyze due to the larger number of overlapping frequencies and the long relaxation time (time in which the spin system returns to its native state) that increase the signal assignment complexity (Frueh et al. 2013).

In NMR experiments the sample is exposed to a magnetic field that influences the spin of the atomic nuclei. In addition to the external magnetic field, the local magnetic field in which nuclei are immersed changes according to the surrounding groups and the relative distances between the atoms. In fact, the reciprocal influence between chemical groups is inversely proportional to their distance. The NMR signal is recorded as a sum of radiofrequency signals decaying after the simultaneous excitation of all the atomic spin transitions. The position, the intensity and the multiplicity of the NMR peaks obtained after Fourier transform of the decaying radiofrequency signal give indications regarding the chemical and geometrical surroundings of each nucleus. For the structural determination of biological macromolecules, the Nuclear Overhauser Effect (NOE) is particularly important as it provides information on nuclei that are less than 5Å apart and it greatly contributes to the determination of the geometrical arrangement of the protein in space (Bax, Kontaxis, and Tjandra 2001). The structure of the specimen is reconstructed by assigning the NMR resonances to each precise atom of the protein sequence and, thus, reconstructing the 3D arrangements of the backbone of the protein by taking into account the distance constrains exerted by the NOE signals (Tolman et al. 1998) (Figure 1.3). A great advantage of NMR is that it takes into account the flexibility of the protein domains and can, therefore, determine the dynamic movements that the protein undergoes in solution.

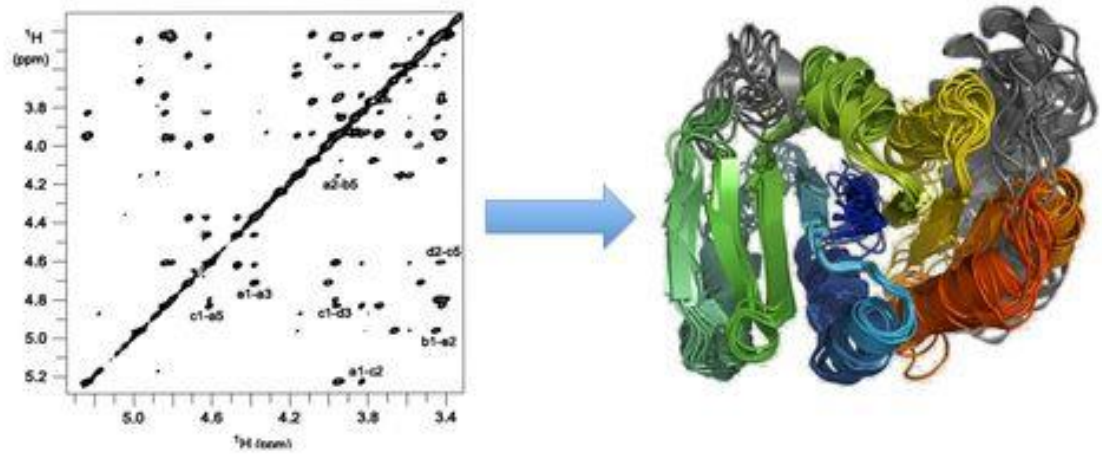

Figure 1.3: Schematic representation of the protein structure determination from NMR data. © 2009 - 2014 TUM Technische Universität München

Due to software improvements and the development of solid state NMR, it is now possible to determine protein structures up to 50 kDa (Frueh et al. 2013). Solid state NMR is particularly useful for membrane proteins embedded in lipid bilayers and allows to observe the influence of lipids on protein conformations (Marassi and Opella 2008).

1.4. Complementary techniques

Despite the great importance of X-ray crystallography, NMR and Cryo-EM as elective techniques for the structural determination of proteins, other techniques cover often neglected aspects of structural biology, such as protein dynamics, protein-ligand or protein-protein interactions. Complementary methods include:

- Small Angle X-ray Scattering (SAXS)
- Circular Dichroism (CD)
- Raman Spectroscopy
- Infrared Spectroscopy (IR)
- Fluorescence Spectroscopy
- Mass spectrometry

Small Angle X-ray Scattering (SAXS) analyzes protein conformation in solution (Pelikan, Hura, and Hammel 2009). This technique allows the low-resolution structural characterization of the three-dimensional structure of macromolecules, the determination of the oligomeric state of proteins, the identification of the formation of complexes or of large conformational

rearrangements induced by ligands or buffer components. SAXS does not require a crystalline sample, the specimen used is a solution of around 1 mg/ml of highly pure protein (Pelikan, Hura, and Hammel 2009).

This technique is based on the elastic scattering of the collimated and focused X-ray beam on the macromolecules in solution. The scattering depends on the molecule concentration, the contrast and the inter-molecular interactions within the solution (Mertens and Svergun 2010). Considering the scattering angle, it is possible to reconstruct the low-resolution structure of the macromolecule.

Generally, to obtain consistent structural information, the low-resolution data obtained from SAXS are combined with the high-resolution structural data obtained via X-ray crystallography on single domains of the protein (Pelikan, Hura, and Hammel 2009) (Figure 1.4).

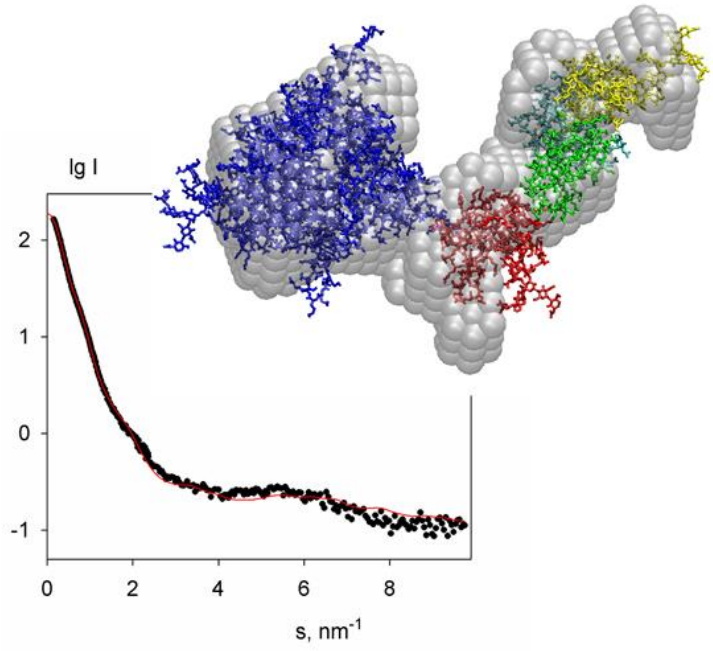

Figure 1.4: Schematic representation of the fitting of crystal structures of single domains in the envelope determined by SAXS data. From Saxier website

In addition, SAXS is a valuable tool to validate and simplify NMR analysis. In fact, the interpretation of NMR spectra of big proteins is complicated by the overlapping signals. SAXS data may give information of the overall shape of the molecule reducing the ambiguity of NMR data interpretation (Mertens and Svergun 2010).

Circular Dichroism (CD) is a valuable technique to investigate the secondary structure of proteins (Greenfield 2009). Since the CD signal between 185 and 230 nm is sensible to the variation of the secondary structure, CD measurements can be used to follow protein conformational changes due to small molecule binding, or unfolding due to chaotropic agents or temperature variations (Miles and Wallace 2016; Greenfield 2009). CD is based on the differential interaction of chiral molecules with the circularly polarized light. In the case of unknown protein samples, the CD spectra in the 185-230 nm region can be compared with those of proteins with a precise secondary structure (α-helix, β-sheets or disordered regions), allowing to determine the secondary structure content of the unknown protein (Greenfield and Fasman 1969) (Figure 1.5). The conformational variations are followed by recording CD spectra in different conditions.

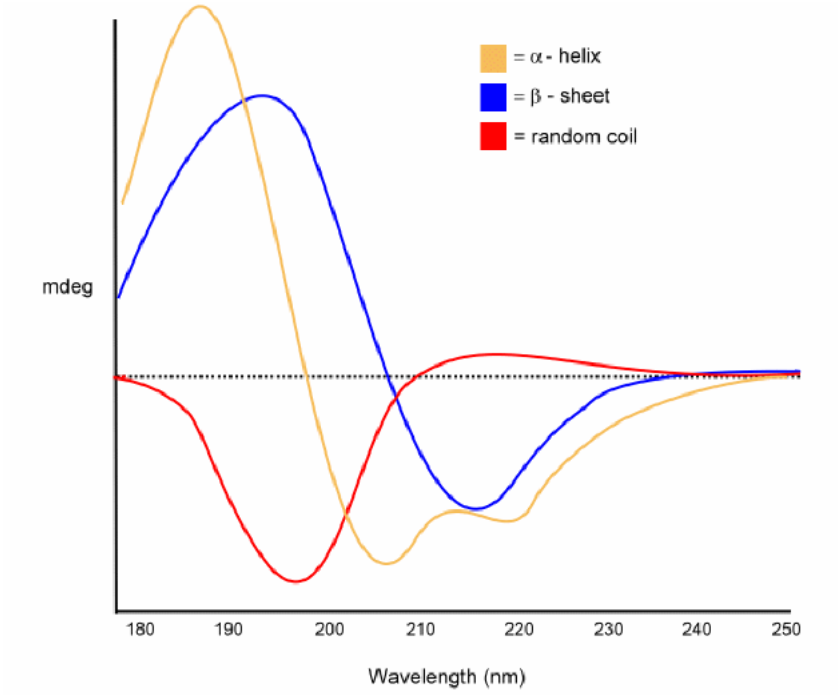

Figure 1.5: CD spectra of different secondary structures. From Pronalyse website

Raman spectroscopy follows the vibrational modes of functional groups and specific amino acid residues when excited at a precise wavelength, providing information on the secondary structure of the protein and the occurrence of conformational rearrangements (Rygula et al. 2013). The bands corresponding to the amides are detected at diverse wavenumbers depending on the secondary structure and the overall folding of the protein. In addition, due to the strong Raman signal of aromatic groups, this technique can follow changes in the surroundings of specific tryptophan, tyrosine and phenylalanine residues. Raman has been used for the study of protein

folding, protein-ligand structures, drug screening, protein assembly and to perform quality controls on protein-based pharmaceuticals (Tuma 2005).

InfraRed (IR) spectroscopy is a widely used technique for the determination of small molecule structure via detection of the vibrational modes of specific groups. IR light promotes vibrational transitions of the atomic polar bonds resulting in stretching and bending phenomena that are characteristic and depend on the nature of the bond (single, double or triple) and the atoms involved (Barth 2007). The position of the peaks corresponding to Amide I and II in IR spectroscopy is related to the secondary structure of the protein and the information obtained with this technique is complementary to that gained by Raman spectroscopy analysis. In fact, the wavenumber of the peaks vary according to the secondary element of the polypeptide chain (Barth 2007).

Fluorescence spectroscopy can be used to investigate protein folding and unfolding processes by recording the intensities of aromatic residues, in particular tryptophan, that are sensitive to environmental changes occurring during protein unfolding, such as a diverse exposure of the hydrophobic residue to the solvent (Moon and Fleming 2013). Tryptophan residues can also be used as intrinsic fluorophores to investigate protein dynamics and interactions (Chattopadhyay and Raghuraman 2004). When more than one fluorophore is present in the protein sequence, or is introduced through chemical modifications, the fluorescence spectroscopy technique FRET (Forster Resonance Energy Transfer) can be used to determine intramolecular rearrangements. The energy transfer measured by the FRET technique occurs between a fluorophore and an acceptor that are located within 10 nm. When donor and acceptor fluorophores are located on different molecules, FRET analysis can be used to investigate intermolecular interactions (Ghisaidoobe and Chung 2014). Fluorescence spectroscopy measurements are very useful also in the preparatory stages of structural determination, taking advantage of fluorescent tags, such as the GFP tag, that allow to determine the localization of the tagged protein within the cells and to specifically detect its presence during expression and purification procedures (Drew et al. 2001).

Mass Spectrometry (MS) is a valuable technique to gain structural information in case of proteins difficult to crystallize, including flexible proteins, samples with glycosylations and proteins that interact with lipids that cannot be properly detected with other techniques. In recent years, in order to study protein samples with minimal disruption of their folding and without hampering their interactions, native MS was developed, a technique able to study proteins preserved in non-

denaturing conditions within the gas phase. With this method, it is possible to evaluate the stoichiometry of the protein complexes identifying the complex-forming subunits (Figure 1.6). Moreover, the structure of nucleic acid binding proteins, difficult to determine via crystallography or cryo-EM, can be investigated with this technique. MS is also used for the identification of annular lipid belts associated with membrane proteins: as annular lipids are often crucial for membrane protein activity, structural information of these components gives a deeper understanding of mechanisms of action of membrane proteins (Liko et al. 2016).

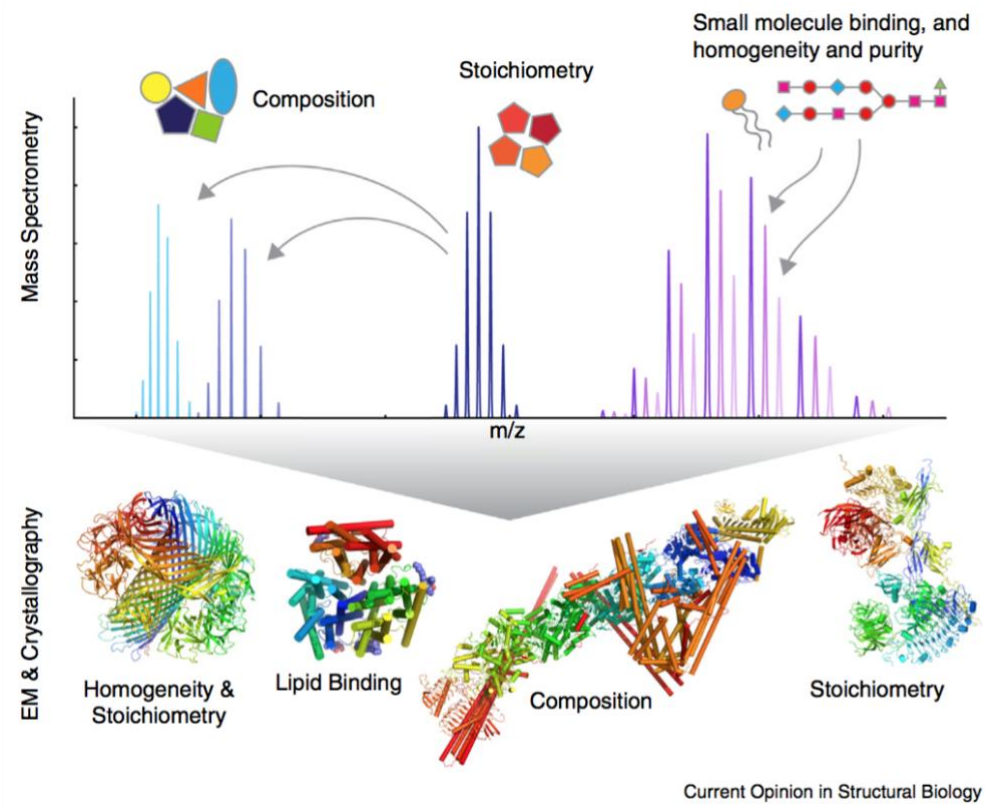

Figure 1.6: Schematic representation of the information provided by mass spectrometry to complement EM and crystallographic techniques

2. THE TRANSLOCASE Wzx: Introduction

2.1. Pseudomonas aeruginosa

Pseudomonas aeruginosa is a gram-negative bacillus that acts as an opportunistic pathogen. It was isolated for the first time in 1882 by Gessard in blue-green pus infections. *P. aeruginosa* is commonly present in the environment, but it infects only individuals with compromised defense mechanisms (Lyczak, Cannon, and Pier 2000), such as AIDS patients, patients undergoing chemotherapy treatment, Cystic Fibrosis patients, or patients with severe burns. In these cases, however, causes of infection can be as simple as the use of soft contact lenses.

P. aeruginosa is reported to be the third leading cause of nosocomial infections (Elamin et al. 2017). Multi-drug resistant strains contaminate floors, bed rails and sinks of hospitals and may be spread through the hands of medical staff. In addition, it may persist in a patient even after various cycles of antibiotics (Lyczak, Cannon, and Pier 2000). This pathogen is responsible for the high mortality rate in critically ill patients even when the infection is treated with appropriate antibiotics, due to the numerous drug-resistant forms of *P. aeruginosa* that develop spontaneously (Hauser 2012). In these infections an early start of adequate therapy is essential to improve patients' outcomes, while inappropriate therapy is reported to favor the development of Multi Drug-Resistant *Pseudomonas aeruginosa* (MDRPA) (Obritsch et al. 2005). MDRPA is an important determinant in hospital mortality due to the limited therapeutic options available (Kollef 2000; Kang et al. 2003). The insurgence of multidrug resistance is associated with a 3-fold increase in patients mortality (Obritsch et al. 2005). The lack of antimicrobial drugs effective against MDRPA strains gave input to the research of new drugs targeting *Pseudomonas* virulence factors (Hauser 2012).

Pseudomonas is not the only bacterium that causes life-threatening infections, but it is part of a very serious problem that is going to worsen in the next decades. In fact, the 2013 Center for Disease Control (CDC) report claims that more than 2 million individuals per year acquire antibiotic resistant bacteria causing about 23˙000 deaths only in the U.S. (Centers for Disease Control and Prevention. Threat Report 2013: Antibiotic/Antimicrobial Resistance. Centers for Disease Control and Prevention; 2013). Further researches have estimated that in the next thirty years more than 10 million people per year will die for the same reason (Neill 2014).
Considering these numbers, it is clear that antibiotic resistance is not only a global medical issue but also an economic emergency (Fields, Lee, and McConnell 2017).

The development of new specific and effective antimicrobial drugs, with novel mechanisms of action and new specific targets, should be a priority for the scientific community. This work is aimed at the structural characterization of *P. aeruginosa* Wzx flippase, one of the components of the Wzy-pathway for the synthesis of Lipopolysaccharide (LPS) O-specific antigen. Considering its involvement in one of the major virulence factors of *P. aeruginosa*, this protein may be an interesting drug target for new antimicrobial drugs, or for antibiotic adjuvants, to overcome the drug resistance issue.

2.1.1 Virulence factors

In its arsenal, *P. aeruginosa* has numerous virulence factors that allow persistence in the host and propagation in the infected organism (Sato, Okinaga, and Saito 1988). The first mechanism that facilitate bacterial infection is the quorum-sensing that regulates gene expression patterns involved in the production of elastase, pyocyanin and other proteases in response to high bacterial density (Hauser 2012). These toxins are able to degrade collagen and disrupt the host basement membrane allowing bacterial dissemination (Bejarano et al. 1989). Another *Pseudomonas* virulence factor is the type III secretion system that mediates the injection of a set of toxins into the host cells. However, the major responsible for *Pseudomonas* virulence is the LPS. This molecule helps bacterial evasion from host defense mechanisms via inhibition of the host immune reactions that follow surface deposition C3b complement (Ricklin et al. 2010), protection against serum-mediated lysis (Dasgupta et al. 1994) and by formation of the biofilm architecture (Lau et al. 2009). For example, bacteria play a fundamental role in Cystic Fibrosis (CF) pathogenesis through the interaction of their LPS with the CF transmembrane regulator (Schroeder et al. 2001).

2.1.2 Resistance

Infections caused by *P. aeruginosa* are particularly difficult to eradicate due to natural or acquired high resistance of this bacterium to antimicrobial drugs. The highly impermeable cell wall of this species, 12 to 100 times less permeable compared to *E. coli* (Hancock 1998), results in a low susceptibility to most antibiotics. The outer membrane of this pathogen has a limited number of channels for the passage of small molecules, acting as a selective barrier for the uptake of antibiotics. In addition, in *Pseudomonas* the removal of potentially harmful compounds is facilitated by the presence of rapid efflux pumps, either expressed constitutively or induced by the presence of the drug (Breidenstein, de la Fuente-Núñez, and Hancock 2011). Another intrinsic protection mechanism that can be used by this microorganism is the production of β-lactamases that break the β-lactam ring present in many antibiotics, inactivating the drug. Strains of *P.*

aeruginosa with alternative resistance mechanisms, acquired or adaptive, have been reported in different studies (Sacha et al. 2008).

Acquired mechanisms are mediated by the internalization of DNA fragments, such as plasmids, transposons, integrons and porophages that contain antibiotic resistance genes, incorporated in the bacterial cell through transformation, conjugation or transduction mechanisms. Alternatively, resistance may arise after spontaneous mutation in genes regulating expression of efflux pumps, production of β-lactamases, small-molecule uptake mechanisms, or mutations that alter antibiotic targets. The accumulation of mutations can greatly increase the bacterium resistance to drugs, transforming it in a so-called "superbug" (Breidenstein, de la Fuente-Núñez, and Hancock 2011).

Adaptive mechanisms are inducible processes that may be triggered by environmental stimuli such as pesticides, pH, divalent cations and sub-inhibitory concentrations of antibiotics. When exposed to gradually increasing doses of antibiotics, bacteria transiently change their phenotype in order to survive to normally lethal concentrations of drugs. The adaptive mechanisms are reversible and the normal phenotype appears after antibiotics are removed (Breidenstein, de la Fuente-Núñez, and Hancock 2011).

Biofilm production. In addition to acquired and adaptive protection mechanisms, *Pseudomonas* can transit to a mucoid phenotype producing a biofilm of alginate and other polysaccharides, that protects bacteria from the aggression of the host immune system. The biofilm confers resistance to antibiotics creating a suitable niche for the bacteria to proliferate, allowing their survival even in environments with limited iron, phosphate or nutrient sources, and increasing their ability to adhere to surfaces (Lyczak, Cannon, and Pier 2000). The protection conferred by this matrix is so robust that, in chronic infections such as lung infections often developed by Cystic Fibrosis patients, bacteria are able to downregulate LPS production, further decreasing immunogenicity and increasing the possibility to evade host defense mechanisms (Maldonado, Sá-Correia, and Valvano 2016). Due to the development of mucoid phenotypes, *P. aeruginosa* chronic lung infections are the primary cause of mortality in Cystic Fibrosis patients (Lyczak, Cannon, and Pier 2000).

In the normal phenotype, however, cell wall integrity is essential for bacterial survival and persistence in the environment. Knock-out mutants of cell wall biosynthesis have a lower growth rate in minimal medium, display changes in cell morphology and a higher sensitivity to macrophage-mediated killing. Compared to the wild type, mutants unable to synthesize a functional cell wall show a dramatic decrease of virulence and pathogenicity (Elamin et al. 2017).

Considering the essential role played by enzymes involved in cell wall biosynthesis, new antimicrobial agents targeting these enzymes may be an interesting and innovative strategy for the treatment of *P. aeruginosa* infections, helping to overcome bacterial antibiotic resistance.

2.2. Bacterial cell wall and plasma membrane

Since bacterial cells are usually exposed to a hostile environment, their cell wall evolved in order to isolate the bacterium from environmental changes, to protect it from hazardous molecules, to maintain cell shape in non-isotonic environments, and to allow the selective passage of nutrients.

In 1884 Christian Gram developed a staining procedure that allows the classification of bacteria in two general classes: gram-positive bacteria retain Gram stain[1], while gram-negative bacteria do not. The stain retention is based on differences in the structure of the bacterial cell envelop (Figure 2.1). Bacteria belonging to each class share similar structural features, but also a great deal of differences, brought by evolutionary processes that allow bacteria to improve their persistence in inhospitable environments.

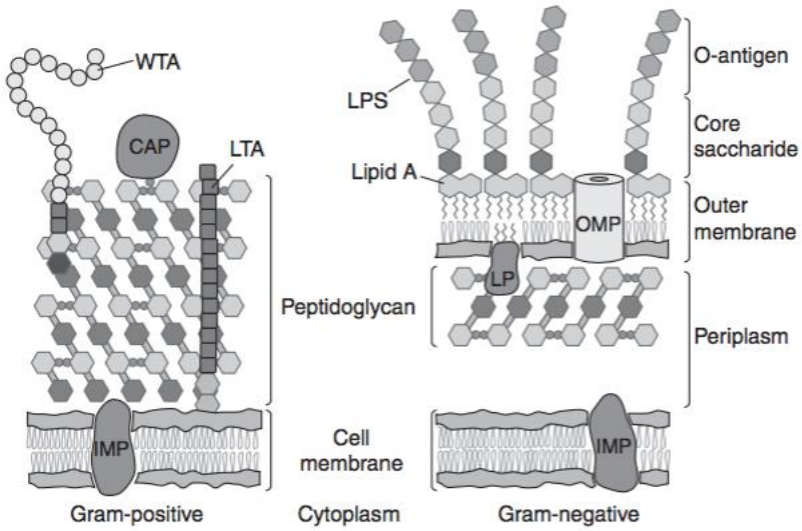

Figure 2.1: Depiction of gram-positive and gram-negative cell envelopes: CAP, covalently attached protein; IMP, integral membrane protein; LP, lipoprotein; LPS, lipopolysaccharide; LTA, lipoteichoic acid; OMP, outer membrane protein; WTA, wall teichoic acid. Cold Spring Harb Perspect Biol 2010.

[1] Through this dissertation, the capitalization of the Gram name follows the CDC guidelines: "*Gram should be capitalized and never hyphenated when used as Gram stain; gram negative and gram positive should be lowercase and only hyphenated when used as a unit modifier".* From CDC webpage updated on May 2016.

2.2.1 The cell wall of gram-positive bacteria

Gram-positive bacteria possess a single phospholipidic membrane protected by a thick layer of peptidoglycan. This rigid polymer, that contributes to the maintenance of the cellular shape, is formed by repeated units of N-acetyl glucosamine-N-acetyl muramic acid, cross-linked via pentapeptide side chains (Vollmer, Blanot, and De Pedro 2008). Having to overcome the turgor pressure exerted on the plasma membrane, the peptidoglycan in gram-positive bacteria is formed by many layers, with a variable thickness of 30-100 nm.

In the layers of peptidoglycan, long anionic polymers mostly composed by glycerol phosphate, ribitol phosphate or glucosyl phosphate repeats, known as teichoic acids, are inserted. These polymers are found in a wide range of gram-positive bacteria and constitute over 60% of the peptidoglycan. According to their structure, teichoic acids are divided into 2 classes: the first includes teichoic acids anchored to the head groups of phospholipids, the lipoteichoic acids, often functionalized with D-Alanine or a sugar moiety; the second class includes the wall teichoic acids, covalently attached to the peptidoglycan via a phosphodiester bond extending perpendicularly to the peptidoglycan mesh (Neuhaus and Baddiley 2003).

The peptidoglycan has also a protective function for gram-positive bacteria, constituting a barrier to potentially harmful compounds. In fact, its biosynthesis, and especially the formation of peptide crosslinks, has evolved in order to enhance impermeability to β-lactamic antibiotics (Rohrer and Berger-Bächi 2003; Sauvage et al. 2008). These compounds mediate bacterial death by interfering with cell wall components, especially with the murein biosynthesis (Kong, Schneper, and Mathee 2010).

The gram-positive bacteria cell wall has a wide variety of embedded proteins, interacting with the internal constituents of the cell wall in different ways. The adhesins, peripheral membrane proteins, are associated through noncovalent polar interactions with the peptidoglycan (Scott and Barnett 2006) or with the teichoic acids. Other cell wall proteins are covalently attached to membrane lipid anchors or to the peptides within peptidoglycan layers (Dramsi et al. 2008; Sjoquist et al. 1972; Fischetti et al. 1990), or have functional interactions with the cell surface polymers. Finally, proteins deputed to peptidoglycan biosynthesis are anchored to the cytoplasmic membrane. The composition of surface proteins is strongly correlated to the environment that surrounds the bacteria (Pollack and Neuhaus 1994). For example, when required by external conditions the bacterium is able to express, on its surface, proteins involved in evasion from host defense mechanisms, in internalization of metals essential for enzymatic activities (e.g. iron), in phage binding, or in cell wall degradation.

2.2.2 The cell wall of gram-negative bacteria

The cell envelop of gram-negative bacteria is formed by three layers: the outer membrane; the periplasmic space, an aqueous compartment containing the peptidoglycan network; and the inner membrane (Glauert and Thornley 1969) (Figure 2.2).

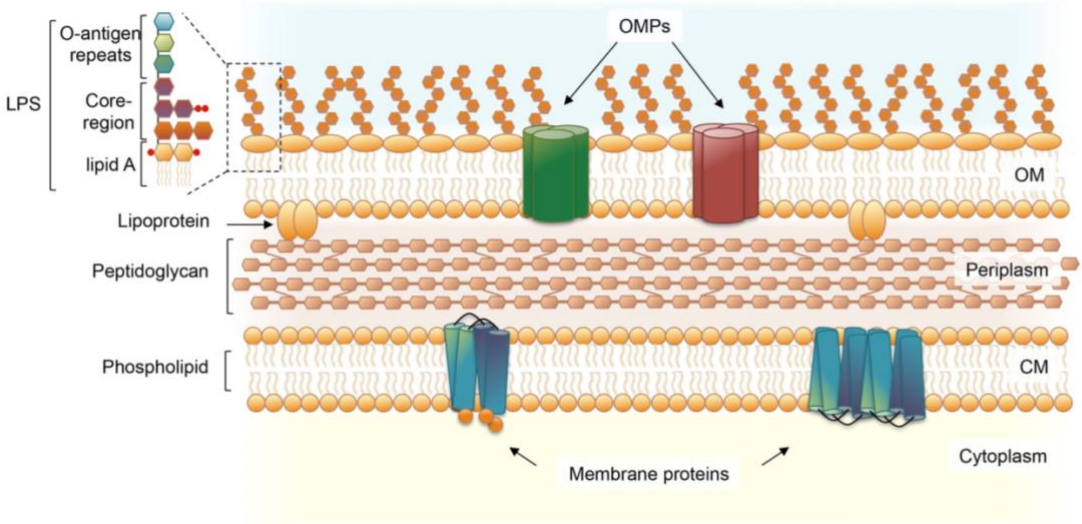

Figure 2.2: Gram-negative bacteria cell wall (Maldonado, Sá-Correia, and Valvano 2016)

The outer membrane, present only in gram-negative bacteria, is not a phospholipidic bilayer, as in typical cell membranes. In fact, the phospholipids are present only in the periplasmic leaflet, whereas the outer leaflet is composed by glycolipids, especially the lipopolysaccharide (LPS) (Kamio and Nikaido 1976).

There are two classes of proteins on the outer membranes, the lipoproteins and the β-barrel proteins. The former are peripheral membrane proteins, known as Braun's lipoproteins or mureins, linked to lipids of the inner leaflet of the outer membrane through covalent bonds formed by an N-terminal cysteine residue (Sankaran and Wus 1994). These proteins have the important function of connecting the outer membrane with the underlying peptidoglycan layer.

Almost all of the integral membrane proteins of the outer membrane belong to the second class, the β-barrel proteins, having a β-barrel tertiary conformation. Despite their similar structure, β-barrel proteins have a variable number of transmembrane β-strands and differ for their multimeric assembly. These proteins have multiple functions: some are responsible for the passive diffusion through the outer membrane of small molecules such as mono- and disaccharides, amino acids, maltose, maltodextrins and anions such as phosphate. Larger β-barrel proteins, the porins, with 20-24 transmembrane β-strands limit the diffusion of hydrophilic molecules larger than 700 Da, working as gated channels and transporting with

high affinity large ligands such as vitamin B-12 and Fe-chelates (Nikaido 2003). Some of the β-barrel proteins have also enzymatic functions, such as phospholipases (Snijder et al. 1999), proteases (Vandeputte-Rutten et al. 2001), and enzymes introducing modifications in the LPS (Hwang et al. 2002). The catalytic sites of all these enzymes are located within the outer leaflet or face the exterior of the cell (Silhavy, Kahne, and Walker 2010).

The peptidoglycan layer underneath the outer membrane of gram-negative bacteria is only a few nanometers thick, much thinner than in gram-positive bacteria. In fact, in gram-negative microorganisms the control of the cellular shape is mostly performed by the external membrane (Silhavy, Kahne, and Walker 2010). As in gram-positive species, linear glycan strands, formed by disaccharide repeat units, are coupled to peptides by glycosidic bonds, creating a mesh-like framework.

The periplasm, the aqueous environment hosting the peptidoglycan layer, is more viscous than the cytoplasm (Mullineaux et al. 2006) and densely packed with proteins, such as periplasmic binding proteins, chaperone-like proteins and various types of enzymes (Ehrmann 2007). This bacterial compartment is believed to be the precursor of eukaryotic cells lysosomes (Duve and Wattiaux 1966) and allows bacteria to isolate potential harmful enzymes, such as RNAses or alkaline phosphatases that in the cytoplasm could damage the integrity of the cell.

Finally, the inner membrane, a common feature of both gram-positive and -negative classes of bacteria, is the more internal component of the gram-negative cell envelop. The inner membrane is constituted by a lipid bilayer and is the site of all those membrane-associated functions that in eukaryotic cells are carried on by organelles. Among them: energy production, lipid biosynthesis, protein secretion and transport (Silhavy, Kahne, and Walker 2010).

2.3. Lipopolysaccharide

Located on the outer leaflet of the outer membrane of gram-negative organisms, the LPS is a fundamental part of the defense mechanisms of gram-negative bacteria as it provides protection to the cell by acting as an effective barrier for hydrophobic molecules and preventing access to deleterious molecules such as antibiotics, bile salts, detergents and cationic antimicrobial peptides. (Nikaido 2003; Silhavy, Kahne, and Walker 2010). LPS helps bacterial colonization of the environment and, therefore, it is actively involved in bacterial infection pathogenesis (Whitfield and Trent 2014). In addition, as the human innate immune system is sensitized to this molecule, the LPS has a very important role in bacterial virulence and is the main responsible for the endotoxic shock (Raetz and Whitfield 2002).

The LPS is constituted by 3 components (Figure 2.3): the lipid A, a glucosamine disaccharide bound to six or seven acyl chains, that anchors the LPS to the outer leaflet of the outer membrane and is common to all gram-negative bacteria; a conserved polysaccharide core that contributes to the integrity of the outer membrane; and a polysaccharide chain, the O antigen, of variable length and composition (Raetz and Whitfield 2002; Whitfield and Trent 2014). The composition of the O antigen is used to classify bacteria by their antigenic properties, dividing a single bacterial species in serotypes. LPS molecules are strictly bound to each other taking advantage of the presence of Mg^{++} ions that neutralize the negative charges of lipid A phosphate groups. The high saturation of the acyl chains of lipid A allows a tight packing of LPS molecules.

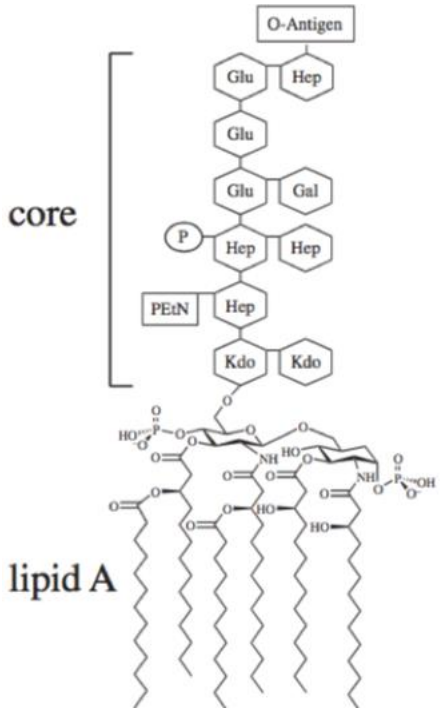

Figure 2.3: Schematic representation of the LPS.(May et al. 2015)

Some bacterial strains have an LPS constituted only by lipid A and the core oligosaccharide, the so-called “rough” LPS; in others all three features are present (“smooth” LPS).

The opposite permeabilities of the outer and the inner membranes confer a high degree of protection to bacteria. In fact, the outer membrane serves as a barrier for small hydrophobic compounds, controlling their diffusion through the outer membrane porins. If a small hydrophobic molecule is allowed to reach the periplasmic space through the outer membrane porins, it can easily diffuse through the phospholipidic membrane, as the inner membrane is more permeable to hydrophobic compounds. On the contrary, the inner membrane is impermeable to small hydrophilic molecules, allowing their access only through highly regulated transporters. The opposite permeability properties of inner and outer membranes are one of the challenges in antibiotic development. When the

asymmetry of the membrane is broken, as in case of LPS disaggregation, phospholipid bilayer patches substitute the missing LPS on the outer membrane. These patches allow the diffusion of small hydrophobic compounds increasing the sensitivity of the bacterium to toxic molecules. Bacteria such as *P. aeruginosa* cannot survive without LPS (May et al. 2015).

In addition, LPS has a considerable influence on outer membrane proteins (both lipoproteins and β-barrel proteins) acting as a chaperone, helping protein oligomerization and maintaining gating functions of β-barrel proteins. In fact, the disruption of the LPS assembly dramatically compromises the function of these protein and alters the access of nutrients into the cell (Zhang, Meredith, Kahne 2014). Inhibition of LPS production prevents bacterial growth and stress response activation due to the accumulation of mistargeted or misfolded outer membrane proteins. In case of severe damage to the LPS, the increased presence of aggregated outer membrane proteins is detected by the sensor protein DegS that initiates a proteolytic cascade (Walsh et al. 2003; Alba and Gross 2004). LPS disruption affects also the inner membrane since the accumulation of glycolipids involved in LPS biosynthesis compromises its functions and prevents the proper assembly of inner membrane proteins (Rick et al. 1988; Rick et al. 1998; Meredith et al. 2007; Typas et al. 2017). Considering its important functions, a disruption of the LPS barrier, for example by inhibiting the LPS biosynthetic pathway, greatly influences bacteria homeostasis, reducing the resistance to antibiotics. For this reason, molecules able to interfere with LPS biosynthesis may be interesting as antibiotics or antibiotic adjuvant molecules.

2.3.1.Lipid A

Lipid A is constituted by a glucosamine dimer, linked to a variable number of acyl chains, usually 6, by ester and/or amide linkages (Figure 2.4A). The sugar units bind two phosphate groups at the reducing end of the first and in position 4 of the second and bear further glycosylations (not shown in Figure 2.4) at the 6'-position with two residues of 3-deoxy-D-manni-oct-2-ulosonic acid. The first of these glycosyl groups is the attachment point of the core region (Maldonado, Sá-Correia, and Valvano 2016).

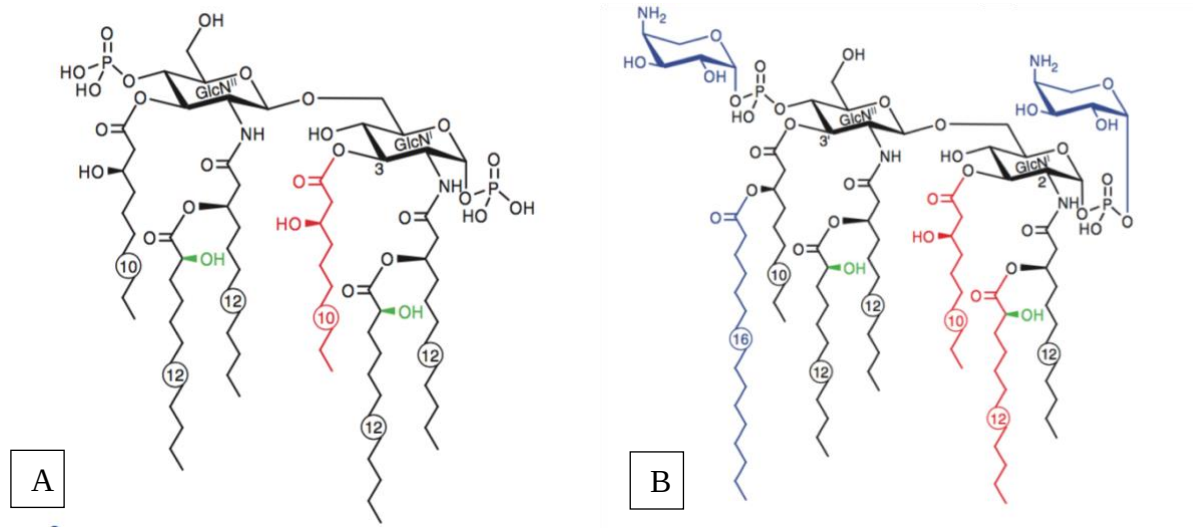

Figure 2.4: A) Typical lipid A structure; B) modification on lipid A structure. From (J. D. King et al. 2009)

Lipid A is recognized by macrophages, monocytes and dendritic cells, causing a robust inflammatory response (Park et al. 2013). In bacteria, modifications occurring on the Lipid A acylation pattern or addition of positively charged glycosyl residues on the phosphate groups (Raetz et al. 2007) confer protection against host immune defenses, decreasing the inflammatory response and increasing the resistance against cationic antimicrobial peptides (Raetz et al. 2007; Molinaro et al. 2015) (Figure 2.4B). Lipid A is synthesized in the inner leaflet of the inner membrane, where a nine-enzyme pathway converts the precursor Uridine-diphosphate-N-acetylglucosamine (UDP-N-acetyl-glucosamine), to lipid A and binds it to two residues of 3-deoxy-D-manni-oct-2-ulosonic acid. This molecule becomes the acceptor of the core oligosaccharides that are linked via glycosyl transfer reactions starting from nucleotide sugar precursors (Whitfield and Trent 2014).

2.3.2.The core oligosaccharide

The core oligosaccharide chain is formed by two parts, the inner core whose residues are usually conserved among bacterial species and an outer core that has a more variable structure, with some changes even in different strains of the same species (King et al. 2009). Decorations of the core oligosaccharide are present in different species. For example, in *Pseudomonas aeruginosa*, the heptose sugars of the inner core undergo phosphorylation associated with higher resistance to antibiotics and an increased membrane impermeability (Walsh 2000). The core is formed by a series of cytoplasmic glycosyl transferases that mediate the addition of the sugar to the Lipid A-Kdo2. The Kdo sugars are bound to the Lipid A by the enzyme WaaA (Whitfield and Trent 2014). Then the sugar chain is elongated by the heptosyltransferases and further glycosyl transferases to

form the specific core sequence. Finally, the core is phosphorylated by WaaP (King et al. 2009; Latino, Caroff, and Pourcel 2017).

Once assembled, the lipid A-core complex is transferred to the periplasmic leaflet of the inner membrane by MsbA, an ABC transporter (Whitfield and Trent 2014). The presence of the core oligosaccharide is essential for LPS transport to the outer membrane (Delucia et al. 2011).

2.3.3.O antigen

The O antigen is constituted of linear or branched repeated oligosaccharide units and is the most exposed part on the surface of the gram-negative bacterial cell (Whitfield and Trent 2014). These sugar chains have multiple functions: they contribute to the evasion from the host immune system, such as the complement cascade, delay internalization and recognition by epithelial cells, and enhance intracellular survival, adhesion and protection against oxidative stress (Murray, Attridge, and Morona 2006; Duerr et al. 2009; Saldías, Ortega, and Valvano 2009; West et al. 2005; Berry et al. 2009).

In *P. aeruginosa,* two types of O-antigen molecules have been recognized through gel separation, namely the oligosaccharides of the "A-band" and of the "B-band". Both these molecules are linked to the lipid A core (Sadovskaya et al. 2000; Knirel et al. 2006) but are constitutively different and their biosynthetic pathways are distinct (King et al. 2009; Lam et al. 2011).

The "A-band", also known as common antigen, is a homopolymer of D-rhamnose, usually 70 sugars long, that causes a weak immunogenic response (King et al. 2009). On the contrary, the "B-band", or specific antigen, is a sugar heteropolymer whose variability, even within the same species, is the basis for bacterial identification through serotyping. In addition, the "B-band" is highly immunogenic and leads to the development of a robust antibody response. This exerts a selective pressure in chronic infections towards strains lacking the ability to produce the "B-band" O antigen (King et al. 2009). For example, in Cystic Fibrosis chronic infections, *P. aeruginosa* strains produce a mucoid polysaccharidic biofilm that protects bacteria from the environment and allows them to survive without the immunogenic specific antigen (Hancock et al. 1983; Govan and Deretic 1996).

2.3.3.1. O antigen biosyntesis

For different bacterial species, the biosynthetic routes for common and specific O antigens are different. There are three main mechanisms for O-antigen production and translocation: the Wzy-dependent pathway, the ABC-transporter dependent pathway and the synthase-

dependent pathway (Keenleyside and Whitfield 1996; Lam et al. 2011; Greenfield and Whitfield 2012; Valvano 2015). In *P. aeruginosa* the common and specific O antigens are formed and transported through the first two pathways. The ABC transport system, constituted by Wzm-Wzt proteins, is involved in the translocation of the common antigen (Figure 2.5, right panel). The Wzy-dependent pathway is deputed to the synthesis and the translocation of the O-specific antigen (King et al. 2009; Lam et al. 2011) (Figure 2.5, left panel).

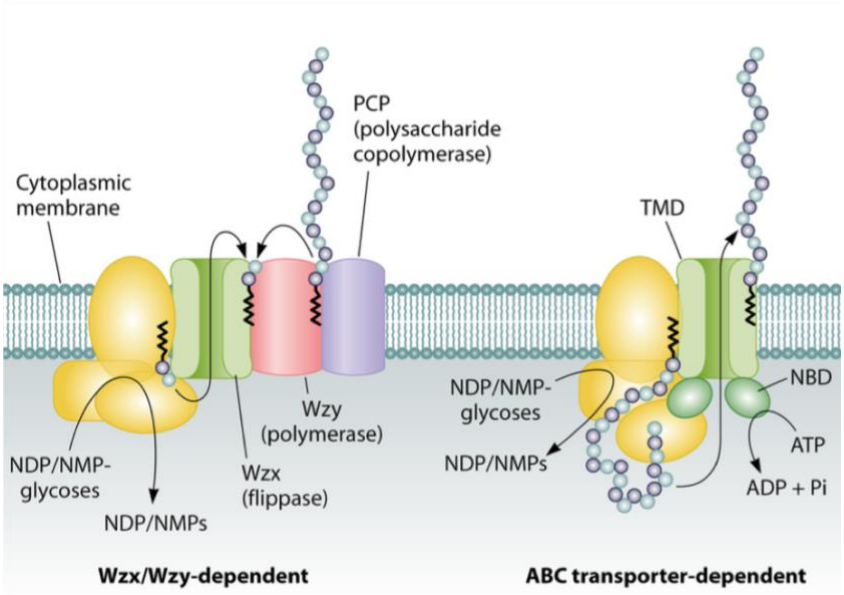

Figure 2.5: Schematic representation of Wzx/Wzy- and ABC transporter-dependent pathways for O-antigen biosynthesis. From(Cuthbertson, Kos, and Whitfield 2010a)

For both O-antigen components of *P. aeruginosa*, the sugar chain is formed onto the C_{55}-undecaprenyl phosphate (Und-P), used as scaffold, through the action of a set of glycosyl transferases, each catalyzing the binding of a specific glycosydic monomer. The first of these glycosyl transferases, the protein WbpL, forms a Und-P-P-sugar intermediate and is common to both Wzy- and ABC transporter-dependent pathways. A specific set of glycosyl transferases, proteins WbpX, WbpY and WbpZ, is deputed to the biosynthesis of the common antigen from the precursor GDP-D-rhamnose. Another set of glycosyl transferases, different for each serotype, is involved in the biosynthesis of the short repeated units that form the specific antigen (King et al. 2009; Lam et al. 2011).

For the common antigen, the polymerization of the whole glycan chain is carried out in the cytoplasm via addition of monomers at the reducing terminus of the lipid linked intermediate. The mature common antigen is then translocated through the inner membrane towards the

periplasmic leaflet by an ABC transporter that couples the substrate flipping with the hydrolysis of ATP (Rocchetta and Lam 1997; Cuthbertson, Kos, and Whitfield 2010b).

For the specific antigen, the repeated subunit, a short oligosaccharide constituted by a variable number of monomers, is formed in the cytoplasmic space and then translocated to the periplasmic leaflet of the inner membrane, where all the repeated units are later polymerized to form the complete polysaccharide. These tasks are performed by an assembly of three enzymes acting sequentially, the Wzx/Wzy/Wzz assembly, composed of an O-antigen flippase, a polymerase and a chain regulator protein, respectively.

In the periplasmic leaflet, both the common and the specific antigens are linked to the lipid A-core oligosaccharide assembly by the enzyme Waal (Abeyrathne et al. 2005; Ruan et al. 2012). Finally, the newly assembled LPS is transported though the periplasm and located on the outer leaflet of the outer membrane by the Lpt (LPS transport) pathway (May et al. 2015; Simpson et al. 2015). This biosynthetic route includes: (1) the LptBFG complex that actively extracts LPS from the periplasmic leaflet of the inner membrane, (2) proteins LptCA and YhjD that promote LPS transition through the periplasm, and (3) the assembly of outer membrane proteins LptDE, YtfN, YfgH, and YceK that promotes the correct insertion of the LPS in the outer membranes (May et al. 2015; Babu et al. 2011; Simpson et al. 2015). During the transport through the periplasm, the LPS may undergo further covalent modifications (Raetz et al. 2007), specifically developed by bacteria to adapt to the environment and often influencing the microorganism virulence.

The correct functioning of the whole machinery that produces the LPS is crucial for bacterial survival. Consequently, proteins participating in this complex biosynthesis are potential targets for antibacterial therapy. For example, the inhibition of the first steps of LPS biosynthesis, such as the formation of lipid A and its binding to the core oligosaccharide, may cause the lack of oligosaccharide lipid A-core complex available for O-antigen binding. In turn, this causes the accumulation of Und-PP-O antigen complex in the inner membrane, an assembly that has been proved to be toxic for the cell (Yuasa, Levinthal, and Nikaido 1969). In fact, both LPS and peptidoglycan biosynthetic pathways necessitate this precursor and the sequestration of Und-P prevents both biosynthetic routes.

2.4. The Wzy pathway

Despite the sequence variability of proteins involved in the pathway, that matches the variability of the polysaccharides produced by different bacterial strains (Raymond et al. 2002), and the different roles covered by this synthetic route, the scheme of the Wzy-dependent pathway is conserved among both gram-negative and gram-positive bacteria (Figure 2.6). In different species this pathway is involved in the synthesis of the heteropolymeric O antigen, in the synthesis of the common antigen (enterobacteria), in the production of other polysaccharides, such as exopolysaccharides, spore coat, adhesive holdfast and capsular polysaccharides (Whitfield 2006; Toh, Kurtz, and Brun 2008; Müller et al. 2012).

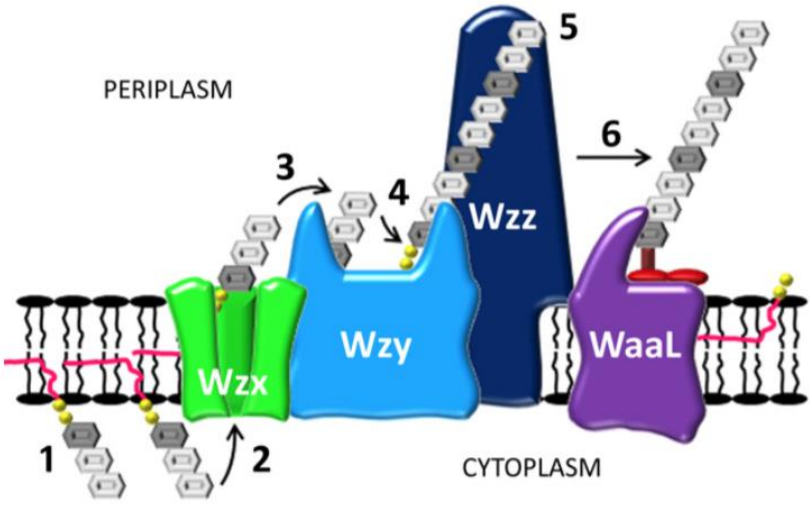

Figure 2.6: Schematic representation of the Wzy-dependent pathway: 1. Polysaccharide repeat units are built in the cytoplasmic space. 2. UndPP-linked repeat units are flipped from the cytoplasmic to the periplasmic leaflet by Wzx. 3. A UndPP-linked repeat unit binds to Wzy in the periplasmic space. 4. Wzy mediates polymerization of the repeat units. 5. The polymerization extent is governed by the chain length regulator Wzz, 6. The newly synthesized polysaccharide is ligated to the lipid A-core oligosaccharide complex by WaaL (Salim T. Islam and Lam 2013)

In the model of this pathway, proposed by Whitfield (Whitfield 1995) and confirmed by recent studies, the first step occurs in the cytoplasmic leaflet of the inner membrane, where an O-antigen repeat unit bound to the UndPP carrier is flipped to the periplasmic leaflet of the inner membrane by the flippase Wzx (D. Liu, Cole, and Reeves 1996) (Figure 6, steps 1-2). The O-antigen subunits are then polymerized on the periplasmic leaflet of the inner membrane by the Wzy polymerase (Robbins et al. 1967; Dasgupta et al. 1994; Woodward et al. 2010) that adds each repeat unit at the reducing terminus of the nascent sugar polymer, generating a new glycosidic linkage (Robbins et al. 1967) (Figure 6, steps 3-4). The length of the sugar chain is regulated by the polysaccharide co-polymerase Wzz (Figure 6, step 5). After the protein Waal catalyzes the O-antigen binding to the lipid A-core oligosaccharide assembly (Abeyrathne et al. 2005; Abeyrathne and Lam 2007b; Han et al. 2012; Ruan

et al. 2012) (Figure 6, step 6), the mature LPS is transported to the outer membrane through the Lpt pathway (Silhavy, Kahne, and Walker 2010).

2.4.1.Wzx: O-antigen flippase

Proteins deputed to the translocation of phospholipids and glycolipids across the membrane are generally called flippases. Members of this large class cover very different functions, from the formation and maintenance of the membrane asymmetry, to the translocation of molecules between membrane leaflets using lipid carriers. Flippases may be divided in two categories based on the energetics of their mechanism of action. Flippases deputed to the translocation of phospholipids and glycolipids transfer their substrates against gradient coupling the flipping with an antiport translocation of other species or through ATP hydrolysis (Kuroda and Tsuchiya 2009; Menon 1995). When the translocation follows the gradient, as for the protein Wzx of the Wzy-dependent pathway, no energy source is required and the flippase simply facilitates the diffusion of the lipid-based compound between the leaflets.

The protein Wzx mediates the translocation of the negatively-charged oligosaccharide O units bound to the Und-PP carrier from the inner to the outer leaflet of the inner membrane (Knirel et al. 2006). Wzx belongs to the Polysaccharide transporter (PST) family (Hvorup et al. 2003), one of the four families of the multidrug/oligosaccharidyl lipid/polysaccharide (MOP) exporter superfamily (Hvorup et al. 2003). The PST family has two main subfamilies, one deputed to the export of the lipopolysaccharide O antigen in gram-negative bacteria, the second involved in the export of exopolysaccharides or capsular polysaccharides in both gram-positive and negative bacteria (Hvorup et al. 2003). In addition, PST systems of both archaea and bacteria are involved in the transport of other classes of carbohydrates such as teichuronic acids (Soldo et al. 1999).

The sequence homology between Wzx orthologs in different organisms is quite low, reflecting the extensive variety of UndPP-linked O antigens (Islam and Lam 2013). The flippase seems to be able to discriminate the entire O-unit structure (Wang, Yang, and von Bodman 2012), but the chemical identity of the first sugar is crucial for initial substrate binding. In addition, only the main sugar chain, the side chains and the chemical modifications of the native O units are able to accommodate in Wzx cationic cavity, ensuring the good degree of selectivity of the protein (Islam et al. 2012). In fact, the flippase Wzx, even when overexpressed, cannot successfully translocate exogenous O units (Hong and Reeves 2014).

Considering the essential function of this protein in the O-antigen biosynthetic machinery and the lack of homologous proteins in mammals, Wzx is an interesting drug target, with an expected low probability of off-target interactions and related side effects. Moreover, the low sequence homology between Wzx flippases in different bacterial strains opens the possibility of strain specific antibiotics, or antibiotic adjuvants (Islam and Lam 2013). In this view, knowledge regarding the protein structure would be a major help in the design of a compound capable of binding to the active site and inhibiting its action (Blundell 1996; Anderson 2010).

Wzx structural studies: state of the art

Due to the complexity of overexpression, purification and crystallization of membrane proteins, to this date the only structural information on Wzx comes from studies of topological mapping, mainly conducted on the sequence of Wzx from the strain PAO1 of *P. aeruginosa* (serotype O5) (Abeyrathne and Lam 2007a). Prediction algorithms suggest that Wzx_{PAO1} is an integral membrane protein formed by 12 transmembrane segments with both N- and C-terminal domains located in the cytoplasm (Islam and Lam 2013) (Figure 2.7).

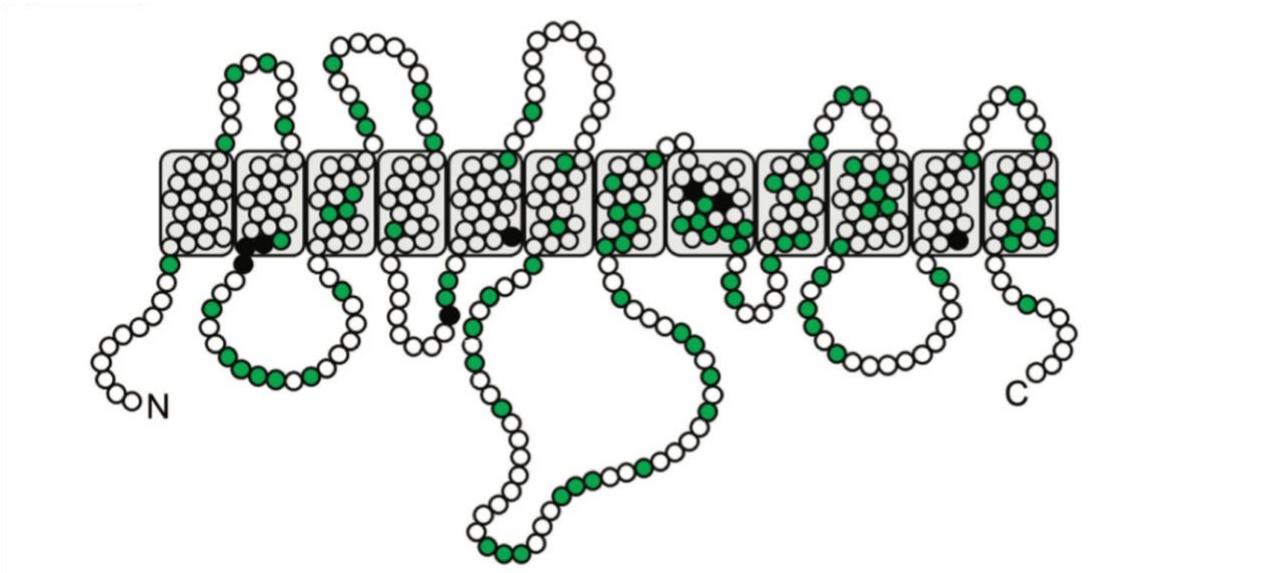

Figure 2.7: Wzx_{PAO1} topology map. The grey squares represent transmembrane segments, circles are the protein residues, with black filling for functionally important amino acid residues and green filling for residues not essential to protein activity, as determined via mutagenesis studies.(Salim T Islam and Lam 2014)

Islam and Lam (Islam et al. 2012) created a Wzx homology model based on the crystallographic structure of NorM from Vibrio cholerae El Tor, another member of the MATE family. The model was validated via comparison with Wzx homologs in other

microorganisms and with random C-terminal truncations that allowed the determination of the positions of transmembrane segments (Figure 2.8).

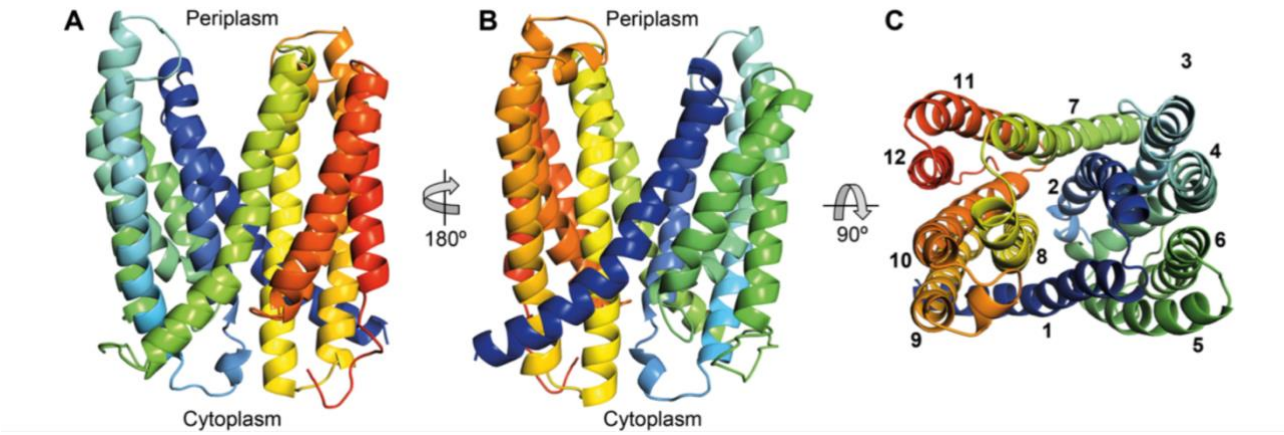

Figure 2.8: Model of the Wzx$_{PAO1}$ tertiary structure, based on sequence homology with known structures (Salim T. Islam et al. 2012)

According to topology predictions and to homology modelling, the cytoplasmic region of Wzx$_{PAO1}$ is composed by three large loops, the larger of which connects transmembrane segments (TMS) 6 and 7 and is probably involved in substrate recognition (Islam et al. 2010). On the opposite side, the periplasmic region seems less organized compared to the cytoplasmic side, confirming that the stereospecific interactions with the substrate happen in the cytoplasmic leaflet of the membrane (Marolda, Vicarioli, and Valvano 2004), whereas the final extrusion in the periplasmic leaflet does not require high substrate specificity (Islam et al. 2012). Considering the characteristics of the luminal space and the overall structure of the protein, the UndPP-linked O-antigen repeated unit is likely to enter only partially in the Wzx$_{PAO1}$ lumen. The positive charge of this region probably interacts with the pyrophosphate-linked O units, while the highly hydrophobic C_{55} tail of the UndPP lipid carrier remains embedded in the inner membrane (Zhou and Troy 2005).

Through mutagenesis studies, Islam and colleagues were able to determine the residues of Wzx$_{PAO1}$ directly involved in O-unit loading into the protein channel and those mainly involved in substrate translocation (Islam et al. 2012). Considering the residues identified by mutagenesis, their study proposes a mechanism of action for Wzx$_{PAO1}$(Figure 10). Positively charged residues are likely to be essential for the interaction with the complementary negatively-charged UndPP-linked O unit, during both substrate recognition and translocation (Islam et al. 2012; Islam, Eckford, et al. 2013a). In fact, Arg146 of Wzx$_{PAO1}$, located in the proximity of the cavity, seems to be involved in initial substrate recognition, whereas the

luminal residues Arg59 and Lys272 are involved in substrate translocation. On the contrary, the negatively charged residues buried in the helical bundles may push the anionic substrate through the cavity by charge repulsion. Glu61 and Asp269 residues seem to be involved in substrate translocation trough the cavity during Wzx_{PAO1} conformational changes. These anionic residues may have an energy-coupling function interacting with the O unit and the positively charged residues of the protein (Islam et al. 2012). The presence of aromatic residues in the sugar binding site is a common feature for carbohydrate-binding proteins (Malik and Ahmad 2007; Elumalai et al. 2010). In Wzx_{PAO1}, the luminal Tyr60 and Phe139 residues may be deputed to substrate binding during O-unit translocation (Islam et al. 2012). The predicted exit site of the substrate is located in the periplasmic portal between TMS1 and TMS9. In this way the flipped unit is ready for the polymerization promoted by Wzy.

As many other members of the MATE family, the flippase Wzx_{PAO1} works with an antiport mechanism, coupling substrate translocation with the transport of another species in the opposite direction (Kuroda and Tsuchiya 2009). Together with the translocation of the O antigen from the cytoplasmic to the periplasmic leaflet of the inner membrane, Wzx_{PAO1} transports protons (H^+) towards the cytoplasm (Islam , Eckford, et al. 2013b). According to the proposed mechanism, in a cytoplasmic facing conformation (Figure 2.9A) a UndPP-linked O unit enters between the TMS 1 (cyan cylinder) and 9 and is loaded via a stereospecific interaction with Arg59 and Tyr60 located on TMS2. The binding of the O unit causes a rearrangement in TMS8 and 11 (yellow cylinder) weakening the binding between the Asp269 and Asp359 dyad and promoting H^+ release in the cytoplasm (Figures 2.9B and 2.9C). Proton release causes a relaxation of the protein structure towards a periplasmic-facing conformation, resulting in O unit flipping across the membrane (Figures 2.9D and 2.9E). In an O unit-bound periplasmic-facing conformation, a proton from the periplasmic space binds the dyad formed by Asp269 and Asp359 causing a rearrangement of the Lys272 on the TMS8 (yellow cylinder). This in turn promotes the shift of TMS11 away from TMS1 and towards the TMS10 (orange cylinder) (Figure 2.9F). In this conformation the O unit disengages from Phe139 diffusing toward the lumen whereas the UndPP linker transits across the acyl chains of the membrane toward the exit portal (Figure 2.9G). Once the O unit is released (Figure 2.9H), a conformational change leads to the proton-bound inward-facing conformation, that can bind another UndPP linked O unit (Islam, Eckford, et al. 2013a).

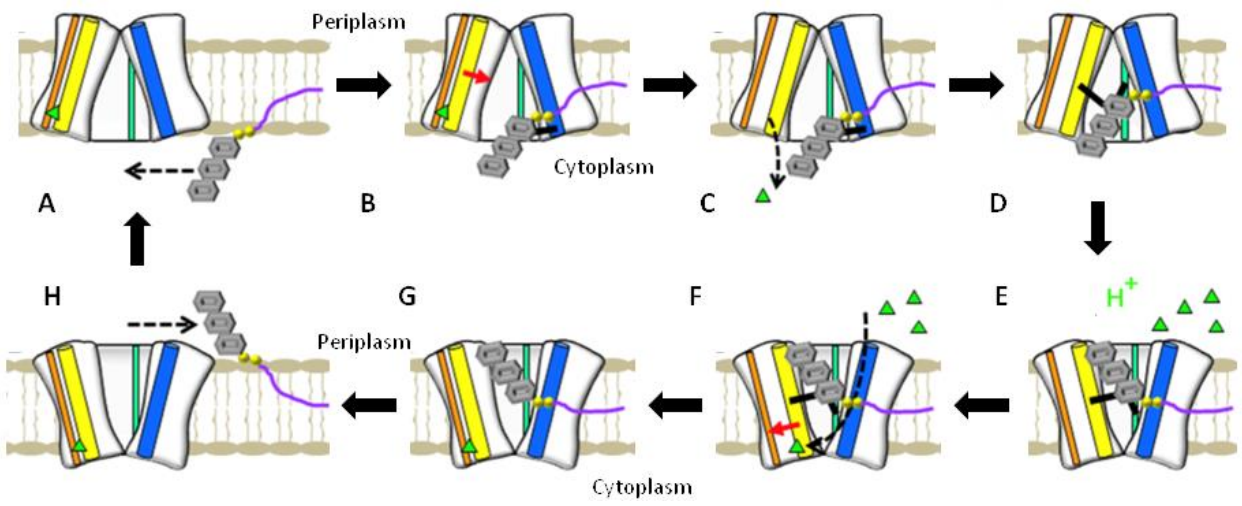

Figure 2.9: Proposed mechanism for the flippase Wzx. (A) H^+-bound conformation, open towards the cytoplasm, (B) loading of a UndPP-linked O unit, (C) H^+ (green triangle) release in the cytoplasm promoted by the O unit, (D) O unit-bound cytoplasm-facing conformation, (E) O unit-bound periplasm-facing conformation, after substrate flipping, (F) binding of H^+ promotes disengagement of the lipid substrate, (G and H) release of flipped O unit. TMS1 and TMS2, in blue; TMS4, in cyan; TMS8 and TMS11, in yellow; TMS10, in orange. Modified from (Salim T. Islam, Eckford, et al. 2013b)

2.4.2.Wzy O antigen polymerase

The O-antigen polymerase Wzy is an integral membrane protein that displays high sequence variability between different bacterial strains. Sequence-based predictions suggest that Wzy has 14 transmembrane segments with two large periplasmic loops and two cytoplasmic loops (Islam et al. 2010) (Figure 2.10). It is likely that in the membrane the polymerase forms a dimer that is functionally active. This was suggested considering the dimerization of the polymerase detected in native SDS-PAGE (Zhao et al. 2014), and consistent with previous studies of analogous O-antigen polymerases in other strains (Islam and Lam 2014).

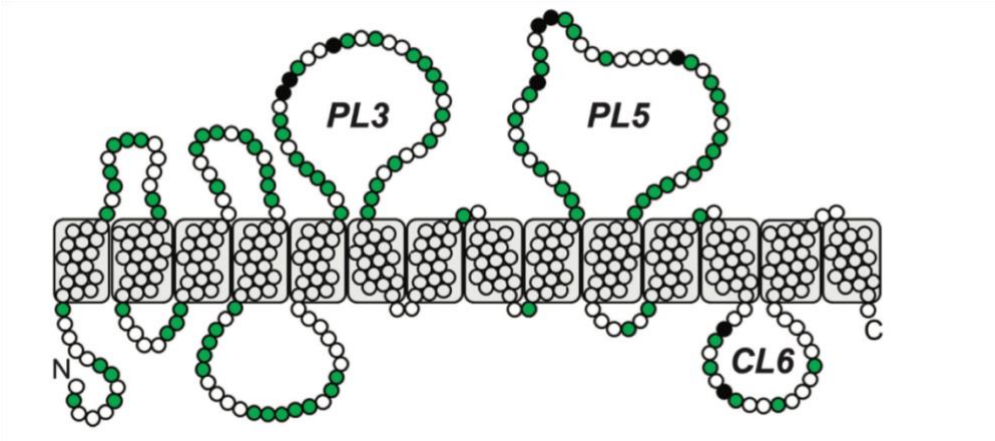

Figure 2.10: Wzy$_{PAO1}$ topology map. The grey squares represent transmembrane segments, circles are the protein residues, with black filling for residues involved in protein activity and green filling for not essential residues determined via mutagenesis studies. (S T Islam and Lam 2014)

Despite having high sequence homology, the periplasmic loops have a different charge distribution, with a net positive charge for the periplasmic loop 3 (PL3) and a net negative charge for PL5. Charge distribution on the periplasmic side is essential for protein activity, and altering the charge of loops PL3 and PL5 compromises Wzy functionality (Islam et al. 2011; Islam, Huszczynski, et al. 2013). A characteristic of both loops is the presence of conserved arginine residues. They are involved in the polymerization mechanism and their mutation affects protein activity. In particular, mutagenesis studies show that not only the charge of the arginine residues is pivotal for catalysis, but also their specific stereochemistry, since substitution with lysine is sufficient to sensibly reduce activity. Evidence that arginine residues are involved in interaction with the oligosaccharide is supported by the fact that these residues are commonly present in polysaccharide or carbohydrate binding enzymes (Malik and Ahmad 2007; Elumalai et al. 2010). Loops PL3 and PL5 are considerably conserved among Wzy homologues (Islam, Huszczynski, et al. 2013) but, while the former, positively charged, is deputed to the binding of a single O unit, the latter, with a net negative charge, binds the growing sugar chain. PL3 acts as a Lewis acid recruiting a new negatively-charged UndPP-linked O unit. In contrast, PL5 acts as a retaining arm for the growing chain and, having a lower affinity for the sugar chain, it is responsible for the release and re-binding of the polysaccharide after the addition of a new subunit. This mechanism proposed by Islam and co-workers (Islam et al. 2011) was named “catch-and-release” and does not require divalent cations for O-antigen polymerization (Woodward et al. 2010).

On the opposite side of the membrane, the cytoplasmic loops are involved in the interaction with proteins Wzz_1 and Wzz_2, responsible for regulation of the polysaccharide chain length. An alteration of this region affects chain length regulation (Islam, Huszczynski, et al. 2013).

2.4.3.Wzz O-antigen chain regulator

The O-antigen chain regulator Wzz is formed by two hydrophobic α-helical segments, one located at the N-terminus and one at the C-terminus of the protein (Bastin et al. 1993; Burrows, Chow, and Lam 1997), enclosing a long soluble periplasmic domain. The periplasmic domain assembles in a bell-shaped structure, highly conserved in different bacterial strains despite the low sequence homology (Kalynych et al. 2012)(Figure 2.11). Wzz is present in an oligomeric state, although the number of subunits assembled is not yet clear, since different crystallographic and cryo-electron microscopy structures show different assemblies, from hexamers to dodecamers (Larue et al. 2009; 2011; Collins et al. 2017). Currently, no information is available on the effective number of monomers that associate in vivo due to the high flexibility of the

protein. Collins and co-workers suggest that the oligomeric state depends on Wzz interaction with other proteins within the bilayer (Collins et al. 2017).

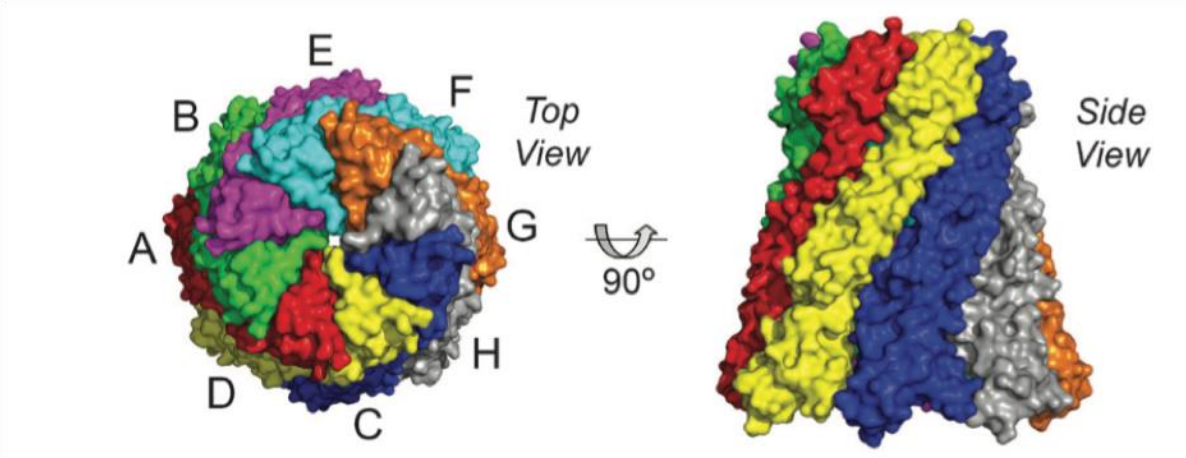

Figure 2.11: One of the experimental structures of the Wzz biological assembly (S T Islam and Lam 2014)

Distinct electrostatic moieties present on the outer surface of Wzz1 homologs are likely to control the interaction with the O antigen, while the transmembrane segments are probably essential for the interaction with Wzy.

The mechanism of chain length regulation by Wzz has not been fully elucidated, but Islam and Lam proposed the "hybrid Chain-feedback-Ruler" model as a possible mechanism to explain the observed Wzz activity (Islam and Lam 2014). In this model, after a few cycles of O-antigen polymerization by the Wzy dimer, the sugar chain is long enough to bind on the outer surface of Wzz. The co-polymerase keeps the sugar chain in a conformation that allows the addition of further sugar units. As the chain elongates, it begins to form high-order structures and these structures, more rigid compared to the linear chain, destabilize the Wzz-polymer interactions. Once the polymer reaches the apex of the Wzz outer surface, it causes a mechanical feedback that promotes its disengaging from the polymerase Wzy. The fully polymerized UndPP-linked O antigen becomes the substrate for the proteins Waal that catalyzes its ligation to the lipid A-core oligosaccharide complex.

2.5. Membrane proteins

Membrane proteins are essential for cell homeostasis and for the response to extracellular stimuli since they are often involved in signaling cascade pathways (Almén et al. 2009). They are divided in numerous families according to their role and functions. Moreover, another classification takes into account their association with the phospholipid bilayer.

The functional families of membrane proteins are:

Receptors are proteins that mediate the cellular response after the interaction with a ligand. This family includes G protein-coupled receptors, receptor-type protein kinases, receptors of the immunoglobulin superfamily and the Scavenger receptors.

Transporters are deputed to the translocation of substrates across the membrane by using gradients or by coupling the transport with exergonic chemical reactions. They are divided into different functional classes: channels, solute carriers, active transporters and other transporters. This large family includes also auxiliary transport proteins whose role is to modulate the activity of other transporters. The proteins belonging to this class usually present a high number of transmembrane segments.

Enzymes bound to the membrane are divided in Oxidoreductases, Transferases, Hydrolases, Lyases, Isomerases and Ligases depending on the reaction catalyzed.

The proteins that do not fit in the already mentioned classes are inserted in the **miscellaneous** group that is further divided into four subclasses: ligands, structural/adhesion protein, proteins with other functions and proteins with unknown function (Almén et al. 2009).

Considering their association with the membrane, proteins can be divided in integral membrane proteins, when they have a significant portion of their mass embedded into the membrane, or peripheral membrane proteins, when only a small portion is associated to the membrane surface (Arinaminpathy et al. 2009). Integral membrane proteins are approximately 20-30% of the proteins encoded by the human genome (Krogh et al. 2001), while the membrane associated proteins represent about 10-20% (Wallin and Heijne 1998).

Prediction of membrane topology is usually facilitated by the fact that transmembrane segments of integral membrane proteins are characterized by an abundance of hydrophobic amino acid residues that find a favorable environment between the acyl chains of the phospholipids. In addition, specific patterns of hydrophilic and hydrophobic residues can be recognized, allowing a discrete reliability in the prediction of the transmembrane regions. Compared to soluble proteins, transmembrane regions are less diverse in their secondary structure motifs: integral membrane proteins can have all α-helical transmembrane domains, forming well-packed bundles across the membrane, or all β-sheet domains, forming β-barrels (Cowan and Rosenbusch 1994) (Figure 2.12).

The number of the transmembrane segments (TMS) and the position of the N- and C-terminus varies among the classes of membrane proteins. However, the majority of proteins with an odd number of TMS present an extracellular N-terminus whereas the C-terminus is more commonly located in the cytoplasm since it is usually deputed to the interaction with cytoplasmic proteins. Usually, the integral membrane proteins with an even number of membrane spanning domains present both termini inside the cell (Almén et al. 2009).

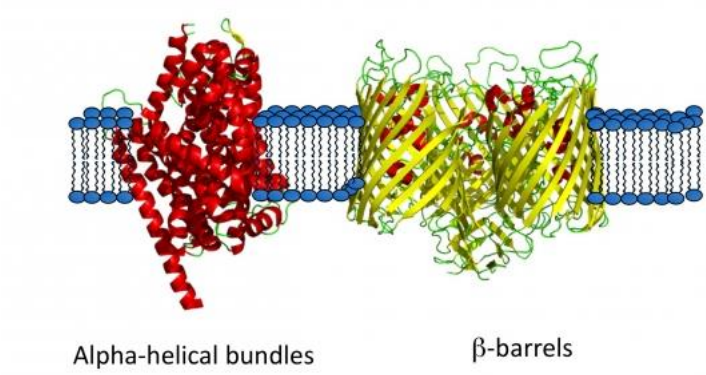

Figure 2.12: Secondary and tertiary structures of membrane proteins. Biochemistry, University of Toronto

Membrane proteins play essential roles in numerous physiological pathways such as molecular recognition, energy transduction and ion flux regulation.

For example, membrane proteins are involved in the cytoskeletal protein anchorage and in the interaction with the extracellular matrix contributing to the maintenance of the cellular shape. In addition, membrane proteins located in the mitochondria are deputed to energy production via the respiratory chain. Cell membrane adhesion molecules, such as the integrines, are involved in cell trafficking and differentiation, covering critical roles in inflammation and immune system regulation (Tan, Hwee, and Chung 2008). The transmembrane transduction receptors bind to a specific extracellular ligand and promote an intracellular signal cascade in response to a specific external signal. The G-protein coupled receptors and the neurotransmitters receptors, among others, belong to this class. Another essential role performed by membrane proteins is the transport of molecules and ions across the membrane. The transporters are divided in channels, that allow the passive movement of specific solutes through their pore, and in carriers that promote the translocation of their substrate after selectively binding the molecule. These macromolecules may discriminate between different solutes mediating the translocation of only a specific class. One of the most studied class of transporter are the ligand and voltage-gated ion channels that mediate the transport of ions across the membrane modulating the membrane potential and allowing the transmission of the synaptic signal.

These channels, such as the sodium-potassium pump, are essential for muscle and neuron functionality (Tan, Hwee, and Chung 2008).

Due to their important roles in biological functions membrane proteins represent more than 60% of drug targets in different therapeutic areas. Drugs may modulate the normal activity of these molecules to obtain the desired effect such as the modulation of GABA receptor to cause sedation (Overington, Al-Lazikani, and Hopkins 2006). Moreover, the malfunction of these proteins may cause severe disorders such as immune deficiencies, Alzheimer and Parkinson diseases or alteration of the central nervous system (Tan, Hwee, and Chung 2008; Ryback 2001).

Despite their relevance and abundance in nature and their importance as drug targets, membrane protein structure and mechanism are still insufficiently understood and they represent only the ~2% of all structures in Protein Data Bank (PDB) (Sarti et al. 2019). Our insufficient structural knowledge of membrane proteins is a limiting factor for the design of more potent and selective drugs. The lack of information regarding membrane proteins is often connected with their hydrophobic nature that makes their handling more difficult compared to most of the soluble proteins. Despite the recent technical and methodological improvements, expression, solubilization, purification and crystallization of membrane proteins are still challenging tasks.

2.5.1.Membrane protein expression, solubilization and crystallization

Membrane proteins may be expressed in bacteria, yeast, insect cells and mammalian cell lines depending on the origin of the protein and the necessity of post translational modifications or specific membrane-targeting systems. The post translational modifications are characteristic of the eukaryotic cells, so, if such modifications are essential for protein stability, the expression should not be done in bacteria. Compared to soluble proteins, the biosynthesis of membrane proteins has significant differences as these proteins need to be immediately inserted in the membrane to adopt their correct folding, due to their highly hydrophobic external surface, not stable in an aqueous environment (Carpenter et al. 2008). To direct this process, membrane proteins have a signal peptide at the N-terminus that is recognized by the signal recognition particle (SRP) (Huber et al. 2005). This interaction mediates the translation of the system across the cytoplasm until it reaches the membrane where the growing protein dissociates from SRP and interacts with the Sec translocon via SRP receptor binding (Luirink and Sinning 2004; Dalbey, Wang, and Kuhn 2011) (Figure 2.13, step a). The insertion within the lipid bilayer is mediated by Sec61α in eukaryotic cells and in SecYEG in bacteria and is driven by the hydrophobicity of the

newly translated helices that favorably interact with the phospholipid acyl chains (E. Park and Rapoport 2012; Hessa et al. 2007) (Figure 2.13, step b). Due to the importance of the N-terminal peptide in membrane protein folding process the addition of an amino terminal fusion tag for protein expression negatively influences the folding in 25% of the proteins with a cytoplasmic N-terminus (Daley et al. 2005; Kim et al. 2006; Wallin and Heijne 1998) and severely prevents the translocation across the bilayer when the N-terminus is extracellular (Rahman et al. 2007; Monné et al. 1999; 2005).

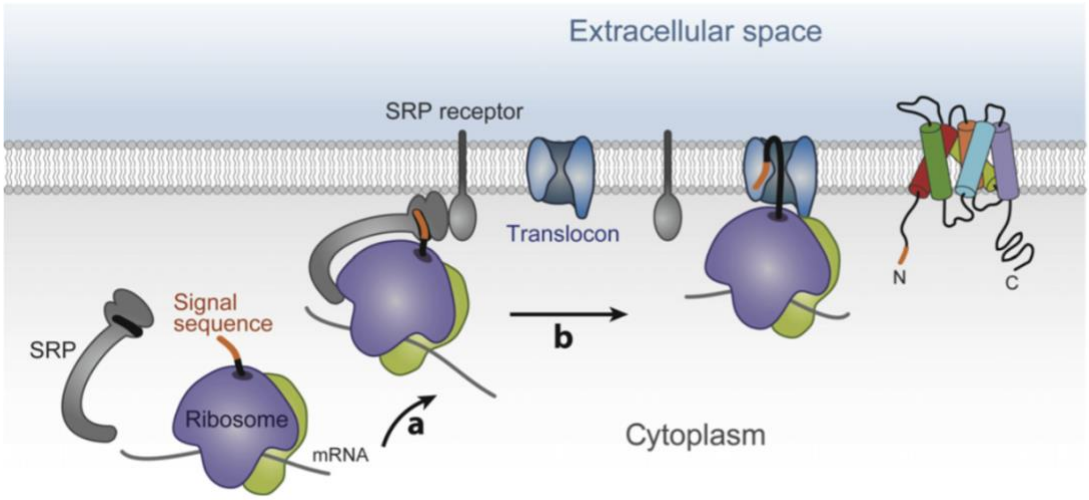

Figure 2.13: Representation of membrane protein translation and folding process. From (Kang, Lee, and Drew 2013)

Due to their localization, membrane proteins are generally expressed in lower yields compared to soluble proteins, as the restricted space of the membrane limits the number of proteins that can be inserted without affecting the stability of the whole membrane. Moreover, the expression of these protein is often toxic for the host, resulting in even lower yields. In addition, after expression, the protein may have low stability, especially if obtained from a heterologous expression system, and may suffer partial proteolysis (Arinaminpathy et al. 2009). For these reasons, membrane proteins are often expressed as chimeric proteins bound to a large affinity tags such as Glutathione-S-Transferase (GST), Maltose-binding protein (MBP) or the Green Fluorescent Protein (GFP) that may improve protein stability (Kobe and Williams 2015).

The addition of a GFP tag, often at the C-terminal of the target protein in order to avoid interference with the signal peptide, may be a powerful strategy to determine the correct folding and localization of the protein in the membrane. In fact, GFP fluorescence is only visible if the domain is properly folded and, due to its localization at the C-terminus, the GFP adopts the correct folding only if the membrane protein at the N-terminus is correctly inserted into the host membrane (Carpenter et al. 2008). Misfolded membrane proteins usually form large aggregates

due to their high hydrophobicity and are isolated in inclusion bodies by the host cell. When the chimeric protein is segregated in inclusion bodies, the GFP fluorescence is not detectable (Drew et al. 2001). Moreover, when unfolding events occur during the purification steps required for structural studies, an irreversible precipitation of the membrane protein is the usual outcome. Therefore, recording the fluorescence intensity of the GFP chimeric proteins can be a useful indication during all the steps of protein expression, solubilization and purification to determine the best operating conditions.

Once these highly hydrophobic proteins are expressed, their purification and crystallization are only possible if they are removed from the lipid environment and solubilized in a suitable detergent solution. These surfactants are amphiphilic molecules able to create micelles and to remove the protein from the phospholipidic bilayer while retaining their native conformation, by shielding their hydrophobic surface from the aqueous solution. Detergents properties should be carefully evaluated to be compatible with the protein purification steps and the characterization experiments planned. Moreover, they must be able to solubilize the protein without causing aggregation or misfolding (Privé 2007). In addition, an excess of detergent may remove the proximal lipids that are often essential for protein stability (Moraes et al. 2014).

Even in the most suitable detergent, membrane proteins are not indefinitely stable in micelles. In fact, while the micelle simulates the hydrophobicity of the membrane environment, it is not able to exert the lateral pressure that is required to maintain protein folding (Privé 2007). In addition, detergents may negatively interfere with the crystallization processes decreasing the surface suitable for protein-protein interactions, hampering crystal genesis and causing phase separation (Moraes et al. 2014). Due to the lower impact on protein-protein contact formation, small micelle-forming detergents are preferred in crystallography due to the higher resolution obtained in the X-ray diffraction patterns. On the other hand, these surfactants are harsher and may cause protein aggregation (Kang, Lee, and Drew 2013).

Due to the large hydrophobic surfaces, membrane protein crystals are formed through a lower number of protein-protein contacts and contain a higher amount of solvent compared to soluble proteins. These crystals are often smaller, more fragile, more sensitive to radiation damage, less ordered and with a higher mosaicity compared to crystals of soluble proteins (Moraes et al. 2014). Consequently, they yield X-ray diffraction data with a lower and often anisotropic resolution.
Tags added to recombinant proteins are often removed prior to crystallization using protease cleavage. Some short tags, in particular, lack a defined three-dimensional structure and can be

highly flexible creating an entropic impediment to crystal formation (Carson et al. 2007). However, large tags such as GFP or GST (Glutathione-S-transferase) may improve the overall solubility of the chimera and may provide additional surface areas for intramolecular interactions required for crystal lattice formation (Kobe and Williams 2015). This expedient is especially used for integral membrane proteins that lack large polar surfaces to create crystal contacts (Kobe and Williams 2015).

Another technique adopted to increase surface contacts is the mutation of precise residues located on the protein surface, often introducing cysteine residues. Otherwise, histidine or other metal-ligating residues may be added to introduce metal binding sites. However, these modifications may influence the protein native folding, whereas the addition of a soluble fusion partner may confer the same properties without disrupting the protein conformation (Leibly et al. 2015).

This expedient was successfully used for the crystallization of G-protein coupled receptors (GPCRs), where a soluble protein, such as Lysozyme, was fused to the receptor (Thorsen et al. 2014; Miller-Gallacher et al. 2014; Cherezov et al. 2007) .

In the case of poorly diffracting membrane protein crystals, the structural determination after data collection may be challenging for the difficulty in phasing low resolution data. In fact, all the methods to solve the phase problem of unknown protein structures are hampered by the low quality of the datasets. Structure determination with molecular replacement may be performed only if a homologous protein has already been solved.

Otherwise, the phase problem can be solved by obtaining a heavy-atom derivative or seleno-methionine labelled crystals. Unfortunately, both procedures may severely affect crystal quality increasing their fragility and sensitivity to radiation damage preventing their use for data collection (Kang, Lee, and Drew 2013). In this case, the presence of a large tag may be useful as it can be used to solve the phase of an unknown membrane protein by molecular replacement (Kobe and Williams 2015).

3. AIM OF THE STUDY

The aim of this project is the characterization of *Pseudomonas aeruginosa* Wzx O-antigen flippase, a possible target for antibacterial therapies due to its involvement in the O-antigen biosynthetic pathway. To date, the structure of this integral membrane protein has not yet been characterized, due to its low expression yield and stability. Therefore, the first goal of this project was to set up expression and purification procedures that yield a considerable amount of protein and to obtain a protein sample stable enough for characterization experiments. Considering the pathogenicity of the bacterium *P. aeruginosa*, the protein was not extracted directly from its native species, but it was obtained from recombinant overexpression in a different bacterial species (nonpathogenic *Escherichia coli*), allowing also for the insertion in the protein sequence of tags useful for purification and protein detection. The second aim of this project was the structural characterization of Wzx to gain insights on its secondary structure and fold.

4. RESULTS AND DISCUSSION

4.1. Cloning of the gene for the Wzx O-antigen flippase from P. aeruginosa

The Wzx gene was amplified from *P. aeruginosa* PAO1 genome and cloned in the expression vector pWaldo, obtained from the plasmid repository Addgene (see Material and Methods). In this plasmid, often used for overexpression of membrane proteins (Drew et al. 2001), the target gene was inserted in a cloning site with a Green Fluorescent Protein (GFP) gene, followed by the sequence coding for a His_8 tag at the C-terminus. For membrane proteins, tags are preferentially added at the C-terminus of the protein, in order to avoid interference with the signal peptide located at the N-terminus. During membrane protein translation, the signal peptide at the N-terminus of the protein sequence allows the correct membrane localization and folding, and it is therefore necessary to avoid wrong protein cellular localization and misfolding.

The GFP tag allows for an easy detection of the protein throughout all the steps of expression and purification. A major issue in overexpression of membrane proteins is their possible segregation in inclusion bodies, in a misfolded or unfolded form. While soluble proteins can be extracted from inclusion bodies and refolded in their native conformation, membrane proteins are very difficult to refold due to their hydrophobic nature. The presence of a fluorescent protein at the C-terminus can be used as an indicator of the folding state. The GFP only emits an intense fluorescence signal if the target membrane protein is correctly inserted in the membrane, whereas the signal is quenched if the protein is segregated in inclusion bodies (Drew et al. 2001). In addition, unfolding of the membrane protein during purification usually results in aggregation and precipitation, reducing the fluorescence in the soluble fraction. Therefore, GFP was used as a folding indicator in both the expression and purification steps.

The His_8 tag is a very common and useful tag, mostly used in the purification protocol, taking advantage of its affinity to a resin containing divalent metal cations such as Ni^{2+} or Co^{2+}. After the initial purification experiments, considering the unexpectedly low binding observed in metal affinity chromatography, the His tag was elongated to 10 histidine residues using PCR techniques.

In the pWaldo plasmid, the target gene is under the control of a T7 promoter that allows for a tight control of overexpression. The use of inducible promoters is particularly beneficial for the expression of toxic proteins, as bacterial growth may be affected by the accumulation of basal levels of the toxic protein. Overexpression of membrane proteins often results in cell suffering due to the excess of polypeptides inserted in plasma membrane.

The cloning result was checked via control PCR using T7-T7 term primers to verify the insertion of Wzx gene. The positive clones were sent for sequencing. The positive plasmids were transformed in XL1Blue cells inoculated in LB broth supplemented with Kanamycin, only the pWaldo transformed clones would have the gene that confers resistance to this antibiotic.

4.2. Overexpression of the O-antigen flippase Wzx

In order to obtain the high yields of the target protein required for the structural characterization, a careful optimization of the overexpression conditions is required, taking into account the host strain, the induction conditions and presence of additives in the media. Taking advantage of the presence of the GFP tag, the fluorescence intensities of the bacterial culture was used as an indication of the best expression conditions, i.e. those that resulted in the highest yields of correctly folded protein.
The first overexpression tests were performed in two bacterial strains, namely the commercial *E. coli* strains BL21(DE3) and Lemo21(DE3).

- BL21(DE3) pLys E is one of the most commonly used bacterial strain for protein expression, due to the presence of a T7 polymerase gene in the bacterial DNA under the control of an inducible promoter, that allows for DNA transcription only upon IPTG addition. To further modulate the expression of the target protein, glucose may be added to the broth, inhibiting gene transcription until IPTG addition.

  The freshly transformed bacteria were inoculated in three different conditions, all with 34μg/ml Chloramphenicol and 50μg/ml of Kanamycin that allow the selective growth of bacteria transformed with pWaldo: LB broth, LB broth supplemented with 1% glucose and with 2% glucose, with the last giving the best results in the pre-induction phase, i.e. a higher optical density indicating a good replication rate of the bacteria. Overexpression yields were evaluated using different concentrations of IPTG (0.2, 0.2 and 0.5 mM IPTG) and induction lengths (5 hours or overnight). In addition, tests were performed at two different temperatures (37°C for 5h induction and 20°C for overnight). Protein production was determined by measuring the fluorescence intensity of the culture (Table 4.1).

Table 4.1: Test expression on BL21(DE3) cells. I: induced cells NI: not induced cells

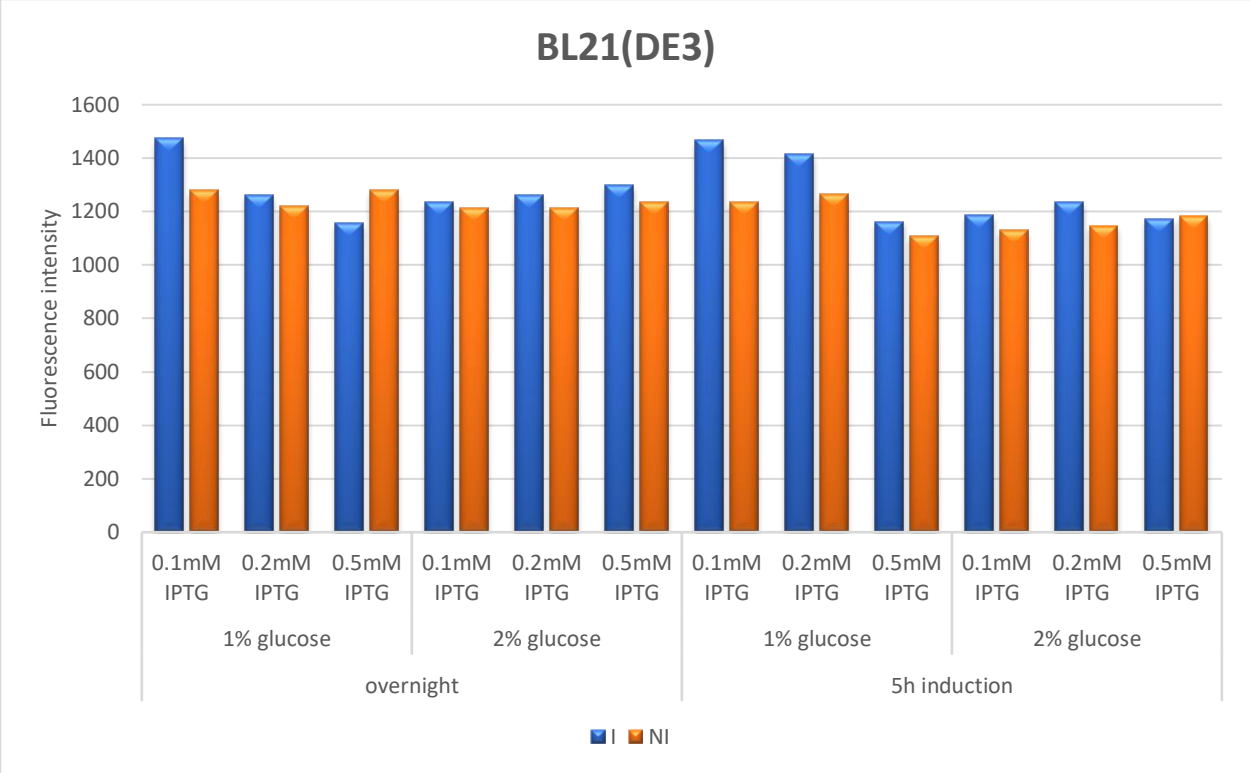

No significant variation between the overnight and the 5h inductions was observed. However, both led to a poor amount of protein. Interestingly, in both conditions the IPTG concentration increase lead to a decrease of fluorescence intensity. This could be explained considering the protein toxicity. Strong IPTG induction causes a protein accumulation in the bacterial membrane that probably leads to cell death. 0.1 mM IPTG inductions at 20° and 37°C yielded the highest amount of protein, the low temperature was preferred to avoid possible proteolysis. Since the final protein yield was low, a different host was chosen for Wzx expression.

- The Lemo21 bacterial strain is a commercially available *E. coli* strain optimized for the expression of toxic and membrane proteins (Wagner et al. 2008). It contains the Lemo plasmid that allows a fine tuning of the expression conditions and inhibition of the basal expression. Upon rhamnose addition, this bacterial strain produces lysozyme (lys Y), that represses the T7 promoter, reducing expression of the protein during pre-induction culture. The Lemo plasmid contains also a gene for Chloramphenicol resistance, to allow selection.
  Lemo21 cells were inoculated in LB supplemented with Kanamycin and Chloramphenicol. The broth was supplemented with diverse concentrations of L-rhamnose, 0.2mM, 0.5mM, 0.75mM, 1mM and 2mM. Induction was obtained with a constant amount of IPTG (0.4mM)

following the manufacturer instructions. Different induction lengths (5h and ON) and temperatures (37°C for the 5h induction and 20 °C for the overnight) were tested (Table 4.2).

Table 4.2: Test expression with Lemo21 competent cells. I: induced cells, NI: not induced cells

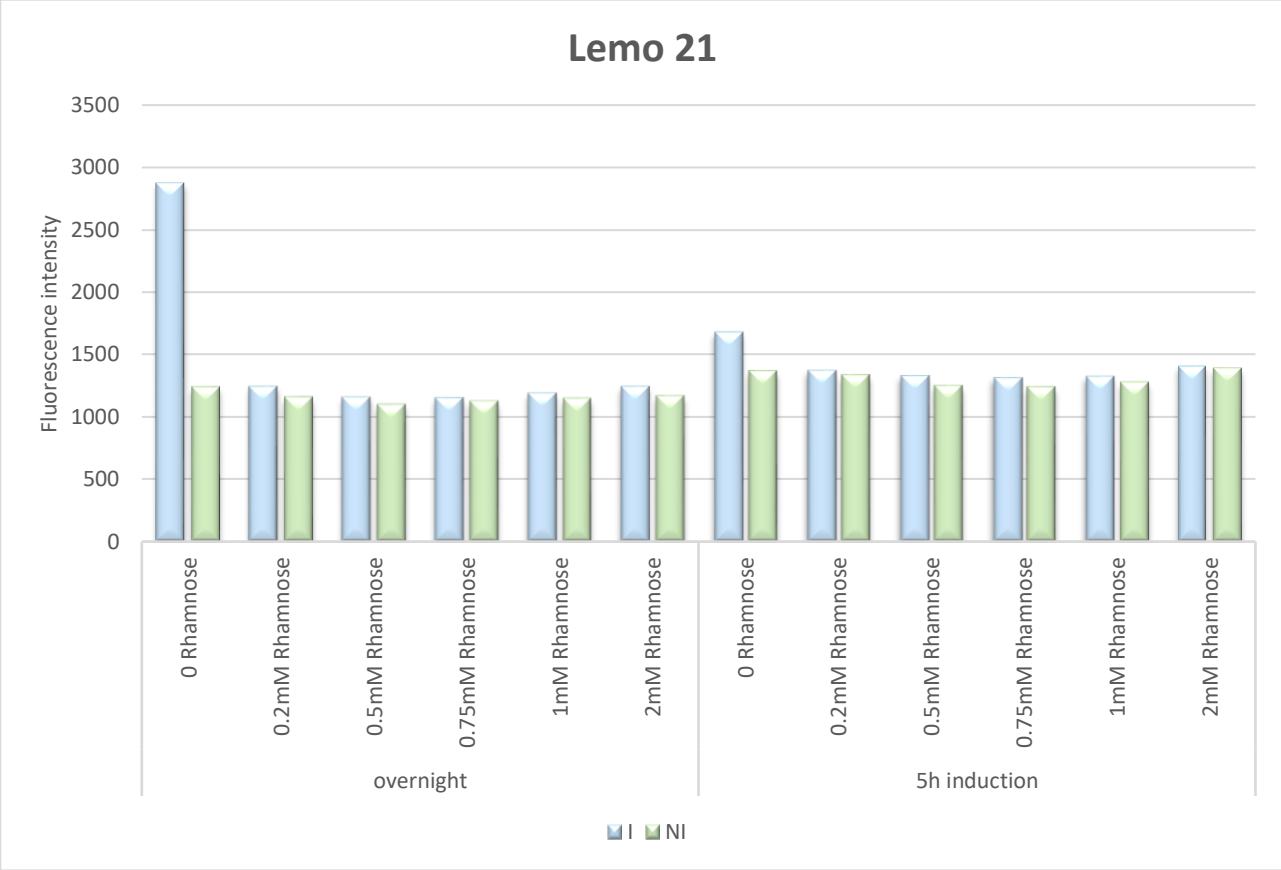

5h induction results in lower protein production compared to overnight. Interestingly, the fluorescence intensity of the culture was inversely proportional to the concentration of rhamnose. This highlights the role of the sugar in inhibiting protein expression. However, final protein yield was higher without rhamnose. The condition yielding the best results was without rhamnose with an overnight induction at 20°C.

Expression tests allowed to select the best conditions for protein production. In the following experiments, protein expression tests were successfully scaled up. The *P.aeruginosa* Wzx flippase protein was recombinantly overexpressed in the Lemo21 strain, at 20°C in LB medium without supplements and with an overnight induction.

After expression, cells were lysed using a homogenizer and membranes were separated through ultracentrifugation.

4.3. Protein solubilization

Membrane proteins are naturally embedded in the phospholipidic bilayer that protects their hydrophobic portions from the aqueous environment. In addition, the membrane exerts a lateral pressure that contributes to maintaining protein folding. Protein extraction from the membrane is required for purification, a step essential for protein characterization (Seddon, Curnow, and Booth 2004). Detergents are used to remove proteins from the membranes and to solubilize them in aqueous buffers by interacting with their hydrophobic regions, maintaining the correct protein folding and activity. The optimal detergent has to be carefully selected for each specific protein, as mild detergents may not be able to efficiently solubilize the protein, while harsh detergents may cause protein unfolding and precipitation (Privé 2007). A detergent screening is a required preliminary step for every membrane protein study.

For each detergent, the surfactant properties are strongly dependent on concentration. In particular, detergent concentrations under a specific value, characteristic of each detergent, do not display the typical micelle formation. Such concentration is defined as Critical Micelle Concentration (CMC). Above the CMC, the detergent behaves as surfactant.

Membranes containing the recombinant Wzx overexpressed were solubilized in different detergents (OG, DM, DDM, LDAO, and $C_{12}E_8$, see Materials and Methods for detergent structure) at a concentration corresponding to 10x CMC, and protein stability, folding and dispersion state were tested. The solubilization was performed at 4°C for 1h under slow agitation. Longer incubations were tested but revealed no improvements compared to the 1-hour solubilization. After the incubation, a first assessment of solubilization efficiency could be done by observing the turbidity of the solutions: LDAO and DM solutions were clear compared to the others. For all samples insolubilized material was removed by ultracentrifugation. As observed prior to ultracentrifugation, LDAO and DM samples showed almost no insoluble fraction, whereas OG had the highest amount of insoluble material. $C_{12}E_8$ and DDM showed intermediate solubilization properties. The fluorescence intensity of the supernatant was recorded for all the samples (Table 4.3), confirming the qualitative observations.

Table 4.3:Fluorescence intensities of the samples solubilized in different detergents. Error bars: standard deviation on repeated measurements

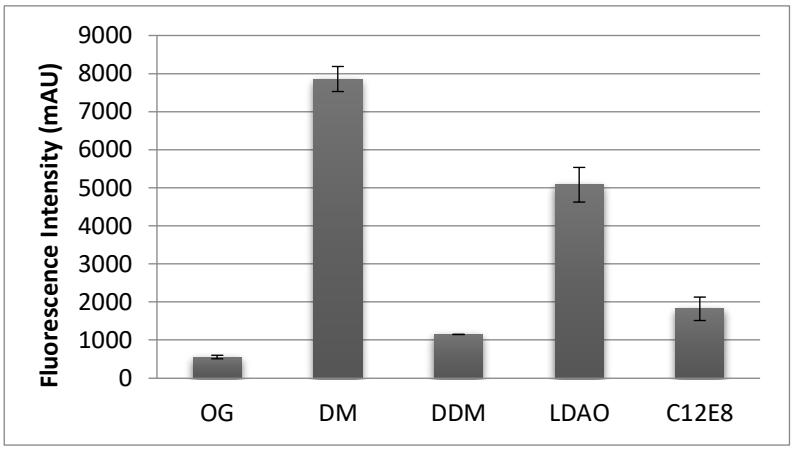

4.4. Protein purification: first affinity chromatography tests

The planned purification protocol included a first step of affinity purification through affinity chromatography with a resin containing divalent metal ions (Immobilized Metal Affinity Chromatography, IMAC). The histidine tag present at the C-terminus of the protein construct is able to selectively bind to divalent metal cations, while untagged proteins do not bind to the resin with specific interactions and are removed during wash steps. In a second purification step, required to obtain the highly pure protein necessary for crystallization trials, the use of Size Exclusion Chromatography (SEC) was expected to remove contaminants and protein aggregates.

To define an optimal purification protocol, the first tests were conducted using the different detergent solubilized protein samples obtained in the previous step and a Co^{2+} resin, in order to determine the detergent effect on resin binding. In fact, protein interactions with the resin may be hampered by a detergent-induced conformation or by the presence of a large detergent micelle that may hide the histidine tag, preventing its complexation with the stationary phase. In the different detergent conditions, the protein was eluted from the resin with a similar imidazole concentration. Imidazole competes with the His tag for Co^{+2} binding, causing protein release from the resin.

Eluted fractions were loaded on SDS-PAGE gels. The gels were stained with Coomassie staining to reveal presence of protein bands and to compare their position with the commercially available molecular weight markers (Figure 4.1A). In addition, despite the denaturant conditions of the gel, a residual folded GFP is present in the band with the target construct and can be revealed analyzing the fluorescence of the SDS-PAGE gel before staining (Figure 4.1B). GFP in-gel fluorescence allows the identification of the protein band without the necessity of a Western Blot analysis, often negatively affected by poor transfer on the blot membrane.

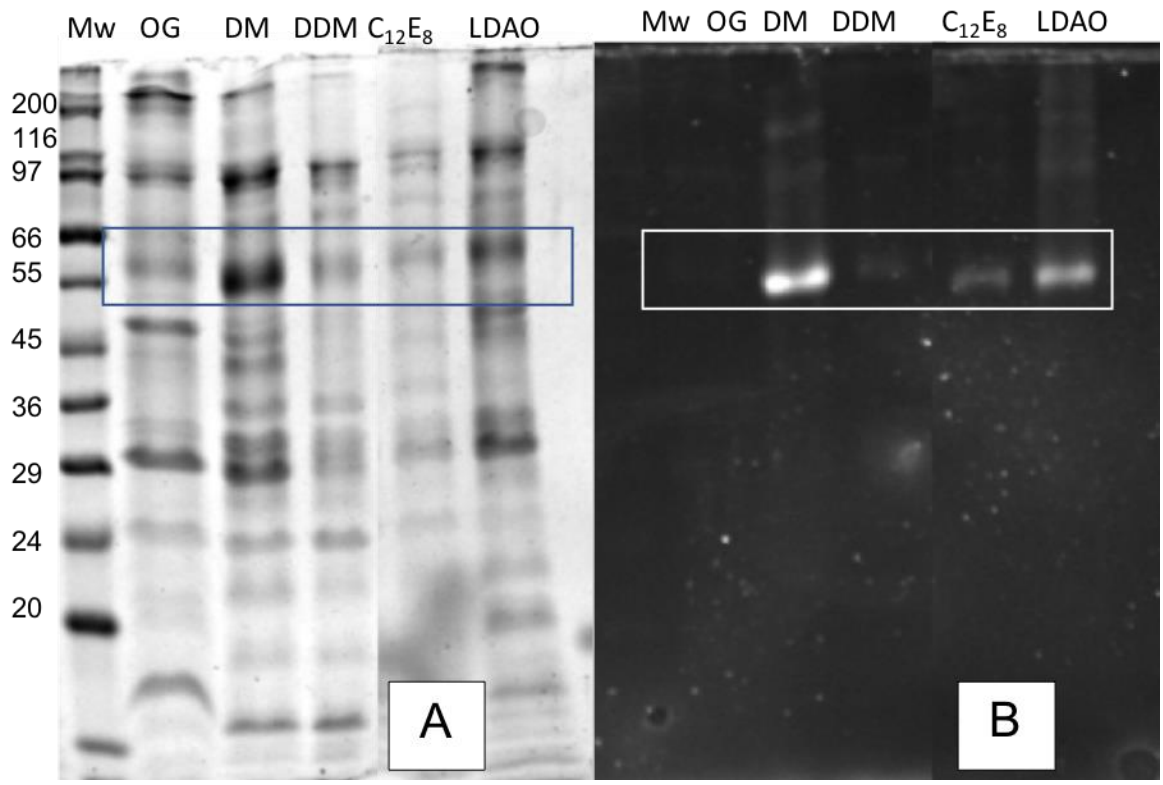

Figure 4.1: SDS-PAGE gel of the IMAC eluates from different detergent test, (A) stained with Coomassie Blue staining and (B) revealed through in-gel fluorescence.

Analysis of the SDS-PAGE gel revealed that DM efficiently solubilizes the protein and do not interfere with its interaction to the resin containing divalent metal ions. This result was confirmed by the measurement of low fluorescence intensity for the unbound fraction (flow-through), revealing a good binding affinity. Positive results were obtained also with LDAO, that seems less efficient than DM in the solubilization step, but that allows good binding of the protein to the resin. For the other detergents tested, solubilization and resin-binding were significantly lower.

Considering the large amount of contaminants, further optimization of the IMAC conditions was required. LDAO was chosen to solubilize the protein for these preliminary tests to determine the best affinity chromatography protocol, due to the low micelle size of this detergent, more suitable to the characterization experiments planned. Two different IMAC resins were tested, containing Ni^{2+} ions or Co^{2+} ions, respectively.

Analysis of the fluorescence intensity (Figure 4.2) of the fractions revealed the Ni^{2+} resin had the higher binding efficiency. However, the Coomassie staining of the SDS-PAGE gel shows that a larger amount of contaminants was present in the fractions eluted from Ni^{2+} resin, while Co^{2+} allowed for a better purification.

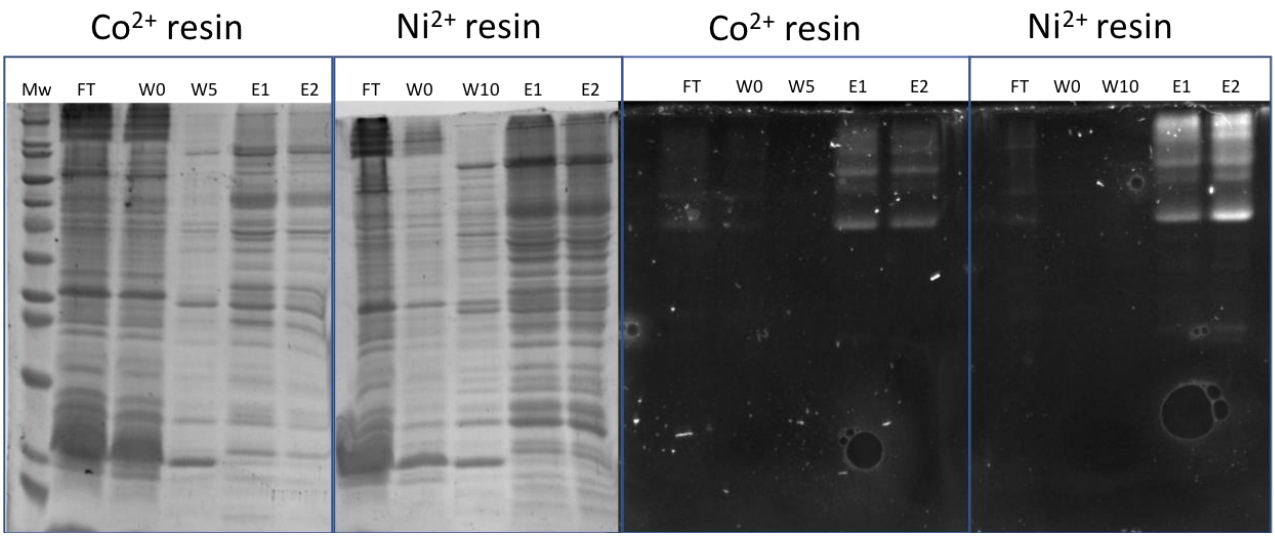

Figure 4.2: SDS-PAGE analysis of the purification test with different IMAC resins. A) Coomassie blue stained gel; B) in-gel fluorescence. MW: molecular weight; FT: Flow Through; W0: wash without Imidazole; W5: wash with 5mM Imidazole; W10: wash with 10mM

Considering these results, the Co^{2+} resin was selected for the IMAC purification step of *P. aeruginosa* Wzx, considering the higher purity of the eluted fractions. Eluates were pooled considering their fluorescence intensity and concentrated to 800µl to be injected in SEC column.

4.5. Protein purification: size exclusion chromatography

Size Exclusion Chromatography (SEC) is a technique used to separate macromolecules according to their molecular weight and shape. The sample is loaded onto a column constituted by a porous gel matrix and elution is run until all molecules exit the column. Larger molecules or protein aggregates cannot enter the gel pores and are eluted in the first fractions, while smaller molecules are eluted in subsequent fractions, with larger retention volumes as their size decreases. Despite the fact that SEC retention volume is influenced not only by protein mass but also by its shape, SEC may be used with some approximation to determine the oligomeric state of the sample, by comparison of the sample chromatogram with the elution volume in the same conditions of standard proteins with known molecular weights. Using this technique, it is usually possible to discriminate between a monomer, an oligomer and a larger aggregate.

SEC purifications were performed on IMAC eluates in DM (10x CMC) and in LDAO (10x CMC) to evaluate the different effect of these detergents on protein aggregation. Before injection in the SEC column, samples from IMAC purification experiments were concentrated, and the concentrated solutions were further centrifuged to remove precipitate that may damage the SEC matrix. The presence of protein in the SEC eluted fractions was detected by measuring the absorbance of the solution at 280 nm (Figure 4.3).

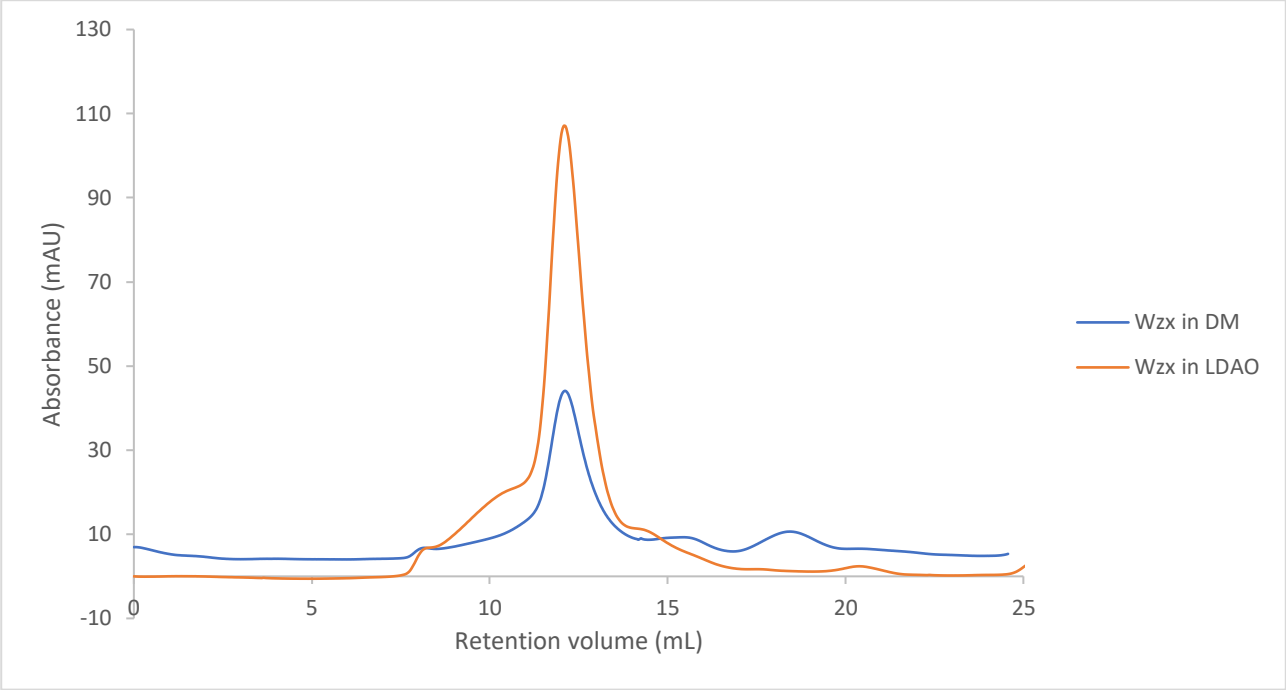

Figure 4.3: Comparison between the SEC peak obtained in DM and in LDAO

While the profile of the chromatograms is similar for the two detergents tested, the absorbance values of the LDAO-solubilized sample are higher, despite the fact that this detergent proved to be less efficient for protein solubilization. This result may indicate a higher destabilization effect on protein folding of DM compared to LDAO, possibly leading to protein aggregation during concentration. Aggregates probably remained on the concentrator device or were removed by centrifugation prior to sample injection in the column.

Fractions obtained from the LDAO SEC purification were loaded on SDS-PAGE gel to check the purity of the sample. Comparative analysis of the Coomassie stained gel and the in-gel GFP fluorescence (Figure 4.4) shows the presence of aggregates of the protein at higher molecular weight even in the samples purified by SEC chromatography, possibly due to sample treatment prior to gel loading (white and blue boxes on the gel). In addition, the Coomassie staining shows the presence of a second band with lower molecular weight (red box). Attempts at identifying the contaminant via mass spectrometry failed due to the low efficiency of the proteolytic digestion of the membrane protein prior to analysis. However, in our laboratory an analogous band was detected in the purification of Wzy, suggesting that the same protein is present in both overexpressed samples. In this case the contaminant, present in larger amounts, could be identified as Cytochrome o Ubiquinol Oxidase from *E. coli*.

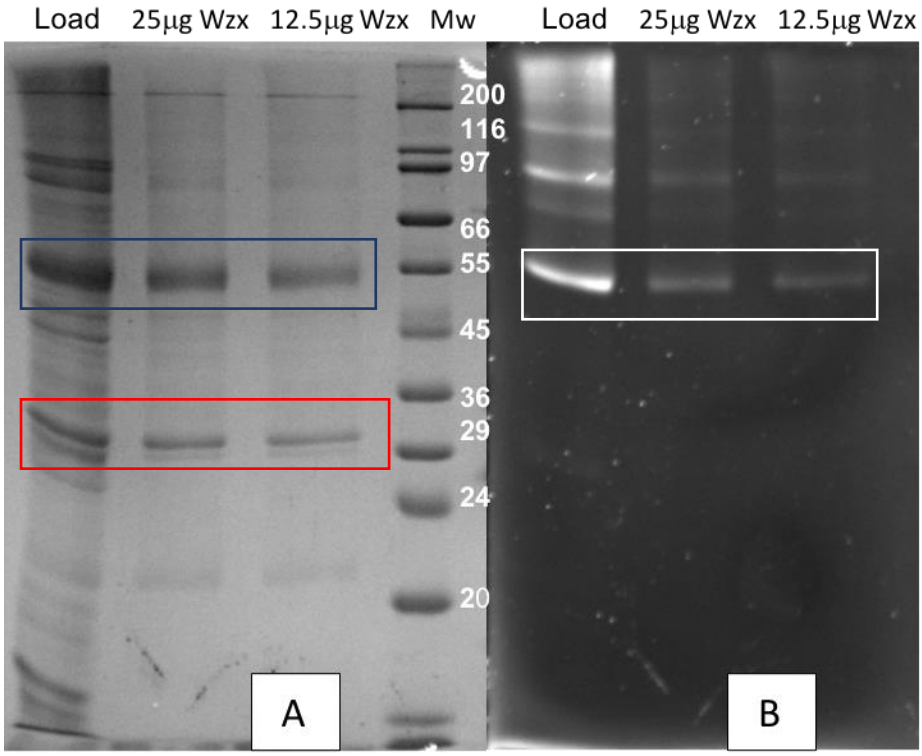

Figure.4.4: SDS-PAGE gel of Wzx purification in LDAO. First lane: Load on SEC, Second lane:25µg Wzx eluted from SEC, Third lane:12.5µg purified Wzx and Molecular weight in the last lane. A) GIOTTO stained, B) in-gel fluorescence

4.6. Protein purification: further affinity chromatography experiments

Unfortunately, the presence of contaminants difficult to remove is a common feature in structural biology research. In addition, the use of detergents may promote the extraction of other membrane proteins from the expression host that may be co-purified with the protein of interest (Wiseman et al. 2014). In such cases, a re-evaluation of all purification steps is required to obtain a sample suitable for structural biology studies.

Our first attempt at optimizing the purification procedure involved the IMAC purification. To remove the contaminant the salt concentration in IMAC buffer was varied: NaCl was increased to 300 mM but no differences were observed in eluate purity. This result suggested that the contaminant was a membrane protein that did not interact with the resin via polar interactions. In addition, it was confirmed that the contaminant interaction with the protein was not mediated by polar residues.

In order to attempt a finer separation of the protein sample and the contaminant in different fractions, we performed an experiment using an imidazole gradient from 5 mM to 150 mM during elution, collecting fractions for every 5 mM increment. The fractions were loaded on SDS-PAGE gel and stained with Coomassie staining (Figure 4.5).

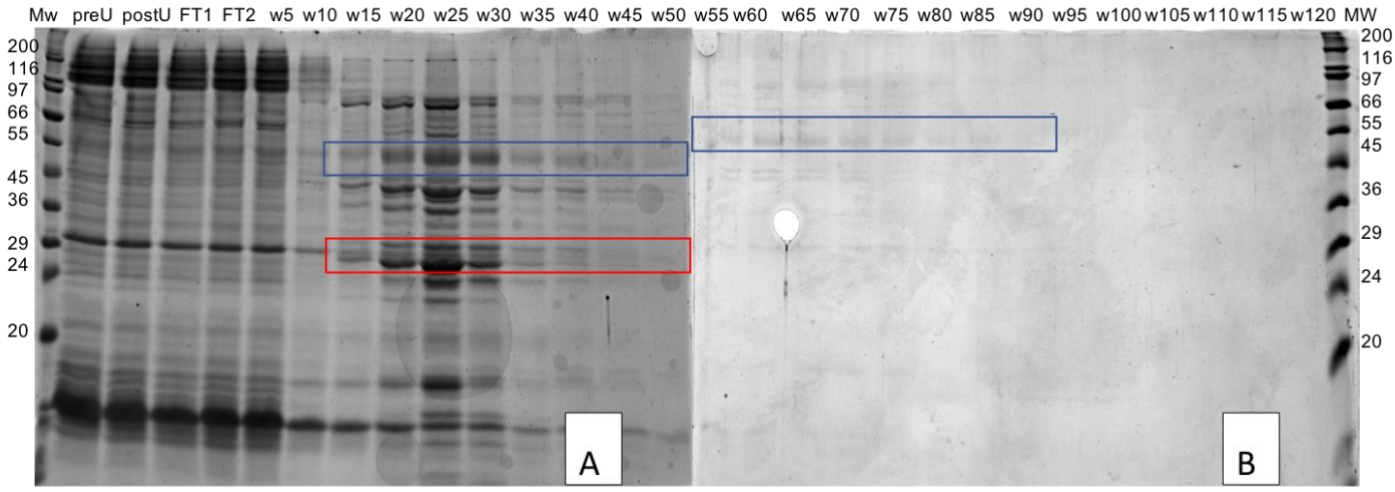

Figure 4.5: SDS-PAGE gels of the Imidazole gradient purification. Gel A: Mw markers-preUltra-postUltra-FT1-FT2-wash from 5mM to 50mM. Gel B: wash from 55mM to 120 mM-Mw markers.

The gel indicated that the contaminant and Wzx are eluted together during the imidazole gradient. Fluorescence measurements confirmed the presence of Wzx in all the fraction despite the difficulty in visualizing the protein band in the gel (Table 4.4). In fact, in all gels from the purification experiments Wzx was poorly stained, increasing the difficulty in detecting the band on the gel.

Table 4.4: Fluorescence intensities measured through the imidazole gradient

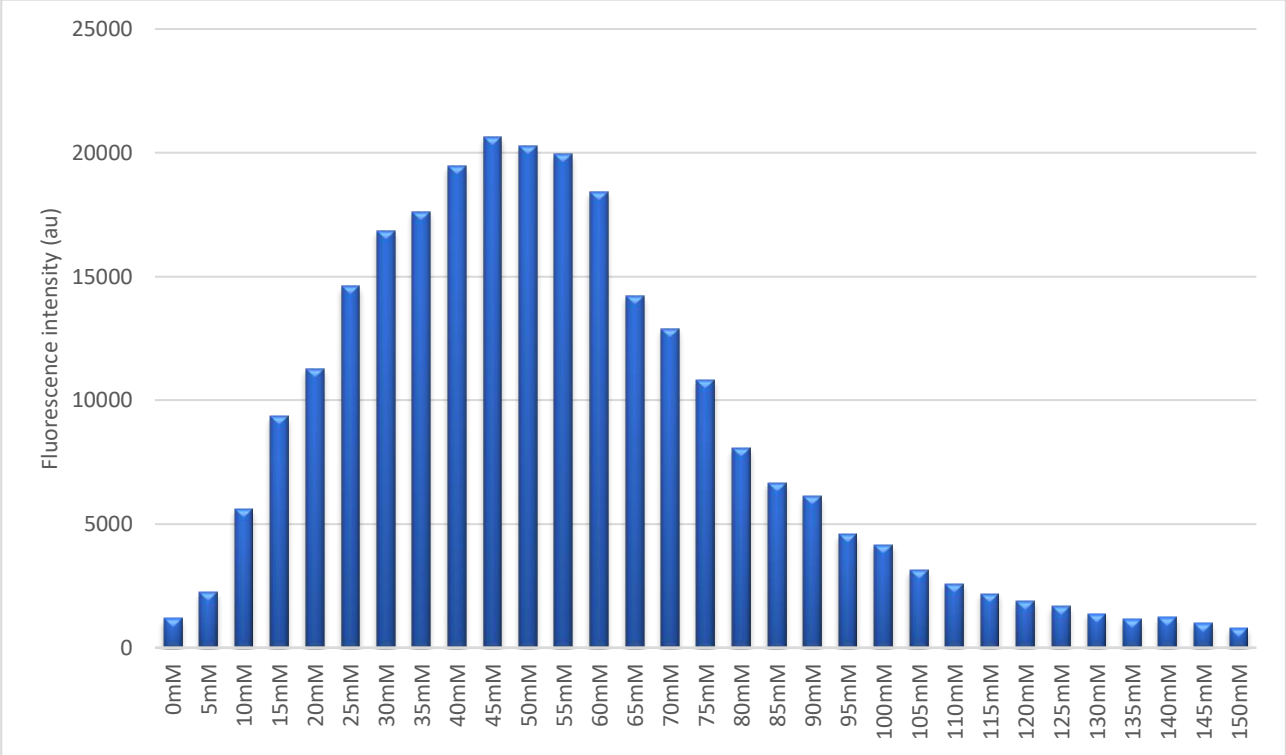

This experiment confirmed a strong interaction between the contaminant and Wzx and a tight binding to the resin. Since this protocol led to a massive protein loss, this technique was not deemed suitable to separate the protein from the contaminant.

4.7. Protein purification: Ion Exchange Chromatography

Ion Exchange chromatography (IEX) is based on the differential binding of proteins to a charged resin. According to its isoelectric point, a protein at a certain pH can be positively or negatively charged. For this chromatography, a positively charged IEX resin is used for negatively charged proteins, and a negatively charged in the opposite situation. The binding strength depends on protein surface charges and the elution is performed with a salt gradient, since ions compete with the protein for the interaction with the resin. This method is not commonly used for membrane proteins due to the low charge present on their surfaces.

Protein sample obtained from IMAC purification was diluted to decrease salt concentration to 20 mM and loaded on a positively charged column for Anion Exchange chromatography. The salt gradient was performed as reported in Materials and Methods. The protein was eluted in a single peak at 340 mM salt.

SDS-PAGE gel analysis showed that Ion Exchange chromatography was not able to separate the target protein from the contaminant as they co-eluted in the same fraction. Considering that LDAO is a zwitterionic detergent, it is possible that the charged groups of the detergent micelle prevent a differential interaction with the cationic stationary phase.

4.8. AntiGFP-resin affinity purification

In order to determine if a selective binding was able to separate the contaminant from Wzx, the sample was loaded on antiGFP-resin, i.e. a resin functionalized with an antibody that binds this tag. However, the majority of Wzx was eluted together with the contaminant suggesting a strong interaction between the two proteins (Figure 4.6).

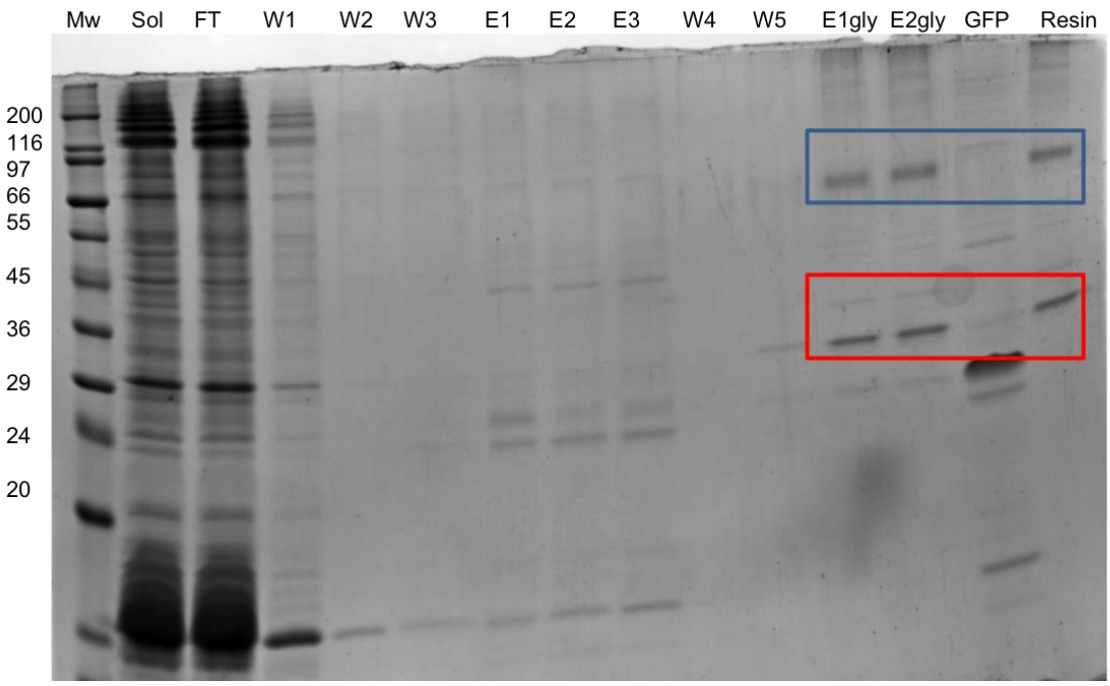

Figure 4.6: SDS gel of GFP resin purification. Sol: solubilized membranes, FT: flow through, W: washes, E: elutions with GFP, Egly: elutions with glycine, GFP used, Resin: resin after elutions. Blue box: Wzx, red box: contaminant

A possible explanation for the behavior observed during the antiGFP-resin purification is that the two proteins, Wzx and contaminant, are solubilized in the same micelle. To disrupt this close interaction, the detergent was changed, in order to modify micelle composition and separate the two proteins.

4.9. Protein purification: detergent exchange from LDAO to $C_{12}E_8$

Considering the poor results obtained from attempts at purification with different techniques, and in particular by the binding of both the target protein and the contaminant to the highly specific affinity resin with a GFP-antibody, it is probable that the target protein, the flippase Wzx, and the contaminant are co-solubilized in the same detergent micelle. To overcome this issue, a further attempt at purification was performed by changing the detergent prior to size exclusion chromatography, to determine if such modification influences the protein or the contaminant stability allowing their separation in two different fractions.

As second detergent, $C_{12}E_8$, a mild detergent, unable to solubilize the protein when used directly on the membranes (see above) but expected to cause little or no destabilization effect on the protein, was chosen. DM was not considered due to its destabilizing effects highlighted by the SEC purification performed previously. In addition, due to the very different nature of $C_{12}E_8$ compared to LDAO, the former may enhance the differences between target protein and contaminant, promoting their separation.

Considering the good results obtained for protein binding to the resin in IMAC purification, the already tested protocol using LDAO was applied. The eluates were pooled together to change the

buffer during the concentration step. The pool was diluted 4 times with a buffer containing $C_{12}E_8$ and incubated for 15 minutes in ice to facilitate the detergent exchange. The sample was then concentrated, and a SEC was performed using a concentration of $C_{12}E_8$ of 10x CMC in the elution buffer.

The resulting chromatogram (Figure 4.7) shows a different profile compared to the similar purification in LDAO or DM. However, separation between protein and contaminant was not successful and instead protein aggregation was observed.

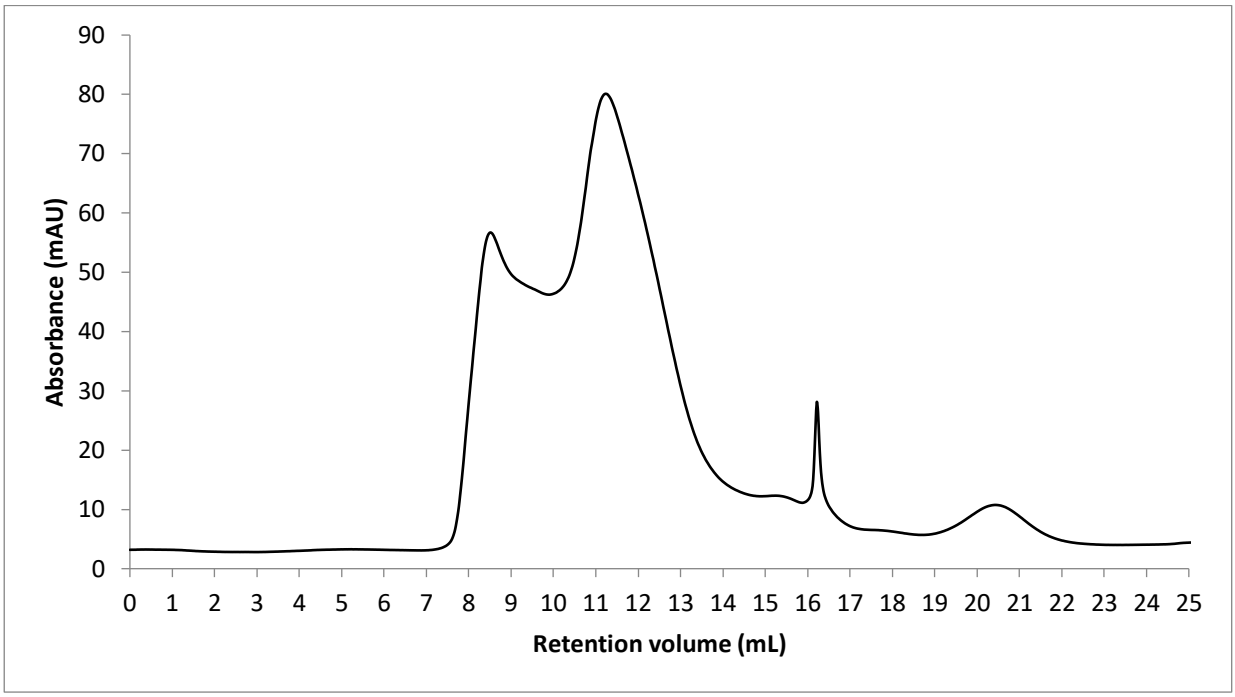

Figure 4.7: SEC purification of Wzx in $C_{12}E_8$, after LDAO-to-$C_{12}E_8$ buffer exchange.

The result suggests that the protein is not stable in the chosen detergent and, while the micelle can be successfully exchanged, this alteration causes substantial protein aggregation.

4.10. Protein solubilization and purification in DDM

Considering the relative stability in DM and the good results obtained for protein solubilization in this detergent, we chose a cognate of DM, the detergent DDM, that has a slightly longer acyl chain compared to DM and is known to have a generally milder effect on protein folding. However, considering that in the initial screening this surfactant did not efficiently solubilize the protein, a higher DDM concentration, 15x CMC (3mM), was tested for the solubilization step, resulting in a better solubilization yield that allowed the purification procedures.

A first step of affinity chromatography followed the same protocol as for the LDAO experiments. Unfortunately, after concentration and SEC purification, the amount of protein was greatly reduced,

possibly due to the same aggregation effects observed for DM. In addition, the chromatogram shows an insufficient separation (Figure 4.8).

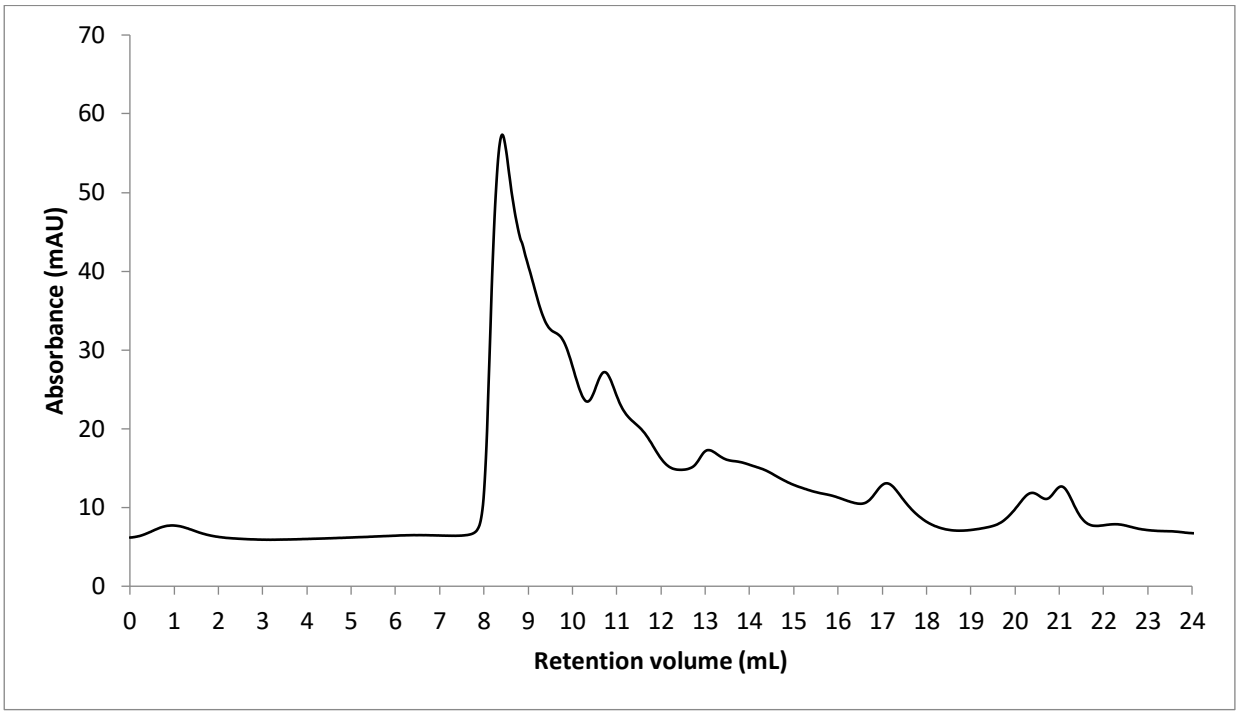

Figure 4.8: SEC purification of Wzx in DDM.

4.11. Crystallization experiments of LDAO-solubilized Wzx protein

Since *P. aeruginosa* Wzx protein is an integral membrane protein completely embedded in the phospholipidic bilayer, with few polar surfaces available for crystal contacts, was decided to maintain the GFP tag in the sample used for crystallization experiments. Considering that no crystal structure of Wzx is available but only a homology model, the GFP tag could be helpful at a later stage to solve the phase problem.

Considering the results obtained from purification tests, crystallization experiments were set up on the protein sample solubilized in LDAO, despite the presence of a contaminant. LDAO purification was chosen due to the higher protein yield of purification, that could be an indication of a higher protein stability in this detergent. In addition, LDAO has the advantage to form smaller micelles compared to DM. The dimension of the micelles is essential especially for integral membrane proteins such Wzx that are completely embedded in the membrane. The smaller micelles cover a lower surface of the protein, allowing intermolecular interactions essential for crystal lattice formation (Privé 2007). Crystallization tests were set up using commercially available kits of sparse matrices of conditions, namely Mem Sys, Mem Start and Mem Gold kits from Molecular Dimensions (see Materials and Methods). These screens were designed to test a wide variety of the most frequent membrane protein crystallization conditions. Crystallization experiments, set up by the sitting drop method using the

Mosquito TT labtech robot, were prepared in duplicate in order to test two different temperatures, 4°C and 18°C, and with different protein concentrations (1.5 - 4.5 mg/ml). Attempts to further increased the concentration failed due to protein aggregation and precipitation on the concentrator.
No crystal formed at 18°C, probably due to the lower stability of the membrane protein at this temperature. However, the experiments at 4°C yielded 3 hits, i.e. conditions where crystals were formed in the solution, that were optimized with further crystallization experiments in order to increase crystal dimension and quality. Interestingly, all the conditions that yielded crystals have a similar pH, from 6.5 to pH 7.5, in HEPES or MES buffer, with high-molecular weight PEG (3000, 4000 or 6000). In the crystallization optimization no crystal grew in presence of MES buffer. However, after 10 days, 8 promising conditions crystallized in the optimization plate of the following condition: 0.05M HEPES pH 7.5; 22% w/v PEG 4000 at 4°C (Figure 4.9).

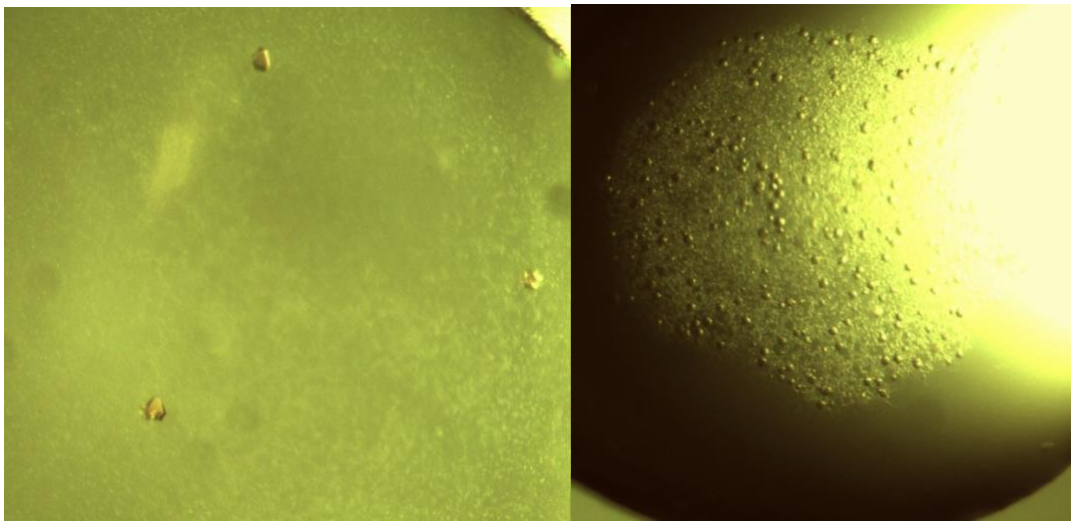

Figure 4.9: Crystals obtained from optimization plates

Crystals were tested at XRD2 beamline of the Elettra Synchrotron (Trieste). Unfortunately, their diffraction was extremely weak. To improve crystals internal order and increase diffraction intensity, crystallization conditions were further optimized using commercial additive screens (HR2-420, HR2-430 and HR2-422 from Hampton Research), starting from the conditions that yielded the larger crystals in the previous tests. In addition, a home-made additive screen was prepared including salts that are known to improve crystal contacts (see Materials and Methods). The hits obtained in the additive screens were reproduced in a larger scale in hanging drop experiments.
Crystals from the optimization/additive tests had a suitable dimension for X-ray diffraction experiments with synchrotron radiation. The low resolution of the data obtained did not allow structure determination, but diffraction spots were sufficient to determine the unit cell parameters (Table 4.5).

Table 4.5: Unit cell parameters of the datasets obtained from crystallization experiments of Wzx in LDAO.

Sample name	A	b	c	α	β	γ	Space group	Resolution
Wzx crystal 1	180.841 Å	181.170 Å	67.271 Å	90°	90°	90°	P21212	7.0 Å
Wzx crystal 2	130.81 Å	154.29 Å	200.53 Å	90°	90°	90°	P212121	9.0 Å

Unfortunately, cell dimensions of crystal 1 were isomorphous to a crystal obtained in our laboratory during crystallization attempts of the protein Wzy polymerase, a physiological partner of the flippase Wzx (a = 180.775 Å, b = 182.613 Å, c = 67.727 Å, α = β = γ = 90°, $P2_1\ 2_1\ 2$). Despite the low resolution of the crystal structure (6 Å) and with the aid of mass spectrometry experiments, it was possible to attribute the electron density observed in the unit cell to Cytochrome o Ubiquinol Oxidase (CUO) (Figure 4.10), a common membrane protein contaminant and one of the proteins of the *E. coli* membrane with the highest expression levels.

Taking advantage of the isomorphism of the crystals, the model obtained for the data collection on crystals grown from Wzy crystallization experiments was used to phase data from Wzx crystallization experiments. Despite the low resolution (7 Å), it was possible to fit the Cytochrome o Ubiquinol Oxidase in the electron density experimentally determined. Due to the extremely low resolution and the few diffraction spots detected, no data processing was possible in neither the samples. No residual electron density was detected, excluding the presence of the Wzx flippase in the unit cell.

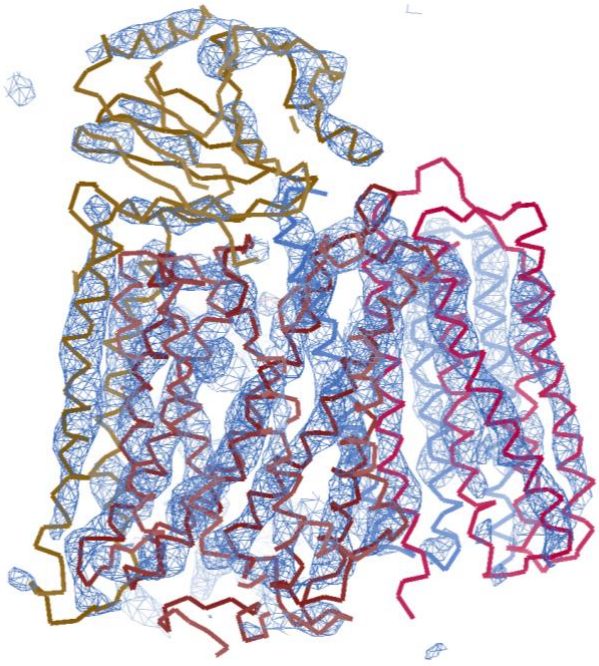

Figure 4.10: Electron density map of the contaminant Ubiquinol Cytochrome C Oxidase determined at Elettra on crystals obtained from the purification and crystallization of the polymerase Wzy.

The larger of the four subunits that form the Cytochrome o Ubiquinol oxidase has a similar molecular weight as the flippase Wzx, explaining the absence of a significant band on the SDS-PAGE gels. Probably the bands of Wzx and of the Cytochrome o Ubiquinol oxidase are superimposed. The second subunit, a 35 kDa polypeptide, corresponds to the lower molecular weight band observed on the gel. The smaller subunits (22KDa and 10KDa) were not detectable on the gel.

For crystal 2 (Table 4.5), a different unit cell was determined from the X-ray diffraction data. However, the resolution was too low (9 Å) to scale the data. In addition, the mosaicity of the crystal was high.

4.12. Optimization of the SEC purification step

To separate Wzx from the contaminant, a SEC purification was performed using a column with a higher number of theoretical plates, that allows a higher resolution in the separation. To this aim, the Superdex 200 10/300 Increase column (GE Healthcare) was chosen.

For this experiment, membrane with overexpressed Wzx protein were solubilized in LDAO and purified through IMAC in the conditions optimized before (see Materials and Methods). Eluted protein was concentrated and loaded on the Superdex 200 10/300 Increase column. The chromatogram shows the separation of the protein sample in two different peaks (Figure 4.11), the fractions were controlled with SDS PAGE (Figure 4.12).

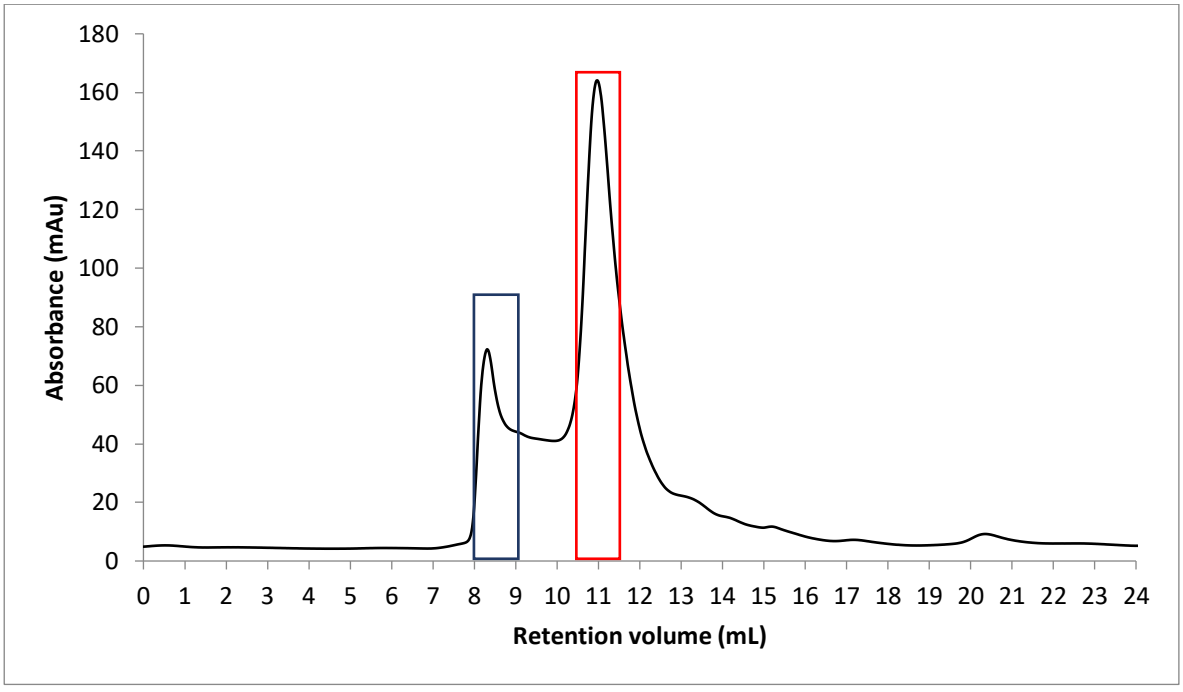

Figure 4.11: SEC purification of Wzx in LDAO using the Superdex 200 10/300 Increase column

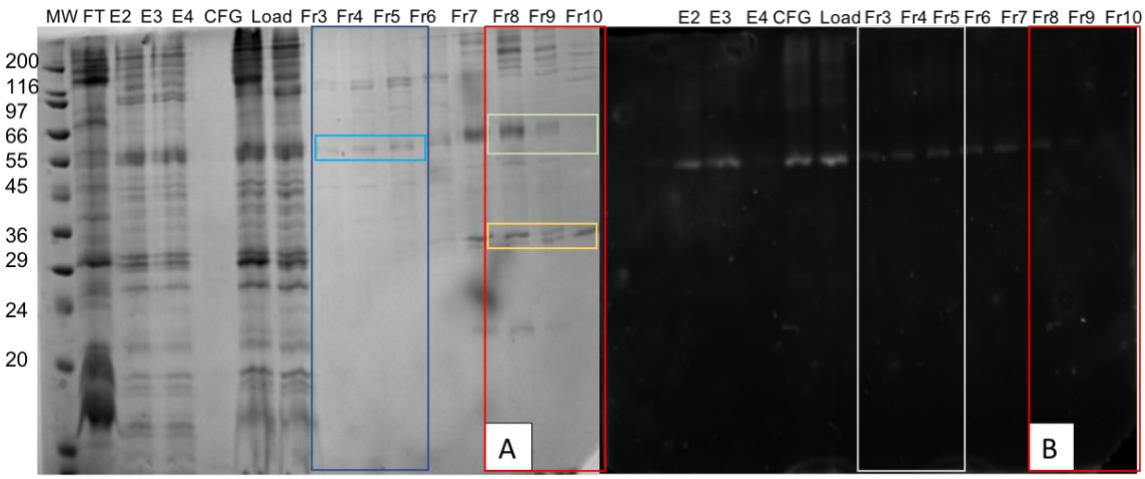

Figure 4.12: SDS-PAGE analysis of fractions eluted from the Superdex 200 10/300 Increase column during Wzx sample purification in LDAO. (A) Coomassie staining and (B) in-gel fluorescence.

Interestingly, the analysis of the fluorescence intensity revealed the presence of the GFP fusion protein in the first peak, eluted at 8.5 ml of retention volume, and in the shoulder, whereas there was a decrease in fluorescence in the main peak. To confirm the presence of the protein mainly in the first peak the fractions were loaded on SDS-PAGE and images of Coomassie-stained gel and of in-gel fluorescence were recorded.

The fraction corresponding to the shoulder between the two peaks was mainly consituted by Wzx. The broad form of the shoulder may be due to the formation of Wzx multimers of different molecular weight. Fractions 3-6 (blue box figure 4.12) of the gel showed only the band corresponding to Wzx, no second band was observed. The in-gel fluorescence confirmed the presence of Wzx (Figure 14.2B). In the following lane, corresponding to the final part of the shoulder, a faint second band at a lower molecular weight appeared, suggesting the presence of a low amount of the Cytochrome o Ubiquinol Oxidase. The amount of this protein is significantly increased in the lanes corresponding to the second peak (red box). The bands at higher molecular weight are probably Wzx multimers. For membrane proteins, the formation of multimers and aggregates in SDS-PAGE running condition is common (Islam, Eckford, et al. 2013a).

Despite the presence of a faint Wzx protein band in the SDS-PAGE analysis of fractions corresponding to the second peak, the fluorescence intensity of these fractions was significantly lower than the first peak demonstrating that the majority of Wzx is eluted in the first peak (Figure 4.13).

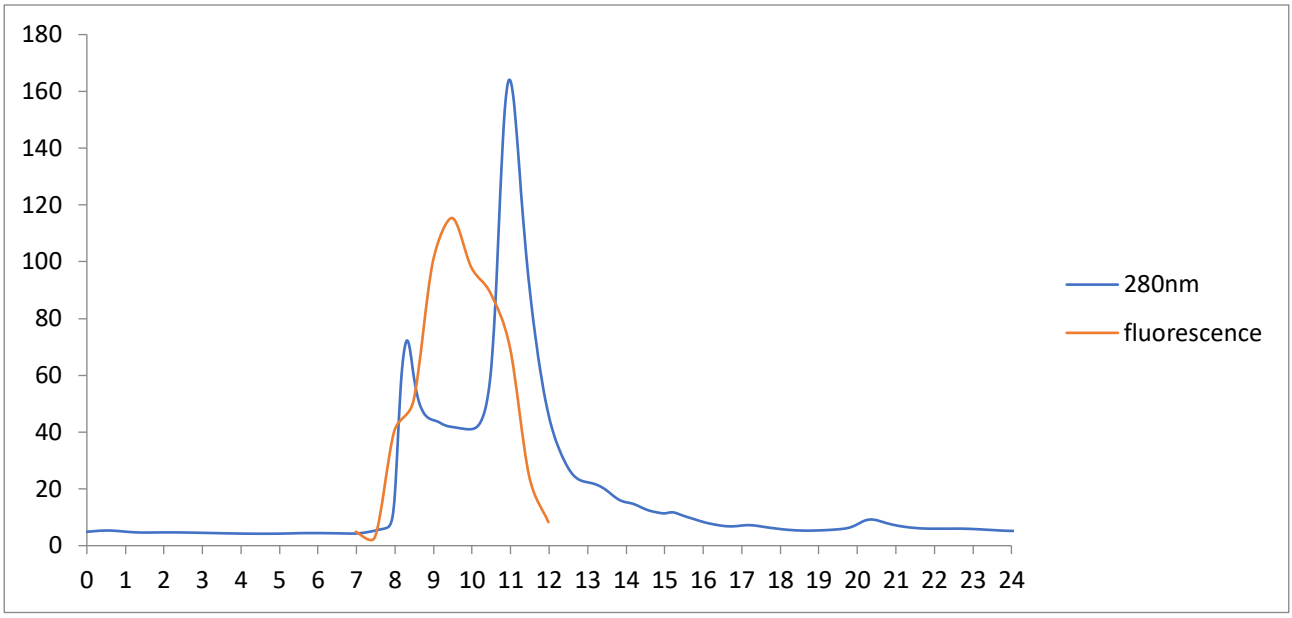

Figure 4.13: Comparison between the chromatogram and fluorescence intensity of the corresponding fractions

The shape of the fluorescence curve may indicate a distribution of Wzx oligomers consistent with the 280 nm absorbance of the shoulder between the two peaks.

From this result, we suggest that the increased efficiency of the SEC column allowed the separation of Wzx from the contaminant. Considering the retention volume that is inversely proportional to the protein molecular weight and the predicted mass of the protein, we speculate that Wzx was eluted in a multimeric form.

4.13. UV visible spectroscopic analysis

To further assess the presence of the contaminant, UV-visible spectra of the combined fractions of the first and the second peak of the SEC purification were recorded. In fact, the Cytochrome o Ubiquinol Oxidase contains heme groups that cause a strong absorption at around 400 nm (Abraham et al. 2001). Spectra of the two peaks are reported in Figure 4.14.

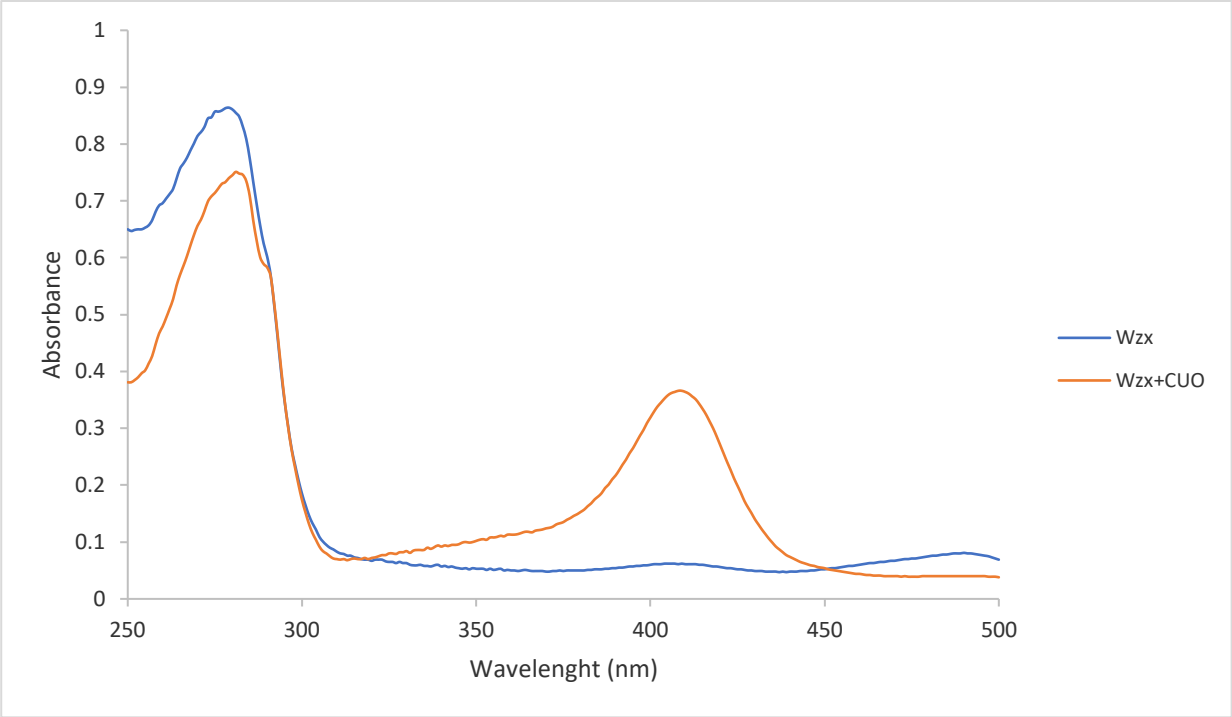

Figure 4.14: UV-visible spectrum of 1st and 2nd peaks from the SEC purification of Wzx in LDAO, using the Superdex 200 10/300 Increase column.

The UV-visible spectra show that the heme absorption peak is present only in the sample corresponding to the second peak and not in the first, thus confirming the effective separation of Wzx from the contaminant.

With the protein sample obtained from the first peak of the SEC purification with the Superdex 200 10/300 Increase column, crystallization experiments were performed using the commercial kits and the preliminary conditions described before. Currently, trials with the purified Wzx sample are ongoing.

4.14. Protein stability: Fluorescence Intensity measurements in temperature gradient

Tryptophan fluorescence can be used to gain information on protein folding and stability, since the fluorescence intensity of this residue depends on its exposure to the solvent. The tryptophan signal varies when the residue is buried in the protein core, usually the case for the native folding, or exposed, often after protein denaturation, and it may be used as an indication of the temperature-driven protein unfolding. The tryptophan residue has an excitation wavelength of 295 nm and the fluorescence intensity is recorded around 340 nm.

To determine protein melting temperature (T_m), spectra of the purified Wzx sample (from the first peak of the purification with Superdex 200 10/300 Increase column, concentration 0.8 mg/mL) were

measured at different temperatures, between 5°C and 70°C. As expected, a strong emission at 338 nm was recorded for all spectra, but with an intensity that decreases significantly with temperature (Figure 4.15).

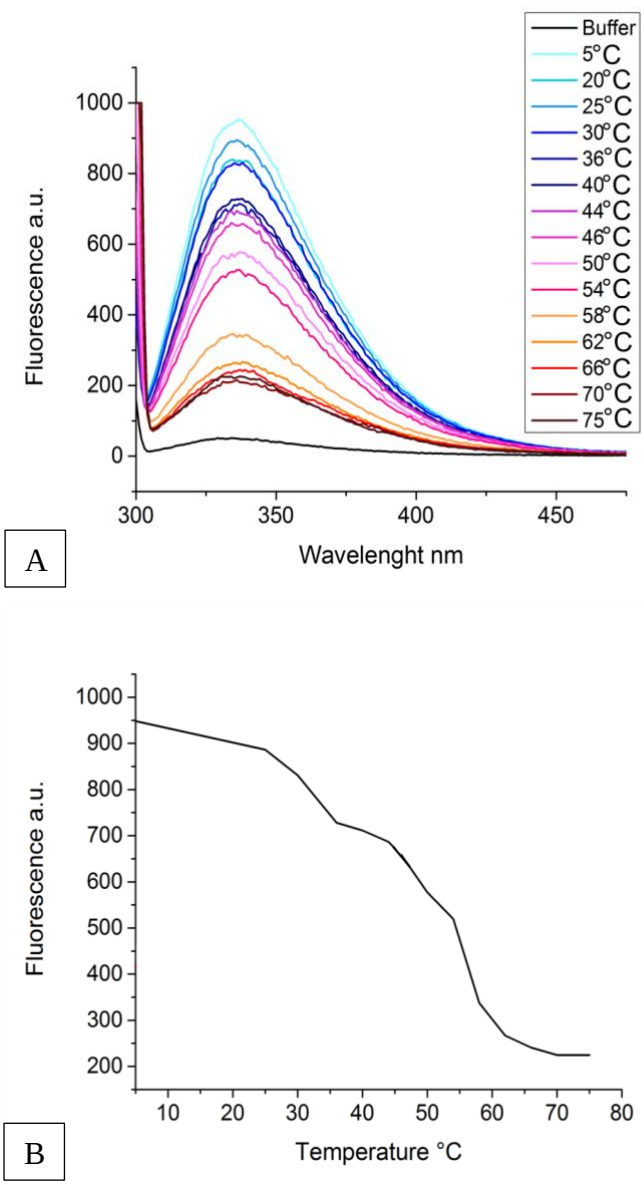

Figure 4.15: Panel A: Fluorescence spectra obtained from a sample of the Wzx protein in LDAO with temperature gradient. Panel B: fluorescence spectrum at 338 nm during the temperature gradient.

From the fluorescence intensity curves two transitions can be observed, the first at 36°C and the second at 46°C. A possible explanation for this behavior is that the first transition is caused by the disassembling of oligomers, while the second is related to protein denaturation. The considerable decrease in fluorescence at 58°C is caused by protein precipitation.

4.15. Protein stability: Circular Dichroism measurements in temperature gradient

Protein secondary structure was also investigated by analyzing the circular dichroism spectra of the sample at different temperatures, in the range of 200 – 250 nm. Circular dichroism is based on the different interactions of the asymmetric elements of the protein with the left- and right-circularly polarized light. The secondary structure elements generate a precise pattern of positive and negative peaks in the CD spectrum. Thus, CD allows the determination of the secondary structure of a protein. Since Wzx has an α-helical structure, negative peaks at 223 and 208 nm were expected. In addition, α-helices usually have a positive peak at 195 nm but in this case the data were cut at 200 nm due to buffer absorption. As for the tryptophan fluorescence analysis, the thermal denaturation of the protein, causing a significant change in its secondary structure, has an important effect on the CD spectrum. The first CD spectrum of the protein purified on the Superdex 200 Increase column, recorded at 4°C using a 0.1 mm cell, shows two minima at 224 nm and at 210 nm, confirming that the protein has a prevalent α-helical structure (Figure 16). In order to follow the thermal denaturation, CD spectra of the protein sample were analyzed between 4° and 80°C, to determine the variation of the α-helix signal during the gradient (Figures 4.16).

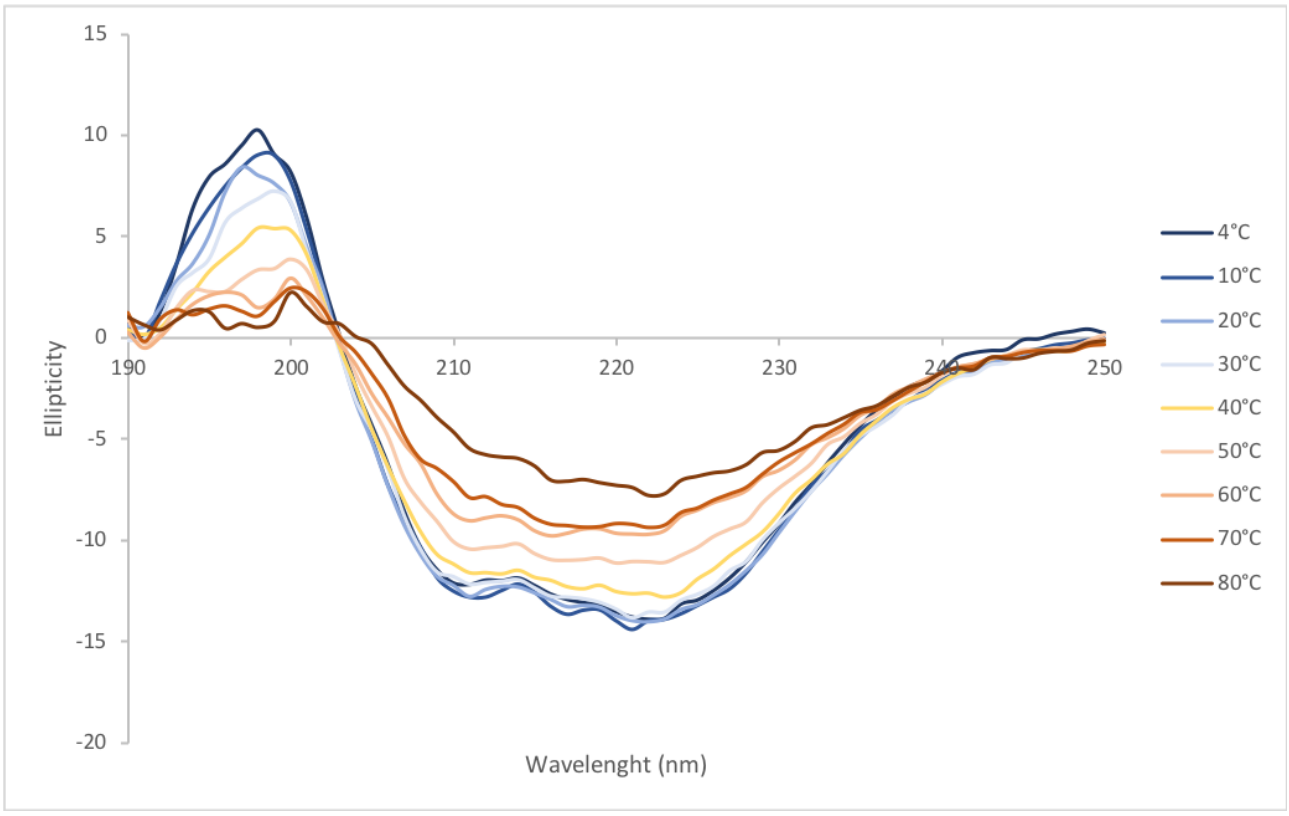

Figure 4.16: CD spectra of the protein Wzx

To determine the melting temperature corresponding to the unfolding process, the same experiment was performed using the 0.2 mm cell. The increase of the optical path allowed to record a stronger signal and to determine an unfolding temperature of about 45°C, confirming the data obtained with fluorescence spectroscopy (Figure 4.17).

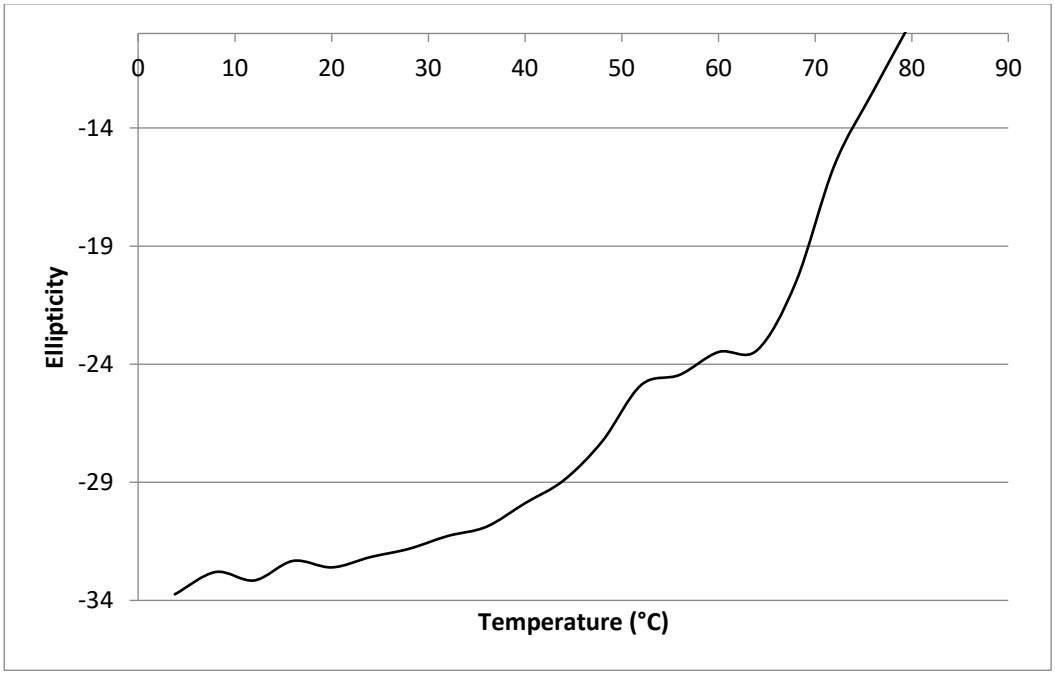

Figure 4.17: temperature-driven change of absorbance at 224nm

4.16. Protein stability: Infra-Red spectroscopy analysis in temperature gradient

Infra-Red (IR) spectroscopy analyses of the Wzx purified samples were performed at the SISSI (Synchrotron Infrared Source for Spectroscopy and Imaging) beamline at Elettra Synchrotron (Trieste).

Data were analyzed considering the Amide I and II range of frequencies, since these signals are originated by the vibrations of the peptide bond. In particular, the Amide I band is due for the 80% to the C=O stretching and 20% and to the C-N out-of-phase. Thus, variation on the HN-C=O bond strength can be assigned to a specific chemical environment, signaling in particular the variation of the H-bond network. Average values assigned to specific secondary structures are summarized in the Table 4.6 (Barth 2007).

Table4. 6: Assignments of different signals (in cm-1) to different secondary structure elements. The values were collected by various authors and evaluated by Goormaghtigh et al. (1994).

Secondary Structure	Average	Extremes
α-helix	1654	1648–1657
β-sheet	1633	1623–1641
β-sheet	1684	1674–1695
Turns	1672	1662–1686
Disordered	1654	1642–1657

It should be pointed out that some authors propose an additional discrimination between parallel and antiparallel β-sheets, considering theoretical calculations on infinite parallel β-sheets. However, the spectra for finite or twisted β-sheets are expected to be similar in both parallel and antiparallel systems.

IR spectra were recorded on a sample deposited onto the diamond crystal of the interferometer and let adhere to the surface, during a temperature gradient from 20°C to 70°C. In addition, the IR spectra at 25°C of the denatured protein after heating was recorded. Figure 4.18 shows the average spectrum obtained by multiple scans for each temperature analyzed. A clear change of band subcomponents during the heating process can be observed in the three-dimensional stack.
The trend can be divided in two subsequent stages. Initially, from 25°C to 35°C, the whole band shifts towards lower wavenumbers (red shift). Then, at 45°C one of the components of this band shifts towards higher wavenumbers (blue shift), peaking at 1660 cm-1. In the final part of the heating process (from 50°C to 70°C), a broadening effect is observed towards lower wavenumbers.

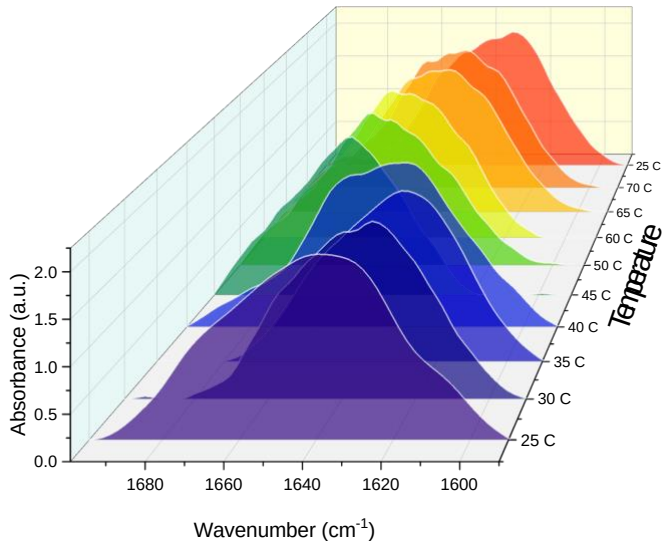

Figure 4.18: 3D stack of the Amide I band at different temperatures.

To better appreciate the band shift and to quantify the variation of each component, the second derivative was analyzed, and six main peaks were identified. The frequencies of these components

were used to guide the Amide I band fit. Figure 4.19 shows the fitting of two of the ten temperature points measured, i.e. the spectrum at 25°C during heating and the spectrum at the same temperature after thermal denaturation. Interestingly, after thermal denaturation the component at 1624 cm-1 increased, whereas the 1605 cm-1 and the 1677 cm-1 components decreased.

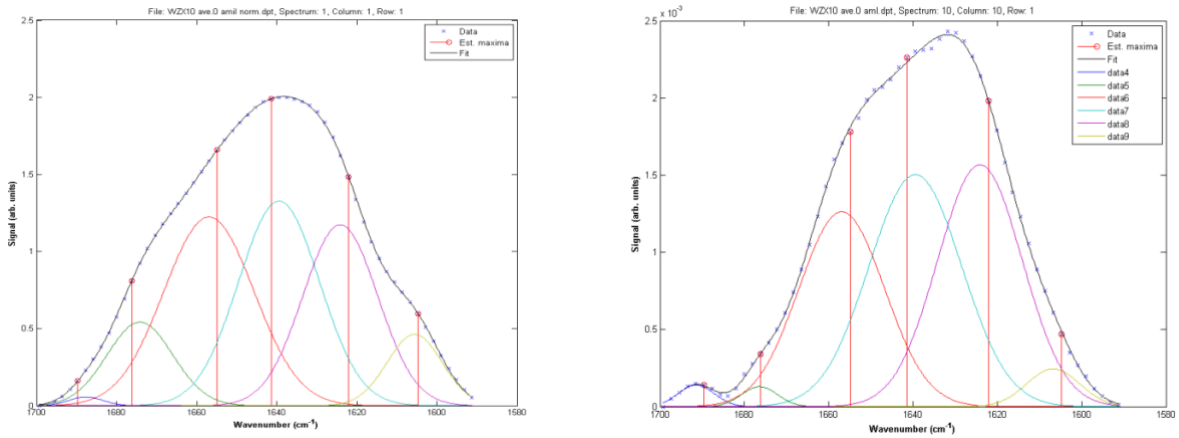

Figure 4.19: Output of the band deconvolution operated with PlotIR. The assumed six components are at: 1690 cm-1, 1677 cm-1, 1655 cm-1, 1641 cm-1, 1622 cm-1, 1605 cm-1

To appreciate the progression of the individual bands during the thermal treatment, the area for each fitted band was plotted in Figure 4.20. The components at 1655 and 1642 cm-1 seem to recover after the end of the thermal treatment.

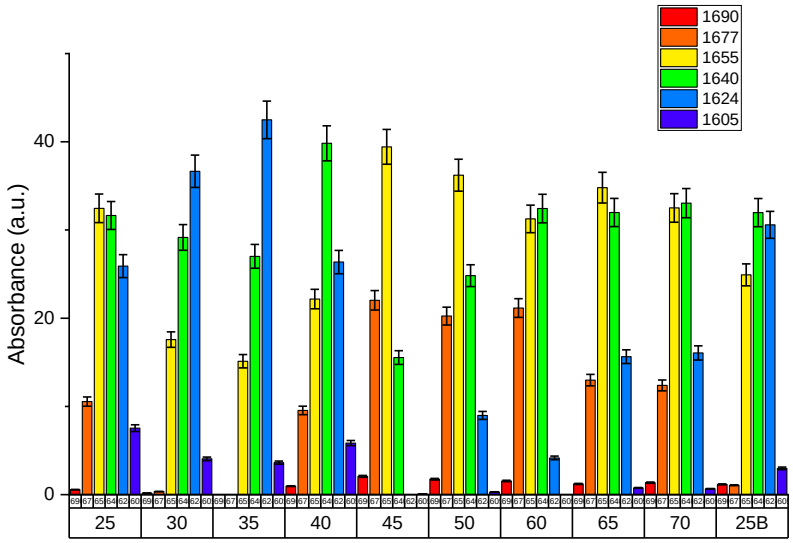

Figure 4. 20: Bar plot representing the variation of the six fitted bands, as band area, while the temperature is changing from 25 °C to 70 °C and back to 25 °C

Analyzing the bar chart, it is possible to better appreciate the two-steps of the denaturation process. In the range of 25-35°C the three main components are at 1655, 1640, and 1624 cm-1; as the temperature increases, the 1624 cm-1 component increases, while the 1655 cm-1 component

decreased. At 40°C this trend ends and at 45°C the 1624 cm^{-1} component becomes barely detectable. At the same temperature, i.e. 40-45 °C, the 1677 cm^{-1} component re-appears. From 45°C to 70 °C the 1624 cm^{-1} component decreases and, reversely, the 1677 cm^{-1} component increases. The component at 1655 cm^{-1} shows a significant increment from 40°C to 45°C, reaching a plateau value almost constant from 50°C to 70°C. In the cooling down step, the 1677 cm^{-1} component almost disappears whereas the 1640 cm^{-1} and 1624 cm^{-1} components recover.

The position of the main peak of the IR data at 1655 cm^{-1} confirms the prevalence of α-helical folding in secondary structure of the Wzx protein, as predicted by homology modeling. The other two main components of the protein at RT could be assigned to turns (1677 cm^{-1}) and disordered structure (1640 cm^{-1}). A third intense component was observed at 1624 cm^{-1}, corresponding to β structures. During the thermal treatment, the α content decreases in favor of a more β-sheet rich structure. At 40-45 °C the trend inverts: the α-helix signal increases and suddenly β-sheet content decreases, passing through a random state (1640 cm^{-1}). After the temperature of 45°C, the interpretation of the spectra becomes less clear. However, the sudden modification in protein secondary structure at 45°C may be the indication of the beginning of the unfolding process.

After the thermal treatment, the protein sample was slowly cooled down to RT. At this stage, the protein secondary structure presents the same three main components observed at the same temperature before thermal denaturation, i.e. at 1655, 1640 and 1624 cm^{-1}. However, their relative intensities are reversed. The impossibility to recover the secondary structure elements after the thermal treatment demonstrates that the protein underwent an irreversible transition.

4.17. Protein stability: Raman spectroscopy analysis in temperature gradient

With Raman spectroscopy the vibrational modes of the Amide I and II of the protein backbone and the peaks corresponding to the aromatic amino acid residues Tryptophan and Tyrosine were analyzed. Spectra were recorded with samples from the first and the second chromatographic peak of the SEC purification with the Increase column, in order to compare the stability of the purified protein and the protein-contaminant mixture. The experiment was aimed at verifying the hypothesis that the presence of Cytochrome o Ubiquinol Oxidase (CUO) has a stabilizing effect on Wzx. This behavior would be consistent with the difficulty in separating the two macromolecules.

The comparison between the Raman spectra of Wzx and Wzx-CUO at 19°C and 70°C shows that at 70°C the Amide I band at 1666 cm^{-1} in the Wzx sample is not detectable, and the proteins appears completely denatured. In the spectrum of Wzx-CUO at 70°C, the presence of secondary structure elements can still be detected. In fact, both the Amide I and the Tryptophan signals are present at 1666 cm^{-1} and 1614 cm^{-1} respectively (Figure 4.21).

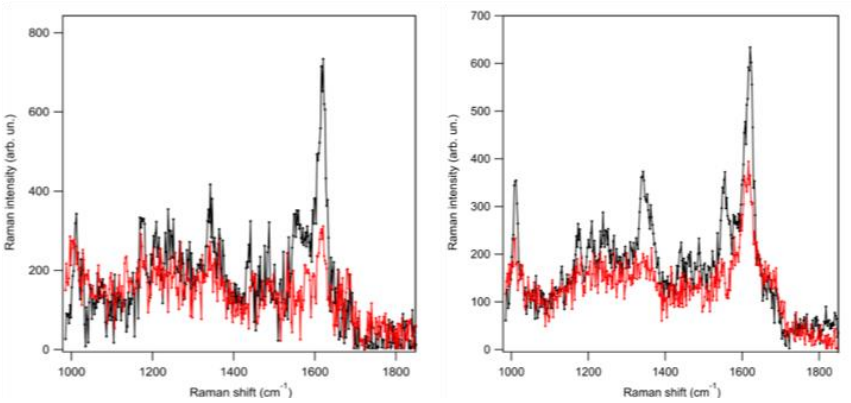

Figure 4. 21: Left: Raman spectra of Wzx-GFP at 19 °C (black) and 70 °C (red). Right: Raman spectra of Wzx-GFP in presence of CUO at 19 °C (black) and 70 °C (red).

This experiment confirmed the hypothesis of a stabilizing effect of the CUO on Wzx folding. This is also suggested by the behavior of the purified sample of Wzx, that forms large oligomers, as proved by the low retention volume of this sample in the SEC purification and by the negative staining EM analysis.

Spectra of a GFP sample were also recorded in the same conditions, to determine the influence of the tag on the Raman spectrum of the sample. Surprisingly, the presence of the GFP protein seems to have little influence on the Wzx spectra.

However, the spectra showed a high signal-to-noise ratio probably caused by the heterogeneity of the sample and by the presence of micelles that increased scattering phenomena. Further experiments will be performed to increase the signal.

4.18. Analysis of the multimeric state: Transmission Electron Microscopy

Transmission Electron Microscopy (EM) is a powerful technique for the visualization of small particles and in the last years demonstrated its potential for the structural determination of proteins with the development of Cryo-EM techniques. However, in order to obtain high-resolution data and to be able to determine the atomic structure of a sample, a high degree of purity is required, avoiding both the presence of unwanted species such as contaminants, and the conformational heterogeneity of the protein.

A first step for the EM analysis of protein samples is the preparation of negatively stained grids, where the protein is treated with a solution containing a heavy atom such as uranium and then analyzed at the microscope. Negative-staining EM allows to evaluate the aggregation state of the protein and the homogeneity of the sample.

To this purpose, images of negatively stained samples of the Wzx flippase peak I purified in LDAO were collected at the University of Trieste using a TEM Philips EM208, equipped with a QUEMSA camera and the software RADIUS. Figure 4.22 shows a representative image of the Wzx sample.

Unfortunately, the EM analysis shows a high degree of heterogeneity of the sample, possibly including multimeric assemblies and probably protein aggregates. The formation of aggregates may be facilitated by the protein solution treatment during grid preparation or by the long exposure to the detergent during purification. The large patches observed in the EM images may be an effect of the zwitterionic detergent on the hydrophilic surface of the grid.

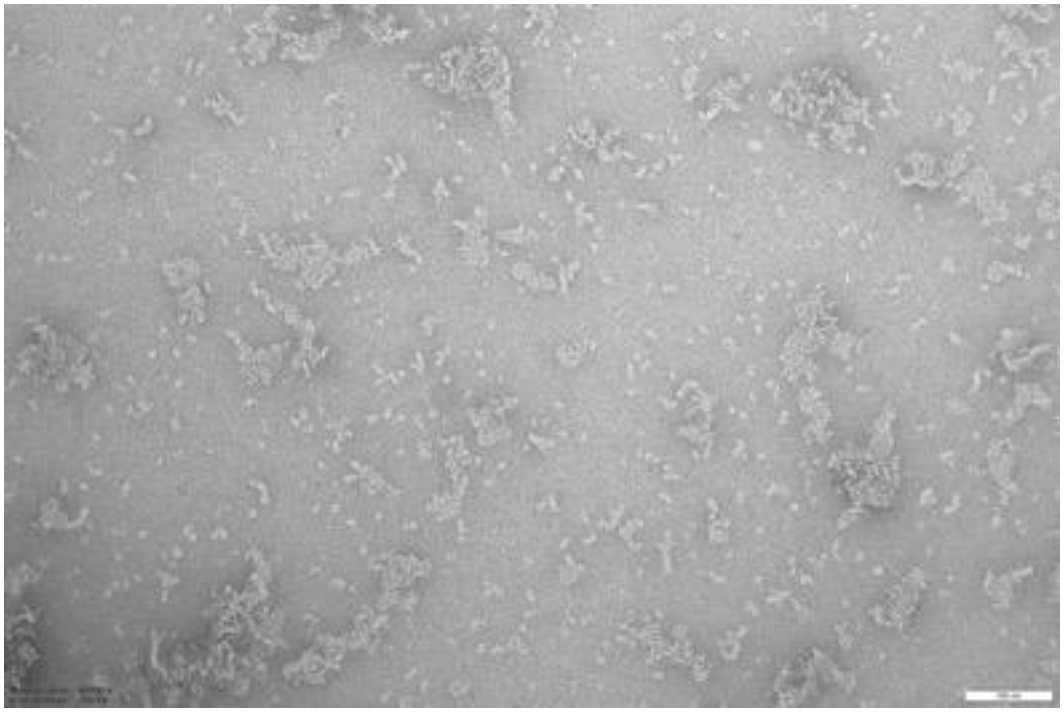

Figure 4. 22: EM image of the Wzx sample after negative straining

5. CONCLUSIONS

The aim of this project was the expression, purification and characterization of the integral membrane protein Wzx of *P. aeruginosa*. *P. aeruginosa* is a very common pathogen with the tendency to develop drug-resistant strains, leading to high morbidity and mortality rates in infected patients. Wzx is one of the members of the Wzy-dependent pathway, responsible for the production of the specific O antigen, an important component of the LPS. In particular, Wzx is deputed at the flipping of the O units from the cytoplasmic to the periplasmic leaflet of the bacterial inner membrane, where the O antigen is polymerized by Wzy. The determination of the Wzx structure may be a starting point for the design of a new class of antibiotics or antibiotic adjuvants against multi drug-resistant strains of *P. aeruginosa*.

During the 3 years of this PhD project, an efficient overexpression protocol for the O-antigen flippase Wzx was set up, yielding amount of protein suitable for the structural characterization. In fact, previous studies were hampered by difficulties in the expression and purification of the protein.

Since membrane proteins are highly hydrophobic and thus insoluble in the aqueous buffers, detergents are required to solubilize the protein and proceed to its purification by chromatographic methods. However, the presence of a harsh detergent may affect the stability and folding of the protein. Therefore, various spectroscopic characterization methods, including IR spectroscopy and circular dichroism, were used to assess the proper folding and to determine the melting temperature of the sample. The choice of the proper detergent was further complicated by the requirements of the crystallization process. The LDAO detergent was chosen for the good results in solubilization tests coupled with CD spectra proving the correct protein folding. In addition, its small micelle size does not affect crystal formation.

The determination of an optimal purification procedure that allowed to obtain a highly pure sample was more challenging. Unfortunately, a contaminant co-solubilized with Wzx showed a strong affinity for the protein and IMAC, antiGFP-based resin, IEX and SEC purifications could not separate the two proteins, even in presence of different detergents, suggesting an interaction between the two. Crystallizations trials of the protein-contaminant sample produced small and poorly ordered crystals. Despite the optimization of crystallization conditions and the further tests conducted in presence of additives, diffraction data could only be collected at low resolution, allowing to determine only the unit cell parameters. However, comparing the cell dimensions with those of another crystal obtained in our laboratory, the sample was identified as a crystal of the *E. coli* membrane protein Cytochrome o Ubiquinol Oxidase.

Further attempts at contaminant removal resulted in the separation of a sample containing only Wzx oligomers, for which the absence of the Cytochrome o Ubiquinol Oxidase was confirmed via UV-visible absorption spectroscopy of the heme group present in the contaminant.

The Wzx oligomeric sample was characterized with fluorescence spectroscopy in temperature gradient to determine the melting temperature, i.e. the temperature at which the protein unfolds. The results indicate that half of the Wzx protein sample is unfolded at about 46°C and the protein precipitates at about 58°C. In addition, another temperature-driven variation in tryptophan fluorescence was attributed to the disassembling of Wzx oligomers. The protein secondary structure was further investigated with circular dichroism, that revealed the characteristic α-helical signal demonstrating the proper Wzx folding in the oligomers.

The variations with temperature of the secondary structure were investigated with IR and Raman spectroscopies in both the oligomeric and the Wzx-contaminant samples. Interestingly, a considerable increment in protein stability in the sample with the Cytochrome o Ubiquinol Oxidase was noticed, suggesting a stabilizing effect of the contaminant and explaining the difficulties in separating the two proteins. The hypothesis that this interaction is maintained in the native environment of the protein, i.e. the cell membrane, needs to be elucidated with different techniques. In particular, as the Cytochrome o Ubiquinol Oxidase protein forming the complex belongs to the host, a similar interaction should be evaluated with the *P. aeruginosa* homolog.

Finally, the oligomeric state of the protein was investigated using negative staining EM, confirming the presence of multimers. Crystallization experiments on the pure flippase are in progress.

As for other integral membrane proteins, the structural characterization of Wzx is complicated by the low stability of the protein extracted from the phospholipidic bilayer. Further structural studies will have to take into account the stability issue, possibly requiring the introduction of stabilizing mutations. In addition, the co-expression and co-purification of Wzx with its physiological partner, the Wzy polymerase, would be interesting to understand the interaction between the two proteins and may result in a sample better suited for the structural characterization.

6. THE KINASE GSK3-β: Introduction

6.1. Protein kinases

Protein kinases (PKs) are enzymes deputed to the transfer of the γ-phosphoryl group from adenosine-5'-triphosphate (ATP) to a hydroxyl group of Ser, Thr or Tyr residues of the target protein, i.e. in the phosphorylation of specific residues. The kinases class is the third most populated protein superfamily and represents almost 2% of human genome (Schwartz and Murray 2011; Johnson and Lewis 2001). The addition of a phosphate group causes a conformational rearrangement of the phosphorylated protein that may lead to an increase or a decrease of its activity (Johnson 1993). The dianionic phosphoryl group is capable to form extensive hydrogen-bond networks that mostly involve nitrogen atoms of the main chain of the protein and side chains of arginine residues (Johnson and Lewis 2001). Since phosphorylation is chemically stable under physiological conditions and ATP is ubiquitous and present at high cellular concentrations, this post-translational modification is widely used as control of biological functions (Westheimer 1987). Therefore, kinases are involved in a huge variety of cellular pathways that are activated or inhibited via phosphorylation such as cell metabolism, DNA replication, gene transcription, protein transport and ubiquitination, cell cycle control, cytoskeleton rearrangement and cell motility (Duong-Ly and Peterson 2014). Kinases play also a critical role in intercellular communication, physiological responses in maintaining homeostasis and in the functioning of immune and nervous systems (Manning et al. 2002).

Since protein phosphorylation is essential in cell functionality, protein kinases activity in strictly regulated via different mechanisms such as transcriptional control, subcellular localization and structural or chemical modification of the kinase.

Mutations and dysregulation of protein kinases are the cause of a diverse group of human diseases such as cancer, diabetes, arthritis neurological and metabolic disorders, leading to the development of kinase agonists and antagonists to be used in therapy (Noble, Endicott, and Johnson 2004; Zhang, Yang, and Gray 2009; Cohen 2002; Hunter, Jolla, and Longfellow 2000).

The design of inhibitors based on the target's structure increases the selectivity and the potency of the so called "smart drugs". The first compound of this class approved for clinical use in 2001 is Imatinib (Gleevec®, Novartis). In that case the elucidation of drug binding mode to the tyrosine kinase Abl and the disposition of the side chains of the kinase gave a major contribution to the design of further compounds targeted against the same protein. These discoveries were possible due to structure resolution of the Abl-Imatinib co-crystal (Noble, Endicott, and Johnson 2004). This result prompted the structural study of kinases that now have become the second most important group of drug targets after G-protein-coupled receptors (Cohen 2002).

6.1.1.Protein kinases classification

The advent of DNA cloning and sequencing techniques allowed the identification in the human genome of 518 kinases-encoding genes (Manning et al. 2002).

Protein kinases may be classified in three families considering the amino acid residue of the target protein that accepts the phosphate group:

1. Ser/Thr protein kinases: This class is constituted by 385 members. These kinases phosphorylate the alcoholic group of a serine and/or of a threonine residue (Manning et al. 2002).
2. Tyr-specific protein kinases: The 90 members of this group catalyze the phosphorylation of the phenolic group of the tyrosine.
3. Dual-specificity protein kinases: able to phosphorylate both Ser/Thr and Tyr residues.

These proteins may be further classified according to structural and functional similarities (Figure 6.1):

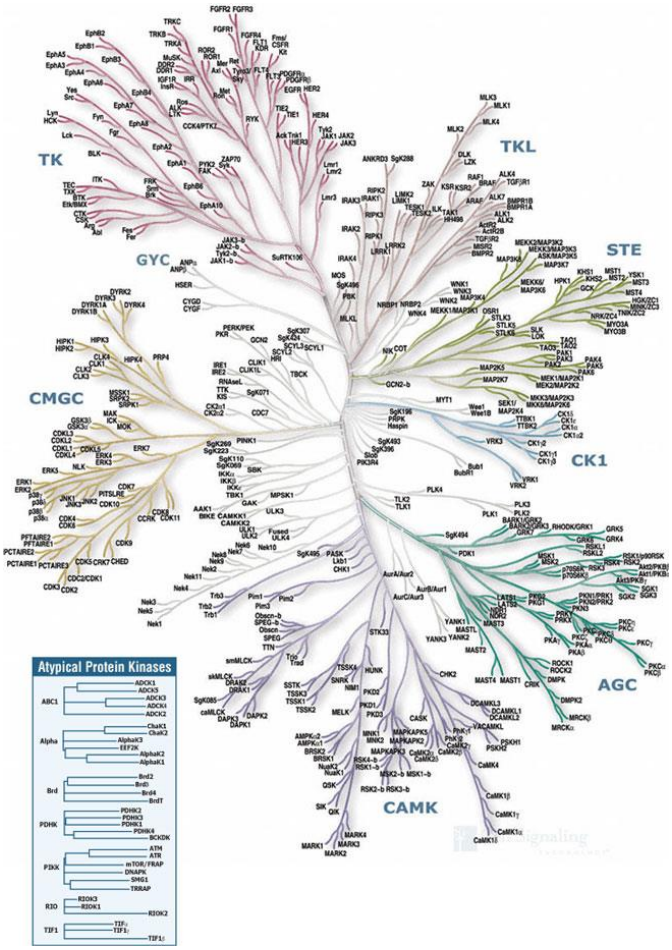

Figure 6.1: The kinome from Cell Signaling website

- AGC (Cyclic nucleotide regulated protein kinase family): this group consists in 63 members. It mainly includes Ser/Thr-specific protein kinases as PKA (cAMP-dependent

protein kinase), PKB (protein kinase B), PKG (cGMP-dependent protein kinase), Aur1/2/3 (Aurora kinase) and PKC (calcium dependent protein kinase).

- CaMK (Kinases regulated by Ca2+/CaM and close relative family): the 74 members of this group are Ca^{2+}/calmodulin dependent protein kinases such as CaMK1/2/4, the MLCK (Myosin light-chain kinase), MAPKAPKs (Mitogen-Activated Protein kinase activating protein kinases) and eleven Nek (Never in mitosis) kinases.
- CK-1 (casein kinase 1 family): in this 12-members group are included the four isoforms of casein kinase 1 (α/γ/δ/ε), the VRK (vaccinia-related kinases) and the TTBK (tau tubulin) kinases.
- CGMC (CDK, GSK-3, MAPK, CDKL): a heterogeneous group of 61 kinases including ten CDKs (cyclin dependent kinase), GSK-3 (glycogen synthase kinase 3) isoforms, MAPK (ERK extracellular signal–regulated kinase) and CDKL (cyclin dependent kinase like).

- STE (related to yeast non-mating or sterile genes): the 47-members group includes MAP kinase cascade families and the MEK proteins, belonging to the Ste7 family. These dual specificity Tyr and Thr kinases phosphoryl ERK/MAP kinases.
- TK (tyrosine kinase): this group consists of 90 members. It includes both receptor TKs (RTKs) as the human epidermal growth factor receptor (HER/EGFR) family and the insulin receptor (IR) and non-receptor (cytosolic) TKs, such as Src kinase, Abl (Abelson tyrosine kinase), and JAK (Janus kinase).
- TKL (tyrosine kinase-like): the structure of the 43 members of this group resembles both the Tyr kinase group and the Ser/Thr one. The group includes the interleukin-1 (IL-1) receptor-associated kinase (IRAK) and the RIPK (receptor-interacting protein kinase) among others.
- RGC (receptor guanylyl cyclase): it is composed by five members that resemble tyrosine kinases.
- OTHER: this is a heterogeneous group counting 83 members.
- ATYPICAL: in this category 40 enzymes are included, such as the pyruvate dehydrogenase kinase (R. J. Roskoski 2015).

6.1.2. Protein kinase structure

Despite the wide variety of metabolic pathways involving kinases, these proteins share the same overall structure (Figure 6.2), as demonstrated by crystal structure comparison. The highly conserved structural features are critical for catalysis and for protein kinase control (Hanks and Hunter 1995).

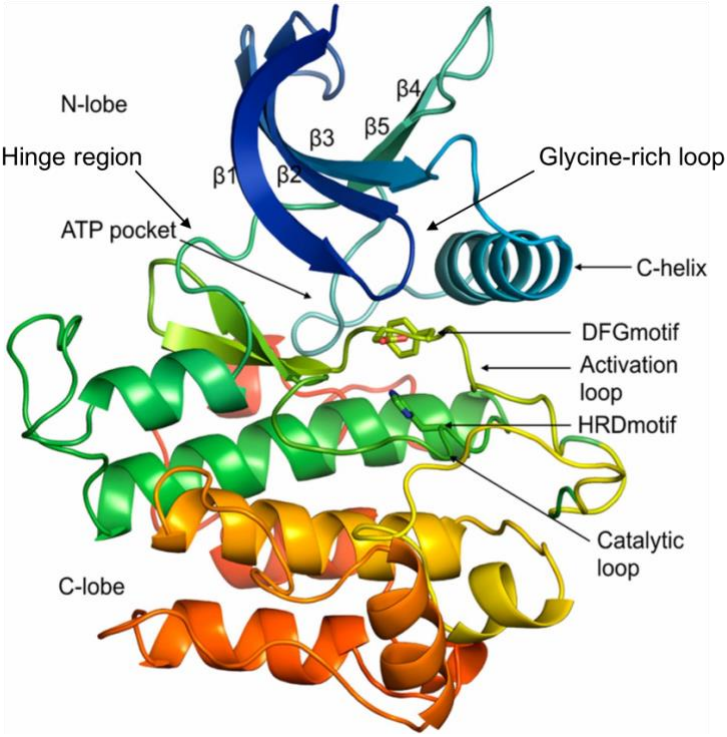

Figure 6.2: Protein kinase structure Vivek Modi, and Roland L. Dunbrack Jr. PNAS 2019;116:14:6818-6827

Generally, protein kinases are constituted by two lobes: the smaller N-terminal lobe, composed of five β-sheets and an α-helix. This domain is involved in the ATP binding. Whereas the larger C-terminal lobe, rich in α-helix structures is involved in the interactions with the peptide substrate (Johnson and Lewis 2001). The two lobes are linked by a hinge region, a short sequence of conserved residues forming hydrogen bonds with ATP's adenine moiety. Within the hinge region, there is a deep cleft that constitutes the active site. In the front pocket of the cleft are located the residues involved in both catalysis and ATP binding. On the opposite side, the back hydrophobic pocket is deputed to regulatory functions (Huse and Kuriyan 2002; Kornev and Taylor 2010). At the N-terminus of the hinge region is located the gatekeeper residue: it controls the access to a hydrophobic pocket that lies behind the adenine-binding pocket of the ATP binding site (Taylor and Kornev 2011). The accessibility to the hydrophobic pocket by kinase inhibitors is determined by the size and hydrophobicity of the gatekeeper residue.

The ATP-binding site consist in a flexible N-terminal loop (G-loop) that contains the motif GXGXXGV, also called the glycine rich loop. This sequence is highly conserved in almost all eukaryotic protein kinases. It has the function of anchoring the nontransferable α- and β-phosphate groups of ATP through ionic interactions (Schwartz and Murray 2011). The glycine rich loop conformation is dynamic, and its conformation depends upon the presence of ligands and the activation state of the catalytic domain.

The C-helix of the N-terminal lobe regulate enzyme activation through its orientation: inward towards the active site in the active state, while in the inactive conformation it is rotated away

from the ATP binding site (Schwartz and Murray 2011). In the active conformation C-helix forms a salt-bridge between its highly conserved Glu and an invariant Lys within the N-terminal lobe, which was demonstrated to be essential for maximal enzyme activity, allowing optimal positioning of the ATP phosphate group.

The catalytic loop is characterized by the HRD motif (histidine-arginine-aspartic acid), which contains a conserved Asp that acts as the catalytic base during the transfer of the phosphoryl group.

The activation loop, located on the C-lobe, is one of the most important control elements of protein kinase activity. This segment is flanked by the highly conserved DFG triplet (aspartic acid-phenylalanine-glycine) and the consensus APE motif (alanine-proline-glutamic acid) (Duong-Ly and Peterson 2014; Steichen et al. 2010). In particular, the Asp of the DFG motif chelates the metal ion(s), usually magnesium orientating the γ-phosphate for transfer and increasing protein phosphorylation activity (Roskoski 2015). In the active state, the Asp side chain points towards the ATP binding site in the so called DGF-in conformation. In the kinases activated via phosphorylation, the phosphate bond formed within the activation loop of the phosphorylation site induces a conformational rearrangement of the loop, allowing peptide substrate binding (Hari, Merritt, and Maly 2008). Usually, kinases are in the inactive form and are activated by autophosphorylation or phosphorylation by other kinases (Manning et al. 2002). Autoinhibitory sequence elements promote the inactivation of the kinases by occupying the peptide binding site preventing real substrate binding (Manning et al. 2002).

6.2. Glycogen synthase kinase 3 (GSK-3)

Glycogen synthase kinase 3 (GSK-3) is a constitutively active multi-potent serine/threonine kinase belonging to the CMGC group. This ubiquitous proline-directed kinase is present in all mammalian cells and has homologues in all eukaryotes. GSK-3 was first identified in 1978 as a key mediator of the insulin pathway, by blocking the incorporation of glucose into glycogen via phosphorylation of glycogen synthase (GS) (Embi, Rylatt, and Cohen 1980). Further studies demonstrated GSK-3 crucial role in the regulation of multiple signaling pathways. It is involved in glycogen metabolism, cell cycle, gene expression, protein synthesis, cellular metabolism, motility, apoptosis, neuroprotection, proliferation and survival by interacting with multiple pathways including Wnt, MAP-kinase (MAPK), or PI3K/Akt signal transduction pathways.

Two GSK-3 isoforms, encoded by distinct genes, were identified: GSK-3α (mapped to chromosome 19q13.2) and GSK-3β (mapped to chromosome 3q13.3). In the isoforms, kinase domains are 98% identical whereas C- and N-terminal regions share only 36% identity (Doble and Woodgett 2003). In

fact, GSK-3α presents an extra N-terminal glycine rich region resulting in higher molecular weight: GSK-3α is 51 kDa, while GSK-3β is 47 kDa (Jacobs et al. 2012; Doble and Woodgett 2003). Further studies identified GSK-3β2, an alternative splicing variant of GSK-3β. The variant contains the splice insert of exon 8b, that encodes a 13-residue extra sequence in the catalytic domain. GSK-3β2, found in human and rodent, presents an altered kinase activity (Mukai et al. 2002). It has a reduced activity towards the microtubule-associated protein tau compared to the more abundant variant (Doble and Woodgett 2003).

Despite their homology, GSK-3 isoforms undergo distinct regulatory mechanisms and exhibit different functions. This is highlighted by the differential presence of GSK-3 isoforms in human tissues. In fact, the α isoform is abundantly present in lung, heart, kidney ovary and testis. GSK-3β is especially observed in lung, kidney and brain. The latter isoform is undetectable in testis. Interestingly, fetal rat brains shows higher GSK-3β concentration compared to adults; this may be connected with the high phosphorylation rate of the microtubule associated tau protein confirming its role in tau hyperphosphorylation (Lau et al. 1999). Therefore, the β isoform is widely studied in neurodegenerative disorders.

6.2.1.GSK-3β structure

Human GSK-3β is a 47 kDa protein formed by 420 amino acid residues (Dajani et al. 2001).

GSK-3β shares many structural motifs with other protein kinases, it presents an N-terminal β-sheet domain coupled to a C-terminal α-helical domain. The N-terminal domain (residues 35-134) is constituted by a closed orthogonal β-barrel formed by seven β-sheet strands. This conformation closely resembles the N terminal domain of tyrosine kinases differing from the Ser/Thr kinase N-termini (Hubbard and Argos, 1994). The β-barrel 5th and 6th strands are connected by a two-turn α-helix (residues 94-104) (Dajani et al. 2001).This α-helix plays key roles in enzyme catalysis in fact, Arg96 is involved in the alignment of the N- and C-terminal domain and in the interaction with the primed phosphorylated substrate (Frame, Cohen, and Biondi 2001). Whereas the active site residue Glu97 forms a slat bridge with the catalytic residue Lys85 within the N-terminal lobe, allowing optimal positioning of the ATP phosphate (Haar, Coll, and Austen 2001). The N-terminal domain is connected to the rest of the kinase via an α-helix (residues 138-149) extending after the 7th strand (Dajani et al. 2001). The ATP binding site is located at the interface of the two domains bordered by the glycine-rich loop and by the hinge region (Haar, Coll, and Austen 2001).

The α-helical domain (residues 152-342) includes a catalytic loop with the highly conserved HRD motif (residues 179-181) and the DFG motif (residues 200-202) (Buch et al. 2010).

Within this domain the residues of the activation segment (210-GEPNVSYICSR-220) and the activation loop (residues 220-226) are also located (Dajani et al. 2001). Tyr216 phosphorylation promotes a rearrangement of the activation segment allowing the correct disposition of the substrate binding site. However, even an unphosphorylated activation loop presents a conformation that resembles the active state of other kinases. This may explain the constitutive activity of GSK-3β.

Beyond this domain, residues 342-386 form a series of short helices and loops that pack against the long helix (residues 155-175) of the α-helical domain (Haar, Coll, and Austen 2001).

6.2.2.GSK-3β regulation

The determination of GSK-3 crystal structure clarified the mechanisms of enzyme control, its necessity of primed phosphorylated substrates and its functionality. Despite non strictly required, the priming phosphorylation increases GSK-3 substrate phosphorylation efficiency by 100-1000 fold (Doble and Woodgett 2003). GSK-3β recognizes the consensus amino acid sequence Ser/Thr-X-X-X-Ser-P/Thr-P. The Ser/Thr residue is GSK-3β phosphorylation target whereas the n+4 Ser-P/Thr-P residue is the primed site already phosphorylated by another protein kinase (Doble and Woodgett 2003). Phosphorylation and priming sites are linked by three residues, usually proline.

In the insulin pathway, GS is previously phosphorylated by Casein Kinase 2 (CK-2), before GSK-3 binding and phosphorylation at different sequential sites (Fiol et al. 1990). However, some substrates such as Axin do not require priming prior to GSK-3β phosphorylation. These proteins display negatively charged residues near the priming position that may mimic a phospho-residue (Doble and Woodgett 2003).

The recognition of the primed substrate is deputed to a basic-residue triad formed by Arg96, Arg180, and Lys205. The triad side chains create a positively charged area that interacts with the negatively charged phosphate group on the primed residue optimizing the orientation of the kinase domain and also placing the substrate in the correct position within the catalytic groove (Doble and Woodgett 2003).

Fully active GSK-3β is phosphorylated at Tyr216 within the T-loop, through a not well clarified mechanism. Several kinases are reported to mediate Tyr216 phosphorylation, but recent evidences suggest an autophosphorylation process, which denotes an intramolecular tyrosine kinase activity (Wang et al. 1994) (Figure 6.3).

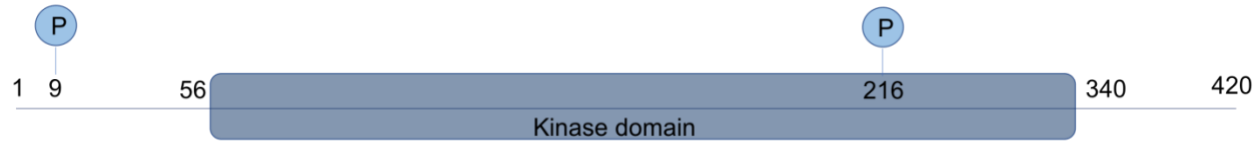

Figure 6.3: schematic representation of GSK3-β

This phosphorylation forces the opening of the substrate binding site facilitating substrate phosphorylation. However, the phosphorylation is not strictly required for kinase activity since in the unphosphorylated state no conformational constrains prevent activity (Dajani et al. 2001).

On the other hand, GSK-3β activity is inhibited through Ser9 phosphorylation by several kinases, including PKB, in response to insulin stimuli, MAPKAP kinase-1, after epidermal growth factor stimulation (Brady, Bourbonais, and Saltiel 1998), p70 ribosomal S6 kinase (Armstrong et al. 2001; U. Krause et al. 2002), PKC (Fang et al. 2002; Li et al. 2000) and PKA (Fang et al. 2002; Ballou et al. 2001). Phosphorylation of Ser9 promotes a folding rearrangement creating a primed pseudo-substrate that intramolecularly binds the positively charged pocket occupying the catalytic groove. This inhibition mechanism is competitive, so a high primed-substrate concentration may compete with the pseudo-substrate and become phosphorylated (Frame, Cohen, and Biondi 2001).

GSK-3β may also be inhibited through formation and disruption of protein complexes, as it happens in the Wnt (Wingless and Int) pathway (Doble and Woodgett 2003).

GSK-3β may also be regulated by N-terminal proteolysis. For example, the proteolytic enzyme calpain is able to remove the regulatory N- terminus of the β isoform generating fragments of about 30-40 kDa. Interestingly, this truncation increases kinase activity, due to the regulatory domain loss.

6.2.3.GSK-3β targets and related pathologies

Considering the range of substrates identified along the years, GSK-3β regulates over 100 proteins involved in metabolic and signaling pathways, as well as transcription factors. A deregulation of those pathways often leads to pathological conditions.

Metabolic pathways

GSK-3 was firstly identified as a negative regulator of glycogen synthesis in the PI3K/insulin signaling pathway. In fact, GSK-3β was shown to inactivate glycogen synthase (GS) via phosphorylation of different serine residues (Embi, Rylatt, and Cohen 1980). After insulin stimulation, the insulin receptor substrates 1 and 2 (IRS1 and IRS2) recruit phosphatidilinositolo-3-kinase (PI3K), that activates PKB by Thr308 and Ser473 phosphorylation. Subsequently, PKB phosphorylates GSK-3β Ser9 preventing glycogen synthase phosphorylation. Active GS

increases glucose storage through glycogen synthesis (Grimes and Jope 2001). Moreover, GSK-3 negatively regulates basal glucose uptake through down-regulation of glucose transporter 1 (GLUT1) expression. Due to its extensive and central role in glucose metabolism, GSK-3 is considered a targetable molecule for the treatment of type II diabetes.

Wnt pathway

The Wnt family of secreted signaling lipoproteins has central roles in embryogenesis, in adult tissue homeostasis and also in human tumorigenesis (Miller 2002). In fact, mutation of several intracellular components is thought to be critical in many forms of cancer (Polakis 2000).

Moreover, Wnt pathway has an important role in neuronal migration, synaptic differentiation, mature synapse modulation and synaptic plasticity.

In Wnt pathway, GSK-3β forms the "destruction complex" together with Axin, APC and β-catenin. In the absence of Wnt signal, active GSK-3 phosphorylates the primed β-catenin on different serine residues (Ser33, Ser37, Ser41) resulting in β-catenin targeting for ubiquitination and consequent degradation by the proteasome (Ciani and Salinas 2005). Axin facilitates β-catenin phosphorylation binding and supporting the different components of the complex. Wnt ligands induce a cascade that promote the occupation of GSK-3 Axin binding site preventing the formation of the GSK-3/Axin/APC/β-catenin complex. Therefore, β-catenin accumulates in the cytoplasm and translocates to the nucleus, where it activates the transcription of target genes (Doble and Woodgett 2003).

Recent advances indicate that GSK-3 also participates in Wnt co-receptor LRP6 activation via phosphorylation, thus suppressing its own activity and stabilizing β-catenin (Chong and Maiese 2004).

However, mutations on β-catenin that prevent its phosphorylation and promote the increase of its levels have been detected in different types of cancer, such as skin, colon, liver, prostate, ovary and endometrium (Polakis 2000).

Hedgehog pathway

The Hedgehog signaling pathway regulates embryonic development, while it is mostly quiescent in adults, except for its role in tissues maintenance and repairing. An aberrant activation of the Hedgehog (Hh) pathway in adults is associated with numerous cancers including lung, prostate, breast, melanoma, colorectal and pancreatic cancer. In children, Hh abnormalities are associated with medulloblastoma and rhadomyosarcoma, malignancies that involve the cerebellum and the muscle, respectively (Scales and de Sauvage 2009). In this pathway, the multi-protein complex

composed of PKA, GSK-3β and Casein Kinase 1 δ (CK-1δ) phosphorylates the Gli (Glioma-associated oncogene) transcription factors. The phosphorylated Gli is subsequently degraded by proteasomes into the C-terminal truncated form (GliR) (Gorojankina 2016). GliR acts as a repressor of Hh target genes into the nucleus (Pan et al. 2006; B. Wang and Li 2006). In this case CK-1δ acts as priming kinase for GSK-3β Gli phosphorylation. Since Hh ligands block Gli phosphorylation promoting the Hh pathway activation, GSK-3β plays a negative role in Hh signaling (Price and Kalderon 2002; Gorojankina 2016). On the other hand, positive regulators of the Hh pathway could be used in neurodegenerative disease treatment. In fact, Hh pathway activation seems to be neuroprotective in Parkinson's Disease (PD) due to its control on the dopaminergic neurons that degenerate in the progress of this pathology. It may also have a regenerative effect by increasing the proliferation and neural differentiation of endogenous precursor cells in the adult brain (Dellovade et al. 2006).

p53 pathway

Tumor suppressor p53 is a key mediator of pro-apoptotic signals in response to DNA damage. Aberration in its apoptotic activity is one of the most common causes leading to malignancies. p53 proteins usually have short life and are stabilized via a multiplicity of post-translational modifications (Oren 2003; Haupt et al. 2003). GSK-3β participates in some of these modification by phosphorylating different p53 residues. Through GSK-3β/nuclear p53 complex formation, the kinase influence p53-induced apoptosis (Watcharasit et al. 2002; Beurel et al. 2004).

Modulating the activity of p53, GSK-3β regulates the p53-mediated transcription of genes (Watcharasit et al. 2003; Beurel et al. 2004), the intracellular localization of the tumor suppressor and also p53 levels via phosphorylation of MDM2 protein (Kulikov, Boehme, and Blattner 2005; Pluquet et al. 2005). In mitochondria, GSK-3β binds the p53 located in that organelle promoting apoptosis (Watcharasit et al. 2003). Moreover, p53 may increase GSK-3β activity via direct binding with the kinase (Beurel and Jope 2008; Watcharasit et al. 2002).

Neuroinflammation

Inflammation is a living tissue response able to counteract harmful stimuli such as infections or wounds and deputed to maintain tissue homeostasis. Inflammation can be divided in acute, that mediates the early responses to the damage and chronic that is caused by persistent stimuli. The inflammatory response involves both the innate system, responsible of the recruitment of immune cells via cytokines production, and the adaptive immunity that involves T cells and antibodies (Streit, Mrak, and Griffin 2004). Chronic neuroinflammation causes microglia and astrocytes

activation that induces the release of pro-inflammatory mediators (cytokines as TNF-α, chemokines MCP-1, interleukins as IL-1β and IL-6 and MIP-1) (Ramesh, Maclean, and Philipp 2013). It may also promote the eventual recruitment of peripheral T-cell infiltrates that cross the Blood Brain Barrier (BBB). However, the persistence of the inflammation causes neuronal damage and contribute to neuronal loss.

Inflammatory processes are pathological mechanisms in many infections such as meningitis, rabies, HIV encephalitis and prion diseases (Streit, Mrak, and Griffin 2004).

Neuroinflammation has a prominent role also in neurodegenerative diseases, such as Alzheimer's disease (AD), amyotrophic lateral sclerosis (ALS), multiple sclerosis and Parkinson's disease (PD) (Glass et al. 2010).

GSK-3 is implicated in the modulation of NF-κB signal pathway involved in the activation of pro-inflammatory genes, in cytokine production and in the modulation of survival, proliferation and differentiation of B and T lymphocytes (Karin 2005; Jope et al. 2017). GSK-3 has a fundamental role in NF-κB gene-specific transcription facilitating NF-κB access to specific pro-inflammatory genes (Steinbrecher et al. 2005; Jope, Yuskaitis, and Beurel 2006).

GSK-3β activation leads to the NF-kB nuclear translocation. Once there, NF-kB forms a complex with CBP (CREB Binding Protein) mediating the transcription of pro-inflammatory cytokines. Moreover, GSK-3β mediates the simultaneous phosphorylation-dependent down-regulation of CREB (cAMP response element binding protein) that is responsible of the production of anti-inflammatory cytokines. Thus, blocking of GSK-3β activity results in inhibition of NF-κB, that reduces inflammatory cytokines, and in activation of CREB, that increases anti-inflammatory cytokine release (Martin et al. 2011). Inhibition of GSK-3β-mediated pro-inflammatory pathways may counteract neuroinflammation in CNS diseases (Jope, Yuskaitis, and Beurel 2006).

Mood disorders

The first evidence of GSK-3β involvement in mood disorders is lithium identification as reversible inhibitor of GSK-3 with an in vitro IC50 of around 2 mM (Jope and Roh 2008). Lithium is widely used as a mood stabilizer in the treatment of bipolar disorder (BD). The variation of the neurotransmitter system induced by drugs currently used to treat mood disorders creates a link between GSK and numerous pathologies. Bipolar disorder, depression and schizophrenia are some of the conditions that are connected with GSK activity (Jope and Roh 2008). In fact, increased levels of pSer9-GSK-3β are reported after the administration of currently used anti-depressant (fluoxetine or imipramine), anti-convulsant (valproate) or anti-psychotic (risperidone,

olanzapine, clozapine) drugs due to the interference with the serotoninergic and dopaminergic transmission modulated by this kinase (Li and Jope 2010).

Neurodegenerative Diseases

Protein kinases including GSK-3β are widely accepted as key components of the molecular mechanisms underlying neurodegeneration and neuroprotection. Here, three neurodegenerative diseases correlated to GSK-3β activity are discussed.

Alzheimer's Disease

Alzheimer's disease (AD) is the most common neurodegenerative and cognitive disorder especially among over 85, and the most prevalent of the tauopathies (Duda et al. 2018). Tauopathies are neurodegenerative disorders characterized by abnormal tau protein deposition in the brain (Kovacs 2017). AD has a multifactorial etiology. In fact, only a minor percentage of patients have a familiar AD while in other cases the insurgence of the pathology can be connected to environmental risk factors.

Four genes are connected to AD: APP (amyloid precursor protein), APOE4 (4 allele of the apolipoprotein E gene), PSEN-1 (presenilin 1) and PSEN-2 (presenilin 2) (Duda et al. 2018). This pathology is characterized by dementia, learning and behavioral impairment, depression and progressive episodic memory loss (Llorens-Martín et al. 2014).

During AD progress, two typical pathological hallmarks appear within specific areas of the brain, i.e. multiple extracellular deposits of senile plaques, composed of amyloid beta (Aβ) peptide, and intracellular neurofibrillary tangles (NFTs), composed of aggregates of the microtubule-associated protein (MAP) tau (Figure 6.4).

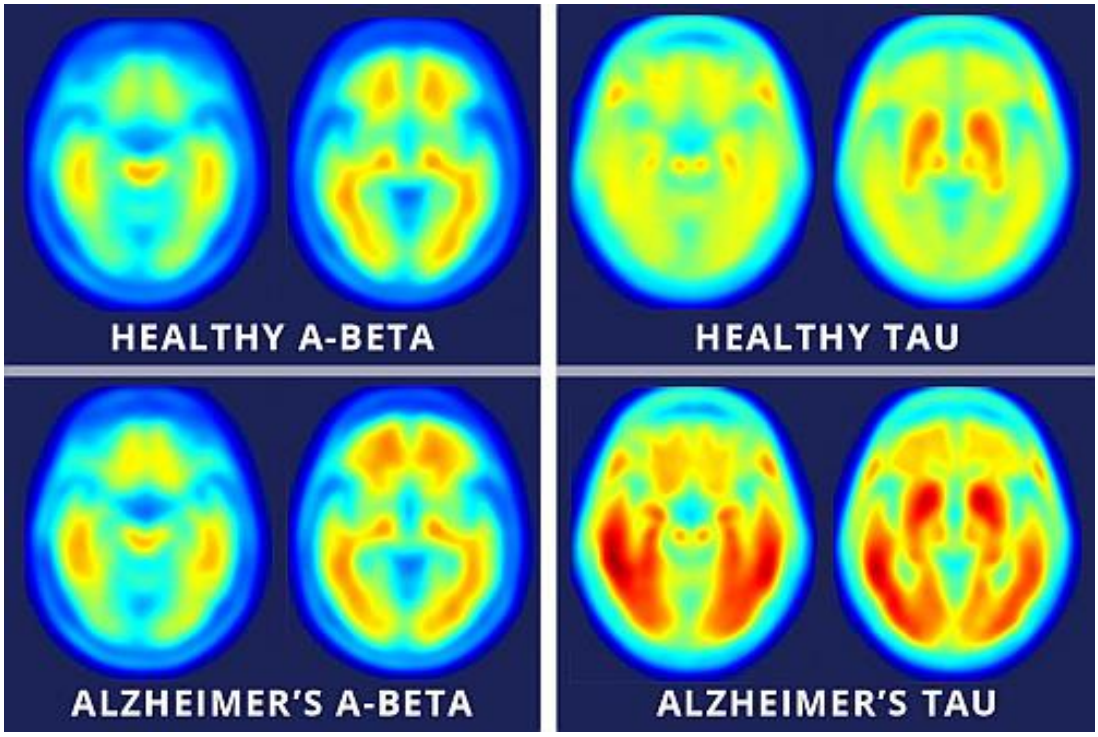

Figure 6.4: β- amyloid and tau protein accumulation in AD. PET brain scan of healthy patients on the top and Alzheimer patients on the bottom. From: New brain imaging agent is marker for progression of Alzheimer's [2016-05-13. Sandra Levy, MedCity News

Aβ protein is a cleavage product of the amyloid precursor protein (APP), a trans-membrane protein whose fate can follow two different routes: the non-amyloidogenic pathway and the amyloidogenic pathway.

In the non-amyloidogenic pathway, APP is cleaved by the α- and γ-secretases producing easily degradable fragments. GSK-3β may interfere with the α-secretase in the non-amyloidogenic pathway, depressing its activity via down-regulation of one of the secretase complex components. It also interferes with γ-secretase cleavage step (Llorens-Martín et al. 2014).

In the amyloidogenic pathway, APP is degraded by β-site APP cleaving enzyme 1 (BACE1), an aspartyl-protease highly expressed in Alzheimer's patients, and the cleaved fragments are then released by the γ-secretase. The released Aβ aggregates into insoluble plaques and oligomers that are able to activate NMDA currents leading to cell death (Deng et al. 2014). The deposition of Aβ seems to be the leading cause of neuroinflammation attracting microglia. These cells are able to phagocyte and degrade Aβ (Frautschy, Cole, and Baird 1992). However, this process is ultimately ineffective or inadequate to face the massive amyloid deposition and neuritic injury (Streit, Mrak, and Griffin 2004). The importance of neuroinflammatory processes in this pathology is demonstrated by the relief mediated by nonsteroidal anti-inflammatory drugs on AD's symptoms (Krause and Müller 2010).

Protein tau is involved in facilitating and regulating microtubule formation and stability. It associates with microtubules and stabilizes their phosphorylation process.

In AD, abnormal tau dissociates from microtubules, destabilizing them and interfering with their cellular mechanisms and transport leading to neurite degeneration (Zhang et al. 2016; Deng et al. 2014). AD's tau forms paired helical filaments (PHF), which tend to clump together forming rigid and insoluble neurofibrillary tangles (NFTs). The hyperphosphorylated tau is often truncated at the C-terminus resulting in resistance to phosphatases and proteases.

Abnormal tau phosphorylation is considered one of the earliest signs of neuronal degeneration and appears to precede tau aggregation or amyloid plaques formation. GSK-3β together with CK-1δ and PKA associates with tau and promotes its phosphorylation (Llorens-Martín et al. 2014). Moreover, CK-1δ can act as priming kinase on tau providing primed phosphorylated substrate to GSK-3β (Singh et al. 1995). Interestingly, tau overexpression increases GSK-3β activity through an increase of oxidative stress and inflammatory processes, thus perpetuating its phosphorylation.

GSK-3β not only hyperphosphorylates tau, but it is also positively regulated by Aβ, linking the two AD's pathological hallmarks. Aβ increases GSK-3 catalytic activity, thus promoting tau phosphorylation (Lei et al. 2011). In addition, GSK-3β is highly involved in AD memory impairment, inflammatory responses, cholinergic deficit and neuronal loss through activation of the intrinsic apoptotic signaling pathway (Hooper, Killick, and Lovestone 2008). In particular, one of the earliest signs of AD is the dysfunction of synaptic plasticity that directly correlates with memory and learning deficiencies. GSK-3β plays a key role in maintaining the equilibrium between LTP (long-term potentiation) and LTD (long-term depression) processes. An increased GSK-3β activity, caused by suppression of Wnt or PI3K signaling, impairs the LTP. Thus, the inhibition of GSK-3β induces LTP and inactivates LTD, strengthening the synaptic efficiency and therefore improving learning and memory (Hooper, Killick, and Lovestone 2008).

Parkinson's Disease (PD)

PD is the second most common neurodegenerative disorder after AD. PD main pathological hallmarks are the progressive degeneration of dopaminergic neurons in the substantia nigra pars compacta of the midbrain and the accumulation of α synuclein-rich eosinophilic inclusions, called Lewy bodies (LB). This pathology is characterized by motor symptoms, such as resting tremor, rigidity, postural instability and bradykinesia. PD symptoms become evident when the dopaminergic neurons decrease to less than 20-40% (Golpich et al. 2015).

These abnormalities result from a complex pathological process that includes oxidative stress, mitochondrial dysfunction, protein aggregation and neuroinflammation that are associated to neuronal loss (DeMaagd and Philip 2015). The PD pathogenesis seems to be ascribed mostly to

environmental factors such as exposure to pesticides and toxins, but also to genetic factors (Golpich et al. 2015).

Notably, GSK-3β seems to participate in PD symptoms by influencing multiple metabolic pathways. The overexpression of α-Synuclein, a presynaptic protein, is believed to promote cellular mortality and synaptic degeneration. In addition, α-synuclein modulates the activation of GSK-3β, enhancing Tyr216 phosphorylation and decreasing Ser9 phosphorylation (Golpich et al. 2015).

GSK-3β is determinant in synuclein aggregation. In fact, GSK-3β phosphorylates the protein (Credle et al. 2015) changing its solubility (Kim, Kågedal, and Halliday 2014).

Dopamine levels are controlled by the D2 receptor and striatal GSK-3β is activated with high dopamine levels. Aberrant activity of the kinase is detected in presence of significantly reduced dopamine levels (Golpich et al. 2015).

In addition, in physiological conditions α-Synuclein may regulate dopamine release. In particular, it is believed to interact with tyrosine hydrolase regulating dopamine precursor synthesis (L-DOPA). Therefore, α-Synuclein availability may indirectly regulate dopamine level (Perez et al. 2002). Interestingly, α-Synuclein accumulates in the Endoplasmic Reticulum (ER), probably leading to ER stress and membrane disruption (Colla et al. 2012). ER stress is associated to inflammatory pathways and oxidative stress that are coupled to GSK-3β elevated activity. GSK-3β is also involved in stress-induced neuronal cell death: this kinase is able to activate caspase-3 and promote apoptosis (Song, Sarno, and Jope 2002).

GSK-3β inhibition is believed to confer protection against MPTP (1-methyl-4-phenyl-1,2,3,6-tetrahydropyridine), 6-OHDA (6-hydroxydopamine) and LPS-induced neurotoxicity (Morales-García et al. 2013; Lei et al. 2011). GSK-3β is implicated in microglial-mediated inflammation and its inhibitors may have neuroprotective effects (Morales-García et al. 2013). Mitochondrial dysfunction also contribute to PD pathogenesis, as mitochondrial GSK-3β is highly susceptible to apoptotic stimuli (Bijur and Jope 2003). Overexpression of the GSK-3β in mitochondria exacerbates the apoptotic effect of other pathways but also decreases ATP production increasing the oxidative stress (King et al. 2008).

GSK-3β is responsible for the phosphorylation of both tau and α-synuclein proteins. Similarly to α-synuclein, also the tau protein seems to be incorporated into the LBs. α-Synuclein directly interacts with tau, promoting its phosphorylation by PKA and mutual aggregation into fibrils.

Amyotrophic Lateral Sclerosis (ALS)

ALS is a lethal progressive neurodegenerative disorder that specifically affects the upper and lower motor neurons in the adult, leading to atrophy of skeletal muscles, spasticity and paresis. ASL prognosis is poor since this pathology leads to death within 5 years from its onset (McGeer and McGeer 2002). Despite most of the cases are sporadic, the 5-10% familiar ALS are characterized by mutations in the gene for the free radical-scavenging metalloenzyme Cu, Zn-superoxide dismutase (SOD1) and in the Tar DNA binding protein 43 (TDP-43) (McGeer and McGeer 2002).

This pathology is characterized by the accumulation of activated microglia and macrophages in the spinal cord and in the motor cortex, leading to massive release of inflammatory cytokines. The neuroinflammation causes the hypertrophy of the gray matter. Instead the white matter cells engorge due to myelin accumulation, losing the ability to perform their function (McGeer and McGeer 2002).

High GSK-3β expression levels are detected in the spinal cord and in the frontal and temporal cortex of ALS patients. Treatment of ALS models *in vitro* and *in vivo* with GSK-3β inhibitors appears to slow the death of motor neurons and the advancement of the degeneration. Probably GSK-3β inhibition may increase cell survival signals that are normally blocked by the kinase via HSTF-1 (heat shock transcription factor-1); an alternative mechanism is the suppression of pro-apoptotic and inflammatory signals such as the release of cytochrome c from mitochondria (Koh, Baek, and Kim 2011).

GSK-3β intervenes in the phosphorylation of the TDP-43 protein, the main component of inclusion bodies in amyotrophic lateral sclerosis (ASL) and responsible of the frontotemporal lobar degeneration (FLTD). GSK-3β inhibition reduces TDP-43 aggregates and their cytosolic accumulation. Moreover, the kinase seems to have a role in TDP-43 nuclear translocation (Moujalled et al. 2013).

6.3. Casein Kinase 1δ (CK-1δ)

Casein kinase 1δ belongs to the Casein kinase family that includes seven isoforms that share a conserved N-terminus, while displaying significant differences in the C-terminal domain (Fish et al. 1995; Rowles et al. 1991; Xu et al. 1995).

The members of this family are mostly involved in the phosphorylation of cytoskeletal proteins such as myosin, tau, spectrin, troponin, ankyrin and α-Synuclein but they also interact with p53 and β-catenin (Behrend et al. 2000; Okochi et al. 2000; Li, Yin, and Kuret 2004).

Since the CK1 family activity modulates essential cell functions such as vesicular trafficking, DNA repair and cell cycle, the levels of these proteins within the cells are highly controlled.

Due to its role in tau processing, an abnormal level of CK1-δ in brain is associated with AD, ALS, PD and other tauopathies (Schwab et al. 2000; Ghoshal et al. 1999; Hu et al. 2003).

6.4. Protein kinase inhibitors

Due to kinases massive involvement in human cellular functions, these proteins have emerged as an important enzyme target for the development of small inhibitors that may be used in the treatment of human diseases (Schwartz and Murray 2011). At present, these drugs are mainly used in cancer therapy. However, there are some compounds used for different pathologies such as tofactinib, that is used in the treatment of rheumatoid arthritis due to its ability to inhibit JAK3, and nintedanib, that inhibits the fibroblast growth factor, successfully contrasting pulmonary fibrosis (Roskoski 2015).

The first protein kinase inhibitor approved for human therapy is Trastuzumab, a monoclonal antibody that inhibits ErbB2 treating ErbB2-positive gastric, breast and gastroesophageal cancers (Roskoski 2014a; 2014b). Subsequently, other large-molecule inhibitors targeting EGFR have been approved for the treatment of metastatic breast cancer (pertuzumab), of colorectal cancer (panitumumab) and of head and neck cancer (cetuximab) (Roskoski 2015).

In 2001 the approval by the FDA of imatinib, the first small molecule inhibitor designed according to the structure of its target, lead to the development of more than two dozens of orally effective compounds such as dasatinib, erlotinib, sunitinib and geflitinib (Figure 6.5).

The assessment of imatinib selectivity for Abl kinase was a breakthrough and opened new possibilities for drugs targeted at the ATP binding site, previously considered not selective due to the high conservation of this moiety throughout the kinome (Zuccotto et al. 2010).

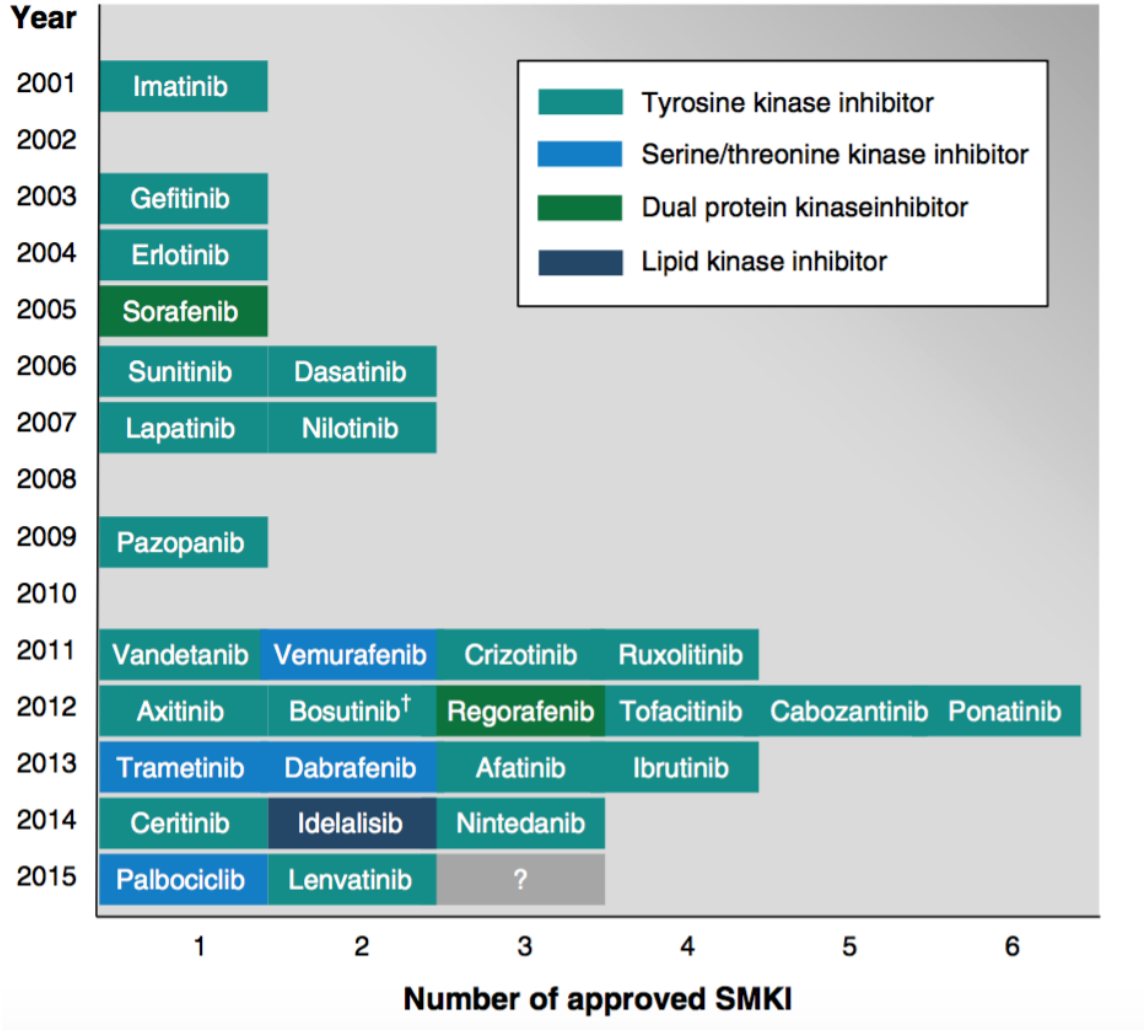

Figure 6.5: Approved KIs until 2015. Drug discovery today 2016

Kinase inhibitors may be classified according to their target binding mode, their binding site and the protein conformation they interact with.

According to the binding mode, kinase inhibitors may be divided in reversible or non-covalent binders, and irreversible, that covalently bind the protein. In addition, these compounds may interact with the active or inactive conformations of the kinase active site. They may also be divided in ATP-competitive inhibitors that interact with the ATP binding site, non-competitive or allosteric inhibitors and in dual inhibitors that simultaneously bind two sites. Moreover, ATP-competitive inhibitors may be divided in type A, that bind the front and the back cleft and near the gatekeeper residue, and type B, that only interact with the front cleft (Roskoski 2016).

The highly conserved ATP-binding site can be divided in five regions:

1. *Adenine region*: it is a generally hydrophobic pocket with amino acids that establish hydrogen bonds with N1 and N6 nitrogen atoms of ATP adenine ring.

2. *Sugar pocket*: a hydrophilic pocket.

3. *Hydrophobic region I*: is located in the backside of the pocket and is often not occupied by ATP. Its size depends on the gatekeeper residue so, the peculiar characteristics of this region are exploited for the design of selective PK inhibitors (Traxler and Furet 1999).
4. *Hydrophobic region II*: as the hydrophobic region I, this region does not participate in ATP binding. Targeting it may increase inhibitor binding affinity towards the kinase.
5. *Phosphate binding site*: it is exposed to the solvent and due to the presence of not-conserved residues could be targeted to increase inhibitor selectivity. On the other hand, the surface of this region has a minor role in enhancing binding affinity (Traxler and Furet 1999).
The design of selective ATP-competitive kinase inhibitors is complicated by the highly conserved structure of ATP-binding site among kinases. In addition, these inhibitors should compete with the high ATP concentration in the cell ([ATP] = 1-5 mM) (Smyth and Collins 2009).

In parallel with the definition of binding-site regions, inhibitors could be distinguished in different classes (Figure 6.6):

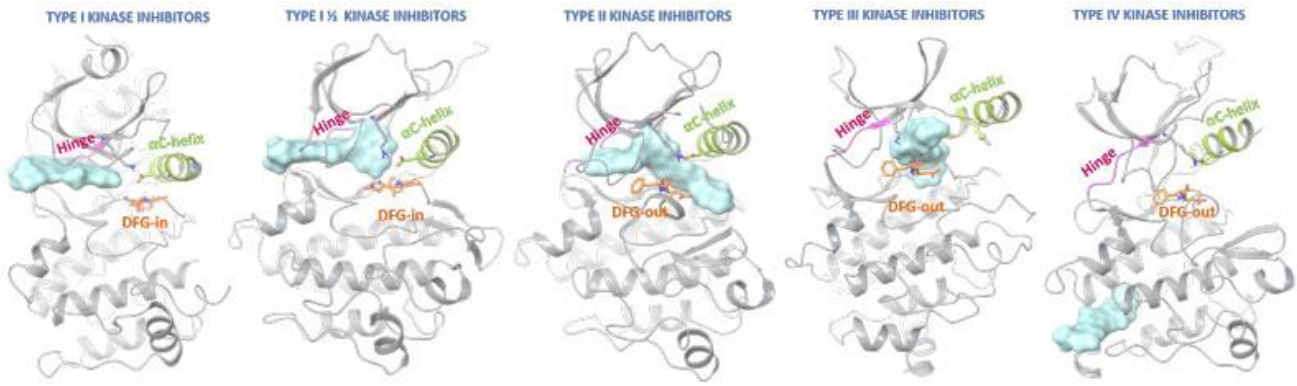

Figure 6.6: Kinase inhibitors classes. From New horizons in next-generation small molecule kinase inhibitors. M. Dobrzanska and K. Gluza. Drug target view,2016.

Type I: This group is constituted by reversible ATP-competitive inhibitors targeting the kinase DFG-in and αC-helix in, or active conformation. In the DFG-in conformation the phenylalanine of the motif packs in a hydrophobic pocket located between the N- and C-lobe allowing the magnesium binding. In the αC-helix in conformation a conserved Glu forms a salt bridge with a lysine residue located in the β3 strand. This conformation promotes the formation of hydrogen bonds between Lys side chain and the ATP phosphates (Modi and Dunbrack 2019). These inhibitors mostly possess a heterocyclic scaffold that forms up to three hydrogen bonds with residues of the adenine-binding region of the ATP pocket. Moreover, functional groups added to the heterocyclic core occupy regions not exploited by ATP in order to improve selectivity and potency (Zuccotto et al. 2010).
Type I 1/2: these inhibitors reversibly bind the DFG-in and αC-helix out conformations. This category of compounds is further divided in type IA that extend out of the ATP-binding site towards the back

cleft and in type IB that only interact with the front cleft. The result of this diverse interaction is the increased residence time of type-IA inhibitors (minutes to hours) compared to type-IB (seconds to minutes).

Type II: these compounds target the DFG-out conformation (inactive conformation) of the kinase occupying part of the adenine binding pocket and forming hydrogen bonds with the hinge region (Roskoski 2016). In this conformation the Phe moves out from the hydrophobic pocket.

These inhibitors may also be divided in type IIA and IIB according to their binding site. The transition to the inactive conformation promotes the movement of the phenylalanine side chain of the DFG loop towards the ATP binding site in a kinase-specific conformation.

Since the inactive state conformation greatly differs between kinases, type-II inhibitors have shown improved target specificity compared to type-I inhibitors. The most famous example of type-II inhibitor is imatinib (c-ABL inhibitor).

Type III: these inhibitors bind an allosteric hydrophobic region within the catalytic domain near the ATP-binding pocket without interacting with the hinge region, and their binding is therefore unaffected by ATP. These uncompetitive inhibitors are characterized by higher selectivity since they target unique binding sites and regulatory mechanisms (Monod, Changeux, and Jacob 1963). Examples of inhibitors of this class are Trametinib that inhibits MEK and is used in the melanoma treatment and Rapamycin that prevent mTORC1 heterodimers formation interfering with kinase activity. This compound is used to prevent rejection after kidney transplantation and for the treatment of renal cell carcinoma (Duong-Ly and Peterson 2014).

Type IV: these allosteric indirect inhibitors bind kinases outside their catalytic domain interacting with enzyme peculiar sequences (Roskoski 2016).

Type V: this group is constituted by bi-substrate, or bivalent, reversible inhibitors. These inhibitors are formed by two conjugated fragments that target different binding sites. These compounds combine the high affinity and potency of active site binding inhibitors, with kinase selectivity due to their interaction with an enzyme-specific site (Lamba and Ghosh 2012).

Type VI: this group is represented by covalent inhibitors that mostly bind the ATP-binding site. The covalent bond irreversibly prevents ATP interaction with the kinase. The long half-life of this covalent bond maximizes the effectiveness of the inhibitor while reduces the exposure to the drug (Roskoski 2016). For example, afatinib, that belongs to this class, covalently binds EGFR and is used in the Non Small Cell Lung Cancer therapy.

Substrate competitive: these inhibitors target the substrate-binding region that is less conserved than the ATP-binding pockets. Despite the high selectivity, small peptides or proteins designed to compete with the substrate present a low potency (Cohen 2002).

The majority of the TKI's FDA-approved belongs to the first and second class, type-II inhibitors demonstrated a higher selectivity compared to type-I. Whereas allosteric, covalent and double inhibitors types are less used in clinic (Figure 6.7).

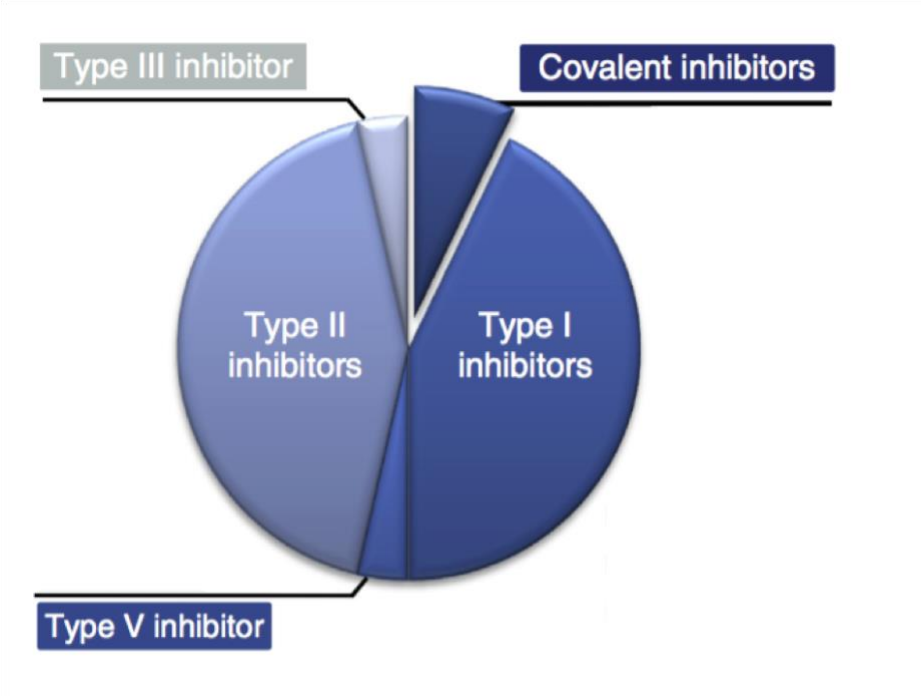

Figure 6.7: Relative abundance of KI's inhibitors FDA-approved. From Drug discovery today 2016

Irreversible inhibitors

Covalent binders share common features such as a heterocyclic core structure (driving portion), generally resembling the reversible ATP-competitive inhibitors. The heterocycle carries an electrophilic "warhead", such as Michael acceptors that covalently interact with a specific cysteine or lysine residue in the target protein (Liu et al. 2014).

Generally, the mechanism of covalent inhibitors is expected to proceed with an initial non-covalent interaction between the molecule and the enzyme, that promotes the small molecule correct orientation within the ATP-binding pocket. Once properly oriented, the warhead-mediated nucleophilic group attacks the kinase creating a new covalent bond (Roskoski 2016).

Irreversible drug-target interaction may potentially cause severe toxicity and long-lasting off-target activity. On the other hand, the long-lasting drug residence within the active site of the kinase may extend the therapeutic activity of the molecule even with low compound concentrations. However, covalent kinase inhibitors with well-balanced molecular recognition and reactivity should provide efficacy, selectivity and the safety margins required for regulatory approval.

6.4.1.GSK-3β Inhibitors

The discovery of GSK-3β key roles in metabolic pathways regulation increased interest in the pharmacologic inhibitors of this kinase.

GSK-3β Inhibitors in Alzheimer's disease

Lithium chloride is one of the first GSK-3β inhibitors used in the treatment of AD for its ability to decrease tau phosphorylation (Tajes et al. 2008). However, lithium treatment has not been associated with clinical benefits in mild AD patients (Hampel et al. 2009).

Other more selective GSK-3β inhibitors were developed for the treatment of this neurodegenerative disorder such as SB216763 (Deng et al. 2014). This compound decreases tau phosphorylation and impacts NMDA inhibiting intracellular Ca^{2+} accumulation (Deng et al. 2014).

Another potential group of drugs are FLZs (N-[2-(4-hydroxy-phenyl)-ethyl]-2-(2,5-dimethoxy-phenyl)-3-(3- methoxy-4-hydroxy-phenyl)-acrylamide). These compounds are synthetic cyclic analogues of natural squamosamide and are able to cross the blood-brain barrier (BBB). Furthermore, they protect against Aβ oligomer production, decrease Tau phosphorylation, increase inactive, Ser9-phosphorylated, GSK3β amounts and improve spatial memory in an animal model of AD (Bao et al. 2013). Other therapeutic molecules are MTs – multitarget drugs that modulate not only GSK3β, but also BACE1 (asparthyl protease-β-secretase), that induces Aβ oligomers production. MTs are effective even in micromolar concentration, are able to cross BBB and decrease NO synthesis, protecting neurons (Prati et al. 2015).

TDZD (thiadiazolidinediones) derivatives such as tideglusib, are ATP-noncompetitive irreversible inhibitors of GSK-3β which stimulate Ser9 phosphorylation. They are effective in lowering Tau activity and amyloid deposition, and in improving spatial memory. Due to its neuroprotective effects (Domínguez et al. 2012; Serenó et al. 2009), tideglusib was examined in clinical trials on AD patients in combination with cholinesterase inhibitor treatment, resulting in high tollerance levels (Del Ser et al. 2013). An additional important family of anti-AD drugs are paullones, including kenpaullone that enhances neurogenesis in hNPC (human neural progenitor cells) and protects neurons against consequences of GSK-3β hyperactivation (Petit-Paitel et al. 2009).

The family of malemides may be useful in the treatment of AD, as these compounds are ATP-competitive GSK-3 inhibitors. SB415286 is a highly selective inhibitor and causes Tau dephosphorylation (Silva et al. 2014; Cross et al. 2001). Indirubines drugs also target GSK-3β, this family include hymenialdisine and menzamine alkaloids. However, they have only been examined *in vitro* or in animal models of AD. Resveratrol and berberine are natural nutraceuticals

that are effective on the PI3K/PTEN/AKT/mTORC1/GSK3 pathway. While the activity of reservatrol is not detectable in AD patients and it has several side effects (Turner et al. 2015), barberine shows a reduction in Aβ levels in mouse model. In addition, this compound improves long-term spatial memory and ameliorate cognitive deficits without detectable side effects (Sundara et al. 2012).

Despite numerous trials, only a few drugs are currently available for AD treatment. Among these, memantine is the only non-competitive NMDA receptor antagonist approved for clinical use. NMDA receptors promote GSK-3 calpain-mediated truncation leading to its activation; memantine inhibits this process (Goi-Oliver, Avila, and Hernández 2009). Moreover, this drug increases inhibitory phosphorylation rate on both GSK-3 isoforms, causing their inactivation and enhancing long term potentiation in hippocampal slices (De Sarno et al. 2006; Turner et al. 2015). Other drugs administered to AD patients are the acetylcholinesterase inhibitors (AChEIs): donepezil, galantamine and rivastigmine (Tayeb et al. 2012). Except rivastigmine, AChEIs protect neurons against Aβ oligomer toxicity and increase their viability by impacting GSK-3 activity throughout the PI3K/AKT pathway. However, most of the acetylcholinesterase inhibitors cause gastrointestinal side effects, such as nausea or diarrhea. Unfortunately, both AChEIs and memantine do not alter AD final outcomes (Tayeb et al. 2012).

GSK-3 Inhibitors in Parkinson's disease

The mechanism of neurodegeneration in PD is poorly understood and current therapies address symptoms instead of preventing neuronal loss. PD's patients have enhanced GSK-3 levels in the brain. Moreover, both active and inactive forms of GSK3β are co-localized with α-Synuclein in Lewy bodies (Noh et al. 2009). GSK-3 isoforms contribution to the pathomechanism of PD is unclear. Only a few GSK-3 inhibitors have reached clinical trials in human subjects, among which tideglusib, LY2090314, enzastaurin and lithium chloride (Pandey and Degrado 2016). Evidences from both animal and in vitro models demonstrate that targeting GSK-3 signaling could be beneficial in preventing neuronal loss in PD (Duda et al. 2018). Inhibition of GSK-3β activity with LiCl or kenpaullone in mice avoided MPP+ induced cell death by blocking changes in the mitochondrial membrane potential and preventing subsequent caspase-9 and -3 activation (Petit-Paitel et al. 2009). GSK-3β roles were identified in phosphorylating Baxα proapoptotic protein, promoting its translocation to mitochondria, oligomerization and pore formation that, in turn, allows cytochrome C transfer to the cytoplasm. Cytochrome C release causes caspases cascade activation that leads to apoptosis (Duda et al. 2018).

In addition, decreased activity of the ubiquitin-proteasome system seems to play a role in PD. In this regard, GSK-3β synphilin-1 phosphorylation may alter its ubiquitination and degradation and thus determine the protein aggregation rate in vitro. This process is suppressed by selective GSK-3β inhibitors SB415286 and kenpaullone as well as by lithium chloride (Avraham et al. 2005). Altogether, altering GSK-3 activity may affect α-Synuclein and synphilin-1 intracellular deposition as well as mitochondrial and ER functions, thus limiting neuronal degeneration rate.
Dopamine D2 receptors may upregulate GSK-3, down-regulating PI3K/AKT activity. Moreover, GSK-3 activity is correlated with dopamine mediated locomotor behavior (Beaulieu et al. 2004). Beneficial aspects of LiCl pharmacological therapy may be partly due to counteraction of lithium and D2Rs on AKT/GSK-3 signaling cascade (Beaulieu et al. 2004). Some psychotic drugs, such as D2R antagonists, affect AKT activity and decrease GSK-3 in the mouse brain (Li, Rosborough, et al. 2007). Therefore, dopamine-based therapies may affect AKT/GSK3 cascade. Indeed, the dopamine receptor D1/D2 family agonist bromocriptine, which is clinically used for PD therapy, regulates GSK-3 by up-regulating AKT activity via nuclear factor-E2-related factor-2 (Nrf2) (Hee et al. 2008). In the late stage of PD, degeneration of cholinergic, serotonergic and noradrenergic neurons takes place. In this regard, serotonin 5-HT1A and muscarinic receptors activation down-regulate GSK-3 activity (Li, Zhu, et al. 2007; De Sarno et al. 2006). Thus, in brain, GSK-3 activity in PD may partly depend on the synaptic transmission affecting the interactions with multiple intracellular signaling proteins.

6.5. SR90 inhibitor

As previously mentioned, GSK3β has fundamental roles in neurodegenerative disorders and together with CK1δ participate to PD and AD pathogenesis.
According to these findings, the dual GSK-3β/CK-1δ inhibitor SR90 was synthesized by the group of Dr. Stephanie Federico of the University of Trieste (Figure 6.8).

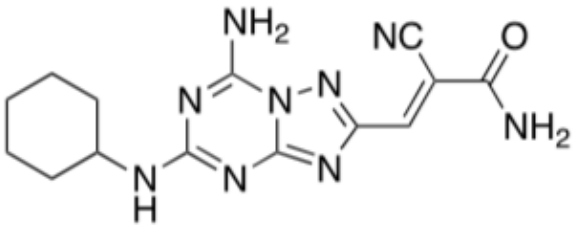

Figure 6. 8: SR90 inhibitor chemical formula

This compound was synthesized starting from the adenine-like [1,2,4]triazolo[1,5-a][1,3,5]triazine (TT) nucleus and its substituents were optimized in order to address both kinases.

Particularly, the 2-cyanoacrylamide group within the TT scaffold was inserted to mediate a reversible interaction with the GSK-3β, whereas an amido moiety was inserted to promote the interaction with CK-1δ.

In computational modelling simulations, the 3-(7-amino-5-(cyclohexylamino)- [1,2,4]triazolo[1,5-a][1,3,5]triazin-2-yl)-2-cyanoacrylamide derivative underwent molecular docking revealing 12 possible orientations of the compound towards GSK-3β Cys199, suggesting a mixed ATP-competitive/non-ATP-competitive interaction. Regarding CK-1δ, this compound seemed to operate with an ATP-competitive inhibition. Interestingly, this compound displays a comparable potency against the two kinases: SR90 has IC_{50} of 0.17 μM and 0.68 μM towards GSK-3β and CK-1δ, respectively.

This compound was tested in order to determine its ability to cross the Blood Brain Barrier with a PAMPA-BBB assay (parallel artificial membrane permeation assay-blood brain barrier). SR90 shoed a mild permeability (1.34 10^{-6} cm s^{-1}), probably due to the compound polar moieties.

However, SR90 has a neuroprotective potential, as proved by *in vitro* models of PD. In fact, it revealed neuroprotective potential on rat PC12 pheochromocytoma cells treated with (4- phenyl-1-methyl-1,2,3,6-tetrahydropyridine (MPTP) or 6- hydroxydopamine (6-OHDA)) neurotoxins. Moreover, this double GSK-3β/CK-1δ inhibitor showed no cytotoxicity up to 10 μM concentrations (Redenti et al. 2019).

Its potential in neuroprotection, double inhibition activity and lack of toxicity makes it a potential lead compound for the design of a new class of GSK-3β/CK1δ double inhibitors.

7. AIM OF THE WORK

This study was performed at the Structural Biology Laboratory of the Elettra Synchrotron (Trieste), in the group of Dr. Paola Storici and in collaboration with Dr. Stephanie Federico of the Department of Chemical and Pharmaceutical Sciences of the University of Trieste.

The aim of this work was the structural characterization of the binding mode of the SR90 inhibitor, a compound synthesized by Dr. Sara Redenti during her PhD in Dr. Federico's laboratory, to the Glycogen Synthase Kinase 3β, obtained by X-ray diffraction on protein crystals. Together with the proof of concept on SR90 interaction with the kinase, this project was also aimed at providing a structural-based tool for the investigation of other inhibitors targeted against this kinase. Providing crystallographic evidences on the interaction of a compound with Glycogen Synthase Kinase 3β could direct the modifications on molecular groups to increase their selectivity and potency.

8. RESULTS AND DISCUSSION

8.1. DNA manipulations

Numerous GSK-3β structures are available on the PDB (Protein Data Bank (www.rcsb.org)) both in the apo form and complexed with a ligand. However, despite the full length kinase was used in most of the crystallization tests that led to structural entries on PDB, the N- and C-termini are often absent in the electron density map due to the high flexibility of these segments (Dajani et al. 2001; Bertrand et al. 2003). Moreover, the resolution of the published GSK-3β structures is generally low, around 2.5/3 Å, probably due to disordered regions that decreased the data quality. In order to obtain a higher resolution, three different constructs were cloned: the full length (1-420) and two truncated forms delimited by residues 25-393 and 35-386, in which the flexible domains that may hamper the crystallization process were removed (Figure 8.1).

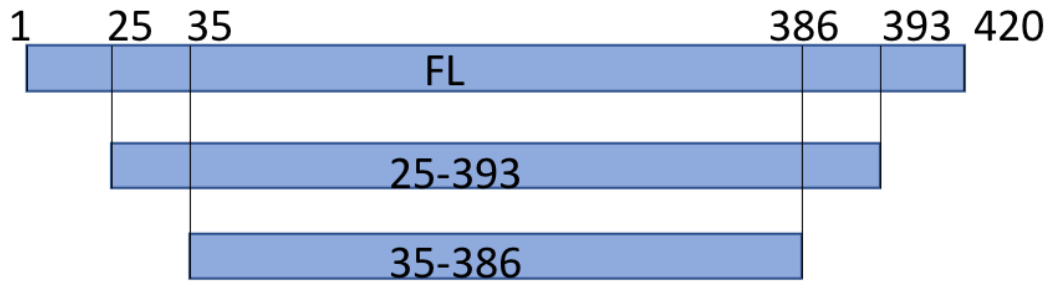

Figure 8.1: Schematic representation of the constructs cloned

The constructs were PCR amplified from human GSK-3β gene (see materials and methods for PCR protocol) and controlled on 1% agarose gel. The bands in Figure 8.2 correspond to the full length (1260 base pair, bp), to the 25-393 construct (1105 bp) and to the 35-386 construct (1054bp).

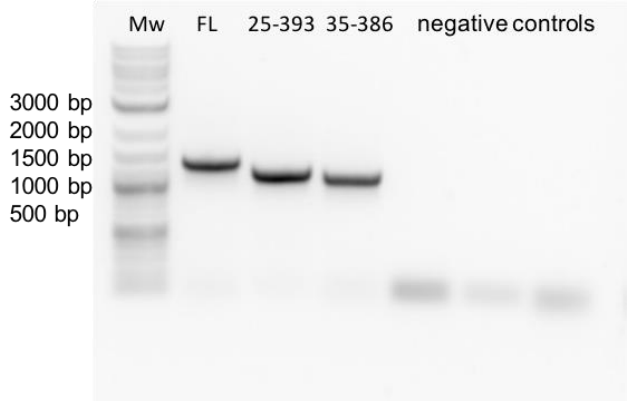

Figure 8.2: 1% agarose gel of PCR amplified constructs. Loading order: Mw, Full Length and truncated constructs 25-393 and 35-386

The constructs were cloned in two different vectors suitable for insect cell protein expression. The plasmids selected were pFB-Bse and pFB-ZB. Both vectors include Ligation Independent Cloning sites.

8.1.1.LIC cloning

In the LIC cloning procedure, the vectors are linearized via digestion with a restriction enzyme (Figure 8.3.1) whereas the insert is amplified with primers that codify for an additional tail (Figure 8.3.2). Afterwards both vectors and inserts are treated with T4 DNA polymerase in the presence of dGTP (vectors) and dCTP (inserts) to create the complementary sticky ends as described in Materials and Methods.

In the subsequent annealing reaction (Figure 8.3.3), the vector and the insert complementary ends interact forming a circular plasmid (Aslanidis and de Jong 1990). The sticky ends sequences ensure the correct insertion of the GOI and prevent the circularization of the empty vector.

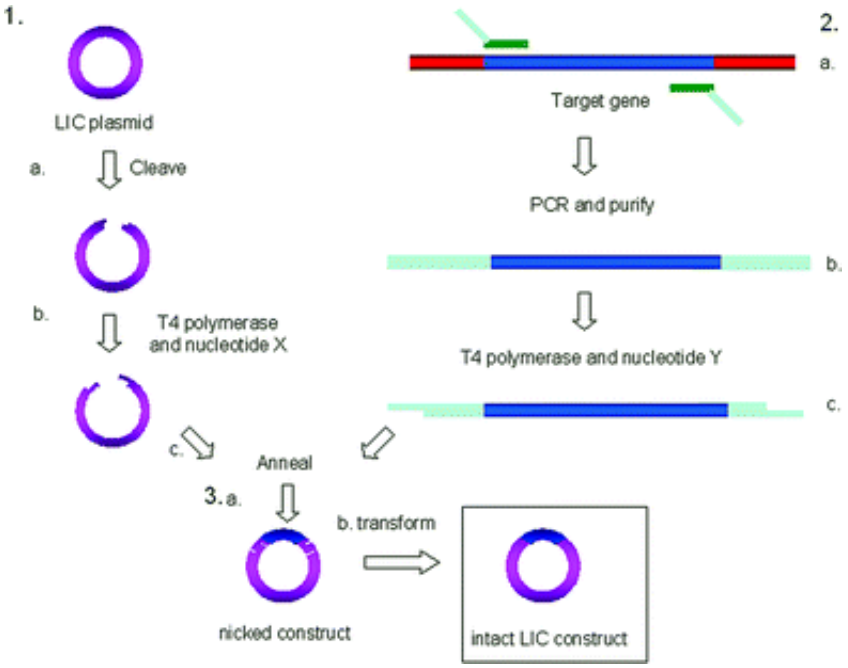

Figure 8.3: Schematic representation of LIC cloning technique. From Org. Biomol. Chem., 2006,4, 1252-1260

The linearized vectors were mixed with the treated inserts for the annealing reaction. The annealing products were transformed in DH5α competent cells and spread on LB agar plates supplemented with ampicillin and 5% sucrose. The sugar was added to the medium to verify the substitution of the SacB gene with the GOI. In fact, the SacB gene codifies for levansucrase that converts sucrose to levan in the presence of sucrose. The accumulation of this product results lethal in gram negative bacteria (Reyrat et al. 1998). The positive clones were sequenced.

8.1.2. Bacmid generation

Baculoviruses are double-strand DNA viruses that infect insects. In the first stage of infection the viral products are separated from the host cell cytoplasm by host-derived membranes. In the late stage of infection, the virus produces a polyhedrin crystalline matrix that substitute the host membrane and protects the viral core from the environment. In the BEVS system, the polyhedrin gene is replaced with the GOI, thus inducing the transcription of the gene in the late infection stage, under the control of the plyhedrin promoter. The elimination of polyhedrin increases safety, since the laboratory-produced viruses are not able to persist in the environment.

The Bac-to-Bac system is based on the site-specific transposition of the selected gene into a bacmid. Initially, the GOI is cloned in a vector containing the transposition sites, then DH10Bac *E. coli* mediate the cassette transposition into the baculovirus genome (Stacey and Davis 2007).

The sequenced plasmids were transformed in EMBacY DH10Bac *E. coli* for GSK3-β gene transposition in bacmid DNA (for full protocol see Materials and Methods). The transposition results were verified with a control PCR.

Table 8.1 reports the constructs cloned and the control PCR results.

Table 8.1: GSK3-β constructs cloned

Construct name	length	Sequencing result	Bacmid generation
pFB-ZB+ GSK-3β FL	6250 bp	✓	✓
pFB-ZB+ GSK-3β 25-393	6095 bp	✓	✓
pFB-ZB+ GSK-3β 35-386	6044 bp	✓	✓
pFB-Bse+ GSK-3β FL	6063 bp	✓	✓
pFB-Bse+ GSK-3β 25-393	5908 bp	✓	✗
pFB-Bse+ GSK-3β 35-386	5857 bp	✓	✓

Unexpectedly, the pFB-Bse GSK-3β 25-393 construct was not efficiently transposed into the bacmid. The procedure was repeated but without results. This particular cDNA sequence seemed to be unstable, and therefore the transfection of GSK-3β 25-393 was only performed with the construct in pFB-ZB vector.

8.1.3. Insect cells transfection

For initial transfection and virus generation a Sf9 cell line was used. Since High 5 cells do not ensure a good virus yield, this cell line was used only for protein expression (Stacey and Davis 2007).

As demonstrated by Figure 8.4, P0 virus was generated inoculating 150 µl of the transfection mix (formed by bacmid DNA, FuGene® reagent and insect cell medium) in 3 mL of $0.5x10_6$ Sf9 cells (see Materials and Methods). The cells were incubated in adhesion for 55/60 hours at 27°C. The schematic representation of the six-well plates with the transfected sample is depicted in Figure 8.4.

After the incubation the wells were analyzed under the microscope to detect eventual bacterial contaminations.

In non-contaminated samples, P0 virus was collected via centrifugation and stabilized with 2% v/v of FBS. 150 µl of the obtained virus were used for the infection of $1.6x10_6$ Sf9 cells. The culture was incubated in adhesion for four days at 27°C to obtain the first amplification of the virus. The P1 viral stock was recovered via centrifugation and stabilized with 10% FBS. The cells pellet was stored at -80°C for a Western Blot. The second amplification of the virus, P2, was obtained infecting 50 mL of $1x10_6$ cells/ml Sf9 cells with 200 µl of P1 stock. The culture was incubated in 200 mL flasks for 4 days at 27°C under agitation.

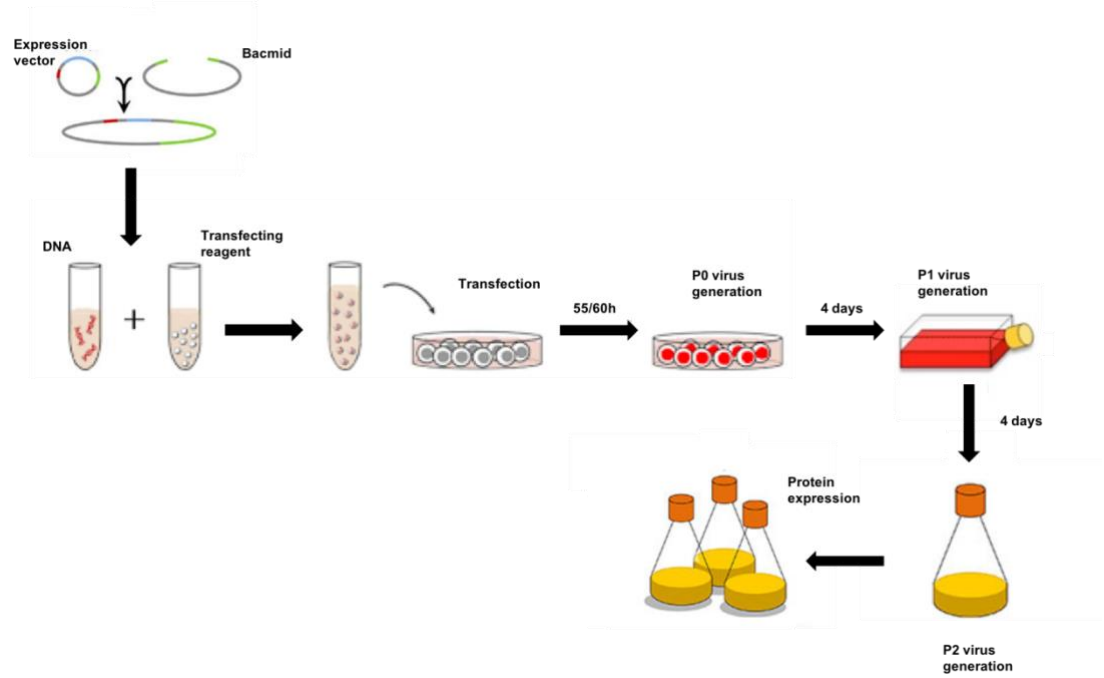

Figure 8.4: Schematic representation of the transfection procedure

Amplification steps were performed to increase virus titer and potency.

The activity of P2 virus was monitored observing cell viability and diameter with Scepter Pipette (Merk). The detection of a high apoptotic peak denoted an excessive activity of the virus that lead to unwanted cell lysis. Also, cell number and diameter gave an information on the stage of the infection: an increased diameter and low cell density indicate virus replication inside the cell, while low diameter and high cell density denote low viral activity (Üstün-Aytekin et al. 2014). During the late stage of infection, Sf9 cells diameter reached 18/20 μm. At this point the P2 virus was collected, stabilized with 10% FBS and stored at 4°C until use. Infected cells with a high density and a diameter of 15/16 μm indicate a non-viable virus. In this case, the cells were discarded, and the virus was amplified again starting from P1 stock.

Western Blot

The WB technique allows the identification of the protein of interest within a mixture using a specific antibody. In this work an anti-His that recognized the tag added at the N-terminus of GSK-3β was used. The WB was performed on the Sf9 cells from the P1 virus amplification step to detect protein production. For all the constructs, thawed cells were lysed by adding 1 mL of lysis buffer and subsequently sonicated for 15", with 5" sonication and 5" stop at 50% amplitude using SonoPlus sonicator (Bandelin). 50 μg/mL DNase and 5 mM $MgCl_2$ were added to the lysed cells, and the mixture was incubated for 10' at room temperature. After the incubation, the sample was centrifuged at 16000xg for 20' at 4°C. 15 μg of the total extract and the supernatant of each construct were loaded on a 12% SDS-PAGE gel for the WB analysis (see Materials and Methods for WB protocol). Nitrocellulose was developed according to standard protocol and the bands corresponding to GSK-3β were detected on the membrane confirming GSK-3β expression.

8.2. Small scale test expression

A small-scale test expression was performed on GSK-3β to determine the best expression conditions. In 24-deep well plates, 2 mL of $1x10^6$ cells/ml were infected with P2 virus. In this experiment two cell lines, Sf9 and High5, and three concentrations of virus, referred to as multiplicity of infection (MOI), were tested. Virus concentration increased 10-folds from one MOI to another so, MOI 2 concentration was 10-folds MOI 1 concentration and 1/10 of MOI 3.

The preliminary test was performed by incubating the infected cells for 72 hours at 27°C under agitation. After the expression, the cells were harvested via centrifugation, lysed and purified in NiNTA columns as described in Materials and Methods. Analyzing the results, it was determined that the Sf9 cell line was not appropriate for GSK-3β expression since the protein was almost undetectable

in the SDS-PAGE gel. The test expression of the FL construct was performed by another PhD student of the Structural Biology Laboratory. As shown in Figure 8.5, in H5 cells the both pFB-ZB and pFB-Bse GSK-3β FL constructs were efficiently expressed with a 3-days expression and a MOI of 2. Comparing the lanes corresponding to constructs, while a single band at higher molecular weight is obtained for the pFB-ZB construct, two bands at a lower molecular weight can be observed in pFB-Bse, suggesting a partial degradation of the kinase. Due to the probable construct instability, the subsequent experiments on the FL were performed using pFB-ZB GSK3-β FL.

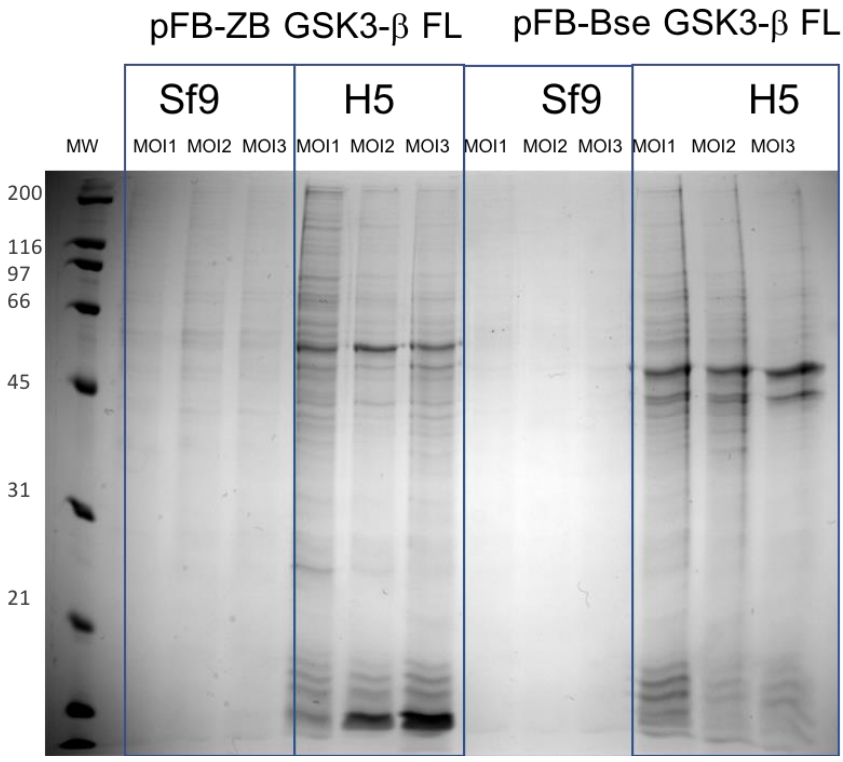

Figure 8.5: Test expression on GSK FL. Gel by Valentina Piretti

Conversely, in H5 cells GSK-3β 35-386 was more efficiently expressed in the pFB-Bse construct, with clearly detectable GSK-3β band in both MOI 1 and 2 lanes (Figure 8.6). However, in this case the MOI 3 sample displayed no protein on the gel, possibly indicating an excess of virus that prevents protein expression and causes cell lysis.

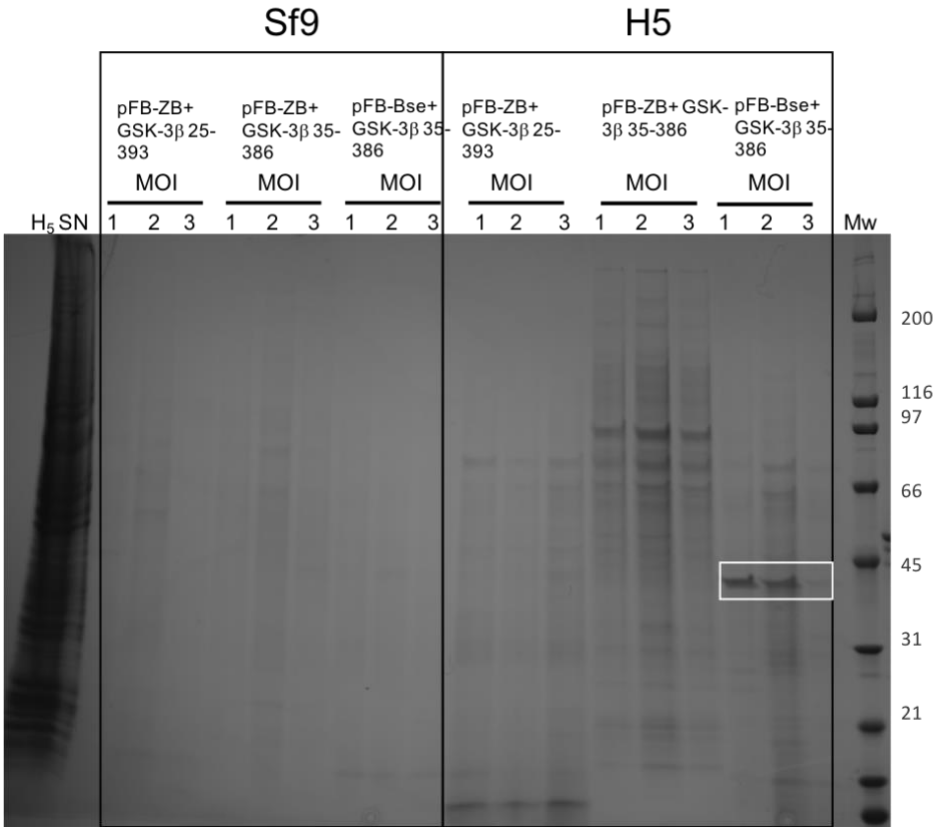

Figure 8.6: Test expression on GSK3-β 25-393 and 35-386. GSK3-β in the white box

To optimize the expression conditions of the shortest construct, an analog test expression was set up with a 48 hours incubation, using only H5 cells.

In this test, the GSK3-β 35-386 construct in pFB-ZB and the 25-393 sample that was poorly expressed in the 3-days test were also included to determine if the low expression was caused by an excessive virus strength.

48h-test expression was performed, and the samples were purified following the same procedure used in the previous experiments. The gels (Figure 8.7) show that pFB-Bse GSK-3β 35-386 was efficiently expressed in 48 hours with a MOI of 1.

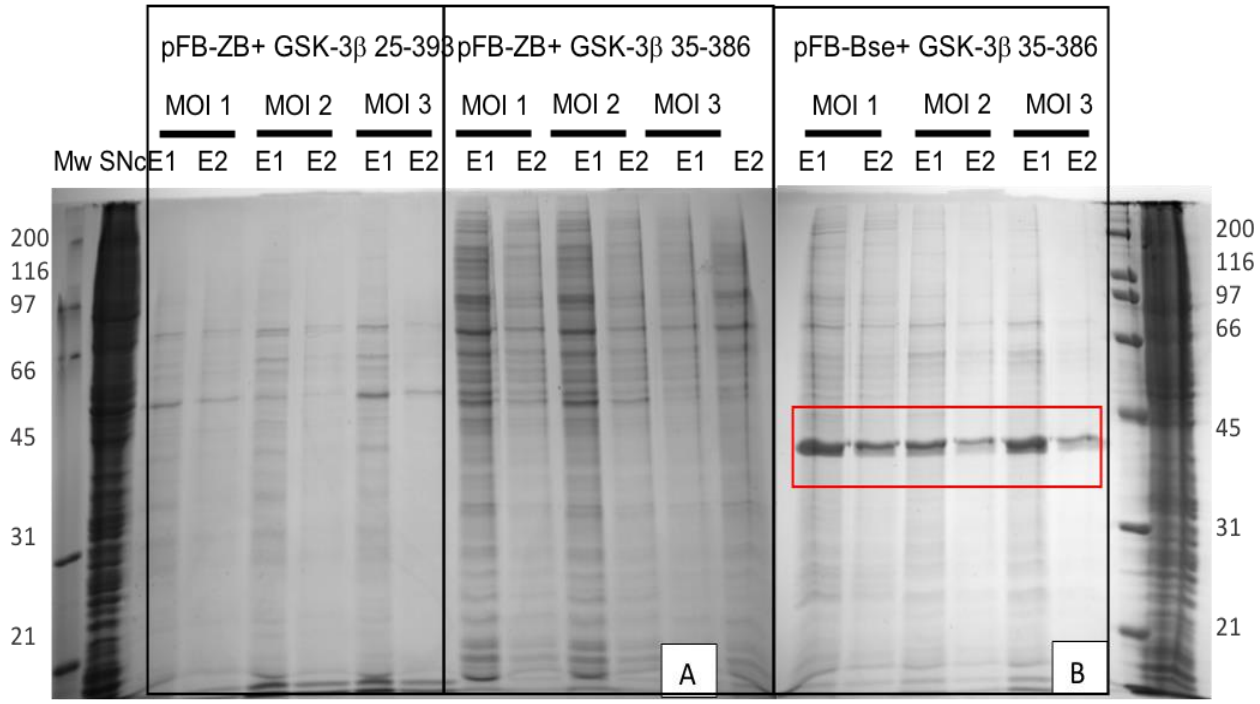

Figure 8.7: SDS-PAGE gels of 48h-test expression. Gel A: Mw, Control SN, E1 and E2 of 25-393 construct at MOI1, MOI2 and MOI3. In the last six lines pFB-ZB 35-386 samples were loaded with the same order. Gel B: E1 and E1 of the three multiplicity of infection of pFB-Bse 35-386.

GSK3-β 25-393 construct demonstrated to be problematic in both the selected vectors since the pFB-Bse construct was not transposed and the pFB-ZB one was not expressed. This suggested an intrinsic instability of the cDNA sequence that may be recovered by changing the vector of modifying the cDNA with other cloning procedures. However, only the more promising constructs were used in further experiments.

Test expression results are summarized in Table 8.2.

Table 8.2: Test expression results

Construct	Expression
pFB-ZB+ GSK-3β FL	✓
pFB-ZB+ GSK-3β 25-393	✗
pFB-ZB+ GSK-3β 35-386	✗
pFB-Bse+ GSK-3β FL	✗
pFB-Bse+ GSK-3β 35-386	✓

Expression conditions:

- pFB-ZB+ GSK-3β FL: 3-days expression with MOI 2
- pFB-Bse+ GSK-3β 35-386: 2-days expression with MOI 1

Repeating the experiments, a baculovirus decrease in potency and vitality was noticed. The virus short life could be caused by the GSK-3β sequence instability that was especially evident on the 25-393 construct but seemed to be common to all constructs. In fact, both FL and 36-386 viruses were not viable after less than one month. Therefore, prior to every large-scale expression, a small-scale test was performed to verify the viability of the virus in order to use the proper MOI during large scale expression or, when the virus was not viable, to prepare a new P2 stock.

8.3. Large scale expression and purification

According to the previous experiments, a 3-days expression was performed for the full length construct and 2-days incubation for the 35-386 construct using the freshly prepared virus. Large scale expression protocol is reported in Materials and Methods.

8.3.1.pFB-Bse GSK-3β 35-386

From the small-scale experiments, the truncated construct seemed to be more stable than the full length. For this protein, a large-scale preparation was purified to set up crystallization trials.

$4.5x10^9$ GSK-3β 35-386 expressing cells were resuspended in 150 mL of lysis buffer and filtered with gauze prior to homogenization. This step resulted essential to reduce cell aggregates that were not efficiently dispersed by pipetting during resuspension. These aggregates tend to clog the homogenizer hampering proper cell lysis. Filtration was preferred to sonication prior to homogenization in order to prevent an excessive oxidation caused by the ultrasounds. Lysed cells were then centrifuged at high speed to remove unlysed cells and organelles. The supernatant of the high-speed centrifugation was loaded on 1 mL of NiNTA resin. The fractions of the IMAC purification were loaded on SDS-PAGE gel to determine the eluates to pool for the IEX (Figure 8.8).

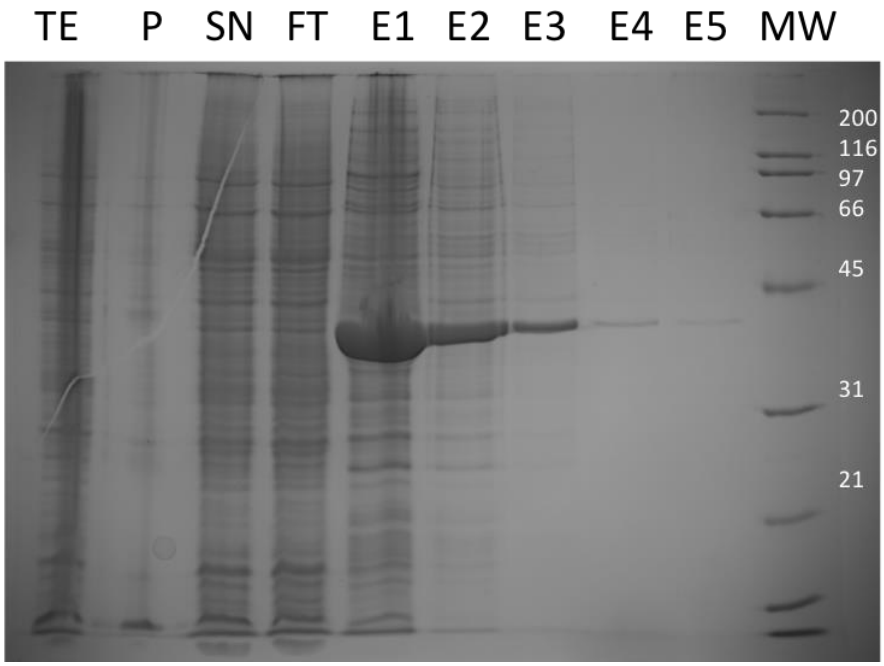

Figure 8.8: 12% gel of 35-386 construct purification. Loading order: TE, P, SN, FT, elutions and Mw

In this case, the first three eluates were pooled and diluted 10 folds to be injected in an IEX column. The cation exchange chromatography was performed immediately after the IMAC to prevent protein degradation. In fact, a degradation was observed in GSK-3β samples dialyzed overnight in an Imidazole-free buffer prior to IEX. Probably, the protein did not tolerate long incubations in presence of imidazole.

The IEX method was optimized to better separate the protein from contaminants. Initially, a 30 mM-to-1 M salt gradient was performed in 20 CV to determine the salt concentration that promotes GSK-3β elution from the column. Then, the method was changed to allow a better separation of the peaks. In the final protocol, a 30 mM-to-260 mM NaCl gradient was performed in 20CV, followed by a 5 CV step at the final concentration and a final gradient to 1M salt in 2CV

In the chromatogram, three peaks were identified, corresponding to different phosphorylated forms of GSK-3β (data not shown) (Figure 8.9). The main peak was isolated and used for the following experiments. Another group that worked in parallel on the FL construct characterized the phosphorylation pattern on the IEX peaks revealing that the main peak corresponds to the unphosphorylated form of the kinase. Comparing the chromatograms, the main peak of GSK-3β 35-386 was also attributed to the unphosphorylated state.

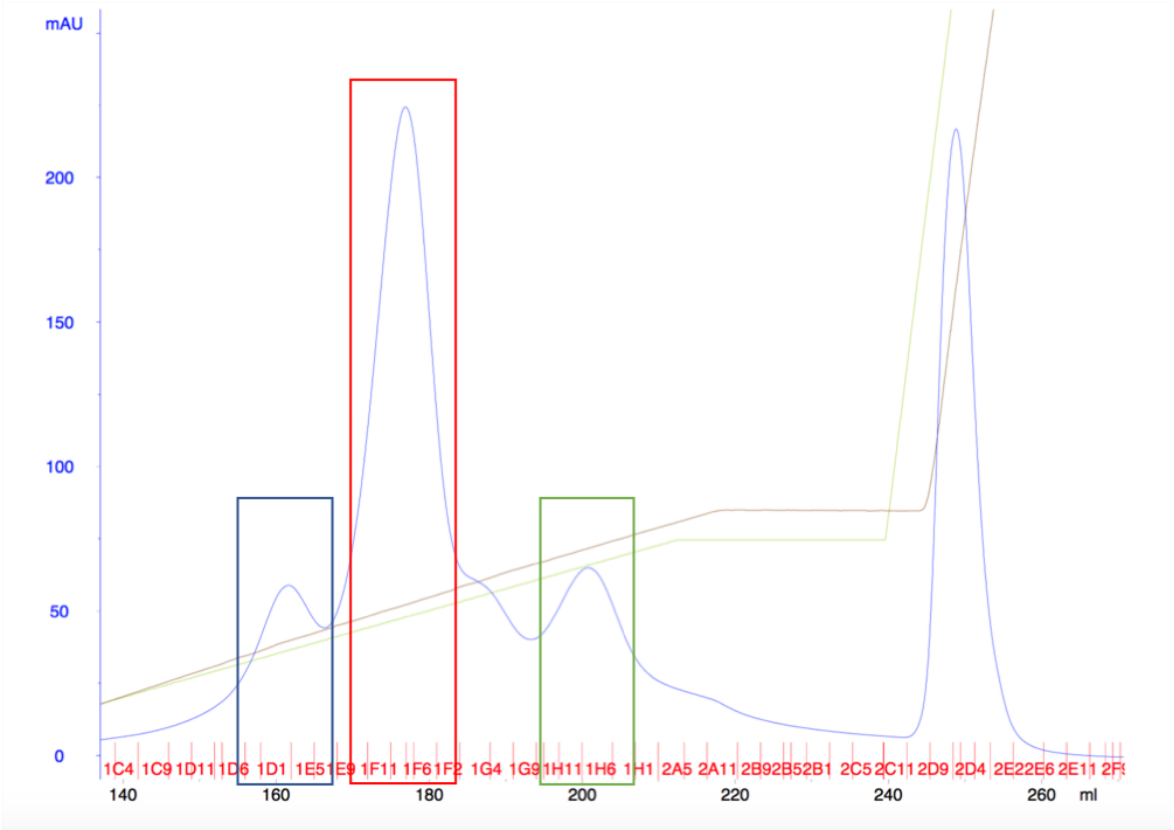

Figure 8.9: IEX peaks. The main peak was used for the following experiments

The IEX fractions corresponding to the main peak (red box) were loaded on 12% gel to verify the sample purity (Figure 8.10).

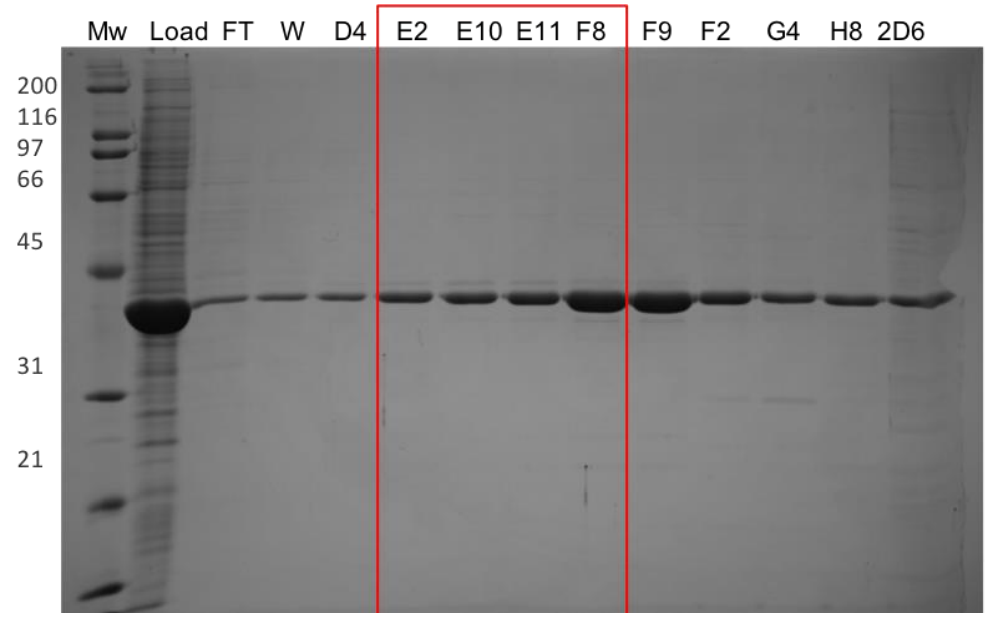

Figure 8.10: 12% gel of IEX on 35-386 construct. Loading order: Mw, Load,FT, W, elution fractions

From the gel, the high purity and quality of the protein sample was verified. Therefore, a further purification step with Size Exclusion Chromatography was deemed unnecessary and was avoided to reduce the amount of sample lost during this procedure.

The fraction corresponding to the main peak were pooled together and dialyzed overnight in TEV buffer with 1/10 of TEV protease to remove the His tag.

The cleaved protein was purified from the protease and the uncleaved kinase using IMAC. NiNTA FT was concentrated and quantified. Dialysis and concentration determined a considerable protein loss. The protein was concentrated to 1.4 mg/mL (38.5 μM) and stored in small aliquots at -80 °C for further use.

Final yield of the main peak (red box in figure 13), peak 2 (blue box) and peak 3 (green box):

Fraction	Total yield	Yield for 1L of culture
Main peak	1.4 mg	0.5 mg/L cell culture
Peak 2	0.75 mg	0.25 mg/L cell culture
Peak 3	0.8 mg	0.27 mg/L cell culture

8.3.2. pFB-ZB GSK-3β FL

In parallel to experiments on GSK-3β 35-386, the work on the full length was continued. Since the protein demonstrated a lower stability compared to the shorter construct in the small-scale expression, a mid-scale purification was performed to investigate the behavior of the protein during purification procedures.

$1.5x10^9$ cells were resuspended in 50 mL of lysis buffer and filtered with gauze before homogenization. The supernatant was loaded in 400 μL of NiNTA resin and incubated 1 hour at 4°C. Both the flow-through and the wash fractions were collected via centrifugation and not by gravity due to the high viscosity of the sample. After the wash the resin was loaded on a column and eluted with 300 mM Imidazole. The eluted fractions were loaded on SDS-PAGE gel to select samples to pool for the following purification step (Figure 8.11).

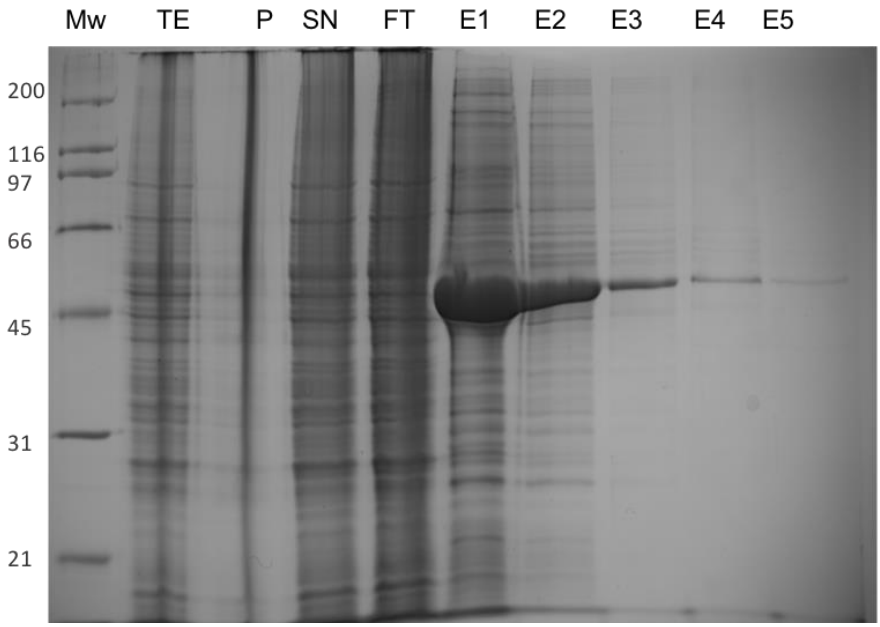

Figure 8.11: 12% SDS-PAGE gel of FL IMAC purification. Loading order: Mw, Total Extract, Pellet, Supernatant, Flow though, and the five eluted fractions.

The E1-E4 eluted fractions were pooled and diluted 1/10 in IEX buffer A to decrease salt concentration prior to injection in HiTrap SP HP 1 mL column with the same method used for the short construct (Figure 8.12).

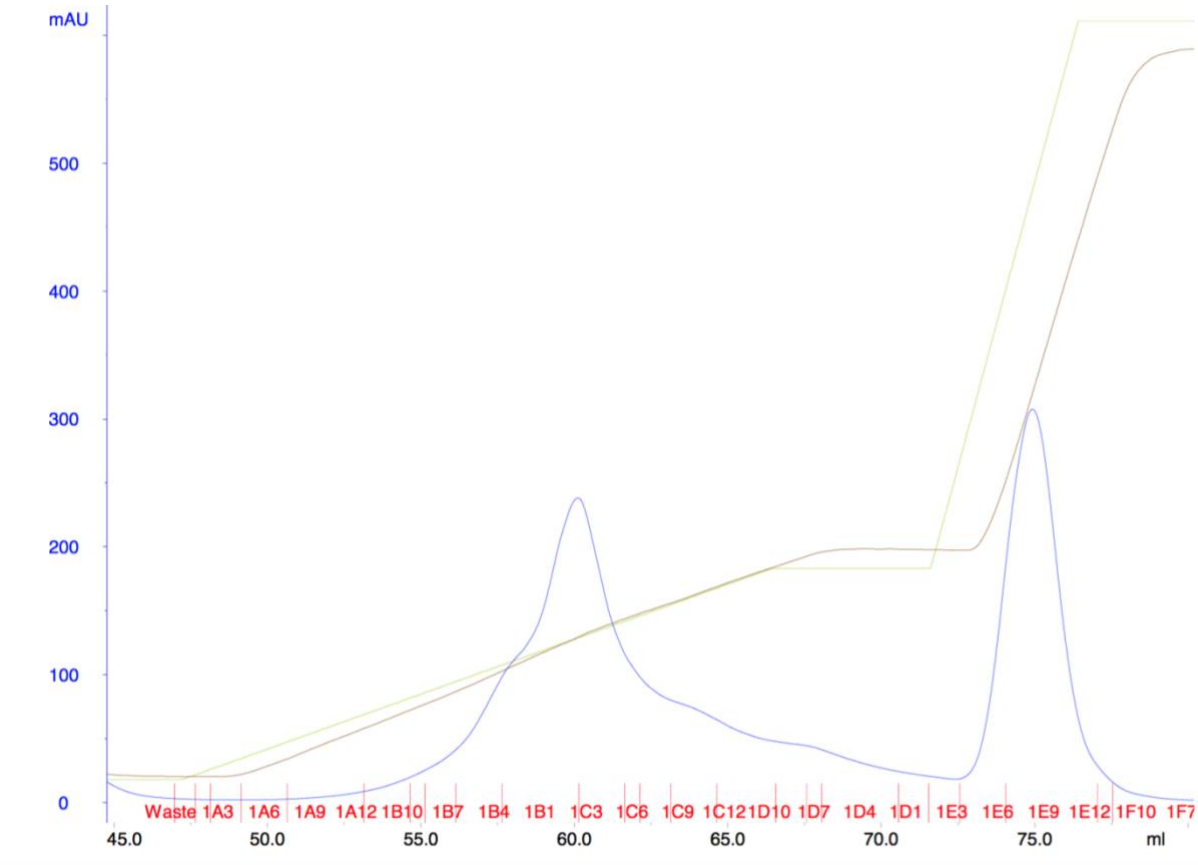

Figure 8.12: IEX of FL construct

The fractions corresponding to the peak were loaded on SDS-PAGE gel to verify the purity of the sample (Figure 8.13).

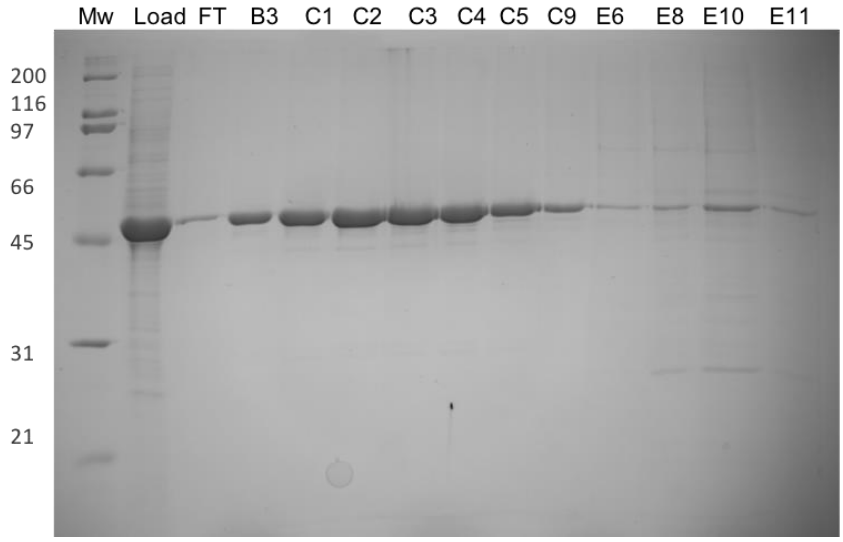

Figure 8.13: 12% gel of IEX fractions. Loading order: Mw, Load, FT, fractions

The fractions corresponding to the center of the peak (C1-C5 fractions) were pooled together and dialyzed overnight in TEV buffer with 1/10 TEV protease to cleave the His tag.

Due to the high purity of the sample, a SEC step was deemed unnecessary and avoided to decrease protein loss.

The cleaved protein was purified from TEV protease and uncleaved GSK-3β via an IMAC step. The properly cut protein was collected in the FT, whereas the TEV and the uncleaved kinase bound to the resins with their His tags and were subsequently eluted (Figure 8.14).

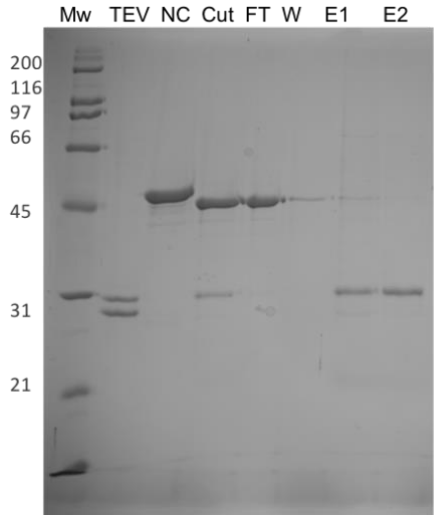

Figure 8.14: 12% gel of the cleaved kinase. Loading order: Mw, TEV, Not Cut, Cut, FT, W, and eluates

When protein sample was concentrated 10 times and quantified with Bradford Assay, a low protein concentration was detected, suggesting a massive protein loss, much higher of the one observed with the short construct. Since the final yield was 0.17 mg, the kinase probably

precipitated during overnight dialysis and concentration step. Thermal Shift Assay was performed in different buffers to find the buffer composition that increased protein stability. However, since the tag removal remained a critical step leading to protein precipitation, it was decided not to cleave the His tag in the following protein preparations. According to results on the crystallization of GSK3-β FL, the kinase can be crystallized even in presence of the His and ZB tags. The pure protein was flash frozen in liquid nitrogen and stored at -80°C.

THERMAL SHIFT ASSAY

TSA provides a fluorescence readout measurement of thermally-induced protein melting. This technique allows the determination of a small molecule or buffer composition effect on protein folding. A variation of protein stability denotes an interaction between the polypeptide and the added component. For this reason, TSA is widely used in drug discovery when High Throughput Screening (HTS) libraries are tested to detect potential hit compounds.

The folding stabilization demonstrated by the increase of protein melting temperature (T_m), may give a preliminary information of inhibitor activity towards the protein. TSA results obtained were in agreement with the enzymatic or radioactive assays, the isothermal titration calorimetry or other assays (Pantoliano et al., 2001).

TSA on GSK-3β FL

The TSA on the FL construct was aimed at determining a buffer composition that increases protein stability, to overcome the problem of protein loss during purification procedures. A limited number of conditions were tested to detect a variation in protein folding stability.

In this experiment the buffer (Tris or HEPES) and its concentration (20mM or 50mM), and the pH (from 7.0 to 8.0) were varied. The concentration of glycerol was also increased to 10%. Buffer compositions are reported in the Table 8.3.

Table 8.3: Buffer tested

	Buffer	NaCl	Glycerol
1	20 mM HEPES pH 7.0	100 mM	5%
2	20 mM HEPES pH 7.5	100 mM	5%
3	20 mM HEPES pH 7.5	150 mM	5%
4	50 mM HEPES pH 7.5	150 mM	5%
5	20 mM HEPES pH 7.5	150 mM	10%
6	20 mM Tris pH 8.0	150 mM	5%
7	50 mM Tris pH 8.0	150 mM	5%
8	20 mM Tris pH 8.0	500 mM	5%

9	20 mM Tris pH 8.0	150 mM	10%
Reference	20 mM Tris pH 8.0	100 mM	5%

The melting temperatures measured on the GSK-3β FL sample are reported in Table 8.4, the standard deviation reported was calculated on the experimental triplicate.

Table 8.4: TSA results

	Melting temperature	Standard deviation
1	41.85°C	± 0.21
2	41.85°C	± 0.21
3	42.60°C	± 0
4	42.00°C	± 0
5	43.20°C	± 0
6	41.47°C	± 0.42
7	41.55°C	± 0.21
8	42.15°C	± 0.21
9	43.05°C	± 0.21
Reference	42.00°C	± 0

The results of this experiment show that an increase of the salt concentration to 150 mM causes an evident decrease of protein stability. The same negative effect was observed using HEPES buffer at pH 7.0 and 7.5 with a 100 mM salt concentration. The negative effect of the pH decrease was minimized by increasing the concentration of NaCl to 150 mM. However, an evident increase in salt concentration to 500 mM did not result in a marked variation of T_m. Interestingly, the addition of 10% glycerol increases protein stability independently on the buffer. According to the result of this experiment, further purifications of GSK-3β FL construct were performed in buffer with 10% glycerol to improve folding stability.

8.4. Characterization of SR90 binding

For the structural characterization experiments of the GSK-3β/SR90 complex the shorter construct was selected due to the higher stability of the structure that would be beneficial for crystallization processes. The complex was initially evaluated with the TSA and subsequently with an activity assay.

8.4.1.TSA on GSK-3β 35-386

This test was performed prior to crystallization trials to determine SR90 effect on GSK-3β folding. A variation of the T_m would denote an interaction between the compound and the kinase that may lead to a stabilization or a destabilization of the folding. GSK-3β 35-386 was incubated in cold room with 3x molar excess of SR90 inhibitor.

Apo-kinase and DMSO-incubated protein were used as controls, as a reference for GSK-3β T_m. Since the inhibitor was solubilized in DMSO, the protein was incubated with the final concentration of DMSO in the sample used for crystallization, 2.8% to evaluate the possible interference of the inhibitor solvent on GSK-3β folding. In Figure 8.15 the melting curves of the samples are reported.

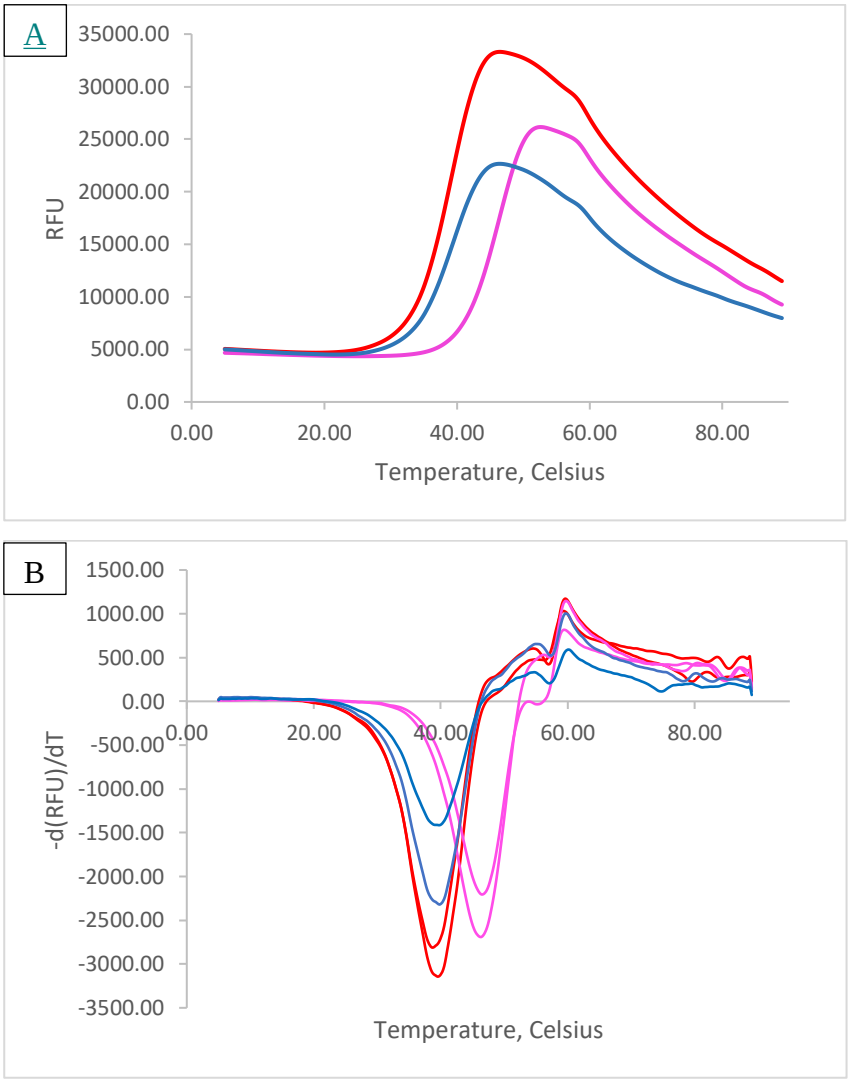

Figure 8.15: TSA melt peak on GSK3-β 35-386. Red curves: Apo, Blu curves: 2.8% DMSO incubated protein and the Pink ones: SR90 incubated protein. Panel A: average of fluorescence intensities, Panel B: derivative results.

The shift of the melting peak indicates a variation in the melting temperature demonstrating the effective binding of the compound.

Table 8.5 reports the results of the experiment: the addition of SR90 inhibitor causes a 7°C increase of the T_m demonstrating a high stabilizing effect of the inhibitor. These data suggested the formation of a strong bond between the protein and the compound, since a weak interactor would influence protein folding only to a limited extent.

As shown in Table 8.5, the DMSO contribution to the increase of GSK-3β 35-386 melting temperature was irrelevant.

Table 8.5: Melting temperatures of the apo GSK-3β 35-386, the DMSO-incubated kinase and the protein incubated with the inhibitor

	Melting temperature	Standard deviation	ΔT
Apo GSK3-β 35-386	39.15°C	±0.64	-
GSK3-β 35-386+ 2.8% DMSO	39.75°C	±0.21	+0.6
GSK3-β 35-386+ SR90	46.35°C	±0.21	+7.2

These results guided crystallization trials: a compound that causes a folding destabilization could interfere with the protein crystallization, whereas in this case the inhibitor could help crystal formation.

8.4.2.SR90 activity and reversibility assays

SR90 IC50

The inhibitory activity of SR90 was preliminarily tested on the commercially available kinase determining an IC_{50} of 0.17 μM. This test was repeated on the GSK-3β 35-386 using KinaseGlo®assay. The phosphorylation activity of the kinase was measured after incubation with serial dilutions of inhibitor. The experiment was performed in triplicate. The IC_{50} was identified at 0.49μM, consistent with the data obtained with the commercially available enzyme (Figure 8.16).

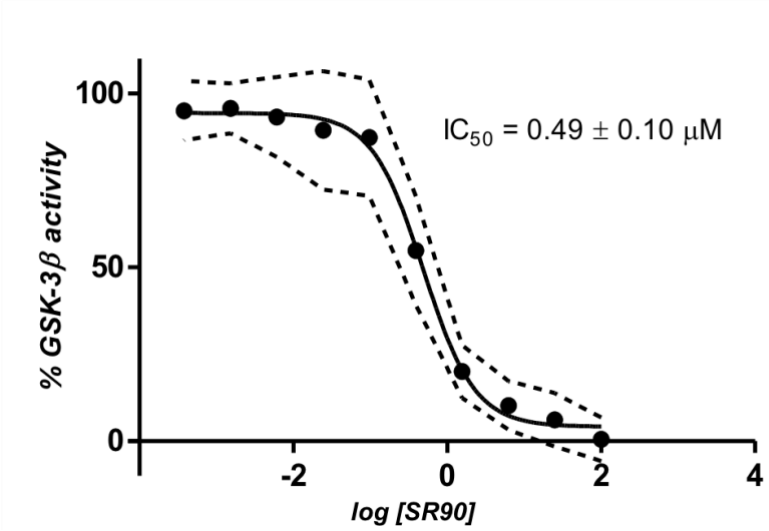

Figure 8.16: SR90 IC_{50} determination on GSK-3β 35-386

SR90 demonstrated a significant activity towards this kinase and a comparable potency on CK-1δ (0.68 μM). Considering its balanced activity on both kinases, SR90 could be a promising lead compound of a new class of inhibitors.

SR90 reversibility assay

A single experiment was performed to determine the kinase recovery from inhibition after compound dilution or after incubations. Despite the inhibitor probable reversible interaction with the kinase, data did not demonstrate a reversible inhibition, nor a kinase activity increase with time. Instead, the bond was proven to be irreversible in those conditions. Further investigations will confirm the irreversibility of the inhibition and will assess the compound behavior in the cell.

8.5. Crystallization on GSK-3β 35-386

As previously mentioned, the GSK-3β construct was selected for crystallization trials due to the extreme flexibility of the N- and C-terminal domains that lead to uninterpretable electron density in the crystals structure (Dajani et al. 2001; Bertrand et al. 2003).

The purified GSK-3β 35-386 was concentrated to 4.4 mg/mL, corresponding to 110 μM. The sample was not further concentrated due to the previously observed protein loss during this procedure. For co-crystallization experiments 330 μM of SR90, solubilized in 100% DMSO, were incubated for 3 hours at 4°C. The final DMSO concentration in the sample was 2.8%, the same tested with the TSA. The selection of the proper crystallization screen was guided by the conditions reported in the published GSK-3β crystal structures. Most of the crystal were obtained with PEG 3350 as precipitant (Haar, Coll, and Austen 2001; Bhat et al. 2003; Bertrand et al. 2003) while in others PEGs at higher

molecular weight were used. Since PEG was commonly present in GSK-3β crystallization conditions the PEG ION screen 1 and 2 were selected for the preliminary tests.

In addition to the protein pre-incubated with the inhibitor, the apo kinase was also tested in this experiment. If the co-crystallization experiments are unsuccessful, apo crystals can be soaked in the inhibitor solution to allow compound diffusion within the already formed crystal lattice.

After 3-days incubation at 20°C crystals were observed only in co-crystallization drops, but within 10 days apo crystals formed too. The faster crystals formation in the drops with the inhibitor confirmed the stabilizing effect of this compound observed in TSA experiments.

GSK-3β/SR90 co-crystals in 0.2 M Sodium malonate pH 6.0, 20% PEG 3350 are shown in Figure 8.17.

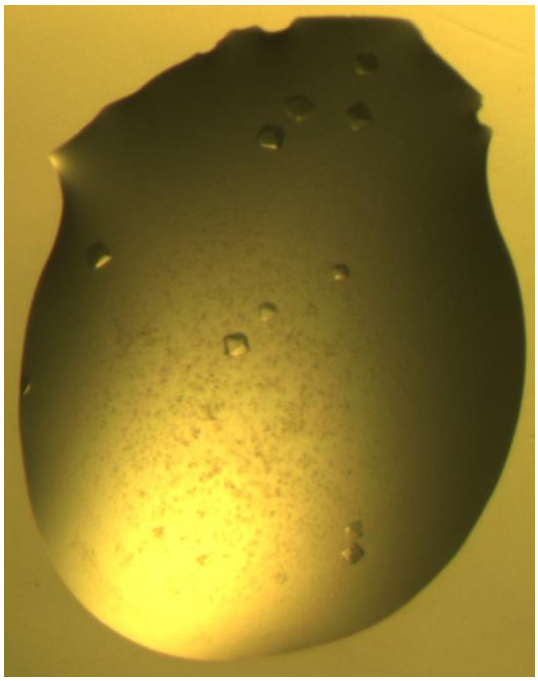

Figure 8.17: Co-crystals obtained from PEG ION screen

Optimizations of the crystallization conditions were performed starting from the conditions:

- 0.2 M Sodium malonate pH 5.0, 20% PEG 3350
- 0.2 M Sodium malonate pH 6.0, 20% PEG 3350
- 0.2 M Malic acid pH 7.0, 20% PEG 3350
- 2% v/v Tacsimate pH 5.0, 0.1 M Sodium citrate tribasic dihydrate pH 5.6, 16% PEG 3350

Hanging and sitting drop optimization plates were set up with both apo and SR90-incubated GSK-3β.

Optimization experiments yielding crystals are summarized in Table 8.6.

Table 8.6: Crystallization results

Conditions	Crystal form	Crystallization technique
16% PEG 3350 0.2M Sodium malonate pH 5.0	Cocrystal	Hanging Drop
18% PEG 3350 0.2M Sodium malonate pH 5.0	Cocrystal	Hanging Drop
20% PEG 3350 0.2M Sodium malonate pH 5.0	Cocrystal	Hanging Drop
22% PEG 3350 0.2M Sodium malonate pH 5.0	Cocrystal	Hanging Drop
22% PEG 3350 0.2M Sodium malonate pH 6.0	Cocrystal	Hanging Drop
16% PEG 3350 0.2M Malic acid pH 7.0	Apo Cocrystal	Hanging Drop Sitting drop
18% PEG 3350 0.2M Malic acid pH 7.0	Apo Cocrystal	Hanging Drop Sitting drop
20% PEG 3350 0.2M Malic acid pH 7.0	Apo Cocrystal	Hanging Drop Sitting drop
18% PEG 3350 2% v/v Tacsimate pH 5.0 0.1M Sodium citrate monobasic trihydrate	Cocrystal	Hanging Drop
20% PEG 3350 2% v/v Tacsimate pH 5.0 0.1M Sodium citrate monobasic trihydrate	Cocrystal	Hanging Drop

In ***hanging-drop plates***, crystals formed within 5 days for both apo and co-crystallization experiments. Interestingly, apo crystals only grew in 0.2 M Malic acid pH 7.0 with 16% (Figure 8.18B), 18% and 20% PEG 3350. Co-crystals grew in 0.2 M Sodium malonate pH 5.0, 16%-18%-20% and 22% PEG 3350 and in 0.2 M Sodium malonate pH 6.0 and 22% PEG 3350. Co-crystals were detected also in 2% v/v Tacsimate pH 5.0, 0.1 M Sodium citrate tribasic dihydrate pH 5.6, 18% (Figure 8.18 A) and 20% PEG 3350.

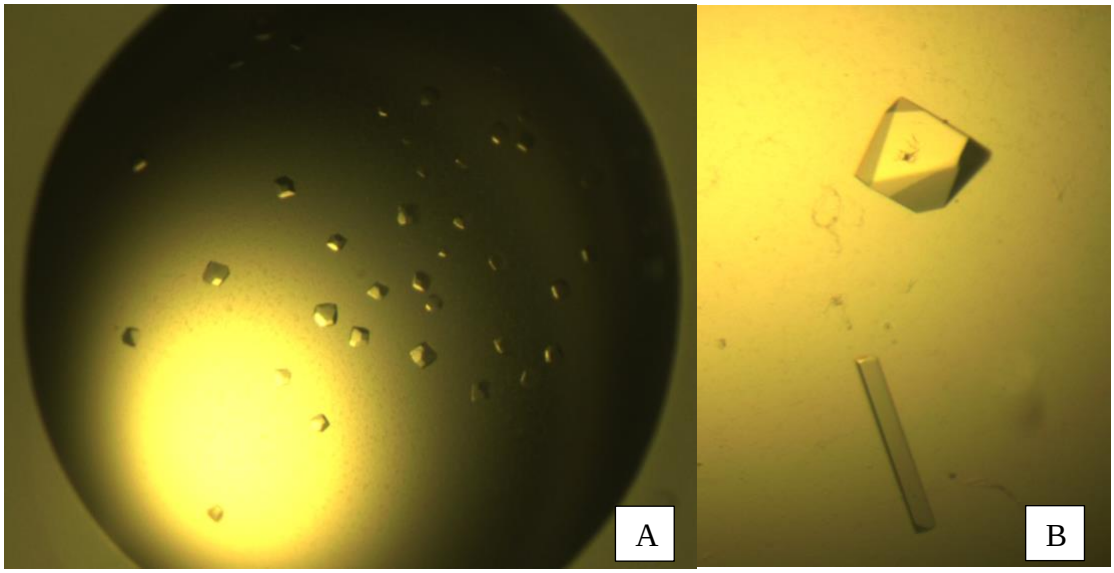

Figure 8.18: Crystals of co-crystallized kinase (A) and apo GSK-3β (B)

In ***sitting-drop plates***, co-crystals grew in 10 days in 0.2 M Malic acid pH 7.0 with 16% ,18% and 20% PEG 3350. The same conditions lead to the formation of apo crystals in hanging drop plates, but the crystal shape was different for sitting drop plates as crystals were flat and small. Notably, in this plate no apo crystals formed.

Cryoprotectant conditions were tested in order to prevent ice formation during data collection. The reservoir solutions were supplemented with the inhibitor at the proper dilution, to assess its possible interference, and 30% glycerol or 20% ethylene glycol. The cryogenic conditions were tested under a 100 K nitrogen flux: the glycerol prevented ice formation, while the ethylene glycol was less efficient in cryoprotecting the crystals.

Diffraction data of the co-crystals fished from the hanging-drops and cryoprotected in 30% glycerol were collected at XRD1 beamline at Elettra Synchrotron Trieste. Unfortunately, due to the low quality of crystal diffraction, these data were not interpretable.

In the apo form hanging drop plate, crystals with different morphologies were observed in the same drop (Figure 8.18B). Both crystal forms were tested using synchrotron radiation. However, only the diamond-shaped crystals gave an interpretable diffraction pattern that was used for structure determination.

Since sitting drop co-crystals were small and considering that the previous diffraction data obtained from co-crystals were not interpretable, in the following experiments the apo crystals were soaked in inhibitor solution. The selected apo crystals from the hanging drop plate (0.2 M Malic acid pH 7.0, 20% PEG 3350) were soaked in a drop formed by the reservoir solution supplemented with 330 μM SR90 for 24 hours. After the incubation the crystals observed under the optical microscope showed the beginning of degradation. Therefore, they were immediately frozen in liquid nitrogen.

8.6. Data collection

X-ray diffraction data of the apo, soaked crystals and the co-crystals were collected at XRD1 beamline at Elettra Synchrotron Trieste, obtaining data at 2.6 Å resolution for the apo crystal, at 2.4 Å for the soaked crystal and at 2.3 Å resolution for the co-crystals fished from the sitting drop plate. The data collection results are reported in Table 8.7.

Table 8.7: Data collection statistics. The values corresponding to the highest resolution shell are reported in parenthesis.

	Co-crystal	Soaked crystal	Apo crystal
Wavelength (Å)	1.00	1.00	1.00
Temperature (K)	100	100	100
Resolution range	47.27 - 2.30 (2.38-2.30)	49.02 - 2.40 (2.54-2.40)	49.23 - 2.60 (2.71-2.60)
Space group	P 21 21 21	P 21 21 21	P 21 21 21
a, b, c (Å)	86.803, 94.542, 106.579	82.526, 83.121, 170.592	82.469, 84.381, 178.190
Mosaicity (°)	0.21	0.25	0.109
Total number of reflections	145310 (14711)	176429 (46048)	363488 (57477)
Unique reflections	39567 (3843)	89376	93759 (14275)
Redundancy	3.7 (3.8)	1.97 (2.02)	3.9 (3.7)
$\langle I/\sigma(I) \rangle$	7.4 (1.5)	5.43 (0.89)	9.25 (2.14)
Rmerge	0.140	0.096	0.124
CC1/2	0.991 (0.570)	0.989 (0.477)	0.995 (0.810)
Rpim	0.084 (0.560)	0.051 (0.474)	0.039 (0.386)
Completeness	99.8 (100)	99.2 (99.3)	99.9 (99.9)

The three structures shared the same space group with minor differences in the unit cell parameters. A research in the Protein Data Bank (PDB) was performed in order to detect a GSK-3β structure with analogous cell parameters to solve the co-crystal structure by molecular replacement. The structure published by Bhat and colleagues (Bhat et al. 2003), PDB code 1Q5K, was used as a model for phasing with MolRep. Structure refinements cycles were performed with Refmac, for the manual fitting of the model in the electron density map the software Coot was used. The final structure was deposited in PDB with code 6H0U (Redenti et al. 2019).

The structures of the soaked and the apo crystals were solved following the same workflow but using the co-crystal structure for the molecular replacement. Refinement statistics are reported in Table 8.8.

Table 8.8: Refinement statistics

	Co-crystal	Soaked crystal	Apo crystal
Resolution (Å)	47.27 – 2.30	49.02 – 2.40	49.23 – 2.60
Number of reflections	37543	46048	37129
Rwork / Rfree (%)	19.2 / 24.0	22.1 / 25.7	21.8 / 27.3
Number of atoms	5722	5810	5764
Protein	5380	5630	5631
Completeness	99.62	99.12	99.86
RMS deviations bonds	0.009	0.013	0.010
RMS deviations angles	1.386	1.949	1.837

8.7. Structures analysis

The crystal structures obtained were analyzed in depth and were compared to elucidate possible variations in the binding mode of SR90. Interestingly, observing the map no electron density corresponding to a phosphate group was detected, confirming the absence of phosphorylation in GSK-3β crystals.

8.7.1.GSK-3β 35-386/SR90 co-crystal

In the crystals structure, GSK-3β forms a dimeric assembly with two molecules in the asymmetric unit (Dajani et al. 2001). The crystal belongs to the orthorhombic space group (P 2_1 2_1 2_1) with the following cell parameters: a= 86.803 Å, b= 94.542 Å and c= 106.579 Å.

The N- and C-terminal ends of the construct (residues 35 and 384-386) were partially disordered as reported in literature (Dajani et al. 2001), an interpretable electron density was visible only for residues 36-383. Moreover, the side chains of surface residues, specially Arg, were less ordered compared to the overall structure.

GSK-3β possesses two phosphorylation sites, Ser9 and Tyr216 implicated in kinase regulation, inhibiting (Ser9) or activating (Tyr216) the kinase (Dajani et al. 2001). Contrary

to the Tyr216, the inhibitory Ser9 was not present in the construct crystallized. However, no electron density corresponding to a phosphate group was detected on the side chain of residue 216, confirming the unphosphorylated state of the kinase.

Two Ramachandran outliers (Arg 220 and Tyr 221) were present in the final structure, despite residues were properly fitted in the electron density map. Other GSK-3β crystallographic structures presented the same outliers suggesting a conserved strained conformation (Bhat et al. 2003; Dajani et al. 2001; Haar, Coll, and Austen 2001; Aoki et al. 2000). In the asymmetric unit, a malonate ion, three glycerol molecules, two chloride ions, a sodium ion, and 266 water molecules were detected.

The crystal structure of GSK-3β 35-386 is presented in Figure 8.19.

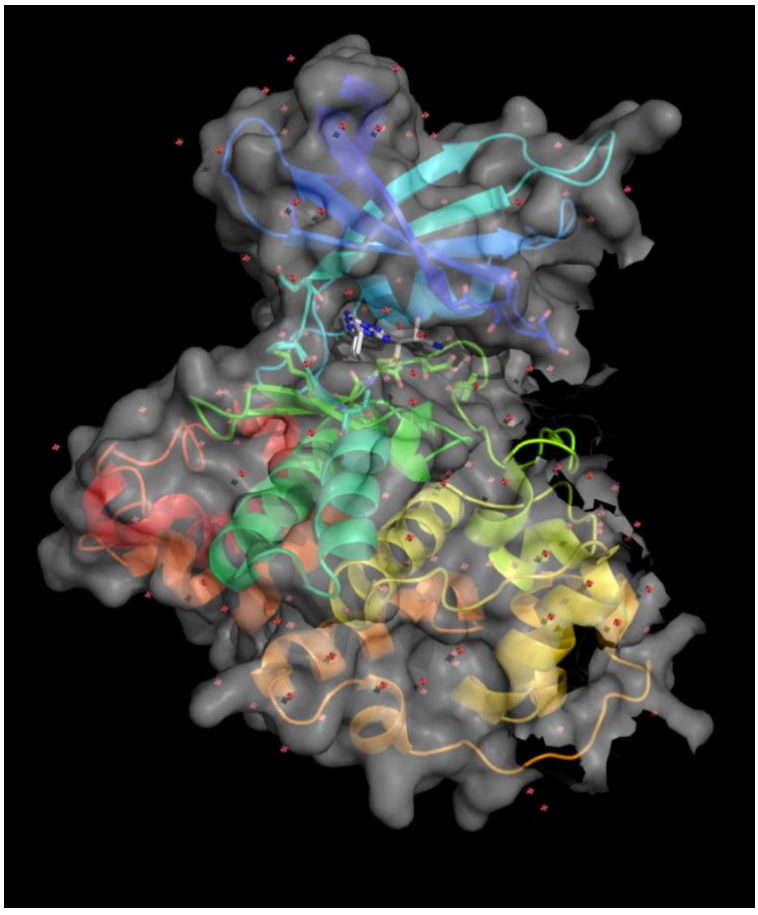

Figure 8.19: Crystal structure of GSK-3β co-crystallized with SR90 inhibitor. PDB code: 6HOU. Chromatic scale: rainbow, from blue at the N-terminus to red at the C-terminus.

An electron density corresponding to the inhibitor was observed in ATP binding pocket, the presence of SR90 bound to the kinase was confirmed with refinement cycles.

To properly determine the compound disposition within the active site of the enzyme, parallel refinements were performed with different conformations of the unbound inhibitor and with the covalently bound one (Figure 8.20).

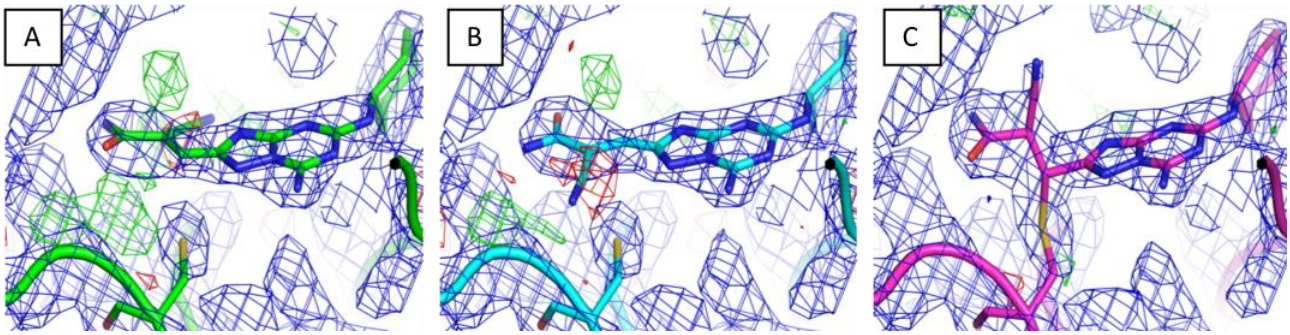

Figure 8.20: Results of the refinement tests using different non-covalently bound conformers of SR90 (A and B) and the SR90-Cys199 bound conformation used in the final refinement (C). Electron density maps are depicted in blue (σ level: 1.0), difference electron density maps are depicted in green (σ level: 2.5) and red (σ level: -2.5). From Redenti et al. 2019

As demonstrated in the Figure, only the covalently bound conformer (Figure 8.20 C) could fit the electron density, reducing the residual difference electron density (red) confirming the irreversible binding mode of SR90 with Cys199, as predicted with computational modelling. SR90 interacts also with Asp133, Lys85, Asp200, Val135 via hydrogen bond formation. In particular, the amide group forms hydrogen bonds with Lys85 and Asp200, whereas the amine group and the nitrogen atom of the heterocycle interact with Asp133 and Val135, respectively. The experimentally determined disposition of the molecule in ATP binding pocket is depicted in Figure 8.21.

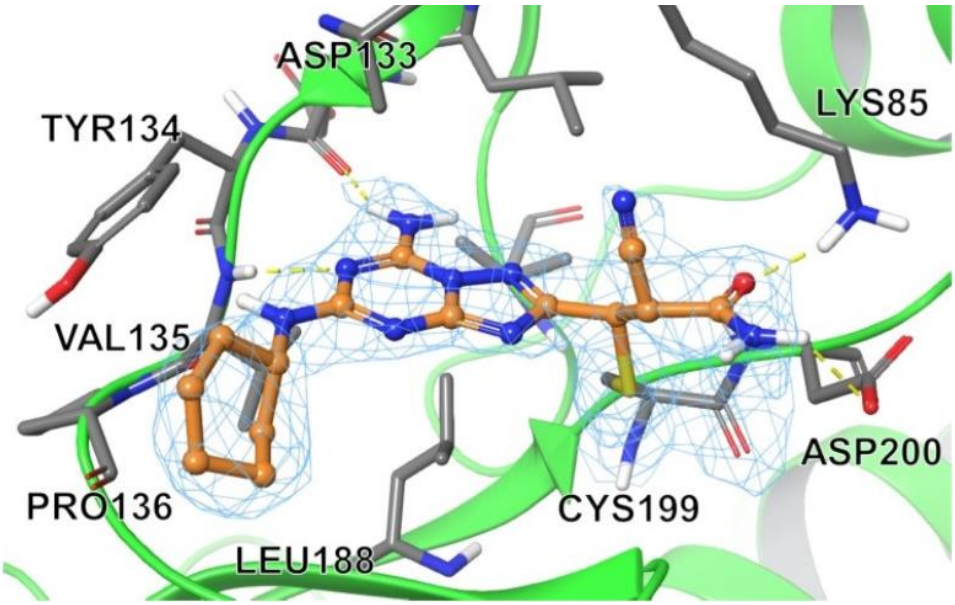

Figure 8.21: SR90 disposition in GSK-3β active site. Inhibitor electron density is represented as a cyan mesh (σ level: 1.0), kinase binding pocket side chains are depicted in grey sticks, SR90 is represented as an orange ball-and-sticks model. From Redenti et al. 2019

From the X-ray structure the configuration of the new stereocenters formed with the Michael reaction could be determined. In this case, the syn addition of SR90 cyanoacrylamido group lead to the R stereo configuration of both carbons. The proposed addiction reaction mechanism is displayed in Figure 8.22.

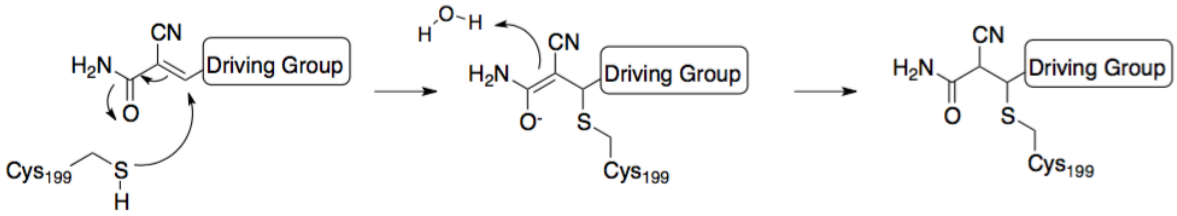

Figure 8.22: Representation of Michael reaction occurred between SR90 and Cys199

Despite the computational modelling predicted the covalent interaction of SR90 with Cys199, the crystal structure revealed a different orientation of compound amide and cyanate groups compared to the predictions.

The differences may be observed superimposing the two models (Figure 8.23). Probably these differences are partially caused by the unpredicted interaction of SR90 amide group with Asp200.

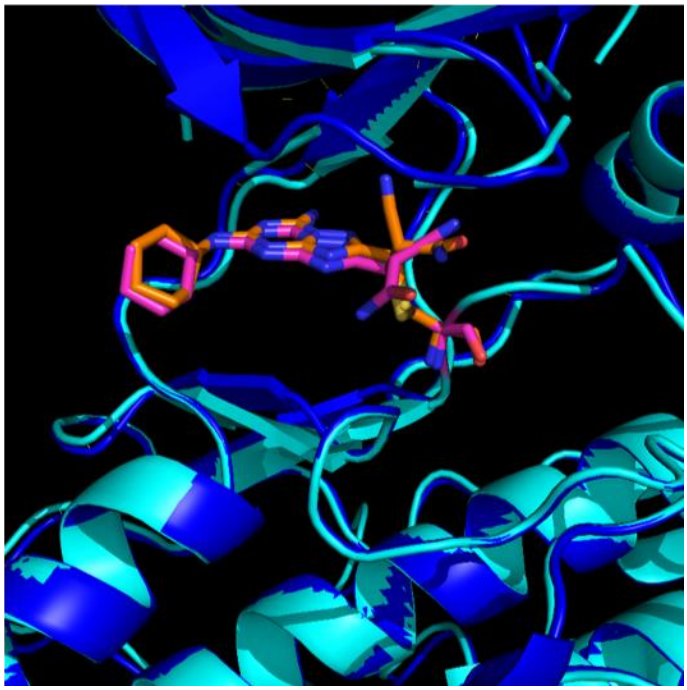

Figure 8.23: Superimposition of the crystal structure of SR90 (orange) bound to GSK-3β (blue), and the computational model with the expected localization of the compound (pink) in the binding site of the protein (cyan).

8.7.2.GSK-3β 35-386 apo and soaked crystals

The structures obtained from apo and soaked crystals displayed two molecules in the asymmetric unit. Despite belonging to the same space group of the co-crystal ($P2_1\ 2_1\ 2_1$), they presented slightly different unit cell parameters, but are isomorphous with the co-crystal. Moreover, the crystal obtained after soaking with SR90 shows a very similar cell compared to the apo, despite the presence of the inhibitor. Probably, SR90 diffusion within the crystal

lattice and the covalent bond formation does not significantly perturb the unit cell parameters, whereas the bound conformation of the kinase promoted the formation of a significantly deformed lattice in co-crystals.

SR90 presence in the soaked crystal was investigated by removing the compound from the reference structure prior to a refinement cycle. In the ATP binding pocket a residual electron density comparable with that observed in the co-crystal map was detected. The inhibitor was subsequently added in the reference PDB and the refinement was launched again allowing the formation of bonds on proximal atoms. As a result, the compound was positioned in the hinge region pocket and the covalent bond with the Cys199 was formed (Figure 8.24).

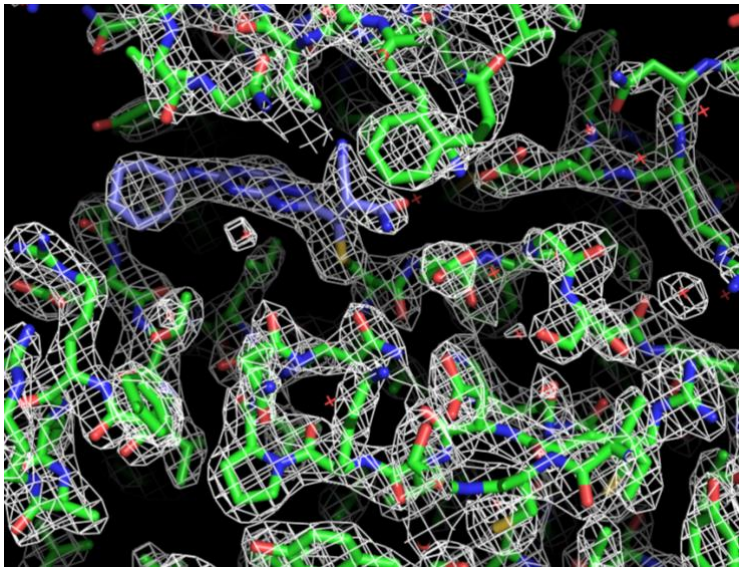

Figure 8.24: Electron density map of soaked crystal

Moreover, the bond distances between SR90 atoms were analyzed, and their values resulted compatible with bonds of already published small molecule crystals with similar features. This demonstrated an unstrained conformation of the molecule.

From these data, SR90 diffusion within crystal lattice of the apo kinase and the formation of a covalent bond within the crystal, with minor differences compared to the co-crystal, were demonstrated (Figure 8.25).

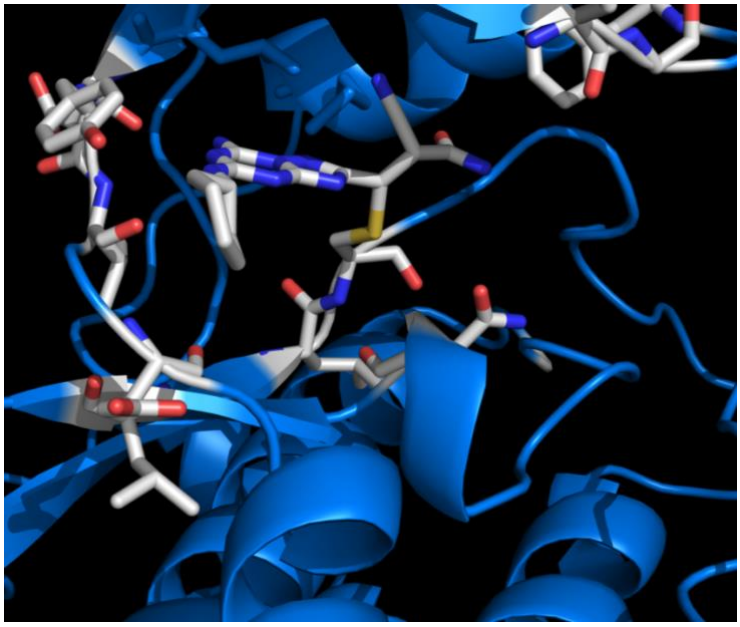

Figure 8.25: SR90 covalent bond with Cys199 in the soaked crystal

8.7.3.SR90 inhibitor

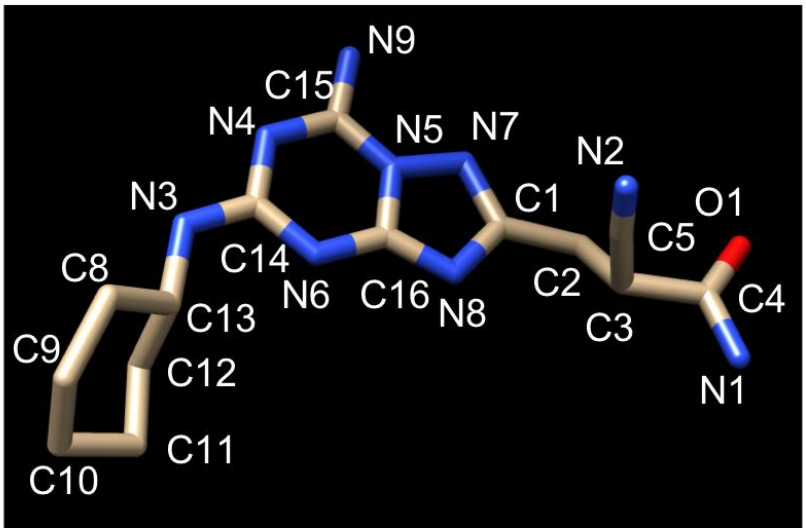

Figure 8.26: SR90 structure

Since a reversible bond was expected, the inhibitor interaction with the kinase was further investigated. Comparing the covalent bond distances between SR90 C2 and Cys199 of the proteins a distance of 1.9 Å in both the soaked crystal and in the co-crystal was measured, indicating no differences in the bond. Furthermore, the pattern of water molecules in the binding site and the surrounding residues demonstrated to be highly similar. To determine the interactions of the compound with the residues near the binding site the structure was analyzed with a Ligplot (Figure 8.27). In the binding site the inhibitor O1 atom interacts with Lys85, N1 with Asp200, N9 with Asp133 and N3 with Val135.

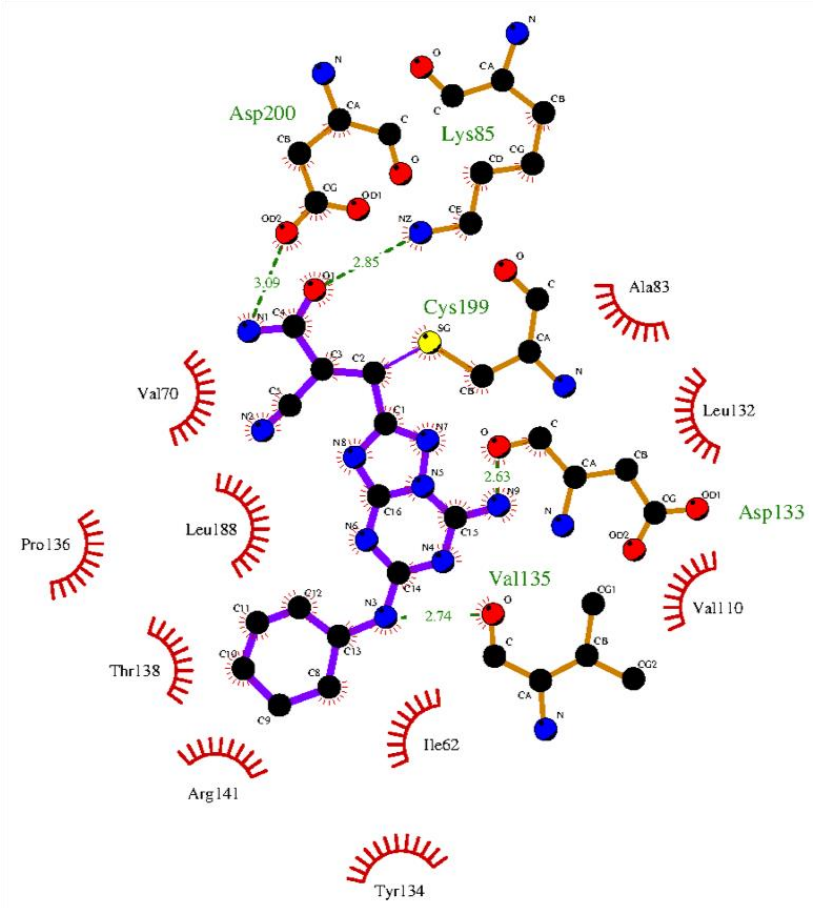

Figure 8.27: Ligplot of SR90 co-crystallized with GSK-3β

The crystal structures demonstrated that SR90 covalent bond with Cys199 is stable and not affected by the small differences in kinase conformation in the two crystals.

8.7.4. Structure comparison: Soak Vs Co-crystal

Overall structure

The structures were superimposed to compare the relative positions of the kinase regions (Figure 8.28).

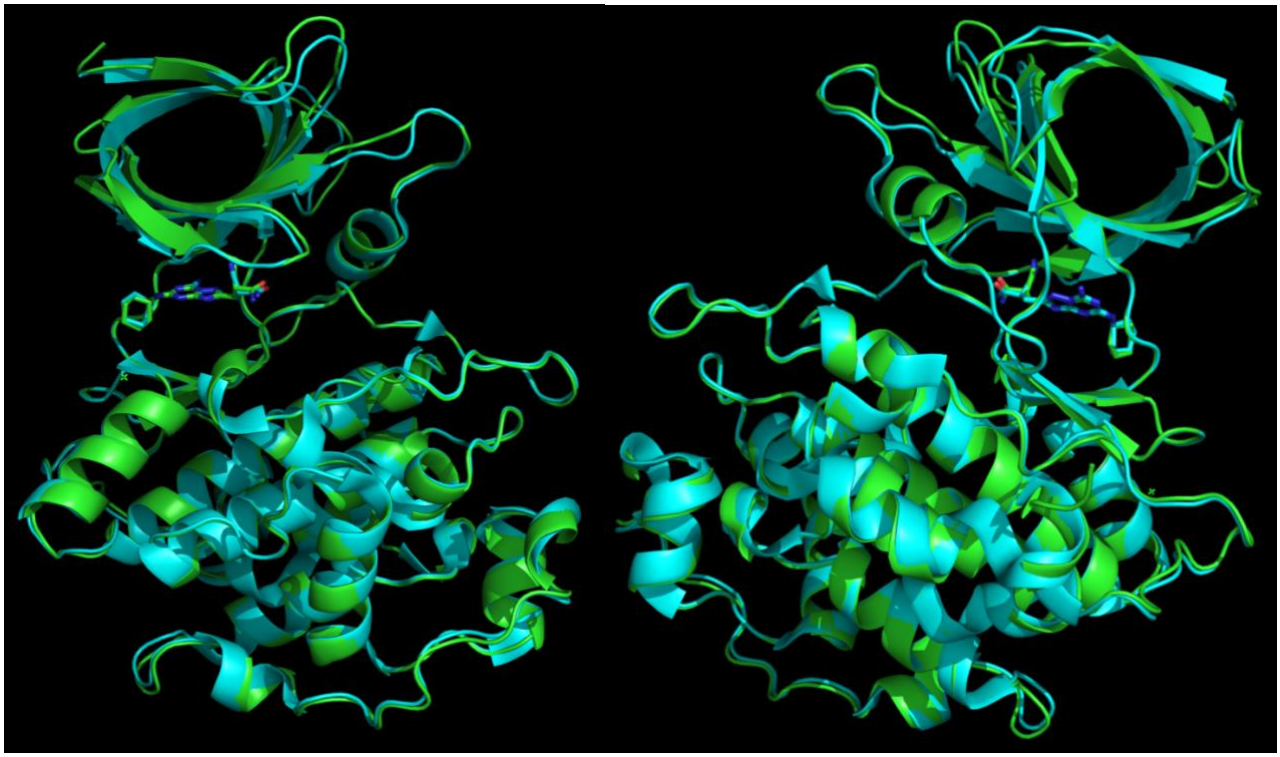

Figure 8.28: Superimposition of the crystallographic structures green: soaked crystal, cyan: cocrystal

The overall structure of the kinase shows a slight change between the co-crystallized and the soaked crystals. The modifications observed could be caused by the slightly different packing within the crystal lattice. The deviation between the main chains of the structures was calculated with Coot by superimposing the coordinates. The maximal deviation calculated was 3.9 Å, probably measured within the N-terminus. In fact, in the loops connecting the β-sheets of the N-terminal region glides and diverse dispositions of the chain can be observed. Moreover, the second β-sheet of the co-crystal is elongated compared to the same segment of the soaked structure, the same variation could be observed in the C-helix. All these modifications resulted in a tilt in the N-terminal β-barrel. However, the variation of the amino terminus did not influence the hinge region and the C-terminal part of the kinase. In fact, the disposition of these regions was very similar in the two crystals.

Comparison on SR90 binding site

The disposition of the inhibitor in the co-crystallized structure and in the soaked crystal was compared (Figure 8.29).

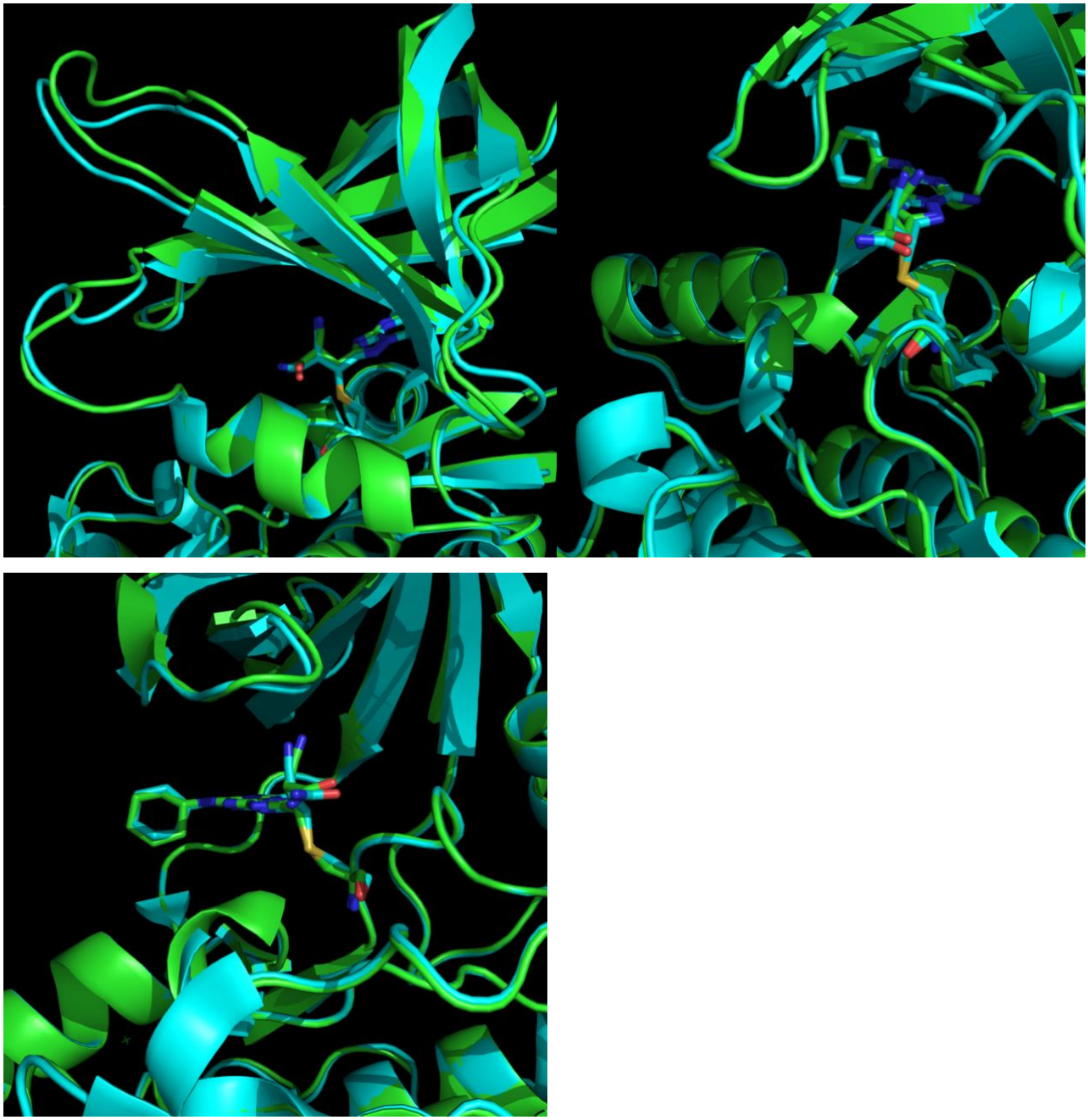

Figure 8.29: Comparison of SR90 binding to the kinase. Cyan: co-crystallized protein Green: soaked one

As can be observed from the Figure, the cyclohexyl is rotated between the two structures, but more interestingly the amide and the cyano groups are tilted. Also, the arrangement of Cys199 displays a different angle, but without preventing the formation of the covalent bond. However, the modifications in binding geometry are not caused by a difference in protein main chain, since the two structures are perfectly superimposable in this region.

8.7.5.Structure comparison: Co-crystal vs apo

Overall structure

These structures displayed the greatest variations between the GSK-3β crystals. The maximal deviation calculated by Coot on the kinase main chain was 4.7 Å. As can be observed in the Figure 8.30, the structure variations are visible along all the sequence. A general shift in the β-sheets was observed and the loops are highly glided resulting in a different conformation of the N-terminus. In this case, significant variations in the hinge region were also observed, especially between residues 133 and 137. However, the chains were superimposable from residues 198 and 205, despite the bond of SR90 to Cys199 in the co-crystal structure. The covalent bond did not modify the morphology of the hinge region. In addition, in the C-terminal domain slight variations in the structures were detected, probably caused by a different molecule disposition in the crystal lattice (Figure 8.30).

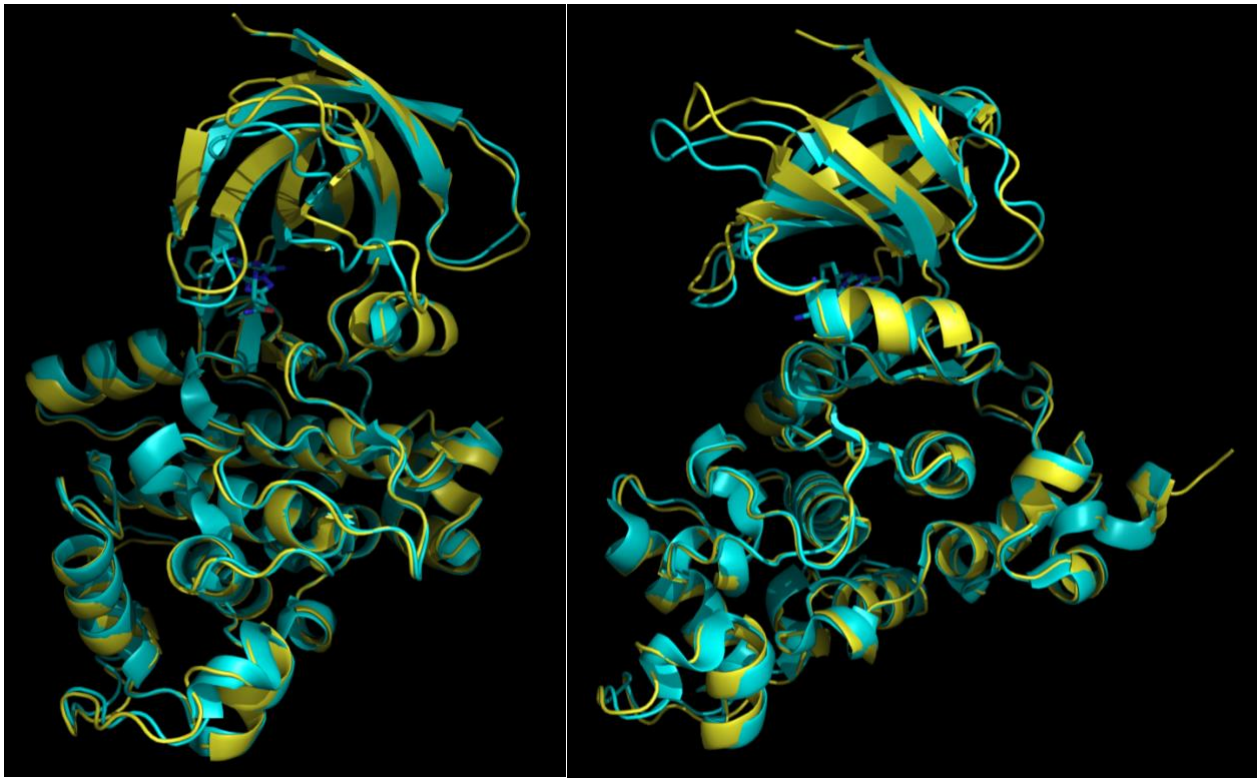

Figure 8.30: superimposition of the cocrystal in cyan and the apo form in yellow

8.7.6.Structure comparison: Apo Vs Soaked

In this case the variations in the structure were minimal. Both crystals displayed very similar unit cell parameters. The maximum deviation between the superimposed main chain was calculated as 3.7 Å. The differences are mostly located within the N-terminal region, with a slightly different position of the loops, while the strands shared a high grade of similarity. A variation in the hinge region between residues 133 and 137 was observed, as previously

mentioned for the co-crystal. The disposition of the helices of the C-terminal domain is highly similar with minor variations (Figure 8.31).

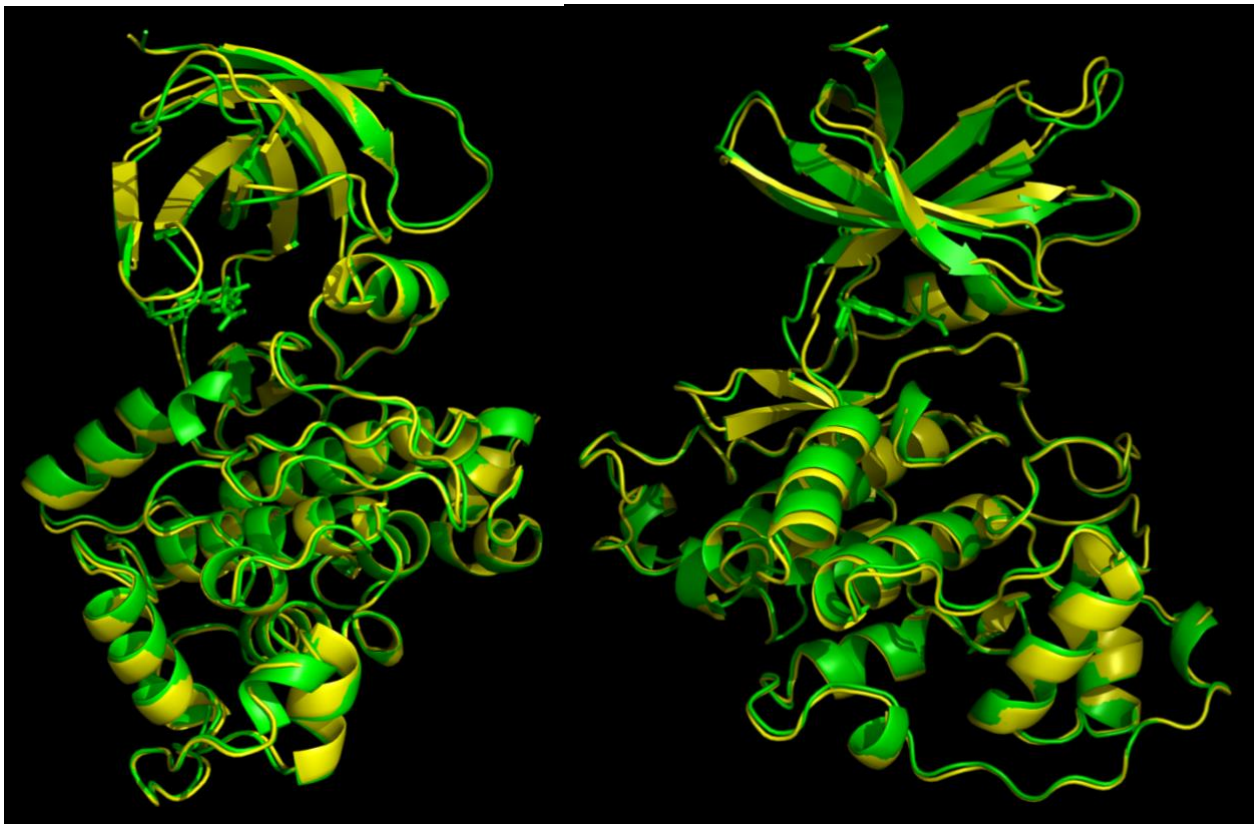

Figure 8.31: superimposition of the apo form in yellow and the soaked crystal in green

8.8. New inhibitors

Due to the good results obtained with the investigation on SR90, the same procedures optimized in this study were used for the structural characterization on other inhibitors synthesized by Dr. Stephanie Federico. In this case the crystal structure of the GSK-3β/inhibitor complex are essential for the understanding of the binding mode, in order to modify the molecule structure to increase the compound potency. In fact, the best strategy could not be divised from the experimental results obtained up to this point.

These compounds are Roscovitine analogs. This small molecule inhibits cyclin-dependent kinases via ATP binding competition and is studied as a potential drug against cancer, inflammation and neurodegenerative diseases (Cicenas, Kalyan, and Valius 2015).

The chemical formula, the BBB permeation capacity and the IC_{50} of the tested compound are reported in Table 8.9. All the inhibitory values reported in this table were determined on the commercial kinase.

Table 8.9: Compound tested with their chemical formula, BBB permeability and IC_{50}

	Formula	PAMPA -BBB	IC_{50} GSK3β (μM)
SR36	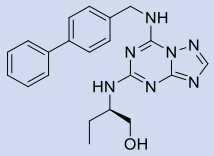	CNS+	2.2
GV18	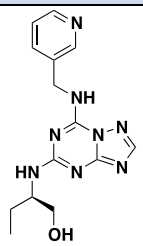	CNS -	1.4
GV19	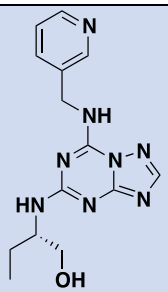	CNS +/-	0.63
GV23	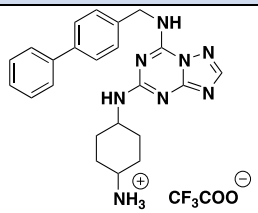	CNS +	2.3
GV24 B 1,3-cis mix	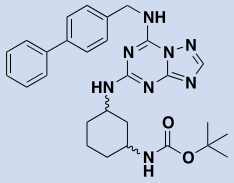	CNS +	0.80
SR90	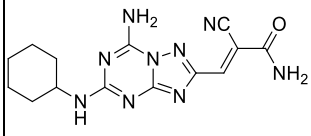	CNS +/-	0.17 Irreversible

As shown in the Table, the inhibitory potency of these inhibitors is lower compared with the IC_{50} of SR90. In fact, these molecules require further optimization.

For these studies, new batches of GSK-3β 35-386 and FL were produced using MultiBac bacmid generation method instead of the Bac-to-Bac used in the previous work. Interestingly, the FL construct expressed following the procedure described in this thesis showed a higher stability compared to the shorter one. It is possible that the different bacmid generation methodology modifies

the folding stability of the proteins. During FL purification steps, the peak corresponding to the phosphorylated kinase was isolated and used for the subsequent experiments.

Cloning, expression and purification procedures were carried out by other members of the Dr. Storici group and are reported elsewhere, while the crystallization and TSA experiments are reported in this dissertation.

Initial Thermal Shift Assay on the inhibitors were performed following the procedure used for SR90, in order to evaluate the compounds effect on kinase folding. Figure 8.32 reports the results of the TSA experiments.

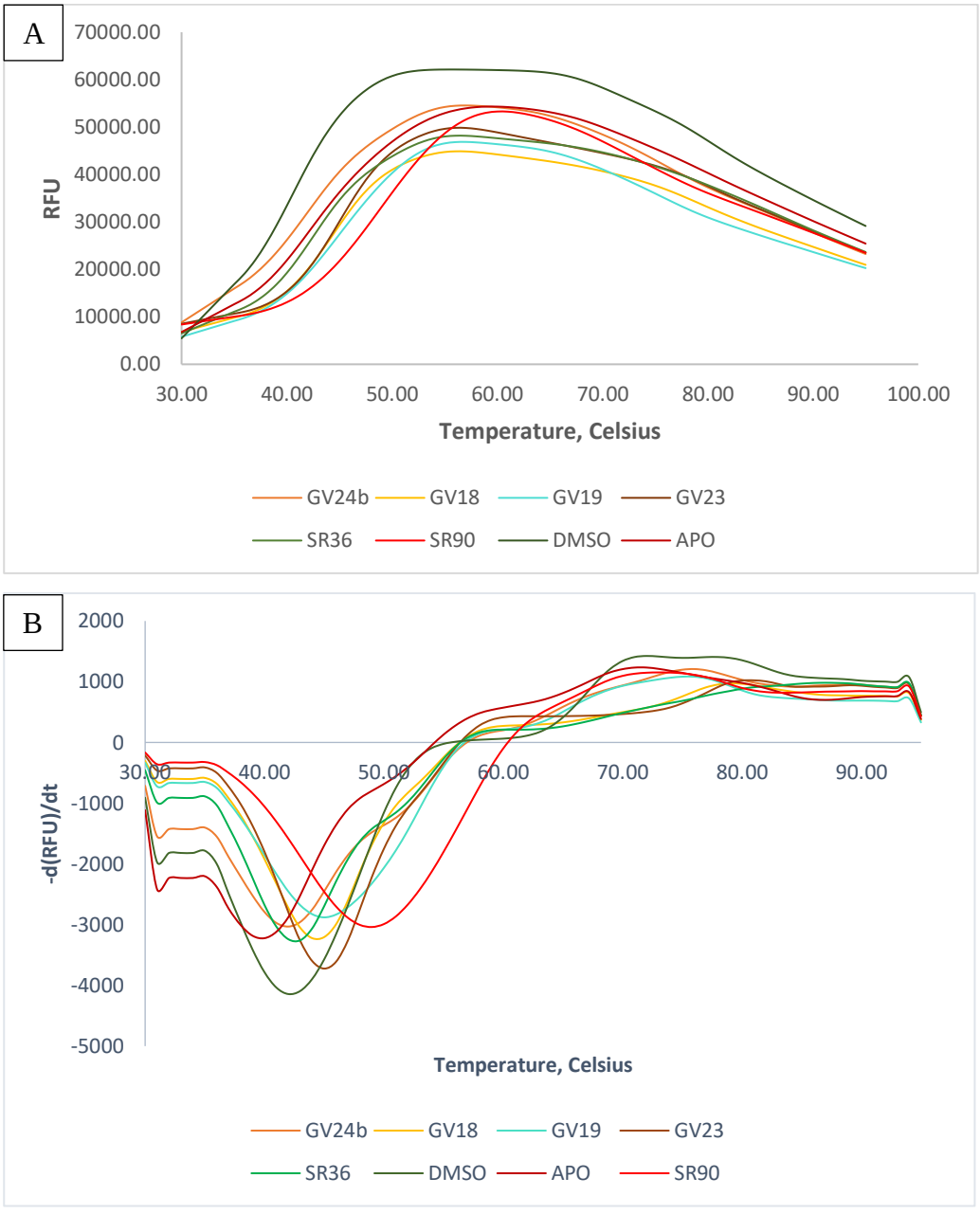

Figure 8.32: TSA melting curve on GSK3-β FL. Panel A: average of fluorescence intensities, Panel B: derivative results.

As for the SR90 inhibitor, also in this case the apo kinase and the protein incubated with DMSO were used as references for the T_m. The results are presented in Table 8.10.

Table 8.10: Melting temperatures determined on the FL construct

Sample	Melting temperature	Standard deviation	ΔT
Apo	40.0°C	±1	-
DMSO	42.0°C	±0.1	+2
GSK3-β+ GV18	44.7°C	±0.58	+4.7
GSK3-β+ GV19	45.0°C	±0.1	+5
GSK3-β+GV23	45.7°C	±0.58	+5.7
GSK3-β+ GV24b	43.0°C	±1.73	+3
GSK3-β+SR36	44.0°C	±0.58	+4
GSK3-β+SR90	48.5°C	±0.70	+8

In this experiment a higher T_m of the apo form compare to the one determined previously on the FL construct can be noticed, probably due to the different bacmid generation procedure and the protein phosphorylation that increased the kinase stability. However, SR90 confirmed to greatly increase GSK-3β folding stability.

Crystallization trials were performed on both constructs. The crystallization conditions were initially screened with PEG ION 1 and 2. No crystal grew in the GSK-3β 35-386 plates, whereas apo crystals of the FL constructs could be obtained. The crystallization condition of the apo kinase were optimized to get larger crystals suitable for diffraction experiments. The apo crystals were soaked in inhibitor solutions and stored in liquid nitrogen. X-rays diffraction data will be collected at XRD2 beamline of Elettra Synchrotron to assess the presence of the inhibitor in the binding site and to investigate the compound binding mode.

9. CONCLUSIONS

This project started with the collaboration of the Dr. Paola Storici group at the Structural Biology Laboratory at Elettra synchrotron Trieste with Dr. Stephanie Federico of the Department of Chemical and Pharmaceutical Sciences of the University of Trieste. This work was aimed at the elucidation of the binding mode of SR90, an inhibitor synthesized in Dr Federico's laboratory, to Glycogen Synthase kinase 3β via X-ray crystallography. This kinase is involved in the regulation of numerous metabolic pathways via phosphate group addition. In particular, it was demonstrated that GSK-3β is involved in neuroinflammation and neurodegenerative processes (Karin 2005; Jope, Yuskaitis, and Beurel 2006). This protein has a fundamental role in the pathogenesis of Alzheimer and Parkinson diseases. In fact, GSK-3β promotes the formation of β amyloid aggregates, the hyperphosphorylation of protein tau and the α-synuclein accumulation, among the most common signs of these pathologies (Llorens-Martín et al. 2014; Deng et al. 2014; Golpich et al. 2015).

SR90 was designed to doubly inhibit GSK-3β and Casein Kinase 1δ (CK1-δ), a kinase also involved in neurodegeneration processes that may act as a priming kinase for GSK-3β substrates (Singh et al. 1995). From computational modelling predictions the compound should reversibly inhibit CK1-δ via an ATP-competitive inhibition and covalently bind Cys199 of GSK-3β with a comparable potency. The identification of a dual inhibitor able to target both kinases may be interesting in the quest for a new lead compound of drugs against the neurodegenerative disorders.

For this purpose, three constructs of GSK-3β, encoding for the full-length kinase and for two N- and C-terminus truncated forms, were cloned. The shorter constructs were selected due to the high flexibility showed by both GSK-3β termini. Flexible regions may hamper the crystallization process and could not be detected in the electron density of the GSK-3β deposited crystal structures (Dajani et al. 2001).

The kinase was expressed in insect cells, the FL and the shorter construct (residues 35-386) revealed the best expression yields and were selected for the scale up. GSK-3β 35-386 construct proved to have a higher stability that increases success rate of the crystallization trials. Prior to crystallization, the influence of SR90 binding on GSK-3β 35-386 was investigated with the TSA. The compound demonstrated to significantly stabilize protein folding, suggesting a strong binding potency towards the kinase. The crystallization experiments were performed on both the apo protein and the kinase pre-incubated with the inhibitor to obtain the co-crystals. From the crystallization experiments the crystals of the apo kinase, the co-crystals of the GSK3-β 35-386 complexed with SR90 and the crystals of the apo kinase soaked in SR90 solution were obtained. In the latter, the diffusion of the

molecule within the already formed crystal lattice is expected. The X-rays diffraction patterns of all the crystals were collected obtaining data at 2.6 Å resolution for the apo form, at 2.4 Å for the soaked crystal and at 2.3 Å for the co-crystal. From the structure of the co-crystal, a residual electron density was detected within the hinge region, consistent with the presence of SR90. Due to the high resolution reached it was possible to investigate the precise disposition of the compound. From different refinement cycles, the presence of a covalent bond of SR90 with the side chain of Cys199 was proven to be the only conformation compatible with the electron density map, as predicted by the computational modelling simulations. However, the molecule disposition was slightly rotated compared to the model, probably due to the molecule unpredicted interaction with a neighboring residue. Data collected from the soaked crystals displayed a similar covalent bond of the inhibitor SR90 with the same GSK-3β residue. From the comparison of the three crystallographic structures slight variation in the α-helical composition of the kinase were detected, the co-crystallized form displaying a higher amount of this secondary structure compared to the apo and the soaked crystals, that showed a higher amount of random structures. However, the co-crystal and the soaked crystal hinge regions were perfectly superimposable.

Moreover, the inhibitory activity of the compound was tested on the expressed kinase determining an IC_{50} value of 0.49 μM, compatible with the one determined with the commercial protein.

This work allowed the determination of the binding mode of SR90 to GSK-3β validating the computational predictions. In addition, the complex crystal structure gave essential information on the disposition of the residues that surrounds the compound binding site.

Despite the initial good results in the small-scale purification tests, the FL revealed a low stability during purification scale up, dialysis and concentration procedures. To determine a buffer composition that stabilizes the FL kinase a Thermal Shift Assay was performed, identifying a promising condition for further purification experiments.

Currently, crystallization trials on GSK-3β FL complexed with other inhibitors from Dr. Federico's laboratory are ongoing. These experiments are aimed at the structural determination of these new protein/inhibitor complexes, to understand their binding mode and direct further modifications on the structures of inhibitors in order to achieve higher potency and selectivity. These experiments will be performed using the same workflow and protocols optimized during this work.

During this work, a reliable protocol to obtain protein-inhibitor complexes for crystallization experiments on GSK-3β was set up and it will be used for further structure-based drug design studies.

10. MATERIALS AND METHODS

10.1. Generic specifications

Unless differently specified, all the reagents were purchased from Sigma-Aldrich; Protease inhibitor cocktails were from Roche; Synthetic oligonucleotides were produced by Sigma; Commercial kits for plasmid DNA extraction and PCR product purification and Mini Prep were purchased by Macherey-Nagel and Sigma; the Ni-NTA resin was provided by Qiagen, Talon resin by GE Healthcare and GFP-trap resin was bought from Chromotek. Phospho Glycogen-Syntase Peptide-2 was purchased by Merk Millipore; the kinase activity assay KinaseGlo® luminescence assay was bought from Promega. The detergents were purchased by Anatrace, Q_5 polymerase and DNTP's were bought from ThermoFisher, DPNI from NEB. Insect cells medium ESF-921™ was purchased by Expression Systems LLC, Davies - USA.

10.2. Buffers

All buffers were filtered at 0.45 μm, unless indicated 0.22 μm. When DTT was included, it was supplemented just prior to use. Buffers used on pre-packed chromatographic columns have been degassed overnight under magnetic stirring to eliminate solubilized gasses, and refrigerated at 4°C prior to use. All solutions were prepared using MilliQ water.

1X TE: 10 mM Tris pH8.0, 0.1 mM EDTA (filtered 0.22 μm)

50x TAE: 242g Tris Base, 57.1 ml acetic acid, 100 ml 0,5M EDTA (to 1L with ultrapure water)

6X DNA Loading Buffer: 60%Glycerol, 10 mM Tris-HCl (pH 7.6), 60 mM EDTA, 0.03% Bromophenol Blue, 0.03% Xylene Cyanol FF

4x SDS-PAGE Sample loading buffer: 200 mM Tris-HCl pH 6.8; 8% SDS; 40% glycerol; 400 mM DTT; 0.08% w/v bromophenol blue

12% running solution for SDS-PAGE: 12% (v/v) Acrylamide/Bis-acrylamide, 30% solution (Sigma-Aldrich), 375 mM Tris pH 8.8, 0.1% SDS, 0.1% Ammonium Persulfate, 0.04% TEMED.

5% stacking solution for SDS-PAGE: 5% (v/v) Acrylamide/Bis-acrylamide, 30% solution (Sigma-Aldrich), 125 mM Tris pH 6.8, 0.1% SDS, 0.1% Ammonium Persulfate, 0.1% TEMED.

SDS-PAGE Running buffer: 25 mM Tris, 192 mM Glycine, 0.1% SDS.

4x SDS-PAGE Sample loading buffer: 200 mM Tris-HCl pH 6.8; 8% SDS; 40% glycerol; 400 mM DTT; 0.08% w/v bromophenol blue.

Western Blot Transfer buffer: 250 mM Tris Base, 192 mM Glycine, 10% methanol.

Western Blot blocking solution: 5% no fat milk, 0.1% Tween 20 in PBS.

PBS: 10mM Na_2HPO_4, 1.8mM KH_2PO_4, 2.7 mM KCl, 1.37 mM NaCl, pH 7.4.

Ponceau stain: 0.15% (w/v) ponceau red, 5% (v/v) acetic acid

TBS buffer: 20mM Tris pH 7.5, 150mM NaCl

10.2.1. Wzx buffers

Membrane Solubilization buffer: 20mM LDAO (10X CMC), 20mM Tris pH 8.2, 150mM NaCl, 1mM PMSF

No detergent buffer: 20mM Trist pH 8.2, 150mM NaCl, 1mM PMSF

Wzx buffer 20mM LDAO (10X CMC), 20mM Tris pH 8.2, 150mM NaCl

IEX buffer 1: 20mM Tris pH 8.2, 7XCMC LDAO

IEX buffer 2: 20mM Tris pH 8.2, 7XCMC LDAO, 1M NaCl

GFP buffer: 10mM Tris pH 8.2, 10X CMC LDAO, 150mM NaCl, 1mM PMSF, 0.5mM EDTA

Competent cells buffer1: 12g/l RbCl,9.9g/l $MnCl*4H_2O$, 1.5ml from a 1M KAc solution pH 7.5, 1.5g/l $CaCl_2*2\ H_2O$, 150g/l Glycerol. Final pH 5.8. filtered 0.22μm

Competent cells buffer2: 0.4ml from a 0.5M MOPS solution pH 6.8, 1.2g/l RbCl, 11g/l $CaCl_2*2\ H_2O$, 150g/l Glycerol. Filtered 0.22μm

10.2.2. GSK3-β buffers

Lysis buffer: 1x COMPLETE EDTA-free Protease Inhibitor,20mM Tris pH 8.0, 500mM NaCl, 10mM Imidazole, 5% glycerol, 1mM DTT

NiNTA Binding buffer: 20mM Tris pH 8.0, 500mM NaCl, 10mM Imidazole, 5% glycerol, 1mM DTT

NiNTA Elution buffer: 20mM Tris pH 8.0, 500mM NaCl, 300mM Imidazole, 5% glycerol

IEX buffer A: 20mM HEPES pH 7.5, 30mM NaCl, 5% glycerol, 1mM DTT

IEX buffer B: 20mM HEPES pH 7.5, 1M NaCl, 5% glycerol, 1mM DTT

TEV buffer: 20mM Tris pH 8.0, 100mM NaCl, 5% glycerol, 1mM DTT

10.3. Bacterial Growth media

Growth media were sterilized in autoclave at 121°C. Eventual supplements were added prior to use.

LB broth (Lennox L broth, Sigma): 10g/L Tryptone, 5 g/L Teast extract, 5 g/L NaCl in deionized water.

LB Agar (Lennox L Agar, Sigma): 10g/L Tryptone, 5 g/L Teast extract, 5 g/L NaCl, 15g/L Agar in deionized water. The complete dissolution of the components occurs in the autoclave. The liquid medium is cooled down to 50°C, at which temperature a desired amount of antibiotic or other components can be added. The liquid LB agar is poured into the Petri dishes and left to cool and solidify. Plates are sealed with parafilm and stored at 4°C for up to maximum two months.

SOC: 2% Bacto-tryptone, 0.5% Bacto-yeast extract, 0.05% Sodium chloride, 2.5 mM Kcl, 10 mM $MgCl_2$ 20 mM Glucose. To prepare 1000 ml of SOC medium: 20 g bacto-tryptone, 5 g bacto-yeast extract and 0.5 g sodium chloride, in 950 mL deionized water; at the end, 2.5 mL of 1 M KCl. pH was adjusted at pH 7.0 with 5 N NaOH (~0.2 mL). Finally, the volume was adjusted at 1000 mL with deionized water. The solution was cooled to 60°C. 20 mL of 1M sterile glucose solution and 5 mL of 2M $MgCl_2$ were added just before use.

LB Agar bacmid plates: LB-AGAR + 50 LB μg/ml Kanamycin, 10 μg/ml Tetracyclin, 1 μg/ml Gentamycin, 40 μg/ml IPTG freshly prepared in H_2O (from 20 mg/ml stock), 100 μg/ml Bluo-Gal freshly prepared in DMSO (from 20 mg/ml stock). The plates were stored at 4°C protected from light for up to 1 month.

1000X Antibiotic solutions (filtered 0.22 μm)

50 mg/ml Kanamycin (in H2O)

34 g/ml Chloramphenicol (in EtOH)

10.4. Bacterial strains

DH5α (Invitrogen) It is the most frequently used *E. coli* strain for routine cloning applications. This strain is renowned for its high transformation efficiency, high plasmid yield and quality.
Genotype: F– Φ80lacZΔM15 Δ(lacZYA-argF) U169 recA1 endA1 hsdR17 (rK–, mK+) phoA supE44 λ– thi-1 gyrA96 relA1

BL21(DE3) pLysE (Novagen) It is the first strain selected for testing protein expression in a prokaryotic system. DE3 lysogen contains T7 polymerase gene, expressed upon IPTG induction. This strain is deficient of *lon* and *omp-t* proteases and is therefore suitable for expression of non-toxic genes.

Genotype: F^- ompT $hsdS_B(r_B^- m_B^-)$ gal dcm (DE3) pLysE (Cm^R)

Lemo 21 (DE3) (New England Biolab): Chemically competent *E. coli* cells with a fine tuning of T7 expression that can alleviate growth inhibitory effects from toxic proteins. Tunable expression is achieved by varying the level of lysozyme (*lysY*) by adding L-rhamnose to the expression culture at levels from zero to 2000 µM.

Genotype: *fhuA2 [lon] ompT gal (λ DE3) [dcm] ΔhsdS/ pLemo*(Cam_R) *λ DE3 = λ sBamHIo ΔEcoRI-B int::(lacI::PlacUV5::T7 gene1) i21 Δnin5* pLemo = pACYC184-*PrhaBAD-lysY*

XL1Blue (Stratagene) These cells are optimized for cloning procedures and for the white-blue color screening.

Genotype: *recA1 endA1 gyrA96 thi-1 hsdR17 supE44 relA1 lac* [$F' proAB lacI^qZ\Delta M15$ Tn*10* (Tet^r)]

EMBacY *E.coli* (kindly provided by Dr. Imre Berger, University of Bristol) was used for bacmid generation. This strain has a viral genome with aBAC helper plasmid for Tn7 transposon enzyme and YFP reporter gene to monitor protein production. It is suitable for the blue-white screening to detect correct plasmid transposition. This strain is protease and chitinase deficient to ensure a reduced proteolytic activity. Resistant to Kanamycin, Tetracycline and Chloramphenicol.

10.5. Insect cells lines

***Spodoptera frugiperda* 9 (Sf9)** insect cell line (Expression Systems LLC, Davies - USA) is derived from pupal ovarian tissue of *Spodoptera frugiperda* IPLB-Sf-21-AE. These cells are a subclone of Sf21 cell line selected for their faster growth rate and higher cell densities. These cells share a uniform diameter at around 14µm. Sf9 may be used for bacmid generation and protein expression.

***Trichoplusia ni* High 5 (H5)** insect cells (Expression Systems LLC, Davies - USA) are derived from the *Trichoplusia ni* embryonic tissue. These cells are only used for protein expression.

10.6. DNA manipulations

10.6.1. Wzx

Wzx gene from *Pseudomonas Aeruginosa* (PAO1) was inserted in pWaldo-GFPd-8His vector (ADDGENE) using the ***Restriction enzyme Free cloning (RF)*** method.

Unlike classical DNA cloning methods that include the use of restriction enzymes to cleave the selected vector and the target DNA, and then a DNA ligase to re-join the ends, the ***PCR-based restriction site-free cloning (RF)*** is based on the overlap extension site-directed mutagenesis technique.

The Restriction Free (RF) cloning technique was selected for its versatility and to avoid the classical restriction enzymes cloning. In fact, restriction enzymes may recognize a sequence within the gene of interest (GOI) resulting in a truncated construct. In addition, the ligation steps that follow DNA cleavage may lead to the circularization of the empty vector or to the inverted insertion of the gene. Instead, RF allows the modification of large parts of the plasmid such as resistance or tag changing without cleaving the vector.

The process consists in two consecutive PCR reaction; in the first a High-fidelity DNA polymerase is used to amplify the insert DNA sequence creating a construct (the desired gene flanked by vector insertion sequences), purified using a DNA gel extraction kit, and then used as megaprimer in a second PCR reaction in which the vector functions as template.

The key of RF is the proper design of primers for the creation of a megaprimer that is a DNA sequence containing the GOI and delimited by two sequences complementary to the vector. The cloning reaction is started by a pair of primers designed with complementary sequence to both the target DNA insert and the selected plasmid (Bond and Naus 2012). The RF primers usually are almost 50 nucleotides long. Half of the primers anneal with the GOI promoting megaprimer creation, the other half becomes the extremity of the megaprimer, complementary to the vector (Zeng et al. 2017). Since the primer sequences are fundamental for cloning success, an online tool is available for proper primer design (Bond and Naus 2012). Once designed, the primer sequences were inserted in NEB online tool to determine the annealing conditions. This step is essential to optimize primer length in order to have a similar GC content between the primers and consequently compatible melting temperatures (T_m).

In the first PCR step the primers anneal on the Wzx gene interacting with their complementary sequences. The product of this PCR is constituted by the gene of interest delimited on each side by the primer sequences complementary with the vector. This fragment of DNA was used as a primer in the following PCR as depicted in Figure 10.1. In the second step of RF cloning, the megaprimer anneals with the vector promoting the amplification of a new plasmid that includes the vector and Wzx.

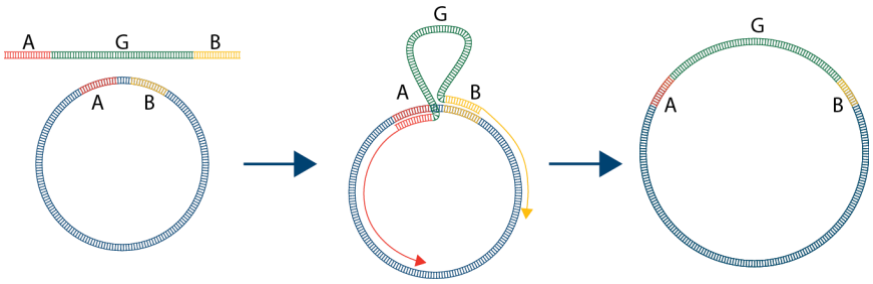

Figure 10.1: RF cloning mechanism. From Integrated DNA technologies.

pWaldo vector (Addgene) encodes for the Green Fluorescent Protein with an 8-histidine tag at the C-terminus of the gene of interest (GOI). (Figure 10.2) In addition, it confers resistance against Kanamycin. The expression of proteins cloned in this vector is under the regulation of lactose *(lac)* promoter. *E.coli lac* operon is a short segment of the bacterial chromosome encoding a genetic switch that responds to glucose and lactose concentrations. Lac repressor binds to the *lac* promoter occluding access of RNA polymerase holoenzyme. Lac repressor binding is weakened in the presence of allolactose or its analog, isopropyl β-D-1-thiogalactopyranoside (IPTG), relieving repression. IPTG removes the repressor and allows RNA polymerase activity weakening *lac* binding.

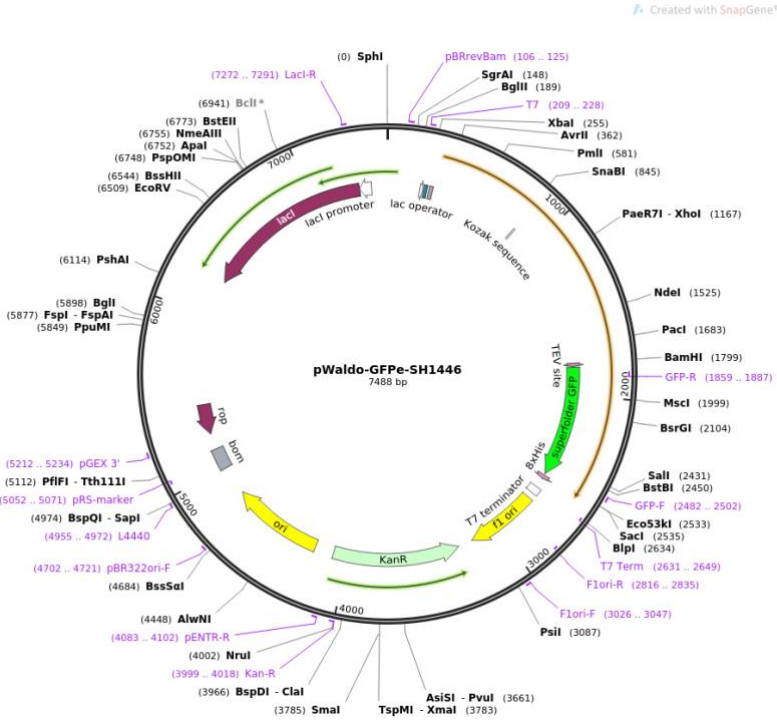

Figure 10.2: pWaldo vector from Addgene

10.6.1.1 Cloning procedures

1 µl (x ng) of PAO1 genome from ATCC was used as template in the amplification reaction of the Wzx gene using a PCR thermal cycler (Prime Thermal Cycler). Forward and reverse primers were designed adding cleavage sites for thrombin. Sequences are reported in Table 10.1.

Table 10.1: Primers sequence

Primer name	Sequence
PAO1_C F1	**GGTGGTTCTAGA**ATGAGTGCGGCTTTTAT
PAO1_C R1	**GCCACGAGGAACTAA**CTTGGCATCTCCCTTGGCA
Primer pWaldoFw	AGAAATAATTTTGTTTAACTTTAAGAAGGAGATATCTAGAATGAGTGCGGCTTTTATC
Primer pWaldoRv	CTCCTCCTTTGCTGAATTGACCCTGACTGCCACGAGGAACTAACTTG
Mutagenesis Fw	(Phos)CATCATCATCACCACCACCACCACCACCACTGAGAT
Mutagenesis Rv	(Phos)GGCCGCAAGCTTTTTGTAG

PCR 1 on PAO1 genome

PCR program:

- 5'@ 98°C
- 30" @ 98°C
- 30" @ 52°C 30 cycles
- 2' @ 72°C
- 6' @ 72°C
- Hold 4°C

PCR mixture:

1µl	PAO 1 genome
0,5µl	primer PAO1_C F1
0,5µl	primer PAO1_C R1
0,5µl	dNTP's
0,25µl	Q_5 polymerase
0,5µl	5X Q_5 Buffer
to 25µl	Water

PCR 1 product was then used as template for the megaprimer creation.

Rf cloning

The first PCR for Megaprimer creation for pWaldo vector was performed as follows:

RF cloning RF1:

PCR program:

- 5’ @ 98°C
- 30” @ 98°C
- 20” @ 56°C — 30 cycles
- 2’ @ 72°C
- 5’ @ 72°C
- Hold 4°C

PCR mixture:

1 µl	PCR1 product
1µl	Primer pWaldo_ Fw
1µl	Primer pWaldo_Rv
1µl	Dntp’s
10µl	5x Q_5 Buffer
0,5 µl	Q_5 polymerase
to 50µl	Water

The megaprimer, resulting from the first PCR, was loaded on agarose gel to verify the correct dimension of the product. The DNA band with the proper dimension was excised from gel and purified with Gene extraction Kit (SIGMA) to recover the DNA. The cloned megaprimer was quantified by spectrophotometry with Simply Nano (GE), and used for the subsequent PCR.

RF cloning RF 2:

PCR program:

- 5’ @ 98°C
- 30” @ 98°C
- 1’ @ 68°C — 30 cycles
- 5’ @ 72°C
- 5’ @ 72°C
- Hold @ 4°C

PCR mixture:

315ng	Megaprimer
65ng	pWaldo
1μl	DNTp's
10μl	5x Q_5 Buffer
0,5 μl	Q_5 polymerase
to 50μl	Water

PCR products were digested for 1 h at 37°C with DpnI restriction enzyme (NEB). DpnI cleaves at methylated sites only (generated during plasmid DNA amplification in *E. coli* dam+ cells, including typical strains for plasmid amplification, such as strain DH5α or XL1 Blue). Therefore, this step degrades the template plasmid but not the PCR product.

The template-free PCR product was then transformed in XL1 Blue competent cells (according to standard protocol) and positive clones were confirmed by DNA sequencing to verify the correct insertion of Wzx gene in pWaldo.

Mutagenesis protocol (pWaldo-WZX-GFP-10His plasmid)

The His tag of pWaldo was elongated to 10 histidine to increase the affinity of the resulting fusion protein with the IMAC resins used for purification procedures. Tag elongation using RF cloning was unsuccessful, probably due to the high homology of the sequence of the tag that did not allow the selective binding of the megaprimer to the vector. Mutation using back to back and phosphorylated primers gave the desired result (Figure 10.3).

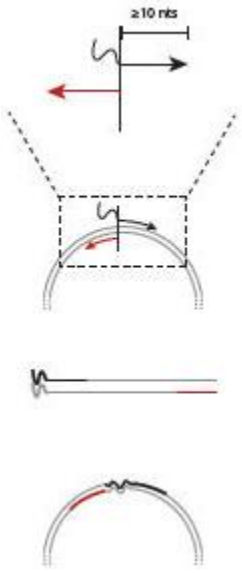

Figure 10.3: Schematic representation of small insertions with mutagenesis protocol. From NEB

PCR program:

- 1'@ 98°C
- 10" @ 98°C
- 30" @ 66°C
- 4'30" @ 72°C

x25 cycles

- 5'@ 72°C

PCR mix:

0.5 µl	Template
12.5µl	Q_5 Hot start mix polymerase
0.5µl	Primer Fw
0.5µl	Primer Rv
To 25µl	Water

PCR product was digested with KLD enzymes (NEB) for 5' at room temperature.

Digestion mix:

1µl	PCR product
5µl	2X KLD reaction buffer
1µl	10X KLD enzymes
To 10µl	Water

10.6.2. GSK-3β

DNA encoding human full-length (FL) GSK-3β was purchased by Genescript.

The oligos for the cloning of three GSK-3β constructs were obtained from Sigma. The chosen constructs are the full-length GSK-3β (residues 1-420) and two N- and C-terminal truncated forms, the first with residues 25-393 and the shorter one with residues 35-386 (Table 10.2).

Oligo Name	Sequence	GC %	Tm
GSK3_L1_M1fw	TACTTCCAATCCATGTCAGGGCGGCCCAGAAC	56	64
GSK3b_L1_G25 fw	TACTTCCAATCCATGAAAGTTAGCAGAGACAAGG AC	42	57
GSK3b_L1_S35f w	TACTTCCAATCCAAGGTGACAACAGTGGTGGCAA C	49	62
GSK3b_L1_A38 6rv	TATCCACCTTTACTGtcaTGCTTGAATCCGAGCATG AGGAG	46	60
GSK3b_L1_N39 3rv	TATCCACCTTTACTGtcaATTTGTGGGGGTTGAAGC AGCTG	46	63
GSK3b_L1_T42 0rv	TATCCACCTTTACTGtcaGGTGGAGTTGGAAGCTGA TGCAG	49	62

Table 10.2: Oligo sequences, in red sequences added for LIC cloning.

The oligos were resuspended in TE buffer at 100 µM concentration for long term storage at -20°C. Prior to use, an aliquot of the oligo solution was diluted to 10 µM in sterile MilliQ water. Aliquots are also stored at -20°C.

A PCR on the DNA template was performed to obtain the desired constructs including the additional sequences for LIC.

GSK-3β FL oligos:

- GSK3_L1_M1fw
- GSK3b_L1_T420rv

GSK-3β 25-393 oligos:

- GSK3b_L1_G25fw
- GSK3b_L1_N393rv

GSK-3β 35-386 oligos:

- GSK3b_L1_S35fw
- GSK3b_L1_A386rv

PCR protocol:

- 1'@ 98°C
- 10" @ 98°C
- 20" @ 65°C x 35 cycles
- 30" @ 72°C
- 2'@72°C
- Hold @ 4°C

PCR sample mixture:

Negative control	Sample GOI	Reagent
5µl	10µl	5X Q_5 reaction buffer
0.5µl	1µl	10mM dNTP's
1.25µl	2.5µl	10µM Fw primer
1.25µl	2.5µl	10µM Rv primer
---	1µl	10ng/µl template DNA
0.25µl	0.5µl	Q_5 High Fidelity DNA polymerase
to 25µl	to 50µl	Water

PCR products mixed with 6X DNA loading buffer were loaded on 1% agarose gel with Syber-SAFE fluorescent stain (Life Technologies). The gel was run in TAE buffer at 80 V and observed under UV lamp to verify the correct construct formation PCR products were purified using Nucleospin PCR cleanup (MN) according to the manufacturer protocol and eluted in 25 µl of TE. Afterwards the eluates were quantified with the NanoDrop (ThermoFisher) spectrophotometer and stored at -20°C.

The constructs were cloned in two different vectors suitable for insect cell expression pFastBac-ZetaBasic (pFB-ZB) and pFastBac-Bse (pFB-Bse) kindly provided by Dr. Opher Gileadi, SGC-Oxford.

pFB-ZB is a baculovirus transfer vector with a 10-His tag and a Z-basic tag followed by a TEV protease cleavage site. The vector includes sites for LIC cloning, Ampicillin resistance (100 μg/ml) and the SacB gene, allowing the negative selection of transformed bacteria on 5% sucrose medium (Figure 10.4). Z-basic tag is a 54 amino acid sequence derived from protein A and subsequently modified to have a positive surface charge (Hedhammar and Hober 2007).

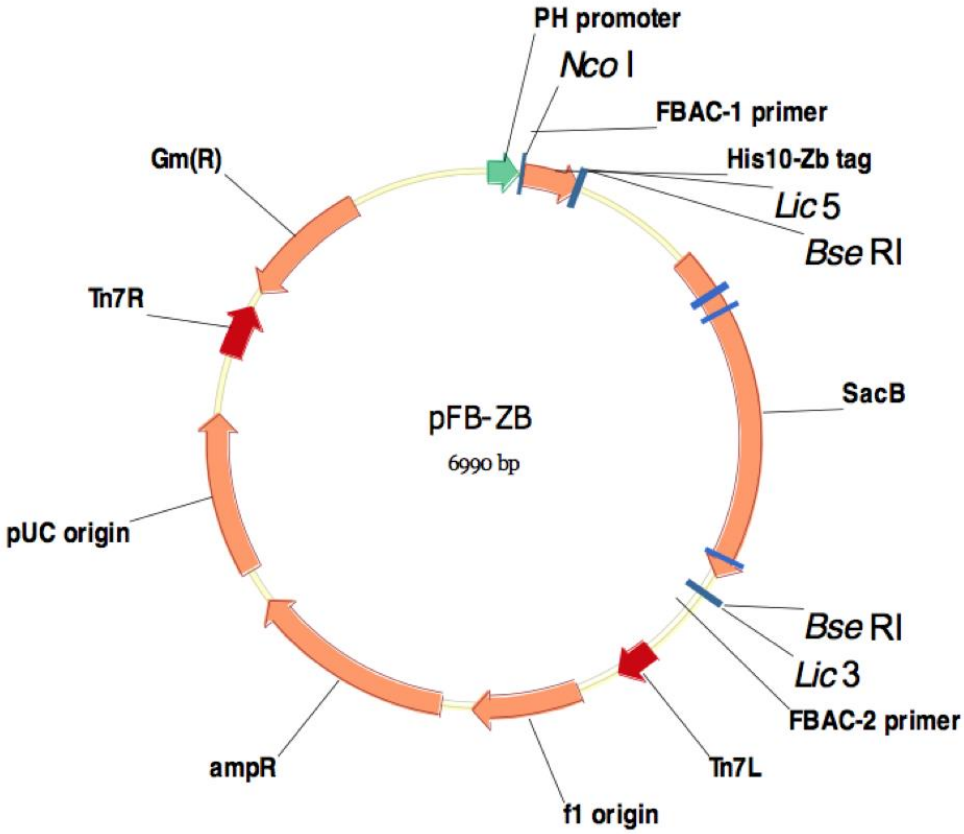

Figure 10.4: pFB-ZB vector from Dr. Opher Gileadi

pFB-Bse is a baculovirus transfer vector with a 6 His tag, a TEV protease cleavage site and an Ampicillin resistance coding gene (Figure 10.5). Also this vector has the SacB gene and sites for LIC cloning.

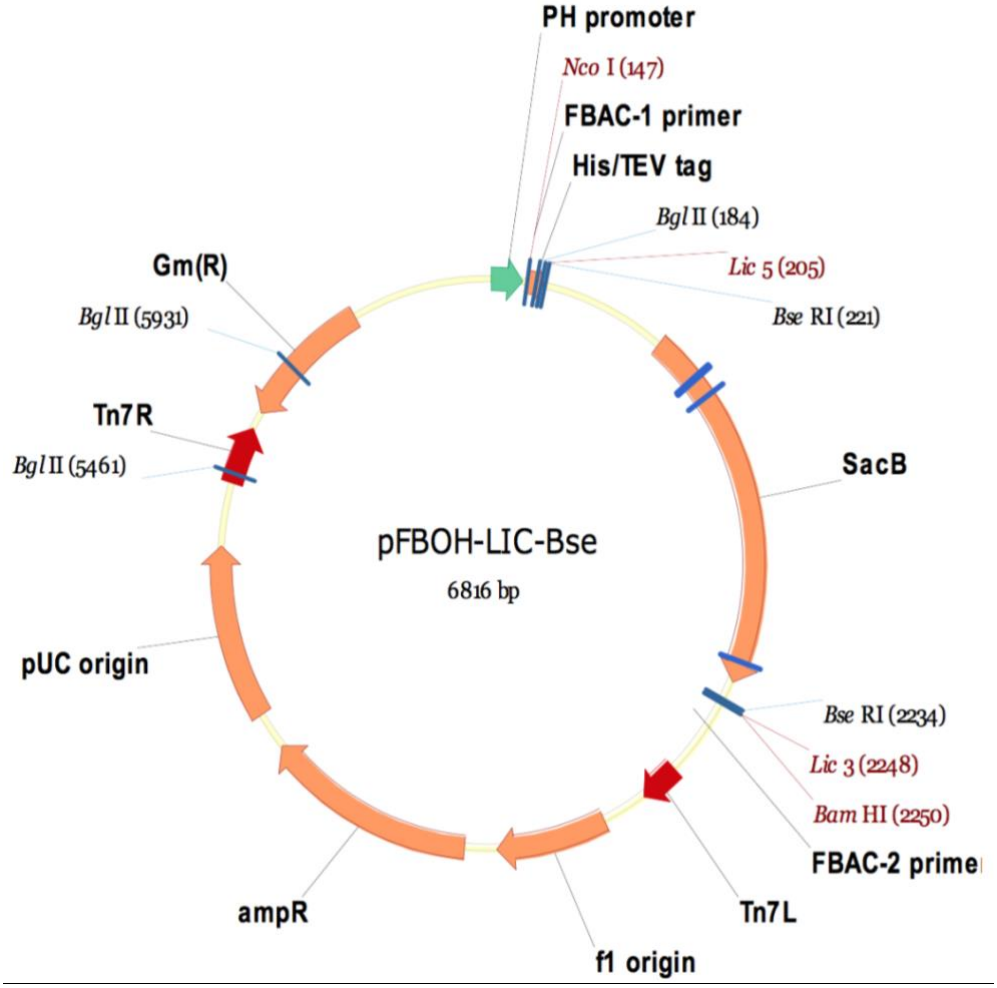

Figure 10.5: pFB-Bse vector from Dr. Opher Gileadi

10.6.2.1. Ligation independent Cloning (LIC)

LIC technique was developed in 1990 to efficiently clone complex PCR mixtures without restriction enzymes.

This cloning technique consist in the addition of complementary 12-nucleotide single strain DNA tails on the insert and on the linearized vector. In particular, the 5'-ends of the insert primers contain additional nucleotide sequences lacking dCMP. In the amplification step these sequences are copied at their 3'ends as sequences lacking dGMP, that can be removed by T4 DNA polymerase in the presence of dGTP. Due to the exonuclease activity of the T4 DNA polymerase, the insert presents definite 5'-single-stranded (ss) tails. The LIC suitable vector is linearized and amplified with primers that promote the addition of 12-nucleotide tails. The vector's tails are digested by T4 DNA polymerase in the presence of dCTP creating ss ends

that are complementary to those of the insert. The circularization is mediated by the interaction of the added tails.

Since identical tails are present at both extremities of the vector, the vector can only interact with the insert, preventing circularization of the empty vector. The product is transformed in bacteria (Aslanidis and de Jong 1990).

Vector linearization

pFB-ZB and pFB-Bse were treated for 2 hours at 37°C with BseRI enzyme that removed the SacB gene.

Reaction mixture:

10 µl	10x NEB Buffer4
5 µg	vector
2 µl	BseRI
To 100 µl	Water

The samples were loaded on 0.8% agarose gel to verify linearization of the vector and elimination of the Sac gene. On the gel were detected pBF-ZB band at 4490bp, corresponding to the vector without the 2000bp of the Sac gene and pFB-Bse band at 4803bp consistent with the elimination of SacB. Also the removed sequence was detectable in gel as a 2000bp band. The vector was subsequently purified with PCR purification kit (MN) and quantified. The linear vector can be stored at -20°C for 1 month or at -80°C up to 6 months.

T4 DNA polymerase treatment of the linearized vector and the insert

The annealing process requires 25-50 ng of treated vector, but the reaction was conducted with 600 ng of vector in order to obtain material sufficient for approximately 20 reactions.

Reaction program:

- 30'@ 22°C
- 20'@ 75°C
- Hold @ 15°C

Reaction mix:

2 µl	10x NEB buffer 2
2 µl	1mg/ml BSA
600ng	Digested vector
0.5 µl	100mM dGTP
1 µl	100mM DTT
0.4 µl	T4 DNA polymerase
To 20 µl	water

The vector solution can be immediately used in the annealing reaction. The final concentration of the insert is 10-20 ng/µl.

The T4 DNA polymerase treatment of the insert was performed using the protocol already described, using 0.02 pmol of insert DNA, sufficient for 10 annealing reactions, and 0.5 µl of dCTP instead of dGTP.

Annealing

The annealing reaction was performed mixing 2 µl of insert DNA (0.02 pmol) and 2 µl of LIC vector (25-50 ng). The mixture was incubated for 20' at room temperature.

Transformation and clone selection

Annealing product was transformed in DH5α competent cells by adding 50µl of competent cells to the reaction mix and then it was proceeded using the standard protocol. Cells were spread on LB Agar plates supplemented with 5% sucrose and 100 µg/ml Ampicillin and incubated overnight at 37°C.

The following day the plates were observed to detect the presence of bacterial colonies.

2 colonies for each plate were picked and inoculated in 2 ml LB supplemented with ampicillin and incubated overnight at 37°C under agitation.

The following day, the overnight inocula were used for Mini Prep (MN) to extract the plasmid. The DNA eluted from the column was quantified and subsequently loaded on agarose gel to verify its dimension. To verify the positive result of the cloning the samples were sent to sequencing.

10.6.3. Baculovirus expression vector system (bevs) (invitrogen)

Baculoviruses are double-stranded DNA viruses that normally infect insect cells. In the so called very late phase of the infection, the virus promotes the expression of polyhedrin that is one of the components of the capsid. These viruses are used as expression vectors replacing

the polyhedrin gene with the recombinant DNA that codifies for the protein of interest. With the modified virus, in the very late phase of infection the strong AcNPV polyhedrin promoter promotes the expression of the desired protein.

Bacmid generation by transposition- Bac-to-Bac Expression System

Once the correct insertion of the gene was verified by sequencing, the plasmid was transformed in EmBacY cells.

1 µl of the virus was transformed in 100 µl of cells and incubated 30' in ice. After 45" heat shock at 42°C the mixture was incubated 3' in ice. The cells were supplemented with 900 µl of 2x LB and incubated under agitation at 37°C for 7 hours.

The transformants were diluted 1:50, 50 µl or 100 µl of the dilution were spread on 10 cm LB-Agar Bacmid plates and incubated upside-down at 37°C for 48 hours, protected from light.

After the incubation, white colonies, for which the transposition was successful, can be distinguished from the blue ones that are negative clones. White colonies were restreaked on 6 cm LB Agar bacmid plates and incubated overnight at 37°C protected from light. When the transposition occurs, the gene insertion disrupts LacZ gene. So, in the presence of IPTG and Bluo-gal the colonies of recombinant bacteria are white whereas if the transposition does not occur the colonies are blue (Figure 10.6).

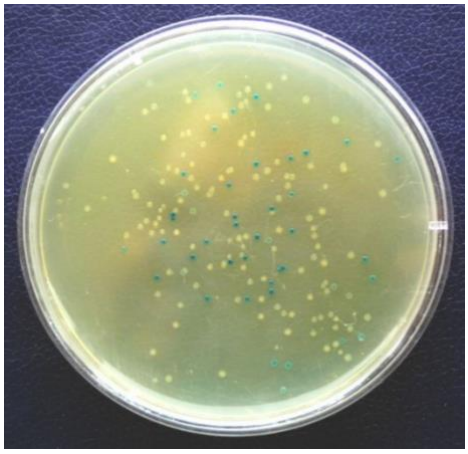

Figure 10.6: LB agar bacmid plate for colony selection

The re-streak is necessary to avoid false positives from the first plates. The positive colonies were inoculated in 10 µl of LB, then 5 µl were used for the control PCR and 5 µl are inoculated in 2 ml LB supplemented with Kanamycin and Gentamycin (7 µg/ml) and incubated at 37°C under agitation.

An aliquot of the overnight inoculum was used for the glycerol stock (final glycerol concentration 15%), the rest was used for the Bacmid Mini prep.

Bacmid mini prep, Imre Berger protocol using MN kit

The bacterial culture was centrifuged for 10' at 3000x g at 4°C and the pellet was resuspended in 300 µl of P1 buffer. Cells were lysed with 300 µl of P2 buffer, the tube was inverted 5-7 times and incubated 5 minutes. The solution was neutralized with 300 µl of P3 buffer, inverted 5-7 times and centrifuged 10' at maximum speed. The supernatant was transferred in a new tube and centrifuged for 5'. The supernatant was transferred in a new tube and 700 µl of 100% isopropanol were added. The mixture is incubated 2h at -20°C. The mixture was then centrifuged, and the supernatant was discarded. The clear bacmid pellet was carefully resuspended for two times in 70% ethanol and centrifuged 5'. After the second centrifuge is essential to work in a sterile environment. The Eppendorf tube was transferred under laminar flow hood and the ethanol was removed. The pellet was dried for 10' and resuspended in 50 µl of sterile water, 1 µl was saved for control PCR and 200 µl of insect cell medium were added on the rest (tube A) (Figure 10.7).

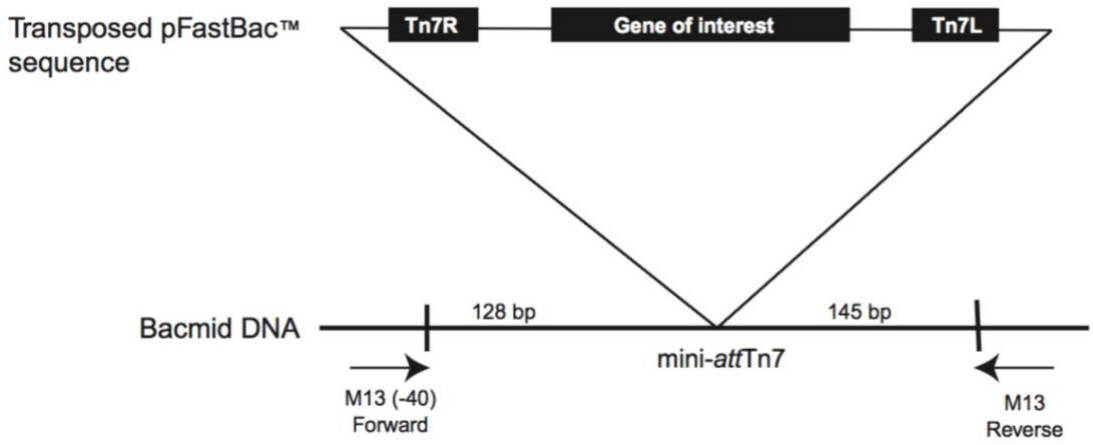

Figure 10.7: Transposition site. From Invitrogen

PCR program:

- 5' @ 95°C
- 15" @ 95°C
- 15" @ 55°C — 25 cycles
- 40" @ 72°C
- 10' @ 72°C
- Hold @ 10°C

PCR mix:

5 µl	5x Wonder Taq buffer
1 µl	10 µM Primer M13 Fw
1 µl	10 µM Primer M13 Rv
1 µl	Template
0.25 µl	Wonder Taq
To 25 µl	Water

PCR products were loaded on 1% agarose gel to control the transposition results. A 300bp band in the gel indicated an empty bacmid whereas positive clones had band at 2300bp+ GOI. So, GSK3-β FL had a band at 3560bp, the 25-393 construct at 3405bp and 35-386 one at 3354bp.

10.7. Bacterial transformation

Transformation in XL1Blue competent cells:

50 µl of XL1 Blue competent cells were transformed with 1 µl of DNA sample and incubated 30' in ice. The cells underwent a heat shock at 42°C for 45". Subsequently the mixture was incubated in ice for 5'. The chilled mixture was supplemented with 250 µl of room temperature SOC medium and incubated for 1h at 37°C under agitation (180 rpm). After 1h, 100 µl of the mixture were inoculated in 5/10 ml of LB supplemented with Kanamycin (50ul/ml) and incubated O/N at 37°C, 180 rpm.

Transformation in BL21(DE3) 21 competent cells:

50 µl of BL21(DE3) competent cells were transformed with 1 µl of pWaldo-WZX-GFP-10His plasmid (70 ng) by incubating 30' in ice. After 45" heat shock at 42°C the mixture was incubated for 3' in ice. Then, it was supplemented with 250 µl of preheated LB and incubated 1h at 37°C shaking at 180 rpm.

100/200 µl of the transformants were inoculated in 10 ml of LB supplemented with Kanamycin (50 µl/ml) and incubated O/N at 37°C, 180 rpm.

Transformation in Lemo 21 competent cells:

pWaldo-WZX-GFP-10His, obtained with RF cloning as described before, was transformed in Lemo21 or BL21(DE3) pLysE competent cells.

50 µl of Lemo 21(DE3) competent cells were transformed with 1µl of pWaldo-WZX-GFP-10His plasmid (70ng). After 30' incubation in ice and 10" heat shock at 42°C, the mixture was incubated

5’ in ice. Then it was supplemented with 950 µl of room temperature LB and incubated 1h at 37°C shaking at 180 rpm.

100/200 µl of the transformants were inoculated in 10 ml of LB supplemented with Kanamycin (50 µl/ml) and Chloramphenicol (34 µg/ml) and incubated O/N at 37°C, 180 rpm.

10.8. Insect cells transfection

Sf9 cells transfection

For each construct, tube A was mixed with a second tube containing 100µl of insect cell medium and 10µl of FuGene® reagent (Promega). This transfection mix was incubated for 5’ at room temperature.

In 6-well plate 3 ml of $0.5x10^6$ Sf9 cells were dispensed in each well ($1.5x10^6$ cells/well). Each construct was tested in duplicate.

150 µl of the transfection mix were added to the cells and the plates were incubated at 27°C for 55-60 hours. After the incubation the cells were collected and centrifuged at 1500x g for 5’. At the supernatant, identified as the P0 stock, 2% v/v of FBS (Foetal Bovine Serum) filtered at 0.22 µm were added to stabilize the virus.

$1.6x10^6$ Sf9 cells were poured in T25 flask (Thermo Fisher), let adhere to the surface and infected with 150 µl of P0 stock. The cells were incubated for 4 days at 27°C. After 4 days the cells were resuspended and centrifuged at 1000x g for 15’, the supernatant was the P1 virus stock. 10% of FBS was added to the P1 stock to stabilize the virus. 50 ml of Sf9 cells ($1x10^6$ cells/ml) were poured in a 250 ml flask (Corning) and infected with 200 µl of P1 virus stock.

The culture was incubated at 27°C under agitation for 4 days. The number and the diameter of the cells was monitored to determine virus activity. After the incubation, P2 virus stock was collected by cell centrifugation as before and supplemented with 10% of FBS.

10.9. Small-scale protein expression

10.9.1. Wzx

Small-scale test expressions are performed to determine the best expression conditions. During this work two bacterial strains (Lemo 21(DE3) and BL21(DE3) pLysE) were tested at different concentration of rhamnose and glucose respectively and with different induction times and IPTG (isopropyl-β-D-1-tiogalattopiranoside) concentrations.

Transformants containing the pWaldo-WZX-GFP-10His plasmid were inoculated in 250 ml of LB supplemented with Kanamycin (50 μl/ml) and Chloramphenicol (34 μg/ml). The Lemo 21 broth was added with different concentrations of rhamnose (0 mM, 0.2 mM, 0.5 mM, 0.75 mM, 1 mM, and 2 mM) whereas BL21(DE3) pLysE both was supplemented with different percentages of glucose (0%, 1%, and 2%).

The cells were grown at 37°C under agitation. Once Lemo 21 cells reached OD_{600} 0.4 (measured with Shimadzu UV-1800 UV spectrophotometer), they were induced with 0.4 mM IPTG at different temperatures and induction times:

- 5h at 37°C
- Overnight at 20°C

BL21(DE3) pLysE cells were grown until OD_{600} 0.6 and induced at different temperatures, times and IPTG concentrations.

Induction at 20°C			Induction at 37°C		
0.1mM IPTG	0.2mM IPTG	0.5mM IPTG	0.1mM IPTG	0.2mM IPTG	0.5mM IPTG
Overnight	Overnight	Overnight	5h	5h	5h

To determine the best expression conditions, the fluorescence intensity of the bacterial culture was recorded and at the end of the induction. Not induced bacteria were used are controls.

10.9.2. GSK3- β

Small-scale expression tests were performed in 24 deep-well plates with two cell lines, Sf9 and H5 cells, at three different values of the multiplicity of infection (MOI) and at two expression times (48h and 72h).

The determination of the proper MOI depends upon virus potency, a strong virus should be used at low titer whereas the MOI 3 is preferred for weak viruses. The correlation between the MOI and the number of infected cells is not linear therefore, MOI 1 is considered as the viral concentration capable to infect 63% of the cells whereas MOI 3 infects the 95% (Figure 10.8) (Stacey and Davis 2007).

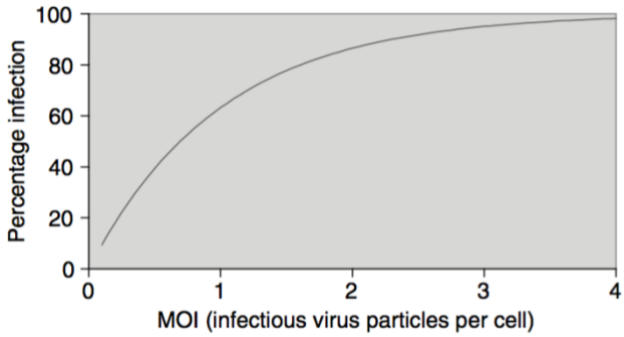

Figure 10.8: Relationship between MOI and infected cells. From Stacey and Davis, 2007

In each well 2ml of $1x10^6$ cells/ml were introduced and infected with:

- 0.66µl of P2 for MOI 1
- 6.66µl of P2 for MOI 2
- 66.6µl of P2 for MOI 3

The plates were incubated for 48h or 72h, at 27°C under agitation.

After the expression the plate was centrifuged for 15' at 500x g at 4°C. The supernatant was discarded, whereas the pellet was washed with 1 ml of PBS with 10% glycerol and centrifuged again for 15' at 500x g at 4°C. The pellet was stored at -80°C.

10.10. Large-scale protein expression

10.10.1. Wzx

Protein expression

To express the pWaldo-WZX-GFP-10His fusion protein 2 ml of the O/N transformants were inoculated in 500 ml LB (total volume of the culture 4 L), supplemented with Kanamycin (50 µg/ml) and Chloramphenicol (34 µg/ml). The cells were grown at 37°C at 180 rpm until they reached OD_{600} 0.4. Once the culture reached the correct density, the flasks were cooled to 20°C. The protein expression was induced by the addition of 0.4mM IPTG, and cultures were incubated O/N at 20°C under agitation. Cells were collected via centrifugation at 4000x g for 10' (Beckman Coulter Avanti J-26-XP). The cell pellet was washed with TBS buffer and centrifuged again at 4000x g for 15'(Hermle z 326K). The pellets were stored at -80°C before cells disruption, in order to improve cell lysis.

Cells lysis and membrane recovery

Frozen bacterial pellet was thawed at room temperature and resuspended in TBS with 1 mM PMSF (phenylmethanesulfonyl fluoride) (Sigma). Once the pellet was homogenously resuspended, lysozyme was added. The bacterial resuspension was incubated for 30' at RT to allow lysozyme enzymatic activity.

The bacterial resuspension was subjected to 3 cycles of homogenization at 1200 psi (APV Lab 2000, GSK) until complete cell disruption. Cell lysates were centrifuged at >4000x g for 20' to pellet cellular debris. The supernatant was ultracentrifuged (Beckman L8-70 ultracentrifuge) at 110˙000x g at 10°C for 1h. After ultracentrifugation, the supernatant was discarded while the bacterial membrane pellet was resuspended in TBS buffer using a potter to increase sample homogeneity. Membrane aliquots were stored at -80°C.

10.10.2. GSK3- β

Trichoplusia ni High 5 (H5) insect cells were infected with the P2 viral stock with the MOI selected from during small-scale expression. The culture ($1,5x10_6$ cells/mL) was incubated in 1 L bottles (Vitlab), for 2 days for 35-386 construct and for 3 days for the full-length construct, at 27 °C, 180 rpm. After the expression, cells were centrifuged at 1000x g at 4 °C for 1 h. Cell pellet was washed with PBS with 10% glycerol and centrifuged for 15' at 1000x g. The pellet was stored at -80 °C until use.

10.11. Solubilization in detergents

Detergents are used to disrupt the phospholipidic bilayer of cell membranes and extract hydrophobic membrane protein without hampering protein folding (Linke 2009). These amphiphilic molecules mimic the lipid bilayer by covering the hydrophobic portion of the protein, thus yielding a protein-detergent complex soluble in aqueous buffers. The optimal detergent retains the protein native folding and functionality, preventing protein aggregation and precipitation. However, the solubilized protein may not be stable in detergent micelles due to the lack of the lateral pressure exerted by the membrane in the native environment (Privé 2007). In some cases, addition of lipids may increase the stability of the sample (Moraes et al. 2014), but at the same time their presence may affect crystal formation.
An important parameter that characterizes surfactant behavior is the critical micelle concentration (CMC) that is the minimal detergent concentration at which micelles form. If the detergent concentration is below the CMC, the detergent is in a monomeric form and does not behave as surfactant. Above the CMC, there is an equilibrium between monomeric detergent molecules and micelles. Detergents are also characterized by the aggregation number, i.e. the average number of monomers forming a micelle, a parameter linked to micelle dimension (Moraes et al. 2014). The concentration of the detergent in the sample must be carefully evaluated, as a low detergent concentration may not be able to fully mask the hydrophobic regions of the protein, resulting in protein aggregation and precipitation (Privé 2007). On the other hand, an excessive concentration of

surfactant may remove the proximal lipid, essential to maintain protein folding, thus resulting in protein unfolding and, eventually, aggregation. A high concentration of detergent may also interfere with the crystallization process causing phase separation (Guan et al. 2006). In addition, at low temperature highly concentrated detergents tend to precipitate in their crystalline form. The temperature in which this phenomenon occurs is called cloud point and is characteristic of each detergent.

Detergents are divided according to the characteristics of their head groups: ionic detergents have a charged head group, nonionic detergents possess uncharged hydrophilic groups, and zwitterionic detergents have opposite charges within the head group. In addition, ionic detergents may carry negative (anionic) charges, such as sodium dodecyl sulfate (SDS), or cationic charges (cationic). Ionic detergents are usually considered among the harshest, frequently causing protein unfolding or denaturation.

- SDS is a C12 detergent with a small, negatively charged head group. Its association and solubilizing properties strongly depend upon the temperature and the presence of salts in the solution. This detergent is known for its denaturing properties on soluble and membrane proteins. However, its ability to solubilize integral membrane proteins is lower compared with its effect on soluble proteins (Figure 10.9).

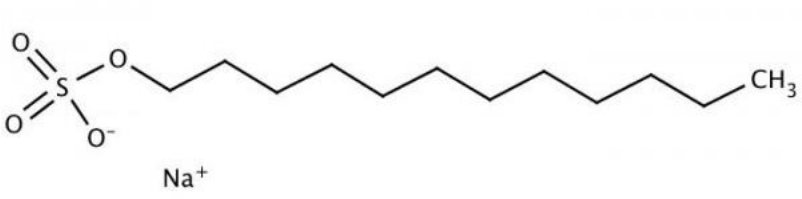

Figure 10.9: Sodium Dodecyl Sulfate (SDS)

On the contrary, nonionic detergents are usually milder since they mostly affect the lipid-lipid or the lipid-protein interactions without affecting protein internal non-covalent bonds. Therefore, this class of detergents is commonly used in solubilization steps of membrane protein research. The most used nonionic detergents are sugar-based detergents such as OG (n-octyl-β-D-glycoside), DM (n-decyl-β-D-maltoside) and DDM (n-dodecyl-β-D-maltoside) thanks to their not denaturing properties. High purity grade of the detergent (>99%) is a crucial parameter for membrane protein research.

- $C_{12}E_8$ (octaethylene glycol monododecyl ether) is a mild detergent with a very low CMC value (Figure 10.10). CMC: 0.09 mM.

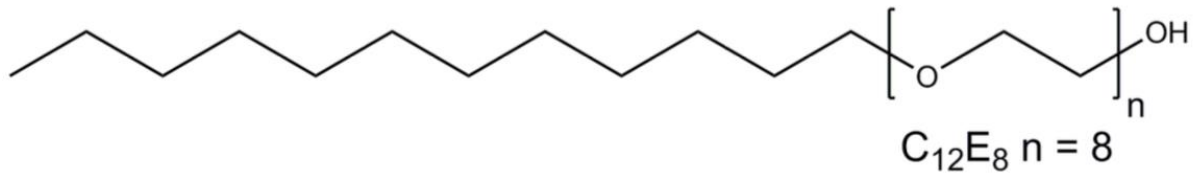

Figure 10.10: Octaethylene glycol monododecyl ether (C12E8)

- OG is a relatively harsh detergent that forms compact micelles. It is commonly used for crystallization (Figure 10.11). CMC: 18-20 mM.

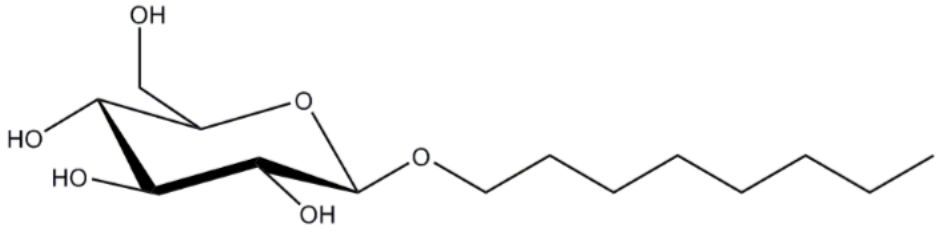

Figure 10. 11: n-octyl- β-D-glycoside (OG)

- DDM is a mild detergent that forms 60 kDa micelles, with a good masking ability for the solubilized proteins. It is used for the solubilization of aggregation prone proteins due to its ability to maintaining protein functionality (Figure 10.12). CMC: 0.2 mM

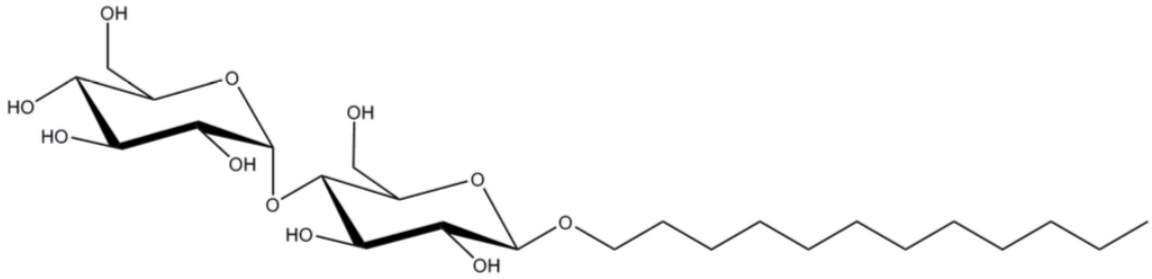

Figure 10.12: n-dodecyl-β-D-maltoside (DDM)

- DM properties highly resemble DDM ones except for its low CMC that makes its removal much easier compared to DDM (Figure 10.13) (Privé 2007). CMC: 1.8mM

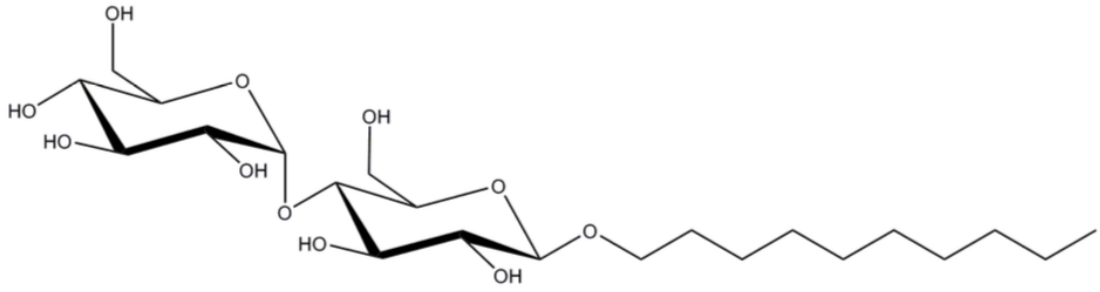

Figure 10.13: n-decyl-β-D-maltoside (DM)

The zwitterionic surfactants combine the properties of the ionic and nonionic classes, resulting milder than the ionic detergents and suitable especially for crystallization and NMR studies. The best known members of this class are CHAPS (3-[(3-Cholamidopropyl)dimetilammonio]-1-propanesulfonate) (CMC: 8mM) and LDAO (lauryldimethylamine-N-oxide) (Moraes et al. 2014).

- LDAO is a C12 zwitterionic detergent that forms small micelles (16kDa) so, it is widely used for crystallization studies. However, it is considered relatively harsh and may promote the denaturation of the protein (Figure 10.14). CMC: 2mM

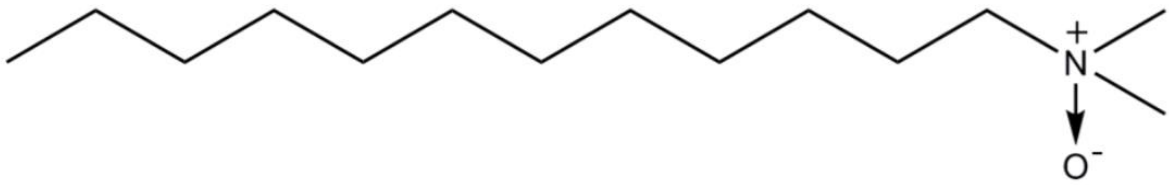

Figure 10.14: Lauryldimethylamine-N-oxide (LDAO)

Membrane protein crystals are difficult to form due to the low number of protein-protein interactions involving the hydrophobic domains, the flexible nature of detergent micelles and the physical properties of the surfactant. The choice a small-micelle detergent, such as OG and LDAO, may allow the formation of a larger number of intermolecular contacts between protein molecules, leading to better diffracting crystals (Privé 2007). On the other hand, these detergents are more denaturing than those forming larger micelles.

Solubilization test

1ml of membranes was resuspended in TBS buffer (corresponding to 50 ml of bacterial culture) and solubilized in 10ml of

- 10xCMC LDAO (20 mM)
- 10xCMC OG (200 mM)
- 10xCMC DM (18 mM)
- 10xCMC DDM (2 mM)
- 10xCMC $C_{12}E_8$ (0.9 mM)

The solution was incubated at 4°C for 1h under agitation. Then the sample was ultracentrifuged at 90000x g and the amount of insoluble material pellet was compared. The supernatant was loaded on 500 µl of Co^{2+} resin (see protocol below) and incubated for 1h in cold room under slow agitation. The sample was transferred to a column (BioRad) and the flow through (FT) was collected. The resin was washed with 10 column volumes (CV) of buffer and subsequently with 10 CV of the buffer

supplemented with 5 mM Imidazole. The protein was eluted with 150 mM Imidazole in 1 CV for 3 times.

The fluorescence intensity of all the fractions was measured with Tecan Infinite M100 Pro to determine Wzx binding to the resin.

Solubilization in DM, LDAO and DDM

The desired amount of resuspended membranes was solubilized in a volume 10x the membrane volume of the following buffer: 20 mM Tris pH 8.2, 150 mM NaCl, 1 mM PMSF, with the chosen detergent. DM and LDAO were added to the buffer at a final concentration 10x CMC, corresponding to 18 mM and 20 mM, respectively. DDM was added at final concentration 15x CMC (3 mM). The mixture was incubated 1h at 4°C under slow agitation. After the incubation the sample was ultracentrifuged at 90000x g for 20'.

Detergent exchange

To replace LDAO with $C_{12}E_8$, the Co^{2+} eluates (see below) were diluted 4 times with the **No detergent** buffer (see above) supplemented with 0.03% $C_{12}E_8$ (final concentration). The mixture was incubated in ice for 15 minutes and subsequently concentrated for SEC on Amicon concentrators with 50 kDa cutoff. The run was performed in the **No detergent** buffer supplemented with 0.03% of $C_{12}E_8$.

10.12. Protein purification

10.12.1. Immobilized Metal affinity chromatography

The IMAC is an affinity chromatography in which proteins are separated according to their affinity for metal ions (e.g., Zn^{2+}, Cu^{2+}, Cd^{2+}, Hg^{2+}, Co^{2+}, Ni^{2+}, and Fe^{2+}) immobilized on an inert polymer matrix (Porath 1989). Histidine, tryptophan, and cysteine present in proteins form complexes with the exposed metal ions. This separation method is especially suited for purifying recombinant proteins with poly-histidine tags. The most widely used are matrices chelating Co^{2+} (commercial product: Talon, from GE Healthcare) or Ni^{2+} ions (commercial product NiNTA, containing the chelating ligand nitrilotriacetic acid, from GE Healthcare) that are adapted to improve purification quality.

The exposed Co^{2+} (Talon resin) or Ni^{2+} ions (NiNTA resin) bind to the imidazole moieties present on the side chains of the poly-histidine protein tags. To elute the target proteins, elution buffer with high concentration of imidazole is applied to the resin to displace the poly-histidine tagged proteins.

10.12.1.1. Wzx

The bacterial membranes were solubilized in the chosen detergent prior to Wzx purification steps. All the purification processes were performed within the same day to decrease the possibility of protein unfolding and denaturation. After solubilization, the sample was purified with two different techniques, an immobilized metal affinity chromatography (IMAC) using Talon Superflow resin (GE healthcare), NiNTA Agarose (GE healthcare) and a Size Exclusion Chromatography with a Superdex G 200 column (GE healthcare) using AKTA FPLC Amersham biosciences p-920.

Co^{2+} and Ni^{2+} IMAC small-scale purification

2 ml of membranes, corresponding to 100 ml of bacterial culture, were solubilized in buffer with 10x CMC LDAO following standard protocol. Solubilized sample was split in 2. Half of the sample was loaded on 600 µl of Co^{2+} resin and the other half on 600 µl of Ni^{2+} resin, the mixtures were incubated for 1h at 4°C under slow agitation. After the incubation the FT was collected. Both the resins were washed with 5 CV of buffer without Imidazole. The Co^{2+} resin was washed with 5 CV of buffer supplemented with 5mM Imidazole, whereas the Ni^{2+} resin was washed with the same amount of buffer supplemented with 10 mM Imidazole. The elution was performed with 1 CV of buffer with 150 mM and 250 mM imidazole, respectively, for Co^{2+} and Ni^{2+} resins.

Mid-scale solubilization test

2 ml of membranes (corresponding to 100 ml of bacterial culture) were solubilized in Wzx buffer with 10x CMC DM, and other 2 ml were solubilized in 10x CMC LDAO. The samples were incubated for 1h at 4C° under slow agitation and subsequently ultracentrifuged at 90˙000x g for 20'. Supernatant was loaded on 1 ml equilibrated Co^{2+} resin and the mixture was incubated for 1h in cold room under slow agitation. The sample was transferred into a 25 ml column (Biorad) and the flow through (FT) was collected. The resin was washed with 10 CV of **Wzx buffer** and subsequently with 10 CV of **Wzx buffer** supplemented with 5 mM imidazole. The protein was eluted for five times with **Wzx buffer** + 150 mM imidazole in 0.5 CV. Eluates were pooled together and concentrated to 800 µl on 50 kDa Amicon concentrators. Samples were centrifuged for 15' at 14˙000x g prior to injection in SEC column. The run was performed in the buffer used for solubilization.

Large-scale purification with Co^{2+} resin

5 ml of solubilized membranes were loaded on 2 ml of equilibrated Co^{2+} resin and incubated in cold room for 1h under slow agitation. After the incubation the sample was transferred on a 25 ml column to collect FT.

The resin was washed with 10 CV of **Wzx buffer** (see above) and subsequently with 10 CV of **Wzx buffer** + 5 mM Imidazole to remove aspecific binding.

The protein was eluted 5 times with 0.5 CV of **Wzx buffer** + 150mM Imidazole. The fluorescence intensity of the fractions was recorded with a microplate reader (Tecan Infinite m 1000Pro) to detect the presence of Wzx+GFP. The fractions with higher fluorescence intensity were pooled together and concentrated to 800µl on 50 kDa Amicon concentrators. The concentrated sample was centrifuged at 14˙000x g for 15' to remove particles and possible aggregates before loading on the SEC column.

Affinity Chromatography protocol with Imidazole gradient

2 ml of solubilized membranes were loaded on 1 ml Co^{2+} resin and incubated for 1h at 4°C. After the incubation the flow through was collected. The resin was washed with 1 CV of buffer without Imidazole and then with a gradient from 5 mM Imidazole to 150 mM Imidazole, in 5 mM increments, with 1 CV each.

Affinity Chromatography with GFP resin

GFP-trap (Chromotek) is a resin designed for immunoprecipitation of GFP fused proteins. It is formed by an anti-GFP Nanobody/ V_HH coupled to agarose beads that allow the detection of the chimeric proteins.

1 ml of solubilized membranes in GFP buffer was loaded on 75 µl of GFP resin and incubated for 1h at 4°C. After FT collection the resin was washed 3 times with 10 CV of GFP buffer. The protein was eluted 4 times with 100 µl of GFP (0.3 mg/ml) for competition. The resin was subsequently washed again with 20 CV of GFP buffer. Despite the GFP competition for resin binding site, Wzx was not eluted in this step. The final 2 elutions were performed with 1 CV of a 0.2 M Glycine solution at pH 2.5. The eluates were collected in a Eppendorf tube with 100µl of GFP buffer to increase the pH of the solution immediately after the elution.

10.12.1.2. GSK3- β

Small-scale purification

Cells pellet was resuspended in 1 ml of lysis buffer (50 mM Tris pH 8.0, 500 mM NaCl, 10 mM Imidazole, 1 mM DTT, 1 mM AEBSF) and incubated for 5' in ice. The cells were disrupted via 2x 5" sonication at 50% amplitude using SonoPlus sonicator (Bandelin).

50µg/ml DNase and 5mM $MgCl_2$ were added to the lysed cells and the sample was incubated for 10' at room temperature (total extract-TE).

The total extract was centrifuged 30' at 16˙000x g at 4°C, the pellet (P) was discarded whereas the supernatant (SN) was loaded on 30 µl of NiNTA resin (CV). The resin was incubated with the sample for 1h in cold room under slow agitation. To collect the flow through (FT) the

sample was centrifuged for 15’ at 500x g at 4°C and the supernatant was discarded. The resin was washed with 1 ml of binding buffer and centrifuged for 2’ at 500x g in cold room (W). The sample was eluted twice with 2 CV of elution buffer, the buffer was incubated for 2’ and the tube was centrifuged for 2’ to collect the eluate.

All the fractions were loaded on SDS-PAGE gel to evaluate the best expression condition.

Large-scale purification

The following protocol was used for the purification of 1 L culture at $1.5x10^6$ cells/mL. The purification of a higher amount of cell culture was performed by scaling up the lysis buffer and the NiNTA volumes.

$1.5x10^9$ cells were resuspended in 50 ml of lysis buffer and filtered with gauze prior to cells disruption. The sample was homogenized (Emulsiflex – Avestin) to disrupt the cells. 10 µl of Benzonase and 5 mM $MgCl_2$ were added and the mixture was incubated at RT for 10 minutes (TE). After the incubation the lysate was centrifuged at 30˙000x g for 1 h, at 4 °C (SN and P). The supernatant was loaded on 400 µl of NiNTA resin (Qiagen) and incubated under slow agitation for 1 h, at 4 °C. The flow-through was collected via centrifugation at 500x g for 15’. The resin was subsequently washed with 20 CV of binding buffer and centrifuged again at 500x g for 15’ to collect the wash. The protein fractions were eluted in 2 CV of elution buffer for five times. The eluates were loaded on SDS-PAGE gel to select the best eluates to pool. The pooled fractions were diluted 1:10 with chilled IEX buffer A to decrease salt concentration before Ion Exchange Chromatography.

10.12.2. Ion Exchange Chromatography (IEX)

Ion Exchange Chromatography is based on the reversible interaction between a charged protein and a chromatographic stationary phase with opposite charge. The net surface charge of a protein varies according to the pH of the buffer. Typically, when the pH is above its isoelectric point (pI), a protein is negatively charged on the surface, so it bind to a positively charged anion exchanger. On the other hand, at a pH below its pI, a protein binds to a negatively charged cation exchanger (Figure 10.15). In IEX, proteins are loaded onto the column at low ionic strength to improve resin binding. Conditions are then altered to differentially elute bound proteins according to the strength of their binding. Elution is usually performed by increasing salt concentration or changing pH in a gradient, or stepwise. The most common salt used in IEX is NaCl, but other salts can also be used.

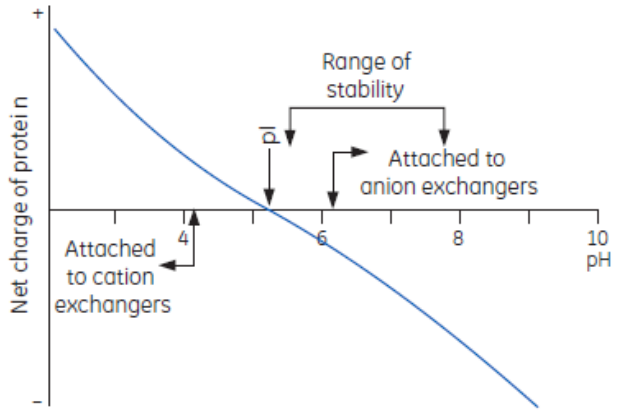

Figure 10.15: ion exchange chromatography choice basing on protein pI

10.12.2.1. Wzx

2 ml of solubilized membranes were purified on Co^{2+} resin as described. The eluted fractions were pooled and subsequently diluted in buffer without salt to decrease NaCl concentration to 20 mM. The protein was loaded on HiTrap Q HP 1 ml column. The column was equilibrated with 5 CV of buffer without salt. A salt gradient from 0 to 1 M salt in 20 CV in IEX buffer 2 was applied. The column was washed with 5 CV of IEX buffer 2.

10.12.2.2. GSK-3β

GSK-3β was further purified by cation exchange chromatography on HiTrap SP HP 1 ml or 5 mL column (GE Healthcare) according to the sample quantity. The protein was purified by applying a salt gradient from 30 mM to 260 mM of NaCl in 20 CV.

The method used is represented in Figure 10.16.

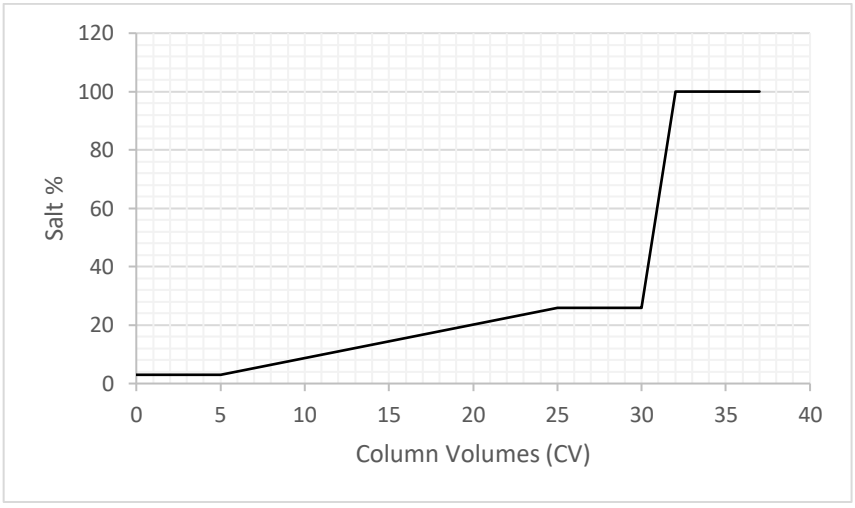

Figure 10.16: IEX method

The eluted fractions were collected and loaded on SDS-PAGE gel to control their composition.

Tag cleavage

The 6His tag was removed by digestion with Tobacco Etch Virus (TEV) protease while dialyzing O/N at 4 °C in TEV buffer. TEV protease has a strict 7 amino acid cleavage recognition sequence of Glu-Asn-Leu-Tyr-Phe-Gln↓Gly/Ser that was introduced in the construct at the N-terminus of the protein sequence. The protein sample was dispensed into the 12-14 kDa MWCO dialysis membrane (SpectraPor, Spectrum laboratories Inc.) together with the selected amount of TEV.

The TEV: protein concentration ratio used was 1:10. The following day, cleaved protein was collected upon a passage on NiNTA beads (Qiagen) to remove TEV and uncleaved protein. The properly cleaved GSK-3β was collected from the FT.

10.12.3. Size exclusion chromatography

Size-exclusion chromatography (SEC) separates molecules according to their molecular sizes in solution; this technique is generally used for the separation of proteins and other water-soluble polymers. In SEC Gel Filtration columns, the particles of different sizes are elute through a porous stationary phase (gel) at different rates (Figure 10.17).

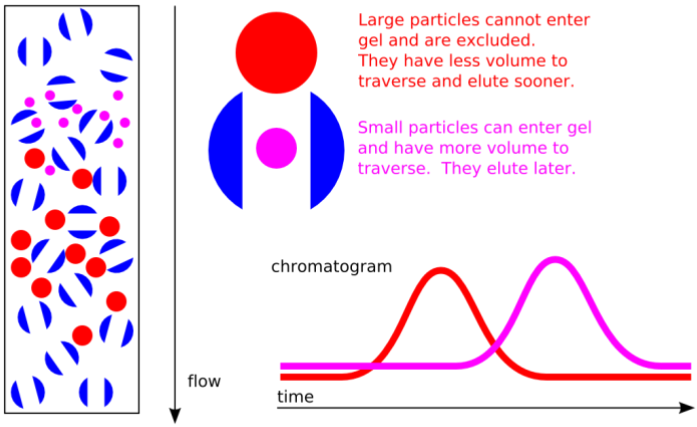

Figure 10.17: Schematic representation of SEC

10.12.3.1. Wzx

Different Size Exclusion columns are available with defined ranges of molecular weights that can be separated. The exclusion limit defines the molecular weight of molecules that are too large to be trapped in the stationary phase and that are eluted with the void volume. The columns employed in this study were Superdex200 10/300 column (with a separation range between 10 and 600 kDa) and Superdex200 10/300 column Increase.

The column, stored in 25% degassed ethanol, was washed with chilled degassed MilliQ water prior to use and then equilibrated with at least 2 CV of **Wzx buffer** filtered and degassed overnight under magnetic stirring in cold room.

The IMAC-purified and centrifuged Wzx protein was loaded on the Superdex200 column for the SEC via a 0.5 ml loop. The flow during the run was constantly maintained at 0.4 ml/min. Fractions eluted from gel filtration were monitored on SDS-PAGE gel to verify the correct molecular weight of the protein and the presence of contaminants. In addition, the fluorescence intensity of the eluates was controlled with a microplate reader (Tecan Infinite m 1000Pro). The fractions with homogeneous protein content were pooled together and eventually concentrated on 50 kDa Amicon concentrators. For crystallization trials Wzx pools were concentrated up to ~3 mg/ml. For fluorescence, IR, Raman spectroscopies and CD the protein was concentrated to 1 mg/ml. For EM analysis further concentration steps were not necessary.

BCA (Bicinconinic Acid- SIGMA) assay and absorption at 280nm with a microvolume spectrophotometer (SimpliNano) were used to determine protein concentration.

10.13. Protein characterization

10.13.1. Fluorescence spectroscopy

In this analytical technique the side chains of tryptophan residues are excited by a radiation at 295 nm and the fluorescence spectrum emitted is recorded from 295 nm to 500 nm. In the spectrum the increase of the peak at 295 nm indicates a higher scattering caused by protein aggregation in the cuvette. The peak around 338 nm corresponds to the maximum of the emitted spectrum. As the protein unfolds, the exposure of the tryptophan side chains to the aqueous environment quenches their fluorescence signal, up to a final plateau value. The temperature at which the fluorescence intensity reaches the medium value between the initial intensity and the final plateau value is defined as melting temperature (T_m) and indicates that half of the protein sample is in an

unfolded state. In addition, protein precipitation effects may cause a dramatic decrease of the fluorescence intensity.

The purified protein was concentrated to 0.8 mg/ml. 800 µl of the sample were pipetted in a 1 ml transparent quartz cuvette and placed in the spectrofluorimeter. Prior to protein analysis, the fluorescence spectrum of the buffer was collected in order to detect possible detergent fluorescence. LDAO does not emit a fluorescence signal in the spectral range analyzed. The protein spectrum was collected applying a temperature gradient. The measures were performed from 8°C to 80°C, with 5°C increments.

10.13.2. Thermal stability assay (TSA)

This technique provides a fluorescence readout measurement of thermally-induced protein melting. The temperature at which a protein melts, T_m, is a measure of protein stability. Thermal Stability Assay (TSA) or Thermofluor uses the signal emitted by a hydrophobic fluorophore (Sypro Orange, Invitrogen) in its bound and unbound states to distinguish between the folded and unfolded states of the protein. At low temperature no fluorescence signal is observed since the protein is properly folded and no hydrophobic surface patches are available to bind the Sypro Orange dye. However, as the temperature increases, the protein starts to melt exposing hydrophobic areas. The fluoroprobe interaction with hydrophobic residues increases the fluorescence signal. The resulting curve is used to determine the melting temperature T_m of the protein. Conditions and components that cause an increase or a decrease in the melting temperature of the protein are stabilizing or destabilizing, respectively (Reinhard et al. 2013).

In this work TSA was used for two purposes: the determination of the influence of the SR90 inhibitor on protein folding and to determine the optimal buffer conditions for the stabilization of GSK-3β.

TSA with SR90

The purified GSK-3β was incubated for 3 hrs at 4°C with 3x molar excess of SR90 solubilized in DMSO. Since the final concentration of DMSO in the mixture was 2.8%, a control of the protein incubated with this concentration of DMSO was added. In white 96-well plates 25 µl of reaction mixtures were prepared as follows:

1.5 µM	kinase final concentration
20 mM	Tris pH 8.0
150 mM	NaCl
10%	Glycerol
1 mM	DTT
5x	Sypro Orange (Invitrogen)
To 25µl	Water

The plate was centrifuged for 1' at 200x g and immediately put into Real Time PCR instrument (CFX96 Touch, BioRad) for Thermofluor run.

Program method:

- 5' at 5 °C
- 0.3 °C increments in 10" every minute ranging from 5 °C to 90 °C

Apo and DMSO-incubated GSK-3β kinase (2.8% final concentration of DMSO) were used as controls. The data were analyzed with Excel for average and standard deviation calculation, and CFX Manager program for graphs.

The same protocol was used for the TSA on the other inhibitor tested on the FL kinase.

TSA on buffers

The protein stability in ten different buffers was investigated to determine the best conditions for protein folding stabilization (Table 10.3).

Reaction method as described in the previous section.

In all the buffers DTT concentration was maintained constant to 1 mM, the TEV buffer was used as control.

Table 10.3: Buffer tested with TSA

	Buffer	NaCl	Glycerol
1	20mM HEPES pH 7.0	100mM	5%
2	20mM HEPES pH 7.5	100mM	5%
3	20mM HEPES pH 7.5	150mM	5%
4	50mM HEPES pH 7.5	150mM	5%
5	20mM HEPES pH 7.5	150mM	10%
6	20mM Tris pH 8.0	150mM	5%

7	50mM Tris pH 8.0	150mM	5%
8	20mM Tris pH 8.0	500mM	5%
9	20mM Tris pH 8.0	150mM	10%
Reference	20mM Tris pH 8.0	100mM	5%

10.13.3. Kinase activity assay

SR90 IC_{50} determination and reversibility assays on GSK-3β (35-386) were performed using KinaseGlo® luminescence assay (Promega). The kinase phosphorylation activity was measured using Phospho-Glycogen Synthase Peptide-2 (Millipore) (sequence: YRRAAVPPSPSLSRHSSPHQ(pS)EDEEE, MW: 3030 Da. Catalogue # 12-241) substrate.

This kit couples the ATP degradation with the mono-oxygenation of luciferin, the process is catalyzed by Ultra-Glo™ Luciferase using the ATP that was not hydrolyzed by the kinase. The reaction produces a luminescence signal that is inversely proportional to kinase activity (Figure 10.18).

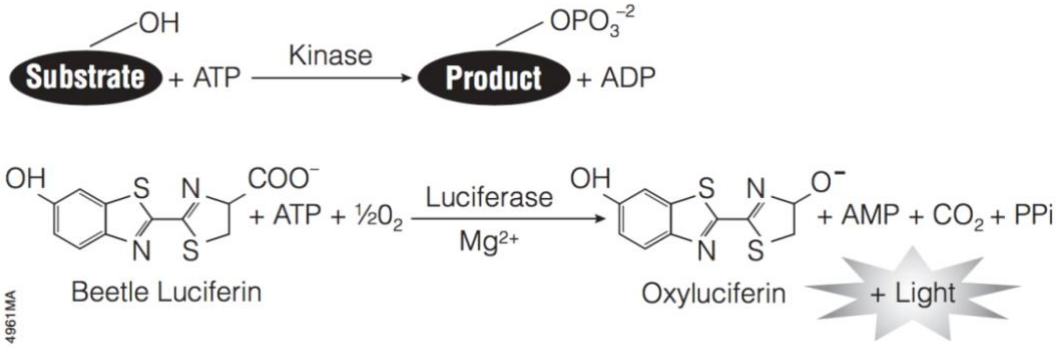

Figure 10.18: schematic representation of the reaction. From Promega bulletin

The kinase activity is proportional to the difference of the total and consumed ATP. The inhibitory activities are calculated considering the maximal activities measured in the absence of inhibitor and the minimal activity measured with a reference inhibitor, following this equation:

Inhibition (%) = (RLU_x – RLU_{CTRL-}) / (RLU_{CTRL+} - RLU_{CTRL-}) x 100

RLU is the Relative Light Unit. RLU_x is the luminescence signal emitted by the kinase mixed with SR90; RLU_{CTRL-} is the luminescence measured in absence of inhibitor (negative control), RLU_{CTRL+} is the luminescence of the positive control in which 100 µM of the compound SB415286 (IC_{50} = 0.103 µM) were added. The positive control is considered as the complete kinase activity inhibition.

Procedure:

The assays were performed in black 96-well plates. The reaction mixture was prepared in 40 µl and incubated for 30' at 30°C. Subsequently 40 µl of Kinase Glo reagent were added, the mixture was incubated for 10' at room temperature protected from light. The luminescence was recorded at 25°C using a Tecan Infinite M100 plate reader.

IC_{50} determination

Reaction mixture:

- 11 nM GSK-3β
- 25 µM GS2 substrate
- 1 µM ATP
- 10 µl of inhibitor at serial dilution from 100 µM to 0.3810 nM
    - 100µM
    - 25µM
    - 6.25µM
    - 1.5625µM
    - 0.3906µM
    - 0.0976µM
    - 0.0244µM
    - 6.1040nM
    - 1.1526nM
    - 0.3810nM

Reversibility assay

The kinase activity recovery was measured upon dilution and after incubation.

Reaction mixture:

- 11 nM GSK-3β
- 25 µM GS2 substrate
- 1 µM ATP
- 10 µMof inhibitor

The florescence was measured after 5', 10', 20', 30', 60', 90' and 120'from the addition of the inhibitor. Otherwise the signal was measured after the 30-fold dilution of the inhibitor mixture, to assess the recovery of the kinase activity.

Data were analyzed using Excel and GraphPad Prism software (version 6.0); IC_{50} curve fits were determined using sigmoidal dose–response (variable slope) equations.

10.13.4. Circular dichroism

Circular dichroism is widely used for the investigation of recombinant protein secondary structure and folding due to the strict correlation between CD spectra and protein conformation. In addition, it may be used to study protein binding interaction. This technique is used to monitor protein conformational changes caused by temperature gradient, residue mutations or addition of small molecules. However, CD data yield information on the overall secondary structure and folding, but not residue-specific information.

CD measurements are based on the unequal absorption of right- and left-handed circular polarized light by asymmetric molecules.

The polarized light is obtained using prisms or filters that promote light electric field (E) sinusoidal oscillation in a single plane. Frontally, the sinusoidal wave of a linearly-polarized radiation can be visualized as of two identical circular vectors that rotate clockwise (E_R) and counterclockwise (E_L), out of phase of 90°. Proteins and other asymmetrical molecules absorb to a different extent the two components of the non-polarized light, resulting in a rotation of the polarization plane of the light. The transmitted light is elliptically polarized due to the variation of the electric field vectors.

Protein characteristic structural elements differentially interact with CD radiation resulting in peculiar spectra, indicative of the secondary structure (Greenfield 2009). In particular, α-helical secondary structures present negative bands at 222 nm and 208 nm and positive one at 193 nm (Holzwarth and Doty 1965). β-sheets are characterized by a negative band at 218 nm and positive one at 195 nm (Greenfield and Fasman 1969), whereas disordered proteins display a low ellipticity above 210 nm and negative bands at 195 nm (Venyaminov et al. 1993).

In this work the purified protein was analyzed against a temperature gradient with Jasco J-815 CD spectrometer to determine Wzx melting temperature. The protein at 1 mg/ml was pipetted into 0.2 or 0.1 mm cuvette. After buffer subtraction, a temperature gradient was applied to the protein from 4°C to 80°C with 5 accumulations every 2°C.

The data were plotted using Excel.

10.13.5. EM analysis

Transmission Electron Microscopy, later referred to as Electron Microscopy (EM), is a commonly used technique for the three-dimensional determination of protein structure. In the negative staining technique, the sample is dispensed on a grid and subsequently embedded in a heavy metal solution that protects the specimen from dehydration caused by the microscope

high vacuum and increases the background scattering signal. However, the stain induces a preferred orientation of the specimen on the grid (Ohi et al. 2004). Due to the low resolution obtained with this technique, negative staining EM technique is used for to determine the coarse features of the specimen and to evaluate the monodispersity of the sample prior to cryo-EM (Kumar et al. 2017; Mitra 2019).

In this work, Wzx samples at a concentration of 0.2 mg/ml were used to prepare EM grids. The grids were charged for 5' in UV ozone cleaner and subsequently 3.5 µl of protein were loaded on the grid. The drop was incubated for 1' on the grid and subsequently dried with filter paper. 3µl of Uranil acetate solution were applied twice on the grid, incubated for 1' and dried with filter paper. Dried grids were transferred on the sample holder and introduces in the microscope.

The images were collected at the University of Trieste using the TEM Philips EM208 with QUEMSA camera and the software RADIUS.

10.13.6. IR spectroscopy

Infrared spectroscopy is a commonly used technique for the determination of specific functional groups in molecule structures. It is especially used for small molecules but can be applied to gain information on protein secondary structures. The technique is not influenced by protein dimension. In recent years, it has been used for the investigation of protein folding and of post-translational modifications essential for protein activity, such as phosphorylation.

IR spectroscopy is based on the vibrational transitions of molecular states caused by the excitation promoted by infrared light. The position of the resulting absorption bands depends on the nature and strength of the bond. Variations in the band position give structural information on the tested molecule (Barth 2007). In particular, IR spectroscopy can be used to investigate the folding and aggregation states of a protein by the analysis of the backbone Amide I and II signals that are weakly affected by the contribution of side chains. The Amide I band signal mostly comes from the C=O stretching, minor contributions are given by CN stretching, CCN deformation and NH bending. Amide II signal is dependent on NH plane bend, CN stretching with minor contributions from CO bending and CC and NC stretching.

When the protein unfolds Amide I band assumes a broaden shape near 1650 cm^{-1} whereas the detection of a band below 1620 cm^{-1} indicates protein aggregation and the formation of intermolecular β-sheets. In the folded protein, α-helices absorb at 1655 cm^{-1} whereas β-sheets

yield bands near 1630 cm^{-1}, 1685 cm^{-1} and 1622 cm^{-1} depending on their parallel or antiparallel disposition (Barth 2007).

Wzx sample was purified according to the above described protocol. Sample measurements were performed at the SISSI (Synchrotron Infrared Source for Spectroscopy and Imaging) beamline of the Elettra Synchrotron (Trieste), using an off-line source and a temperature controlled, in vacuum, single reflection, broadband, ATR (attenuated total reflection), Platinum from Bruker Optik GmbH, Ettlingen. The ATR accessory is mounted on a VERTEX 70v interferometer, Bruker. 20 μl of the sample solution were deposited on the diamond crystal and dried for 30" to let the proteins adhere onto the crystal surface. Then the crystal was covered with a cap in order to preserve the air around the sample and the instrument was evacuated to 10 mbar. The ATR accessory has a heating strip near the crystal that can operate up to 100 °C. Each spectrum was recorded by acquiring 128 scans at 10 kHz scanner speed using a broad band DTGS (deuterated triglycine sulfate) detector, and for each temperature spectra were recorded in triplicate. Before each experiment the background was recorded with the same acquisition parameters used for the experiment. For the background measurements no sample was loaded onto the crystal. In order to efficiently remove the buffer signal from the protein bands, a series of buffer spectra were recorded every 5 °C from 20°C to 70°C. Data were averaged and preprocessed in OPUS (Bruker), with a baseline correction, cut in the Amide I and II range (1700-1480 cm^{-1}), normalization and differentiation using Savitzky –Golay smoothing filter (5 points of smoothing, 3rd degree polynomial function and 2nd degree derivative). The Amide I range was exported in ASCII and deconvolved using PlotIR, a Matlab-based program developed in-house (Cervelli et al. 2012) selecting 6 sub bands of the Amide I, based on the calculated second derivative, fitting parameters: 2 wavenumbers allow variation, FWHM variation 10-30 wavenumbers, signal threshold 0.001 a.u., wavenumber range 1700-1590 cm^{-1}, peaks selected 1690 cm^{-1}, 1677 cm^{-1}, 1655 cm^{-1}, 1641 cm^{-1}, 1622 cm^{-1}, and 1605 cm^{-1}. Results were analyzed and plotted using OriginPro 2019 (OriginLab Corporation).

10.13.7. Raman spectroscopy

Raman spectroscopy is a noninvasive technique that provides information from various samples important in biology and medicine. Raman follows the vibrational modes of functional group and it may provide insight in protein structures.

In protein samples, the Raman characteristic bands are associated with the CONH group, referred to as amide A (NH stretching, about 3500 cm^{-1}) and amide B (NH stretching, about 3100 cm^{-1}).

Also amide I to VII at their characteristic wavenumbers are measured to elucidate the secondary structure of proteins. In fact, the position of amide I and III is correlated with α-helical or β-sheet motifs. In particular, amide I bands are detected at 1662-1655 cm^{-1} for α-helix and at 1674-1672 cm^{-1} for β-sheet, whereas amide II presents bands at 1272-1264 cm^{-1} and 1242-1227 cm^{-1}, respectively for α-helix and β-sheet. Thus, variations in protein secondary structure may be detected by the shift of the band wavenumbers. Raman spectroscopy may be used for the description of the side chains of specific residues, such as tryptophan, that presents a doublet at 1360/1340 cm^{-1}, and tyrosine, that shows two peaks at 860/833 cm^{-1} (Rygula et al. 2013).

UV Raman measures were performed at BL10.2-IUVS beamline at Elettra Synchrotron Trieste (D'amico et al. 2013). Raman spectra were collected at 244 nm excitation wavelength in backscattering geometry using a triple stage spectrometer (Trivista, Princeton Instruments) with a spectral resolution of about 8 cm^{-1}. Wzx was analyzed in Suprasil quarts cuvettes that were horizontally oscillated during the data collection to prevent sample photodamaging caused by the long exposure to UV radiation. The oscillation was controlled in order to avoid a significant scattering volume variation during the measurements.

The Raman spectra were collected for 3 hours with a UV excitation of 40 μW.

Data were averaged and processed by removing background, signals of the empty cell and of the buffer. Acquisition parameters were kept constant during the experiments; baseline correction by a low order polynomial function was applied to remove the fluorescence from the spectra, wavenumber scale was calibrated with cyclohexane as a standard. Results were analyzed and plotted using Igor Pro Version: 7.0.8.1 2019 (Wavemetrics Corporation).

Table 10.4 reports the assignments of vibrational peaks of the aromatic residues.

Table 10.4: Band assignment

Peak (cm-1)	Amino acid / Amide	Vibrational mode
1010	Trp	W16 (symmetric pyrrole out-of -phase breathing)
1173	Tyr	Y9a
1209	Tyr	Y7a
1238	Amide III	C-N + N-H
1342	Trp	W7 (pyrrole ring vibration)
1362	Trp	
1559	Trp+ Amide II	W3 (C2-C3 stretching mode of the pyrrole ring)
1623	Trp + Tyr	W2 Trp (phenyl mode with some contribution from the pyrrole N1C8 stretching) + Y8 (in plane ring stretching)
1666	Amide I	C=O

In this study, signals of tryptophan, phenylalanine and tyrosine residues of purified Wzx at 0.3 mg/ml were followed. Accumulation spectra were collected at 244 nm and at three different

temperatures (292 K (19°C), 323 K (50°C), 343 K (70°C)) to determine secondary structure modifications during the thermal treatment. In this experiment the pure Wzx sample (after the removal of the contaminant) and the second peak of the SEC with Superdex200 Increase column, in which the contaminant is present, were analyzed. Figure 10.19 displays an example of peak attribution on the Wzx sample from peak II at 19°C (Oladepo et al. 2012).

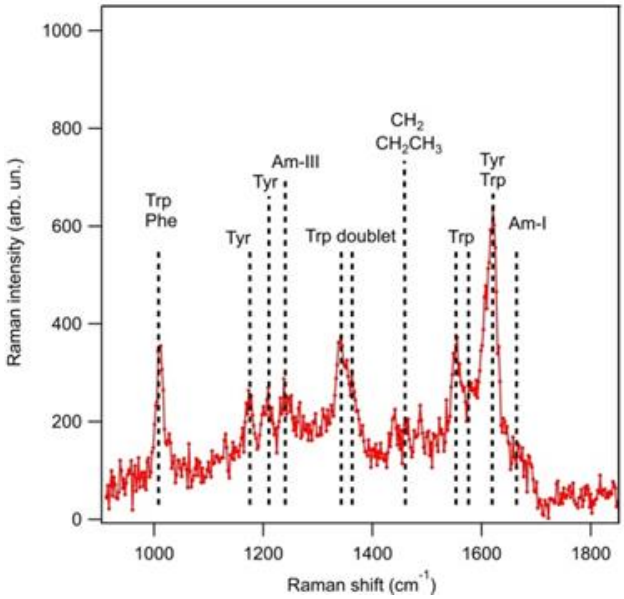

Figure 10.19: Peaks assignment for the sample Wzx-contaminant at 19°C

10.14. Crystallization

The determination of the three-dimensional structure of biological macromolecule at atomic revolution provides a unique understanding of protein function and a major help for the design of selective inhibitors. Protein crystals are three-dimensional periodic arrays of molecules in which the solvent content is around 30-70% (Parker 2003), but it can be higher especially in membrane protein crystals. To determine the structure of a protein via x-ray diffraction an ordered disposition of the molecules is required to increase the signal as the scattering of an individual molecule is too weak to be measured. To obtain high resolution-diffracting crystals the protein sample should be pure and homogeneous (Bergfors, 1999; McPherson, 1999).

Prior to crystallization plate setup the protein should be concentrated avoiding aggregation or precipitation. For soluble proteins the concentrations commonly used are of 5-50 mg/ml, whereas for membrane proteins the concentration is usually lower due to their low solubility and their aggregation propensity (Dessau and Modis 2010). In order to form crystals, the molecule should be in a supersaturated state, to reach this state the high concentrated protein is mixed with a precipitant.

The phase diagram (Figure 10.20) describes the crystallization process: the vertical axis shows the protein concentration, whereas the horizontal axis indicates the precipitant concentration.

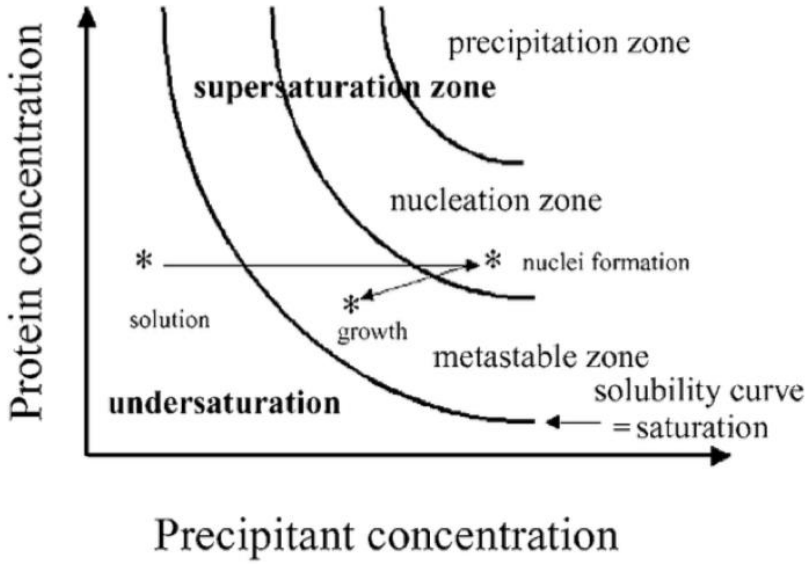

Figure 10.20: Phase diagram (Parker 2003)

At low concentration of both the components, i.e. in an undersaturation condition, the protein remains in solution. As the concentration of protein and/or the precipitant increases, due to the water diffusion outside the drop, protein solubility decrease until it reaches a supersaturated condition in the nucleation zone. At this point the protein may aggregate forming amorphous or microcrystalline precipitates, if the supersaturation is excessive; positive results are obtained when the protein organizes in an ordered crystal lattice. While the protein crystallizes, protein concentration in solution decreases and reaching a condition within the metastable zone. In this zone formation of new crystal nuclei is kinetically unfavored, but crystal dimensions can increase (Parker 2003).

Crystals may be obtained with two main techniques: vapor diffusion and batch crystallization.

In the ***vapor diffusion method***, a drop formed by a mixture of protein and precipitant is sealed in a chamber with a reservoir of pure precipitant. Water vapor slowly diffuses out of the drop until it equalizes the osmolarity of the precipitant. During this process the drop dehydrates causing a slow concentration of both the protein and the precipitant until the system reaches the equilibrium with the formation of crystal nuclei.

In the ***batch method*** the protein is immediately brought to a nucleation condition by mixing with a sufficient amount of precipitant. This method is usually performed under paraffin or mineral oil to prevent drop dehydration (Dessau and Modis 2010).

In this work, crystallization experiments were conducted using the vapor diffusion technique with two different procedures, the hanging drop and the sitting drop. In both cases the plate wells are filled

with reservoir solution that is usually formed by a precipitant agent, a buffer and salts or additives, that help the protein crystallization process.

In the sitting drop setup, a drop containing protein and precipitant is deposited in the suitable well next to the larger well containing the reservoir solution. The system is closed to allow vapor diffusion until equilibrium. The sitting drop setup is mostly used for the initial screen of crystallization conditions. For this purpose, sparse matrix screens that contain a wide variety of conditions are commercially available. Conditions of the screens are usually selected among those that demonstrate the highest success rates for protein crystallization.

In the hanging drop setup, technique, the drop containing protein and precipitant solutions is placed on a cover slide and hang onto the reservoir solution by flipped the cover slide. The system is sealed to allow vapor diffusion until equilibrium. This technique is mostly used for the optimization of crystallization condition previously determined. Optimization screens can be prepared by varying precipitant concentrations, pH or adding additives, in order to improve crystal dimension and internal order and, as a result, the resolution of the X-ray diffraction data.

10.14.1. Wzx

Sitting drop

While a huge variety of screens is available for soluble proteins, for membrane protein crystallization the choice is more limited. In this study the MEM START/MEM SYS and the MEM GOLD screens from Molecular Dimensions were used.

The purified protein was concentrated to 3mg/ml.

Wells of the 96-well plates (Corning) were filled with 80 μl of reservoir solution. Drops containing protein and reservoir solutions were made using a Mosquito nanoliter TTP Labtech instrument and dispensing 200 nl of protein solution and 200 nl of precipitant, maintaining the protein/precipitant ratio to 1:1. The plates were sealed with transparent tape and stored at 18°C or at 4°C.

Hanging drop

For the hanging drop experiments, 24-well plates were used. Wells were filled with 1 ml of reservoir solution. Then a silicon grease ring was dispensed around each well. The cover slides were cleaned with 100% ethanol prior to use. Equal volumes of the protein (concentrated to 3 mg/ml) and the reservoir solution were pipetted onto the cover slides. Then, each cover slide was flipped on the respective reservoir solution and gently pressed to seal the well with the grease.

In this work, all the crystallization solutions were filtered at 0.22 μm to eliminate the impurities. Plates were stored at 18°C and at 4°C.

According to the hit determined with Sitting drop kit screening (0.05M HEPES pH 7.5; 22% w/v PEG 4000) a optimization plate in hanging drop was set up as shown in table 10.5.

Table 10.5: crystallization conditions in the optimization plate for Wzx

13% PEG 4000 0.05M HEPES pH 7.5	16% PEG 4000 0.05M HEPES pH 7.5	19% PEG 4000 0.05M HEPES pH 7.5	22% PEG 4000 0.05M HEPES pH 7.5	25% PEG 4000 0.05M HEPES pH 7.5	28% PEG 4000 0.05M HEPES pH 7.5
13% PEG 4000 0.05M HEPES pH 7.2	16% PEG 4000 0.05M HEPES pH 7.2	19% PEG 4000 0.05M HEPES pH 7.2	22% PEG 4000 0.05M HEPES pH 7.2	25% PEG 4000 0.05M HEPES pH 7.2	28% PEG 4000 0.05M HEPES pH 7.2
13% PEG 4000 0.05M HEPES pH 6.9	16% PEG 4000 0.05M HEPES pH 6.9	19% PEG 4000 0.05M HEPES pH 6.9	22% PEG 4000 0.05M HEPES pH 6.9	25% PEG 4000 0.05M HEPES pH 6.9	28% PEG 4000 0.05M HEPES pH 6.9
13% PEG 4000 0.05M HEPES pH 6.5	16% PEG 4000 0.05M HEPES pH 6.5	19% PEG 4000 0.05M HEPES pH 6.5	22% PEG 4000 0.05M HEPES pH 6.5	25% PEG 4000 0.05M HEPES pH 6.5	28% PEG 4000 0.05M HEPES pH 6.5

To improve crystal internal order and increase the diffraction a series of additives were tested. The additive screens HR2-420, HR2-430 and HR2-422 from Hampton Research were used with a sitting drop setup. In addition, a salt and additive screen was prepared with condition that usually promote crystallization (Table 10.6).

Table 10.6: Additive and salts screen

0.01M Lithium sulfate	0.05M Lithium sulfate	0.1M Lithium sulfate	0.01M Lithium acetate	0.05M Lithium acetate	0.1M Lithium acetate
0.01M Lithium chloride	0.05M Lithium chloride	0.1M Lithium chloride	0.01M Ammonium sulfate	0.05M Ammonium sulfate	0.1M Ammonium sulfate
0.01M Ammonium carbonate	0.05M Ammonium carbonate	0.1M Ammonium carbonate	0.01M Ammonium chloride	0.05M Ammonium chloride	0.1M Ammonium chloride
0.01M Magnesium sulfate	0.05M Magnesium sulfate	0.1M Magnesium sulfate	0.01M Magnesium chloride	0.05M Magnesium chloride	0.1M Magnesium chloride
0.01M Calcium chloride	0.05M Calcium chloride	0.1M Calcium chloride	0.01M Calcium acetate	0.05M Calcium acetate	0.1M Calcium acetate
0.1M Ammonium sulfate	0.15M Ammonium sulfate	0.2M Ammonium sulfate	0.1M Ammonium carbonate	0.15M Ammonium carbonate	0.2M Ammonium carbonate
0.1M Ammonium chloride	0.15M Ammonium chloride	0.2M Ammonium chloride	0.1M Lithium sulfate	0.15M Lithium sulfate	0.2M Lithium sulfate
0.05M Lithium acetate	0.1M Lithium acetate	0.15M Lithium acetate	0.05M Lithium chloride	0.1M Lithium chloride	0.15M Lithium chloride

At regular intervals of days, the plates were checked to verify the presence of crystals. The drops may present three diverse situations: crystals, clear drop or precipitation.

The amorphous precipitation, a brownish powder with no distinct shape, occurs when the precipitant concentration is too high and the protein aggregates. The clear drop phenomenon occurs when the solution is undersaturated and the protein remains in solution.

To collect the X-ray diffraction data, crystals are fished with cryo-loops and cryoprotected with the reservoir solution supplemented with the chosen cryoprotectant, generally 30% glycerol that prevent ice formation during flesh freezing. The cryogenic conditions were tested at the Elettra

Synchrotron by adding 10%, 15%, 20% or 30% of different small molecular weight PEGs (PEG 200, PEG 300 and PEG 400) to the reservoir solution. The solutions were put under the nitrogen flux at 100K to determine the mixture that prevented ice formation.

According to the cryogenic conditions tested, the fished crystals were cryoprotected in 15% PEG 200. Cryoprotected crystals were flesh frozen in liquid nitrogen and stored until data collection.

The data collection was performed at the XRD2 beamline of the Elettra Synchrotron at a temperature of 100 K and a wavelength of 1 Å.

Data collection on crystals obtained in the crystallization experiments for the protein Wzx (table 10.7):

Table 10.7: Data collection statistics

	Cytochrome o Ubiquinol Oxidase	Wzx Crystal 1	Wzx crystal 2
a	180.775 Å	180.841 Å	130.810 Å
b	182.613 Å	181.170 Å	154.291 Å
c	67.727 Å	67.271 Å	200.532 Å
α	90.000°	90.000°	90.000°
β	90.000°	90.000°	90.000°
γ	90.000°	90.000°	90.000°
Space Group	$P2_1\ 2_1\ 2$	$P2_1\ 2_1\ 2$	$P2_1\ 2_1\ 2_1$
Resolution	46.651- 6.321	50.000-7.021	9
I/σ	10.09 (1.42)	7.44 (0.96)	-
R merge	5.8%	5.8%	-

10.14.2. GSK-3β

GSK-3β aliquots were concentrated to 4.4 mg/mL for crystallization trials.

The protein was incubated with 3x molar excess of SR90 for 3h at 4°C. Subsequently the incubated protein and the apo GSK-3β crystallization conditions were screened using PEG ION 1 and 2 commercial screen (Hampton research), using the sitting drop vapor diffusion technique. The wells were filled with 80 µl of reservoir. Crystallization drops were prepared using Mosquito nanoliter TTP Labtech with 0.1 µl protein solution and 0.1 µl reservoir. The plates were incubated at 20°C for 3 days. Crystals were detected in both apo and SR90-incubated wells.

Crystallization optimizations were performed starting from the following conditions:

- 0.2M Sodium malonate pH 5.0, 20% PEG 3350
- 0.2M Sodium malonate pH 6.0, 20% PEG 3350
- 0.2M Malic acid pH 7.0, 20% PEG 3350
- 2% v/v Tacsimate pH 5.0, 0.1M Sodium citrate tribasic dihydrate pH 5.6, 16% PEG 3350

PEG 3350 percentage was variated from 16% to 22% for optimization plates starting from the first 3 conditions, and from 14% to 20% for the last. The optimizations were performed using both the sitting drop and the hanging drop technique with 0.5µl + 0.5µl drops and 1µl + 1µl drops, respectively. Crystallization plates were incubated for 10 days at 20°C.

In soaking experiments, apo crystals were soaked in a 2 µl drop of the reservoir solution supplemented with 3X molar excess of the compound for 24h.

Prior to data collection crystals were cryoprotected in 30% Glycerol and frozen in liquid nitrogen.

10.15. X-ray diffraction structure determination

X-ray diffraction

To visualize atomic scale structures, diffraction experiments are performed using X-rays with wavelength in the order of atomic bond distances, approximately 1 Å. X-ray diffraction is the phenomenon caused by the interference between the scattered waves from the electron density surrounding the individual atoms present in the crystal. ***Bragg's law*** indicates that constructive interference between scattered X-rays that hit a crystal may occur only if the difference between the path of the radiation scattered by atoms on parallel planes is a multiple of the wavelength λ. Therefore, Bragg equation $\mathbf{n\lambda=2d\sin\Theta}$ predicts the position of the diffraction maxima in a diffraction pattern (Parker 2003) (Figure 10.21). The electron density present in each diffraction plane influence the amplitude of the diffracted wave.

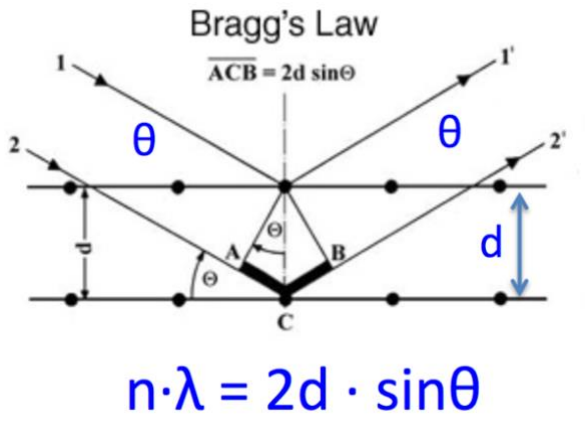

Figure 10.21: Schematic representation of Bragg's law. The arrows represent the incident and diffracted X-ray waves on parallel planes at distance d.

Bragg's law can be visualized by the construction of Ewald sphere. The sphere represents the incident radiation, is centered in the crystal reciprocal lattice and has a radius of 1/λ. Its interaction with the reciprocal lattice defines diffraction conditions for every node of the reciprocal lattice that intercepts the sphere surface (Parker 2003), according to the Bragg's law. In experimental conditions, subsequent rotations of the crystal under the X-ray beam allow interaction of each point of the reciprocal lattice with the Edwald sphere.

To obtain high-resolution data from small and poorly-ordered crystals, high intensity radiation must be used. For protein structure determination on small crystals, X-rays from synchrotron facilities are routinely used. In these facilities electrons are accelerated close to the speed of light by a linear accelerator and subsequently injected into the synchrotron ring. The electron circular orbit is maintained by high energy magnets. High-speed electrons emit an electromagnetic radiation every time their trajectory changes. The emitted radiation is tangent to electron trajectory and is conveyed into beamlines of the synchrotron facility, where monochromators allow the selection of the desired wavelengths.

From the X-ray diffraction pattern the intensity of the structure factors can be obtained. The structure factor is a complex representation of the scattering power of the electron density present in the unit cell of the crystal. The diffraction experiment does not allow to measure the phase of the structure factor. In order to determine the electron density present in the crystal, and therefore the 3D structure of the molecule that forms the crystal lattice, both intensity and phase information of the structure factors are required. To solve the phase problem, three main methods are applied in protein crystallography: the single or multiple isomorphous replacement, the single- or multi-wavelength anomalous scattering and the molecular replacement.

In isomorphous replacement methods, the diffraction patterns are collected on native crystals and on crystals soaked in a solution containing atoms of a heavy atom, such as mercury, platinum, uranium,

lead, gold or lanthanides. When the data of the native and isomorphous crystals are compared, the positions of the heavy atom, whose high electron density causes an intense diffraction signal, can be identified.

In the anomalous scattering methods, incident wavelengths close to the X-ray absorption edges of atoms, usually heavier atoms, present in the crystal are used. In this case, anomalous scattering effects cause changes in the diffraction intensity related to Friedel pairs of diffraction intensities. The comparison between data collected at different wavelengths, usually at least 3, allows to localize the anomalous scatterers in the unit cell. The native atoms of the protein, such as sulfur or metal center of metalloproteins, can be used for anomalous scattering phasing, but often atoms yielding a good anomalous signal are incorporated during crystal preparation, e.g. by expressing the protein with selenium-methionine residues.

The molecular replacement technique may be applied if the protein of interest shares at least 25% of sequence identity with an already known structure. In this case the phases may be solved by locating the known structure in the correct orientation and position in the unit cell of the target protein (Parker 2003).

The crystallographic data obtained in the research work of this thesis were analyzed to determine protein structure. At low resolution (8 to 3.5 Å), only the overall shape of the molecule can be determined. At medium resolution (3.5 to 2.5 Å), the protein main chain and the amino acids side chains can be identified. At high resolution (2.5 to 1.0 Å) the atoms can be individually located and the ordered solvent around protein structure can be distinguished (Parker 2003).

10.15.1. GSK-3β

Data collection, structure solution and refinement

X-ray diffraction data were collected at the XRD1 beamline of the synchrotron Elettra (Trieste, Italy), using monochromatic radiation of 1.00 Å and a Pilatus-2 M (Dectris) detector. Data were indexed, integrated and scaled using XDS (Kabsch 2010).

GSK-3β (35-386) co-crystallized with SR90

The structure was solved by Molecular Replacement with MolRep using 1Q5K structure as reference model (Bhat et al. 2003). Inhibitor and water molecules were removed from the model prior to phase calculation (Vagin and Isupov 2001). Iterative cycles of manual fitting with Coot were used to improve the model. Data refinement was performed using REFMAC5, where 5% of the data were excluded and used for R-free value calculation (Emsley et al. 2010). Coordinates and structure factors were deposited in the Protein Data Bank with accession code 6H0U.

GSK3-β 35-386 apo and soaked crystals

In the soaking technique the inhibitor solution diffuses within the crystal channels filled by the solvent. The soaking time should be long enough to allow the diffusion and the subsequent interaction between the compound and its binding site on the protein. On the other hand, a prolonged soaking may lead to crystal cracking due to the excessive perturbation of the mother solution.

Data obtained from apo and soaked crystals data were processed as described for the co-crystal. However, for the refinement processes the structure of the co-crystal (PDB: 6H0U) was used as reference.

10.16. Generic procedures

Agarose gel preparation:

Agarose is a linear polymer composed of alternating residues of D- and L-galactose joined by β (1→3) and β (1→4) glycosidic linkages. When this matrix is places in an electric field, it allows to separate DNA fragments according to the size.

For 0.9% agarose gel preparation 0.45 g of agarose were dissolved in 50 mL of TAE buffer and heated until complete agarose dissolution. In the agarose solution 4 μL of Gel-Red or 2.5 μL of Pro Safe (Euroclone) were added for a 7x10 gel. The solution was poured into the gel casing tray with a comb with the desired number of wells and let polymerize. Once the gel was formed, the comb was removed, and the gel was located in the running chamber. The sample was added with 6x DNA loading buffer. The chamber was filled with TAE buffer and the sample and a broad range of DNA standards, that allow the evaluation of the DNA dimension, were loaded into the wells. The gel was run at 70 V using an electrophoresis power supply (Major science MP-300V e) and monitored under UV light.

Gel Extraction protocol:

The gel extraction was conducted according to manufacturer's protocol. The DNA fragment of interest was excised from an agarose gel and solubilized in binding buffer via incubation at 60°C. At this temperature, the chaotropic agent in the binding buffer dissolves the agarose matrix. The resulting clear solution was applied to the column, allowing DNA binding of the silica membrane and removal of impurities with a wash step. Purified DNA was eluted from the column with the provided elution buffer.

Competent cells preparation:

Chemically induced competence followed by transformation is a commonly used technique to introduce plasmids or other DNA fragments into *E. coli* strains. Induction of competence increases

the ability of a prokaryotic cell to incorporate plasmid DNA allowing cells to be transiently genetically transformed (Dagert and Ehrlich, 1979). The addition of calcium chloride to a cell suspension promotes the binding of plasmid DNA to lipopolysaccharides (LPS). Positively charged calcium ions attract both the negatively charged DNA backbone and the negatively charged groups in the LPS inner core. The plasmid DNA can then pass into the cell upon heat shock, where chilled cells (4 °C) are heated to a higher temperature (42 °C) for a short time.

Starting from bacteria glycerol stock kept at -80°C, cells were inoculated with a sterile loop into a 100 mL sterile flask containing10 mL LB medium supplemented with the proper antibiotic, and Incubated O/N at 37°C, shaking mode. After incubation the culture was diluted into 200 mL LB, in a 1 L sterile flask, without any antibiotic. Cells were grown at 37°C, monitoring the culture until 0.48 optical density at 600nm (OD600nm). The culture was transferred into sterile 50 ml falcon tubes, kept on ice for 15 minutes and then centrifuged at 1˙000x g for 5' at 4°C. The supernatant was discarded, while the pellet was resuspended in 20 ml **Competent cells buffer1** cold solution and immediately transferred on ice for 5 minutes. The suspension was centrifuged as before, and the pellet was resuspended into 2 ml **Competent cells buffer2** cold solution and transferred on ice for 15'. The competent cells are aliquoted in 1.5 mL pre-cooled tubes and immediately stored at -80°C.

Mini Prep:

Mini Prep is a procedure to isolate plasmid DNA from a small-scale bacterial culture (1-3 ml) of a *E.coli* cloning strain transformed according to the protocol described in the previous section. The procedure was performed using a commercial kit (Sigma), according to the manufacturer's protocol. This plasmid purification protocol is based on a modified alkaline lysis procedure followed by the binding of plasmid DNA to an Anion-Exchange Resin under appropriate low-salt and pH conditions. RNA, proteins, dyes and low molecular weight impurities are removed by low-salt and ethanol washes. Plasmid DNA is eluted in TE buffer.

WB protocol

Western Blot is qualitative analysis used to identify a particular protein in a mixture, using an antibody that recognizes a specific epitope of the protein. In this study the antibody recognizes the His-tag that was added to protein sequence. In this work the wet Western Blot technique was applied. The SDS-PAGE gel was run in presence of prestained markers (PageRuler Prestained Protein Ladder, ThermoFisher). After the run, stacking phase was removed and SDS-PAGE was incubated for 10' in **Western Blot Transfer buffer** together with the filter paper and the sponges. A suitable area of a 0.22 μm nitrocellulose membrane was cut, pre-wet and activated in ultrapure water, and then put in Transfer buffer. The "Sandwich" assembly was prepared.

"Sandwich" assembly:

- 3 x filter papers
- Nitrocellulose
- SDS-PAGE
- 3 x filter papers

Protein transfer from SDS-PAGE to nitrocellulose was run for 1h, 250 mA at 4°C constant into a tank full of transfer buffer

When the transfer was complete, the membrane was blocked by incubation in 5% no fat milk + 0,1% Tween20 (prepared in PBS) to saturate the nitrocellulose. The blocking lasted for 1h at RT or ON at 4°C. The membrane was washed with PBS before incubation with the antibody, α-His Tag HRP-conjugated (#A7058, Sigma), diluted 1:5000 in 1% no fat milk + 0,1% Tween20 in PBS, 1h at RT. Nitrocellulose was washed 3 x 5' with 1% no fat milk + 0,1% Tween20 in PBS and 1 x 10' with PBS only.

The WB was developed with the ECL method by mixing 1:1 (1 ml:1 ml for a 6 cm x 6 cm membrane) ECL Prime Reagents (GE Healthcare) just prior to use. The mixture was poured on the membrane and incubated 1' before the chemiluminescent image acquisition with ImageQuant LAS4000 (GE healtcare).

WB results may also be observed with DAB method using SIGMA FAST 3,3′-Diaminobenzidine tablets. In this case, the tablets (1 silver and 1 gold) were dissolved in 5 ml of H_2O and poured on the membrane. The reaction was stopped by washing with water.

Protein quantification with Bradford assay

This technique is based on the color change of Coomassie Brilliant Blue G-250, from red to blue, upon binding to a protein. The protein-dye complex high extinction coefficient leads to high sensitivity in measurements. The protein binding stabilizes the blue form of the Coomassie dye so, the amount of the complex is proportional to protein concentration. The comparison of the protein absorbance measured at 595 nm with a standard curve allows the calculation of protein concentration. However, this assay is susceptible to interference by elevated concentrations of detergent. In fact, the detergents associate strongly with the Coomassie dye, causing an increase in the absorbance at 595 nm preventing protein quantification. This technique is not used for Wzx quantification due to Bradford sensitivity to detergents. The Bradford assay is linear up to a protein concentration of 2 mg/mL, more concentrated samples require dilution prior to analysis.

Bradford solution was prepared by mixing 1 part of Bradford reagent (Biorad) with 4 parts of ultra-pure water. For the standard curve the following BSA dilutions were prepared: 1 mg/ml; 0.8 mg/mL;

0.6 mg/mL; 0.4 mg/mL; 0.2 mg/mL; 0.1 mg/mL. Afterwards, 4 µl of each sample (standard and protein, eventually diluted) were pipetted into flat transparent 96-well plate (Corning). 200 µl of Bradford solution was added into each well. For both BSA standards and samples a blank was measured for buffer signal subtraction. BSA samples were prepared in duplicate, protein samples were prepared in triplicate.

The plate was incubated for 7 minutes at RT before measuring the absorbance at 595 nm. The total protein concentration was calculated by interpolating the measured sample absorbance on a regression curve created using the BSA standard concentrations.

Protein quantification by Bicinchoninc acid (BCA) assay

The BCA assay detects the cuprous ions generated after the reaction of cupric ions and a protein under alkaline conditions. Bicinchoninic acid sodium salt, is a stable, water-soluble compound that forms an intense purple complex with cuprous ion (Cu^{+}) in an alkaline environment (Smith et al. 1985). The color produced by the reaction of protein with alkaline Cu^{2+} (Biuret reaction) increases proportionally over a range of increasing protein concentrations (Smith et al. 1985).

The reaction mixture was incubated at 60°C to enhance sensitivity. Otherwise the reaction can be conducted at room temperature or at 37°C, but incubation times differ. The complexes formed after incubation has a strong absorption at 562 nm.

Procedure:

25 µl of each sample (standard and protein dilutions) were pipetted into different plate wells (Flat Transparent 96 well plate, Corning). 200 µl of BCA reagent solution (Bicinconinic acid +copper sulfate) was added into each well. The following BSA dilutions were prepared to determine the standard curve: 1 mg/ml; 0.75 mg/mL; 0.5 mg/mL; 0.25 mg/mL; 0.125 mg/mL

The mixture was incubated at 60°C for 30 minutes and absorbance at 562 nm was recorded.

For both BSA standards and Wzx samples a blank was measured in order to subtract the absorbance of the buffer components. Every sample was prepared in triplicate.

The total protein concentration was calculated by interpolating the absorbance value measured on a regression curve created using the BSA standard values.

Acrylamide gel electrophoresis:

The Sodium Dodecyl Sulfate-Poly Acrylamide Gel Electrophoresis (SDS-PAGE) is a technique that allows proteins separation according to the molecular weight in denaturing conditions. The gel can be prepared at different percentages of acrylamide: higher concentrations of acrylamide produce gels with smaller mesh and therefore suitable for smaller protein sizes. The proper percentage of acrylamide depends on the dimension of the protein: to separate Wzx a 14% gel was used, whereas for GSK3-β a 12% gel was used.

The electrophoretic run was performed in **SDS-PAGE Running Buffer** at a constant voltage of 180 V. All the samples were diluted in **SDS-PAGE Sample buffer** 4x and subsequently incubated at 37°C for 15'. Usually soluble proteins are boiled at 95°C with sample buffer prior to gel loading, but membrane proteins tend to aggregate once heated despite the presence of SDS. Even when not heated, membrane proteins often aggregats during the run forming a pattern of oligomers on the gel (Engel, Chen, and Privé 2002). After the run, the gels were stained for visualization with ProBlue Safe stain (Giotto Biotech). Gel images were collected with VWR CHEMI premium imager and ImageQuant LAS4000 (GE healtcare). The presence of Wzx-GFP was also detected via in-gel-fluorescence observation, prior to gel staining. In fact, GFP fusion protein may emit fluorescence under UV lamp even in the denaturing conditions of the SDS-PAGE run. The in-gel-fluorescence observation is a useful technique that allows the correct identification of the desired protein band without the need of a Western Blot (Salim T. Islam, Eckford, et al. 2013a). The fluorescent bands were visualized using VWR CHEMI premium-imager.

11. Acknowledgements

I would like to acknowledge my supervisors Rita De Zorzi and Paola Storici for their support during the PhD.

For the synthesis of SR90 inhibitor I acknowledge Sara Redenti and for the collaboration in the GSK-3β project I would like to thank Stephanie Federico.

I would like to acknowledge Nicola Demitri for the data collection on XRD 1 and 2 beamlines, for the preliminary structure refinement and for the support during data interpretation.

For the TEM analysis I would like to thank Paolo Bertoncin of the University of Trieste, and Catherine Venien-Bryan and Dania of the Pierre and Marie Curie University, Paris.

IR spectroscopy analysis and interpretation were performed in collaboration with Giovanni Birarda and Federica Piccirilli on the SISSI beamline at Elettra Synchrotron.

For Raman spectroscopy analysis and data interpretation I would like to acknowledge Attilio Cesaro, Silvia Di Fonzo and Maria Pachetti of the IUVS beamline of Elettra.

For the valuable discussion and essential support I would like to acknowledge Sabrina Semeraro, Barbara Giabbai, Barbara Medagli, Laura Destefanis and Marta Semrau.

12. Bibliography

Abeyrathne, Priyanka D., Craig Daniels, Karen K.H. Poon, Mauricia J. Matewish, and Joseph S. Lam. 2005. "Functional Characterization of WaaL, a Ligase Associated with Linking O-Antigen Polysaccharide to the Core of Pseudomonas Aeruginosa Lipopolysaccharide." *Journal of Bacteriology* 187 (9): 3002–12. https://doi.org/10.1128/JB.187.9.3002-3012.2005.

Abeyrathne, Priyanka D., and Joseph S. Lam. 2007a. "Conditions That Allow for Effective Transfer of Membrane Proteins onto Nitrocellulose Membrane in Western Blots." *Canadian Journal of Microbiology* 53 (4): 526–32. https://doi.org/10.1139/W07-007.

Abeyrathne, Priyanka D., and Joseph S. Lam. 2007b. "WaaL of Pseudomonas Aeruginosa Utilizes ATP in in Vitro Ligation of O Antigen onto Lipid A-Core." *Molecular Microbiology* 65 (5): 1345–59. https://doi.org/10.1111/j.1365-2958.2007.05875.x.

Abraham, B. D., M. Sono, O. Boutaud, A. Shriner, J. H. Dawson, A. R. Brash, and B. J. Gaffney. 2001. "Characterization of the Coral Allene Oxide Synthase Active Site with UV - Visible Absorption, Magnetic Circular Dichroism, and Electron Paramagnetic Resonance Spectroscopy: Evidence for Tyrosinate Ligation to the Ferric Enzyme Heme Iron." *Biochemistry* 40 (7): 2251–59. https://doi.org/10.1021/bi002121h.

Alba, Benjamin M., and Carol A. Gross. 2004. "Regulation of the Escherichia Coli ΣE-Dependent Envelope Stress Response." *Molecular Microbiology* 52 (3): 613–19. https://doi.org/10.1111/j.1365-2958.2003.03982.x.

Almén, Markus Sällman, Karl J.V. Nordström, Robert Fredriksson, and Helgi B. Schiöth. 2009. "Mapping the Human Membrane Proteome: A Majority of the Human Membrane Proteins Can Be Classified According to Function and Evolutionary Origin." *BMC Biology* 7: 50. https://doi.org/10.1186/1741-7007-7-50.

Anderson, Amy C. 2010. "The Process of Structure-Based Drug Design." *Artificial Intelligence in Medicine* 10: 1118. https://doi.org/10.1016/j.

Aoki, Masaaki, Chizuko Sasaki, Tsukasa Hasegawa, and Takao Matsuzaki. 2000. "Crystallization Papers Expression , Purification and Crystallization of Human Tau-Protein Kinase I / Glycogen Synthase Kinase-3 b Crystallization Papers," 1464–65.

Arinaminpathy, Yalini, Ekta Khurana, Donald M. Engelman, and Mark B. Gerstein. 2009. "Computational Analysis of Membrane Proteins: The Largest Class of Drug Targets." *Biophysics* 14: 1130–35. https://doi.org/10.1016/j.drudis.2009.08.006.Computational.

Armstrong, Jane L., Sylvie M. Bonavaud, Barry J. Toole, and Stephen J. Yeaman. 2001. "Regulation of Glycogen Synthesis by Amino Acids in Cultured Human Muscle Cells." *Journal of Biological Chemistry* 276 (2): 952–56. https://doi.org/10.1074/jbc.M004812200.

Aslanidis, Charalampos, and Pieter J. de Jong. 1990. "Ligation-Independent Cloning of PCR Products (LIC-PCR)." *Nucleic Acids Research* 18 (20): 6069–74. https://doi.org/10.1093/nar/18.20.6069.

Avraham, Eyal, Raymonde Szargel, Allon Eyal, Ruth Rott, and Simone Engelender. 2005. "Glycogen Synthase Kinase 3 ␣ Modulates Synphilin-1 Ubiquitylation and Cellular Inclusion Formation by SIAH IMPLICATIONS FOR PROTEASOMAL FUNCTION AND LEWY BODY FORMATION *" 280 (52): 42877–86. https://doi.org/10.1074/jbc.M505608200.

Babu, Mohan, Hiroyuki Aoki, Wasimul Q. Chowdhury, Alla Gagarinova, Chris Graham, Sadhna Phanse, Ben Laliberte, et al. 2011. "Ribosome-Dependent ATPase Interacts with Conserved Membrane Protein in Escherichia Coli to Modulate Protein Synthesis and Oxidative Phosphorylation." *PLoS ONE* 6 (4). https://doi.org/10.1371/journal.pone.0018510.

Ballou, Lisa M., Pei Yu Tian, Hong Ying Lin, Ya Ping Jiang, and Richard Z. Lin. 2001. "Dual Regulation of Glycogen Synthase Kinase-3β by the α 1A-Adrenergic Receptor." *Journal of Biological Chemistry* 276 (44): 40910–16. https://doi.org/10.1074/jbc.M103480200.

Bao, Xiu-qi, Ning Li, Tao Wang, Xiang-chen Kong, Wen-jiao Tai, Hua Sun, and Dan Zhang. 2013. "FLZ Alleviates the Memory Deficits in Transgenic Mouse Model of Alzheimer ' s Disease

via Decreasing Beta- Amyloid Production and Tau Hyperphosphorylation" 8 (11): 1–11. https://doi.org/10.1371/journal.pone.0078033.

Barth, Andreas. 2007. "Infrared Spectroscopy of Proteins." *Biochimica et Biophysica Acta - Bioenergetics* 1767 (9): 1073–1101. https://doi.org/10.1016/j.bbabio.2007.06.004.

Bastin, David A., Gordon Stevenson, Peter K. Brown, Antje Haase, and Peter R. Reeves. 1993. "Repeat Unit Polysaccharides of Bacteria: A Model for Polymerization Resembling That of Ribosomes and Fatty Acid Synthetase, with a Novel Mechanism for Determining Chain Length." *Molecular Microbiology* 7 (5): 725–34. https://doi.org/10.1111/j.1365-2958.1993.tb01163.x.

Bax, Ad, Georg Kontaxis, and Nico Tjandra. 2001. "Nuclear Magnetic Resonance of Biological Macromolecules - Part B." *Methods in Enzymology* 339 (1997): 127–74. https://doi.org/10.1016/S0076-6879(01)39313-8.

Beaulieu, Jean-martin, Tatyana D Sotnikova, Wei-dong Yao, Lisa Kockeritz, James R Woodgett, Raul R Gainetdinov, and Marc G Caron. 2004. "Lithium Antagonizes Dopamine-Dependent Behaviors Mediated by an AKT ¯Glycogen Synthase Kinase 3 Signaling Cascade," no. 14.

Behrend, L., D. M. Milne, M. Stöter, W. Deppert, L. E. Campbell, D. W. Meek, and U. Knippschild. 2000. "IC261, a Specific Inhibitor of the Protein Kinases Casein Kinase 1-Delta and -Epsilon, Triggers the Mitotic Checkpoint and Induces P53-Dependent Postmitotic Effects." *Oncogene* 19 (47): 5303–13. https://doi.org/10.1038/sj.onc.1203939.

Bejarano, P. A., J. P M Langeveld, B. G. Hudson, and M. E. Noelken. 1989. "Degradation of Basement Membranes by Pseudomonas Aeruginosa Elastase." *Infection and Immunity* 57 (12): 3783–87.

Berry, Matthew C., Gayle C. Mcghee, Youfu Zhao, and George W. Sundin. 2009. "Effect of a WaaL Mutation on Lipopolysaccharide Composition, Oxidative Stress Survival, and Virulence in Erwinia Amylovora: RESEARCH LETTER." *FEMS Microbiology Letters* 291 (1): 80–87. https://doi.org/10.1111/j.1574-6968.2008.01438.x.

Bertrand, J A, S Thieffine, A Vulpetti, C Cristiani, B Valsasina, S Knapp, H M Kalisz, and M Flocco. 2003. "Structural Characterization of the GSK-3 b Active Site Using Selective and Non-Selective ATP-Mimetic Inhibitors," 393–407. https://doi.org/10.1016/j.jmb.2003.08.031.

Beurel, Eléonore, and Richard S. Jope. 2008. "The Paradoxical Pro- and Anti-Apoptotic Actions of GSK3 in the Intrinsic and Extrinsic Apoptosis Signaling Pathways Eléonore." *Bone* 23 (1): 1–7. https://doi.org/10.1038/jid.2014.371.

Beurel, Eléonore, Michel Kornprobst, Marie José Blivet-Van Eggelpoël, Carmen Ruiz-Ruiz, Axelle Cadoret, Jacqueline Capeau, and Christèle Desbois-Mouthon. 2004. "GSK-3β Inhibition by Lithium Confers Resistance to Chemotherapy-Induced Apoptosis through the Repression of CD95 (Fas/APO-1) Expression." *Experimental Cell Research* 300 (2): 354–64. https://doi.org/10.1016/j.yexcr.2004.08.001.

Bhat, Ratan, Yafeng Xue, Stefan Berg, Mats Ormö, Yvonne Nilsson, Ann-cathrin Radesäter, Eva Jerning, et al. 2003. "Mechanisms of Signal Transduction : Structural Insights and Biological Effects of Structural Insights and Biological Effects of Glycogen Synthase Kinase 3-Specific Inhibitor AR-A014418 *." https://doi.org/10.1074/jbc.M306268200.

Bijur, Gautam N., and Richard S. Jope. 2003. "Glycogen Synthase Kinase-3 Beta Is Highly Activated in Nuclei and Mitochondria." *Neuroreport* 14 (18): 2415–19. https://doi.org/10.1097/00001756-200312190-00025.

Blundell, Tom L. 1996. "Structure-Based Drug Design." *Nature* 384 (6604): 23–24. https://doi.org/10.1038/384023a0.

Bond, Stephen R., and Christian C. Naus. 2012. "RF-Cloning.Org: An Online Tool for the Design of Restriction-Free Cloning Projects." *Nucleic Acids Research* 40 (W1): 209–13. https://doi.org/10.1093/nar/gks396.

Brady, Matthew J., Francis J. Bourbonais, and Alan R. Saltiel. 1998. "The Activation of Glycogen Synthase by Insulin Switches from Kinase Inhibition to Phosphatase Activation during

Adipogenesis in 3T3-L1 Cells." *Journal of Biological Chemistry* 273 (23): 14063–66. https://doi.org/10.1074/jbc.273.23.14063.

Breidenstein, Elena B M, César de la Fuente-Núñez, and Robert E W Hancock. 2011. "Pseudomonas Aeruginosa: All Roads Lead to Resistance." *Trends in Microbiology* 19 (8): 419–26. https://doi.org/10.1016/j.tim.2011.04.005.

Buch, Idit, Dan Fishelovitch, Nir London, Barak Raveh, Haim J. Wolfson, and Ruth Nussinov. 2010. "Allosteric Regulation of Glycogen Synthase Kinase 3β: A Theoretical Study." *Biochemistry* 49 (51): 10890–901. https://doi.org/10.1021/bi100822q.

Burrows, Lori L., David Chow, and Joseph S. Lam. 1997. "Pseudomonas Aeruginosa B-Band O-Antigen Chain Length Is Modulated by Wzz (Rol)." *Journal of Bacteriology* 179 (5): 1482–89. https://doi.org/10.1128/jb.179.5.1482-1489.1997.

Carpenter, Elisabeth P., Konstantinos Beis, Alexander D. Cameron, and So Iwata. 2008. "Overcoming the Challenges of Membrane Protein Crystallography." *Current Opinion in Structural Biology* 18 (5): 581–86. https://doi.org/10.1016/j.sbi.2008.07.001.

Carson, Mike, David H. Johnson, Heather McDonald, Christie Brouillette, and Lawrence J. DeLucas. 2007. "His-Tag Impact on Structure." *Acta Crystallographica Section D: Biological Crystallography* 63 (3): 295–301. https://doi.org/10.1107/S0907444906052024.

Cervelli, F, S Carrato, A Mattei, L Benevoli, and L Vaccari. 2012. "Beyond Fingerprints Morphology: Chemical Mapping of Functional Groups." In *2012 Proceedings of the 20th European Signal Processing Conference (EUSIPCO)*, 1509–13.

Chattopadhyay, Amitabha, and H Raghuraman. 2004. "Application of Fluorescence Spectroscopy to Membrane Protein Structure and Dynamics."

Cheng, Yifan, Nikolaus Grigorieff, Pawel A Penczek, and Thomas Walz. 2015. "Primer A Primer to Single-Particle Cryo-Electron Microscopy."

Cherezov, Vadim, Daniel M. Rosenbaum, Michael A. Hanson, Søren G.F. Rasmussen, Sun Thian Foon, Tong Sun Kobilka, Hee Jung Choi, et al. 2007. "High-Resolution Crystal Structure of an Engineered Human B2-Adrenergic G Protein-Coupled Receptor." *Science* 318 (5854): 1258–65. https://doi.org/10.1126/science.1150577.

Chong, Z. Z., and Kenneth Maiese. 2004. "Targeting WNT, Protein Kinase B, and Mitochondrial Membrane Integrity to Foster Cellular Survival in the Nervous System." *Histology and Histopathology* 19 (2): 495–504. https://doi.org/10.14670/HH-19.495.

Ciani, Lorenza, and Patricia C. Salinas. 2005. "WNTs in the Vertebrate Nervous System: From Patterning to Neuronal Connectivity." *Nature Reviews Neuroscience* 6 (5): 351–62. https://doi.org/10.1038/nrn1665.

Cicenas, Jonas, Karthik Kalyan, and Mindaugas Valius. 2015. "Roscovitine in Cancer and Other Diseases Cellular Effects and Preclinical Tests." *Ncbi.Nlm.Nih.Gov* 9 (19): 1–12. https://doi.org/10.2210/pdb2a4l/pdb.

Cohen, Philip. 2002. "Protein Kinases - The Major Drug Targets of the Twenty-First Century?" *Nature Reviews Drug Discovery* 1 (4): 309–15. https://doi.org/10.1038/nrd773.

Colla, Emanuela, Poul H Jensen, Olga Pletnikova, Juan C Troncoso, Charles Glabe, and Michael K Lee. 2012. "Accumulation of Toxic ␣ -Synuclein Oligomer within Endoplasmic Reticulum Occurs in ␣ -Synucleinopathy In Vivo" 32 (10): 3301–5. https://doi.org/10.1523/JNEUROSCI.5368-11.2012.

Collins, Richard F., Vasileios Kargas, Brad R. Clarke, C. Alistair Siebert, Daniel K. Clare, Peter J. Bond, Chris Whitfield, and Robert C. Ford. 2017. "Full-Length, Oligomeric Structure of Wzz Determined by Cryoelectron Microscopy Reveals Insights into Membrane-Bound States." *Structure* 25 (5): 806-815.e3. https://doi.org/10.1016/j.str.2017.03.017.

Cowan, S. W., and Jurg P. Rosenbusch. 1994. "Folding Pattern Diversity of Integral Membrane Proteins" 264 (May).

Credle, J J, J L George, J Wills, V Duka, K Shah, Y-c Lee, O Rodriguez, et al. 2015. "GSK-3 β Dysregulation Contributes to Parkinson ' s-like Pathophysiology with Associated Region-

Specific Phosphorylation and Accumulation of Tau and α -Synuclein," 838–51. https://doi.org/10.1038/cdd.2014.179.

Cross, Darren A E, Ainsley A Culbert, Katy A Chalmers, Laura Facci, Stephen D Skaper, and Alastair D Reith. 2001. "Selective Small-Molecule Inhibitors of Glycogen Synthase Kinase-3 Activity Protect Primary Neurones from Death," 94–102.

Cuthbertson, L., V. Kos, and C. Whitfield. 2010a. "ABC Transporters Involved in Export of Cell Surface Glycoconjugates." *Microbiology and Molecular Biology Reviews* 74 (3): 341–62. https://doi.org/10.1128/mmbr.00009-10.

Cuthbertson, L., V. Kos, and C. Whitfield. 2010b. "ABC Transporters Involved in Export of Cell Surface Glycoconjugates." *Microbiology and Molecular Biology Reviews* 74 (3): 341–62. https://doi.org/10.1128/mmbr.00009-10.

D'amico, Francesco, Makina Saito, Filippo Bencivenga, Marino Marsi, Alessandro Gessini, Gaia Camisasca, Emiliano Principi, et al. 2013. "UV Resonant Raman Scattering Facility at Elettra." *Nuclear Instruments and Methods in Physics Research, Section A: Accelerators, Spectrometers, Detectors and Associated Equipment* 703: 33–37. https://doi.org/10.1016/j.nima.2012.11.037.

Dajani, Rana, Elizabeth Fraser, S Mark Roe, Neville Young, Valerie Good, Trevor C Dale, and Laurence H Pearl. 2001. "Crystal Structure of Glycogen Synthase Kinase 3 ␣ : Structural Basis for Phosphate-Primed Substrate Specificity and Autoinhibition" 105: 721–32.

Dalbey, Ross E., Peng Wang, and Andreas Kuhn. 2011. "Assembly of Bacterial Inner Membrane Proteins." *Annual Review of Biochemistry* 80 (1): 161–87. https://doi.org/10.1146/annurev-biochem-060409-092524.

Daley, Daniel O., Mikaela Rapp, Erik Granseth, Karin Melén, David Drew, and Gunnar Von Heijne. 2005. "Biochemistry: Global Topology Analysis of the Escherichia Coli Inner Membrane Proteome." *Science* 308 (5726): 1321–23. https://doi.org/10.1126/science.1109730.

Dasgupta, T., T. R. De Kievit, H. Masoud, E. Altman, J. C. Richards, I. Sadovskaya, D. P. Speert, and J. S. Lam. 1994. "Characterization of Lipopolysaccharide-Deficient Mutants of Pseudomonas Aeruginosa Derived from Serotypes O3, O5, and O6." *Infection and Immunity* 62 (3): 809–17.

De Zorzi Rita , Wei Mi, Maofu Liao, and Thomas Walz. 2016. "Single-Particle Electron Microscopy in the Study of Membrane Protein Structure." *Microscopy (Oxford, England)* 65 (1): 81–96. https://doi.org/10.1093/jmicro/dfv058.

Dellovade, Tammy, Justyna T. Romer, Tom Curran, and Lee L. Rubin. 2006. "The Hedgehog Pathway and Neurological Disorders." *Annual Review of Neuroscience* 29 (1): 539–63. https://doi.org/10.1146/annurev.neuro.29.051605.112858.

Delucia, Angela M., David A. Six, Ruth E. Caughlan, Patricia Gee, Ian Hunt, Joseph S. Lam, and Charles R. Dean. 2011. "Lipopolysaccharide (LPS) Inner-Core Phosphates Are Required for Complete Lps Synthesis and Transport to the Outer Membrane in Pseudomonas Aeruginosa PAO1." *MBio* 2 (4): 1–9. https://doi.org/10.1128/mBio.00142-11.

DeMaagd, George, and Ashok Philip. 2015. "Parkinson ' s Disease and Its Management" 40 (8): 504–11.

Deng, Yulei, Zhe Xiong, Paul Chen, Jing Wei, Shengdi Chen, and Zhen Yan. 2014. "Neurobiology of Aging b -Amyloid Impairs the Regulation of N -Methyl-D-Aspartate Receptors by Glycogen Synthase Kinase 3." *Neurobiology of Aging* 35 (3): 449–59. https://doi.org/10.1016/j.neurobiolaging.2013.08.031.

Dessau, Moshe A., and Yorgo Modis. 2010. "Protein Crystallization for X-Ray Crystallography." *Journal of Visualized Experiments* 9 (47): 1–6. https://doi.org/10.3791/2285.

Doble, Bradley W, and James R Woodgett. 2003. "GSK-3 : Tricks of the Trade for a Multi-Tasking Kinase." https://doi.org/10.1242/jcs.00384.

Domínguez, Juan Manuel, Ana Fuertes, Leyre Orozco, María Monte-milla, Elena Delgado, and Miguel Medina. 2012. "Evidence for Irreversible Inhibition of Glycogen Synthase" 287 (2):

893–904. https://doi.org/10.1074/jbc.M111.306472.
Drew, David E., Gunnar Von Heijne, Par Nordlund, and Jan-willem L De Gier. 2001. “Green Fluorescent Protein as an Indicator to Monitor Membrane Protein Overexpression in Escherichia Coli” 507: 220–24.
Duda, Przemysław, Janusz Wiśniewski, Tomasz Wójtowicz, and Olga Wójcicka. 2018. “Targeting GSK3 Signaling as a Potential Therapy of Neurodegenerative Diseases and Aging.” *Expert Opinion on Therapeutic Targets* 0 (0): 1. https://doi.org/10.1080/14728222.2018.1526925.
Duerr, Claudia U., Sebastian F. Zenk, Cécilia Chassin, Johanna Pott, Dominique Gütle, Michael Hensel, and Mathias W. Hornef. 2009. “O-Antigen Delays Lipopolysaccharide Recognition and Impairs Antibacterial Host Defense in Murine Intestinal Epithelial Cells.” *PLoS Pathogens* 5 (9). https://doi.org/10.1371/journal.ppat.1000567.
Duong-Ly, Krisna C., and Jeffrey R. Peterson. 2014. “The Human Kinome and Kinase Inhibition as a Therapeutic Strategy,” no. 215. https://doi.org/10.1002/0471141755.ph0209s60.The.
Duve, Christian De, and Robert Wattiaux. 1966. “FUNCTIONS OF LYSOSOMES,” no. September.
Ehrmann, Michael. 2007. “The Periplasm.” *The Periplasm*. https://doi.org/10.1128/9781555815806.
Elamin, Ayssar A., Susanne Steinicke, Wulf Oehlmann, Yvonne Braun, Hanaa Wanas, Eduard A. Shuralev, Carmen Huck, Marko Maringer, Manfred Rohde, and Mahavir Singh. 2017. “Novel Drug Targets in Cell Wall Biosynthesis Exploited by Gene Disruption in Pseudomonas Aeruginosa.” *PLoS ONE* 12 (10): 1–18. https://doi.org/10.1371/journal.pone.0186801.
Elumalai, Pavadai, M. Rajasekaran, Hsuan Liang Liu, and Chinpan Chen. 2010. “Investigation of Cation-π Interactions in Sugar-Binding Proteins.” *Protoplasma* 247 (1): 13–24. https://doi.org/10.1007/s00709-010-0132-x.
Embi, Noor, Dennis B. Rylatt, and Philip Cohen. 1980. “Glycogen Synthase Kinase-3 from Rabbit Skeletal Muscle Separation from Cyclic-AMP-Dependent Protein Kinase and Phosphorylase Kinas.” *Publications of the American Statistical Association* 1 (8): 475–77. https://doi.org/10.1080/15225437.1889.10502791.
Emsley, P., B. Lohkamp, W. G. Scott, and K. Cowtan. 2010. “Features and Development of Coot.” *Acta Crystallographica Section D: Biological Crystallography* 66 (4): 486–501. https://doi.org/10.1107/S0907444910007493.
Engel, Christian K., Lu Chen, and Gilbert G. Privé. 2002. “Stability of the Lactose Permease in Detergent Solutions.” *Biochimica et Biophysica Acta - Biomembranes* 1564 (1): 47–56. https://doi.org/10.1016/S0005-2736(02)00397-8.
Fang, X., S. Yu, J. L. Tanyi, Y. Lu, J. R. Woodgett, and G. B. Mills. 2002. “Convergence of Multiple Signaling Cascades at Glycogen Synthase Kinase 3: Edg Receptor-Mediated Phosphorylation and Inactivation by Lysophosphatidic Acid through a Protein Kinase C-Dependent Intracellular Pathway.” *Molecular and Cellular Biology* 22 (7): 2099–2110. https://doi.org/10.1128/mcb.22.7.2099-2110.2002.
Fields, Francisco R., Shaun W. Lee, and Michael J. McConnell. 2017. “Using Bacterial Genomes and Essential Genes for the Development of New Antibiotics.” *Munchener Medizinische Wochenschrift* 120 (45): 1480. https://doi.org/10.1016/j.bcp.2016.12.002.Using.
Fiol, Carol J, Aiqun Wang, Roger W. Roeske, and Peter J Roach. 1990. “Ordered Multisite Protein Phosphorylation.” *Journal of Biological Chemistry* 265 (11): 6061–65.
Fish, Kimberly J., Aleksandra Cegielska, Michael E. Getman, Gregory M. Landes, and David M. Virshup. 1995. “Isolation and Characterization of Human Casein Kinase Iϵ (CKI), a Novel Member of the CKI Gene Family.”
Frame, Sheelagh, Philip Cohen, and Ricardo M Biondi. 2001. “Explains the Unique Substrate Specificity of GSK3 and Its Inactivation by Phosphorylation” 7: 1321–27.
Frautschy, S. A., G. M. Cole, and A. Baird. 1992. “Phagocytosis and Deposition of Vascular β-Amyloid in Rat Brains Injected with Alzheimer β-Amyloid.” *American Journal of Pathology*

140 (6): 1389–99.
Frueh, Dominique P., Andrew C. Goodrich, Subrata H. Mishra, and Scott R. Nichols. 2013. "NMR Methods for Structural Studies of Large Monomeric and Multimeric Proteins." *Current Opinion in Structural Biology* 23 (5): 734–39. https://doi.org/10.1016/j.sbi.2013.06.016.
Ghisaidoobe, Amar B T, and Sang J Chung. 2014. "Intrinsic Tryptophan Fluorescence in the Detection and Analysis of Proteins : A Focus on Förster Resonance Energy Transfer Techniques," 22518–38. https://doi.org/10.3390/ijms151222518.
Ghoshal, Nupur, John F. Smiley, Anthony J. DeMaggio, Merl F. Hoekstra, Elizabeth J. Cochran, Lester I. Binder, and Jeff Kuret. 1999. "A New Molecular Link between the Fibrillar and Granulovacuolar Lesions of Alzheimer's Disease." *American Journal of Pathology* 155 (4): 1163–72. https://doi.org/10.1016/S0002-9440(10)65219-4.
Glass, Christopher K, Kaoru Saijo, Beate Winner, Maria Carolina Marchetto, and H Gage. 2010. "Mechanisms Underlying Inflammation in Neurodegeneration." *Nih* 140 (6): 918–34. https://doi.org/10.1016/j.cell.2010.02.016.Mechanisms.
Glauert, A M, and M J Thornley. 1969. "The Topography of the Bacterial Cell Wall." *Annual Review of Microbiology* 23 (1): 159–98. https://doi.org/10.1146/annurev.mi.23.100169.001111.
Goi-Oliver, Paloma, Jesús Avila, and Félix Hernández. 2009. "Memantine Inhibits Calpain-Mediated Truncation of GSK-3 Induced by NMDA: Implications in Alzheimer's Disease." *Journal of Alzheimer's Disease* 18 (4): 843–48. https://doi.org/10.3233/JAD-2009-1190.
Golpich, Mojtaba, Elham Amini, Fatemeh Hemmati, Norlinah Mohamed, Behrouz Rahmani, Zahurin Mohamed, Azman Ali, Leila Dargahi, Rasoul Ghasemi, and Abolhassan Ahmadiani. 2015. "Glycogen Synthase Kinase-3 Beta (GSK-3 ␣) Signaling : Implications for Parkinson ' s Disease" 97: 16–26.
Gorojankina, Tatiana. 2016. "Hedgehog Signaling Pathway: A Novel Model and Molecular Mechanisms of Signal Transduction." *Cellular and Molecular Life Sciences* 73 (7): 1317–32. https://doi.org/10.1007/s00018-015-2127-4.
Govan, J. R.W., and V. Deretic. 1996. "Microbial Pathogenesis in Cystic Fibrosis: Mucoid Pseudomonas Aeruginosa and Burkholderia Cepacia." *Microbiological Reviews* 60 (3): 539–74.
Greenfield, Norma, and Gerald D. Fasman. 1969. "Computed Circular Dichroism Spectra for the Evaluation of Protein Conformation." *Biochemistry* 8 (10): 4108–16. https://doi.org/10.1021/bi00838a031.
Greenfield, Norma J. 2009. "Using Circular Dichroism Spectra to Estimate Protein Secondary Structure." *ProQuest Dissertations and Theses* 1 (6): 2876–90. https://doi.org/10.1038/nprot.2006.202.Using.
Grimes, Carol A., and Richard S. Jope. 2001. "The Multifaceted Roles of Glycogen Synthase Kinase 3β in Cellular Signaling." *Progress in Neurobiology* 65 (4): 391–426. https://doi.org/10.1016/S0301-0082(01)00011-9.
Guan, Lan, Irina N. Smirnova, Gill Verner, Shushi Nagamoni, and H. Ronald Kaback. 2006. "Manipulating Phospholipids for Crystallization of a Membrane Transport Protein." *Proceedings of the National Academy of Sciences of the United States of America* 103 (6): 1723–26. https://doi.org/10.1073/pnas.0510922103.
Haar, Ernst, Joyce T Coll, and Douglas A Austen. 2001. "Structure of GSK3 β Reveals a Primed Phosphorylation Mechanism A" 269 (1995): 593–96.
Hampel, Harald, Michael Ewers, Katharina Bürger, Peter Annas, Anette Mörtberg, Anna Bogstedt, Lutz Frölich, et al. 2009. "Lithium Trial in Alzheimer ' s Disease :," no. June: 923–32.
Han, Weiqing, Baolin Wu, Lei Li, Guohui Zhao, Robert Woodward, Nicholas Pettit, Li Cai, Vireak Thon, and Peng G. Wang. 2012. "Defining Function of Lipopolysaccharide O-Antigen Ligase Waal Using Chemoenzymatically Synthesized Substrates." *Journal of Biological Chemistry* 287 (8): 5357–65. https://doi.org/10.1074/jbc.M111.308486.

Hancock, R. E.W., L. M. Mutharia, L. Chan, R. P. Darveau, D. P. Speert, and G. B. Pier. 1983. "Pseudomonas Aeruginosa Isolates from Patients with Cystic Fibrosis: A Class of Serum-Sensitive, Nontypable Strains Deficient in Lipopolysaccharide O Side Chains." *Infection and Immunity* 42 (1): 170–77.

Hancock, Robert E. W. 1998. " Resistance Mechanisms in Pseudomonas Aeruginosa and Other Nonfermentative Gram-Negative Bacteria ." *Clinical Infectious Diseases* 27 (s1): S93–99. https://doi.org/10.1086/514909.

Hanks, S. K., and T. Hunter. 1995. "The Eukaryotic Protein Kinase Superfamily: Kinase (Catalytic) Domain Structure and Classification." *FASEB Journal* 9 (8): 576–96. https://doi.org/10.1096/fasebj.9.8.7768349.

Hari, Sanjay B., Ethan A. Merritt, and Dustin J. Maly. 2008. "Sequence Determinants of a Specific Inactive Protein Kinase Conformation." *Bone* 23 (1): 1–7. https://doi.org/10.1038/jid.2014.371.

Haupt, Susan, Michael Berger, Zehavit Goldberg, and Ygal Haupt. 2003. "Apoptosis - The P53 Network." *Journal of Cell Science* 116 (20): 4077–85. https://doi.org/10.1242/jcs.00739.

Hauser, Alan R. 2012. "So Many Virulence Factors, So Little Time." *Crit Care Med.* 39 (9): 2193–94. https://doi.org/10.1097/CCM.0b013e318221742d.Pseudomonas.

Hedhammar, My, and Sophia Hober. 2007. "Zbasic-A Novel Purification Tag for Efficient Protein Recovery." *Journal of Chromatography A* 1161 (1–2): 22–28. https://doi.org/10.1016/j.chroma.2007.05.091.

Hee, Ju, Kyeong-man Kim, Seong Who, Onyou Hwang, and Hyun Jin. 2008. "Bromocriptine Activates NQO1 via Nrf2-PI3K / Akt Signaling : Novel Cytoprotective Mechanism against Oxidative Damage" 57: 325–31. https://doi.org/10.1016/j.phrs.2008.03.004.

Hessa, Tara, Nadja M. Meindl-Beinker, Andreas Bernsel, Hyun Kim, Yoko Sato, Mirjam Lerch-Bader, Ingmarie Nilsson, Stephen H. White, and Gunnar Von Heijne. 2007. "Molecular Code for Transmembrane-Helix Recognition by the Sec61 Translocon." *Nature* 450 (7172): 1026–30. https://doi.org/10.1038/nature06387.

Holzwarth, G., and P. Doty. 1965. "The Ultraviolet Circular Dichroism of Polypeptides." *Journal of the American Chemical Society* 87 (2): 218–28. https://doi.org/10.1021/ja01080a015.

Hong, Yaoqin, and Peter R. Reeves. 2014. "Diversity of O-Antigen Repeat Unit Structures Can Account for the Substantial Sequence Variation of Wzx Translocases." *Journal of Bacteriology*. https://doi.org/10.1128/JB.01323-13.

Hooper, Claudie, Richard Killick, and Simon Lovestone. 2008. "The GSK3 Hypothesis of Alzheimer's Disease." *Journal of Neurochemistry* 104 (6): 1433–39. https://doi.org/10.1111/j.1471-4159.2007.05194.x.

Hu, Jie Hong, Ken Chernoff, Steven Pelech, and Charles Krieger. 2003. "Protein Kinase and Protein Phosphatase Expression in the Central Nervous System of G93A MSOD Over-Expressing Mice." *Journal of Neurochemistry* 85 (2): 422–31. https://doi.org/10.1046/j.1471-4159.2003.01669.x.

Hubbard, Simon J, and PATRICK ARGOS. 1994. "Cavities and Packing at Protein Interfaces."

Huber, Damon, Dana Boyd, Yu Xia, Michael H. Olma, Mark Gerstein, and Jon Beckwith. 2005. "Use of Thioredoxin as a Reporter to Identify a Subset of Escherichia Coli Signal Sequences That Promote Signal Recognition Particle-Dependent Translocation." *Journal of Bacteriology* 187 (9): 2983–91. https://doi.org/10.1128/JB.187.9.2983-2991.2005.

Hunter, Tony, La Jolla, and Henry Wadsworth Longfellow. 2000. "Signaling — 2000 and Beyond" 100: 113–27.

Huse, Morgan, and John Kuriyan. 2002. "The Conformational Plasticity of Protein Kinases" 109: 275–82.

Hvorup, Rikki N., Brit Winnen, Abraham B. Chang, Yong Jiang, Xiao Feng Zhou, and Milton H. Saier. 2003. "The Multidrug/Oligosaccharidyl-Lipid/Polysaccharide (MOP) Exporter Superfamily." *European Journal of Biochemistry* 270 (5): 799–813.

https://doi.org/10.1046/j.1432-1033.2003.03418.x.
Hwang, Peter M., Wing Yiu Choy, Eileen I. Lo, Lu Chen, Julie D. Forman-Kay, Christian R.H. Raetz, Gilbert G. Privé, Russell E. Bishop, and Lewis E. Kay. 2002. "Solution Structure and Dynamics of the Outer Membrane Enzyme PagP by NMR." *Proceedings of the National Academy of Sciences of the United States of America* 99 (21): 13560–65. https://doi.org/10.1073/pnas.212344499.
Islam, S T, and J S Lam. 2014. "Synthesis of Bacterial Polysaccharides via the Wzx/ Wzy-Dependent Pathway 1." *Canadian Journal of Microbiology*. https://doi.org/10.1139/cjm-2014-0595.
Islam, Salim T., Paul D.W. Eckford, Michelle L. Jones, Timothy Nugent, Christine E. Bear, Christian Vogel, and Joseph S. Lam. 2013a. "Proton-Dependent Gating and Proton Uptake by Wzx Support o-Antigen-Subunit Antiport across the Bacterial Inner Membrane." *MBio* 4 (5). https://doi.org/10.1128/mBio.00678-13.
Islam, Salim T., Paul D W Eckford, Michelle L. Jones, Timothy Nugent, Christine E. Bear, Christian Vogel, and Joseph S. Lam. 2013b. "Proton-Dependent Gating and Proton Uptake by Wzx Support o-Antigen-Subunit Antiport across the Bacterial Inner Membrane." *MBio*. https://doi.org/10.1128/mBio.00678-13.
Islam, Salim T., Robert J. Fieldhouse, Erin M. Anderson, Véronique L. Taylor, Robert A B Keates, Robert C. Ford, and Joseph S. Lam. 2012. "A Cationic Lumen in the Wzx Flippase Mediates Anionic O-Antigen Subunit Translocation in Pseudomonas Aeruginosa PAO1." *Molecular Microbiology*. https://doi.org/10.1111/j.1365-2958.2012.08084.x.
Islam, Salim T., Alexander C. Gold, Véronique L. Taylor, Erin M. Anderson, Robert C. Ford, and Joseph S. Lam. 2011. "Dual Conserved Periplasmic Loops Possess Essential Charge Characteristics That Support a Catch-and-Release Mechanism of O-Antigen Polymerization by Wzy in Pseudomonas Aeruginosa PAO1." *Journal of Biological Chemistry* 286 (23): 20600–605. https://doi.org/10.1074/jbc.C110.204651.
Islam, Salim T., Steven M. Huszczynski, Timothy Nugent, Alexander C. Gold, and Joseph S. Lam. 2013. "Conserved-Residue Mutations in Wzy Affect O-Antigen Polymerization and Wzz-Mediated Chain-Length Regulation in Pseudomonas Aeruginosa PAO1." *Scientific Reports* 3: 1–9. https://doi.org/10.1038/srep03441.
Islam, Salim T., and Joseph S. Lam. 2013. "Wzx Flippase-Mediated Membrane Translocation of Sugar Polymer Precursors in Bacteria." *Environmental Microbiology*. https://doi.org/10.1111/j.1462-2920.2012.02890.x.
Islam, Salim T, and Joseph S Lam. 2014. "Synthesis of Bacterial Polysaccharides via the Wzx/Wzy-Dependent Pathway." *Canadian Journal of Microbiology*. https://doi.org/10.1139/cjm-2014-0595.
Islam, Salim T, Véronique L Taylor, Meng Qi, and Joseph S Lam. 2010. "Membrane Topology Mapping of The" 1 (3): 1–10. https://doi.org/10.1128/mBio.00189-10.Editor.
Jacobs, Keith M., Sandeep R. Bhave, Daniel J. Ferraro, Jerry J. Jaboin, Dennis E. Hallahan, and Dinesh Thotala. 2012. "GSK-3β: A Bifunctional Role in Cell Death Pathways." *International Journal of Cell Biology* 2012 (Figure 1). https://doi.org/10.1155/2012/930710.
Johnson, L. N. 1993. "THE EFFECTS OF PHOSPHORYLATION ON THE STRUCTURE AND FUNCTION OF PROTEINS," 199–232.
Johnson, Louise N, and Richard J Lewis. 2001. "Structural Basis for Control by Phosphorylation." https://doi.org/10.1021/cr000225s.
Jope, Richard S., Yuyan Cheng, Jeffrey Lowell, Ryan J. Worthen, Yoel H. Sitbon, and Eleonore Beurel. 2017. "Stressed and Inflamed, Can GSK3 Be Blamed?" *Physiology & Behavior* 176 (3): 139–48. https://doi.org/10.1016/j.physbeh.2017.03.040.
Jope, Richard S., and Myoung-sun Roh. 2008. "Glycogen Synthase Kinase-3 (GSK3) in Psychiatric Diseases and Therapeutic Interventions." *Bone* 23 (1): 1–7. https://doi.org/10.1038/jid.2014.371.

Jope, Richard S, Christopher J Yuskaitis, and Eléonore Beurel. 2006. “Glycogen Synthase Kinase-3 (GSK3): Inflammation, Diseases, and Therapeutics.” *Neurochemical Research* 32 (4–5): 577–95. https://www.ncbi.nlm.nih.gov/pmc/articles/PMC1970866/pdf/nihms24923.pdf%0Ahttp://www.ncbi.nlm.nih.gov/pubmed/16944320.

Kabsch, Wolfgang. 2010. “XDS.” *Acta Crystallographica Section D Biological Crystallography* 66 (2): 125–32. https://doi.org/10.1107/S0907444909047337.

Kalynych, Sergei, Deqiang Yao, James Magee, and Miroslaw Cygler. 2012. “Structural Characterization of Closely Related O-Antigen Lipopolysaccharide (LPS) Chain Length Regulators.” *Journal of Biological Chemistry* 287 (19): 15696–705. https://doi.org/10.1074/jbc.M112.354837.

Kamio, Yoshiyuki, and Hiroshi Nikaido. 1976. “Outer Membrane of Salmonella Typhimurium: Accessibility of Phospholipid Head Groups to Phospholipase C and Cyanogen Bromide Activated Dextran in the External Medium.” *Biochemistry* 15 (12): 2561–70. https://doi.org/10.1021/bi00657a012.

Kang, Cheol-In, Sung-Han Kim, Hong-Bin Kim, Sang-Won Park, Young-Ju Choe, Myoung-don Oh, Eui-Chong Kim, and Kang-Won Choe. 2003. “ Pseudomonas Aeruginosa Bacteremia: Risk Factors for Mortality and Influence of Delayed Receipt of Effective Antimicrobial Therapy on Clinical Outcome .” *Clinical Infectious Diseases* 37 (6): 745–51. https://doi.org/10.1086/377200.

Kang, Hae Joo, Chiara Lee, and David Drew. 2013. “Breaking the Barriers in Membrane Protein Crystallography.” *International Journal of Biochemistry and Cell Biology* 45 (3): 636–44. https://doi.org/10.1016/j.biocel.2012.12.018.

Karin, Michael. 2005. “Inflammation-Activated Protein Kinases as Targets for Drug Development.” *Proceedings of the American Thoracic Society* 2 (4): 386–90. https://doi.org/10.1513/pats.200504-034SR.

Kim, Hyun, Karin Melén, Marie Österberg, and Gunnar Von Heijne. 2006. “A Global Topology Map of the Saccharomyces Cerevisiae Membrane Proteome.” *Proceedings of the National Academy of Sciences of the United States of America* 103 (30): 11142–47. https://doi.org/10.1073/pnas.0604075103.

Kim, Woojin Scott, Katarina Kågedal, and Glenda M Halliday. 2014. “Alpha-Synuclein Biology in Lewy Body Diseases,” 1–9. https://doi.org/10.1186/s13195-014-0073-2.

King, Jerry D., Dana Kocíncová, Erin L. Westman, and Joseph S. Lam. 2009. “Lipopolysaccharide Biosynthesis in Pseudomonas Aeruginosa.” *Innate Immunity* 15 (5): 261–312. https://doi.org/10.1177/1753425909106436.

King, Taj D., Buffie Clodfelder-Miller, Keri A. Barksdale, and Gautam N. Bijur. 2008. “Unregulated Mitochondrial GSK3β Activity Results in NADH:Ubiquinone Oxidoreductase Deficiency.” *Bone* 23 (1): 1–7. https://doi.org/10.1038/jid.2014.371.

Knirel, Yuriy A., Olga V. Bystrova, Nina A. Kocharova, Ulrich Zähringer, and Gerald B. Pier. 2006. “Review: Conserved and Variable Structural Features in the Lipopolysaccharide of Pseudomonas Aeruginosa.” *Journal of Endotoxin Research* 12 (6): 324–36. https://doi.org/10.1179/096805106X118906.

Kobe, Bostjan, and Simon J Williams. 2015. “Fusion-Protein-Assisted Protein Crystallization,” 861–69. https://doi.org/10.1107/S2053230X15011061.

Koh, Seong Ho, Wonki Baek, and Seung H. Kim. 2011. “Brief Review of the Role of Glycogen Synthase Kinase-3β in Amyotrophic Lateral Sclerosis.” *Neurology Research International* 2011. https://doi.org/10.1155/2011/205761.

Kollef, Marin H. 2000. “Inadequate Antimicrobial Treatment: An Important Determinant of Outcome for Hospitalized Patients.” *Clinical Infectious Diseases* 31 (Supplement_4): S131–38. https://doi.org/10.1086/314079.

KONG, KOK-FAI, LISA SCHNEPER, and KALAI MATHEE. 2010. “Beta-Lactam Antibiotics:

From Antibiosis to Resistance and Bacteriology." *Apmis* 118 (1): 1–36. https://doi.org/10.1111/j.1600-0463.2009.02563.x.Beta-lactam.

Kornev, Alexandr P, and Susan S Taylor. 2010. "Biochimica et Biophysica Acta De Fi Ning the Conserved Internal Architecture of a Protein Kinase." *BBA - Proteins and Proteomics* 1804 (3): 440–44. https://doi.org/10.1016/j.bbapap.2009.10.017.

Kovacs, Gabor G. 2017. "Tauopathies" 145. https://doi.org/10.1016/B978-0-12-802395-2.00025-0.

Krause, Daniela L., and Norbert Müller. 2010. "Neuroinflammation, Microglia and Implications for Anti-Inflammatory Treatment in Alzheimer's Disease." *International Journal of Alzheimer's Disease* 2010. https://doi.org/10.4061/2010/732806.

Krause, Ulrike, Luc Bertrand, Liliane Maisin, Maria Rosa, and Louis Hue. 2002. "Signalling Pathways and Combinatory Effects of Insulin and Amino Acids in Isolated Rat Hepatocytes." *European Journal of Biochemistry* 269 (15): 3742–50. https://doi.org/10.1046/j.1432-1033.2002.03069.x.

Krogh, Anders, Björn Larsson, Gunnar Von Heijne, and Erik L.L. Sonnhammer. 2001. "Predicting Transmembrane Protein Topology with a Hidden Markov Model: Application to Complete Genomes." *Journal of Molecular Biology* 305 (3): 567–80. https://doi.org/10.1006/jmbi.2000.4315.

Kulikov, R., K. A. Boehme, and C. Blattner. 2005. "Glycogen Synthase Kinase 3-Dependent Phosphorylation of Mdm2 Regulates P53 Abundance." *Molecular and Cellular Biology* 25 (16): 7170–80. https://doi.org/10.1128/mcb.25.16.7170-7180.2005.

Kumar, Ramakrishnan B., Lin Zhu, Hans Hebert, and Caroline Jegerschöld. 2017. "Method to Visualize and Analyze Membrane Interacting Proteins by Transmission Electron Microscopy." *Journal of Visualized Experiments* 2017 (121): 1–10. https://doi.org/10.3791/55148.

Kuroda, Teruo, and Tomofusa Tsuchiya. 2009. "Multidrug Efflux Transporters in the MATE Family." *Biochimica et Biophysica Acta - Proteins and Proteomics* 1794 (5): 763–68. https://doi.org/10.1016/j.bbapap.2008.11.012.

Lam, Joseph S., Véronique L. Taylor, Salim T. Islam, Youai Hao, and Dana Kocíncová. 2011. "Genetic and Functional Diversity of Pseudomonas Aeruginosa Lipopolysaccharide." *Frontiers in Microbiology* 2 (JUNE): 1–25. https://doi.org/10.3389/fmicb.2011.00118.

Lamba, Vandana, and Indraneel Ghosh. 2012. "New Directions in Targeting Protein Kinases: Focusing Upon True Allosteric and Bivalent Inhibitors." *Current Pharmaceutical Design* 18 (20): 2936–45. https://doi.org/10.2174/138161212800672813.

Larue, Kane, Robert C. Ford, Lisa M. Willis, and Chris Whitfield. 2011. "Functional and Structural Characterization of Polysaccharide Co-Polymerase Proteins Required for Polymer Export in ATP-Binding Cassette Transporter-Dependent Capsule Biosynthesis Pathways." *Journal of Biological Chemistry* 286 (19): 16658–68. https://doi.org/10.1074/jbc.M111.228221.

Larue, Kane, Matthew S. Kimber, Robert Ford, and Chris Whitfield. 2009. "Biochemical and Structural Analysis of Bacterial O-Antigen Chain Length Regulator Proteins Reveals a Conserved Quaternary Structure." *Journal of Biological Chemistry* 284 (11): 7395–7403. https://doi.org/10.1074/jbc.M809068200.

Latino, Libera, Martine Caroff, and Christine Pourcel. 2017. "Fine Structure Analysis of Lipopolysaccharides in Bacteriophage-Resistant Pseudomonas Aeruginosa PAO1 Mutants." *Microbiology (United Kingdom)* 163 (6): 848–55. https://doi.org/10.1099/mic.0.000476.

Lau, K. F., C. C.J. Miller, B. H. Anderton, and Pang Chui Shaw. 1999. "Expression Analysis of Glycogen Synthase Kinase-3 in Human Tissues." *Journal of Peptide Research* 54 (1): 85–91. https://doi.org/10.1034/j.1399-3011.1999.00083.x.

Lau, Peter C.Y., Theresa Lindhout, Terry J. Beveridge, John R. Dutcher, and Joseph S. Lam. 2009. "Differential Lipopolysaccharide Core Capping Leads to Quantitative and Correlated Modifications of Mechanical and Structural Properties in Pseudomonas Aeruginosa Biofilms." *Journal of Bacteriology* 191 (21): 6618–31. https://doi.org/10.1128/JB.00698-09.

Lei, Peng, Scott Ayton, Ashley I. Bush, and Paul A. Adlard. 2011. "GSK-3 in Neurodegenerative

Diseases." *International Journal of Alzheimer's Disease* 2011. https://doi.org/10.4061/2011/189246.

Leibly, David J, Mark A Arbing, Inna Pashkov, Geoffrey S Waldo, Thomas C Terwilliger, Todd O Yeates, David J Leibly, et al. 2015. "Resource A Suite of Engineered GFP Molecules for Oligomeric Resource A Suite of Engineered GFP Molecules for Oligomeric Scaffolding." *Structure/Folding and Design* 23 (9): 1754–68. https://doi.org/10.1016/j.str.2015.07.008.

Lengyel, Jeffrey, Eric Hnath, Marc Storms, and Thomas Wohlfarth. 2014. "Towards an Integrative Structural Biology Approach: Combining Cryo-TEM, X-Ray Crystallography, and NMR." *Journal of Structural and Functional Genomics* 15 (3): 117–24. https://doi.org/10.1007/s10969-014-9179-9.

Li, Guibin, Haishan Yin, and Jeff Kuret. 2004. "Casein Kinase 1 Delta Phosphorylates Tau and Disrupts Its Binding to Microtubules." *Journal of Biological Chemistry* 279 (16): 15938–45. https://doi.org/10.1074/jbc.M314116200.

Li, M., X. Wang, M. K. Meintzer, T. Laessig, M. J. Birnbaum, and K. A. Heidenreich. 2000. "Cyclic AMP Promotes Neuronal Survival by Phosphorylation of Glycogen Synthase Kinase 3beta." *Molecular and Cellular Biology* 20 (24): 9356–63. https://doi.org/10.1128/mcb.20.24.9356-9363.2000.

Li, Xiaohua, and Richard S. Jope. 2010. "Is Glycogen Synthase Kinase-3 a Central Modulator in Mood Regulation." *Neuropsychopharmacology* 35 (11): 2143–54. https://doi.org/10.1038/npp.2010.105.

Li, Xiaohua, Kelley M Rosborough, Ari B Friedman, Wawa Zhu, and Kevin A Roth. 2007. "Regulation of Mouse Brain Glycogen Synthase Kinase-3 by Atypical Antipsychotics" 3: 7–19. https://doi.org/10.1017/S1461145706006547.

Li, Xiaohua, Wawa Zhu, Myoung-sun Roh, Ari B Friedman, Kelley Rosborough, and Richard S Jope. 2007. "In Vivo Regulation of Glycogen Synthase Kinase-3β (GSK3β) by Serotonergic Activity in Mouse Brain" 29 (8): 1426–31.

Liko, Idlir, Timothy M. Allison, Jonathan TS Hopper, and Carol V. Robinson. 2016. "Mass Spectrometry Guided Structural Biology." *Current Opinion in Structural Biology* 40: 136–44. https://doi.org/10.1016/j.sbi.2016.09.008.

Linke, Dirk. 2009. *Chapter 34 Detergents. An Overview*. *Methods in Enzymology*. 1st ed. Vol. 463. Elsevier Inc. https://doi.org/10.1016/S0076-6879(09)63034-2.

Liu, Dan, Robert A. Cole, and Peter R. Reeves. 1996. "An O-Antigen Processing Function for Wzx (RfbX): A Promising Candidate for O-Unit Flippase." *Journal of Bacteriology*.

Liu, Qingsong, Yogesh Sabnis, Zheng Zhao, Tinghu Zhang, Sara J Buhrlage, H Jones, and Nathanael S Gray. 2014. "Developing Irreversible Inhibitors of the Protein Kinase Cysteinome" 20 (2): 146–59. https://doi.org/10.1016/j.chembiol.2012.12.006.Developing.

Llorens-Martín, María, Jerónimo Jurado, Félix Hernández, and Jesús Ávila. 2014. "GSK-3β, a Pivotal Kinase in Alzheimer Disease." *Frontiers in Molecular Neuroscience* 7 (MAY): 1–11. https://doi.org/10.3389/fnmol.2014.00046.

Luirink, Joen, and Irmgard Sinning. 2004. "SRP-Mediated Protein Targeting: Structure and Function Revisited." *Biochimica et Biophysica Acta - Molecular Cell Research* 1694 (1-3 SPEC.ISS.): 17–35. https://doi.org/10.1016/j.bbamcr.2004.03.013.

Lyczak, Jeffrey B., Carolyn L. Cannon, and Gerald B. Pier. 2000. "Establishment of Pseudomonas Aeruginosa Infection: Lessons from a Versatile Opportunist." *Microbes and Infection* 2 (9): 1051–60. https://doi.org/10.1016/S1286-4579(00)01259-4.

Maldonado, Rita F., Isabel Sá-Correia, and Miguel A. Valvano. 2016. "Lipopolysaccharide Modification in Gram-Negative Bacteria during Chronic Infection." *FEMS Microbiology Reviews* 40 (4): 480–93. https://doi.org/10.1093/femsre/fuw007.

Malik, Adeel, and Shandar Ahmad. 2007. "Sequence and Structural Features of Carbohydrate Binding in Proteins and Assessment of Predictability Using a Neural Network." *BMC Structural Biology* 7. https://doi.org/10.1186/1472-6807-7-1.

Manning, G, D B Whyte, R Martinez, and T Hunter. 2002. “The Protein Kinase Complement of the Human Genome” 298 (December).

Marassi, Francesca M, and Stanley J Opella. 2008. “NMR Structural Studies of Membrane Proteins.” *Bone* 23 (1): 1–7. https://doi.org/10.1038/jid.2014.371.

Marolda, Cristina L., Jessica Vicarioli, and Miguel A. Valvano. 2004. “Wzx Proteins Involved in Biosynthesis of O Antigen Function in Association with the First Sugar of the O-Specific Lipopolysaccharide Subunit.” *Microbiology* 150 (12): 4095–4105. https://doi.org/10.1099/mic.0.27456-0.

Martin-Garcia, Jose M., Chelsie E. Conrad, Jesse Coe, Shatabdi Roy-Chowdhury, and Petra Fromme. 2016. “Serial Femtosecond Crystallography: A Revolution in Structural Biology.” *Archives of Biochemistry and Biophysics* 602: 32–47. https://doi.org/10.1016/j.abb.2016.03.036.

Martin, Michael, Kunal Rehani, Richard S Jope, and Suzanne M Michalek. 2011. “Toll-like Receptor—Mediated Cytokine Production Is Differentially Regulated by Glycogen Synthase Kinase 3” 46 (4): 564–74. https://doi.org/10.1016/j.cortex.2009.08.003.Predictive.

May, Janine M., David J. Sherman, Brent W. Simpson, Natividad Ruiz, and Daniel Kahne. 2015. “Lipopolysaccharide Transport to the Cell Surface: Periplasmic Transport and Assembly into the Outer Membrane.” *Philosophical Transactions of the Royal Society B: Biological Sciences* 370 (1679). https://doi.org/10.1098/rstb.2015.0027.

McGeer, P. L., and E. G. McGeer. 2002. “Inflammatory Processes in Amyotrophic Lateral Sclerosis.” *Muscle and Nerve* 26 (4): 459–70. https://doi.org/10.1002/mus.10191.

Menon, Anant K. 1995. “Flippases,” 355–60.

Meredith, Timothy C., Uwe Mamat, Zbigniew Kaczynski, Buko Lindner, Otto Holst, and Ronald W. Woodard. 2007. “Modification of Lipopolysaccharide with Colanic Acid (M-Antigen) Repeats in Escherichia Coli.” *Journal of Biological Chemistry* 282 (11): 7790–98. https://doi.org/10.1074/jbc.M611034200.

Mertens, Haydyn D.T., and Dmitri I. Svergun. 2010. “Structural Characterization of Proteins and Complexes Using Small-Angle X-Ray Solution Scattering.” *Journal of Structural Biology* 172 (1): 128–41. https://doi.org/10.1016/j.jsb.2010.06.012.

Miles, A. J., and B. A. Wallace. 2016. “Circular Dichroism Spectroscopy of Membrane Proteins.” *Chemical Society Reviews* 45 (18): 4859–72. https://doi.org/10.1039/c5cs00084j.

Miller-Gallacher, Jennifer L., Rony Nehmé, Tony Warne, Patricia C. Edwards, Gebhard F.X. Schertler, Andrew G.W. Leslie, and Christopher G. Tate. 2014. “The 2.1 Å Resolution Structure of Cyanopindolol-Bound B1-Adrenoceptor Identifies an Intramembrane Na+ Ion That Stabilises the Ligand-Free Receptor.” *PLoS ONE* 9 (3). https://doi.org/10.1371/journal.pone.0092727.

Miller, Jeffrey R. 2002. “The Wnts.” *Current Biology* 9 (1): 1–15. https://doi.org/10.1016/S0960-9822(99)80029-3.

Mitra, Alok K. 2019. “Visualization of Biological Macromolecules at Near-Atomic Resolution: Cryo-Electron Microscopy Comes of Age.” *Acta Crystallographica Section F: Structural Biology Communications* 75: 3–11. https://doi.org/10.1107/S2053230X18015133.

Modi, Vivek, Dunbrack Jr, Roland L. 2019. "Defining a new nomenclature for the structure of active and inactive kinases" *PNAS* Apr 2019, 116 (14) 6818-6827; DOI:10.1073/pnas.1814279116

Molinaro, Antonio, Otto Holst, Flaviana Di Lorenzo, Maire Callaghan, Alessandra Nurisso, Gerardino D’Errico, Alla Zamyatina, et al. 2015. “Chemistry of Lipid a: At the Heart of Innate Immunity.” *Chemistry - A European Journal* 21 (2): 500–519. https://doi.org/10.1002/chem.201403923.

Monné, Magnus, Guro Gafvelin, Robert Nilsson, and Gunnar von Heijne. 1999. “N-Tail Translocation in a Eukaryotic Polytopic Membrane Protein. Synergy between Neighboring Transmembrane Segments.” *European Journal of Biochemistry* 263 (1): 264–69. https://doi.org/10.1046/j.1432-1327.1999.00498.x.

Monné, Magnus, Tara Hessa, Laura Thissen, and Gunnar Von Heijne. 2005. “Competition between Neighboring Topogenic Signals during Membrane Protein Insertion into the ER.” *FEBS Journal* 272 (1): 28–36. https://doi.org/10.1111/j.1432-1033.2004.04394.x.

Monod, Jacques, Jean Pierre Changeux, and François Jacob. 1963. “Allosteric Proteins and Cellular Control Systems.” *Journal of Molecular Biology* 6 (4): 306–29. https://doi.org/10.1016/S0022-2836(63)80091-1.

Moon, C. Preston, and Karen G. Fleming. 2013. “Using Tryptophan Fluorescence to Measure the Stability of Membrane Proteins Folded in Liposomes” 7256: 189–211. https://doi.org/10.1016/B978-0-12-381268-1.00018-5.Using.

Moraes, Isabel, Gwyndaf Evans, Juan Sanchez-Weatherby, Simon Newstead, and Patrick D.Shaw Stewart. 2014. “Membrane Protein Structure Determination - The next Generation.” *Biochimica et Biophysica Acta - Biomembranes* 1838 (1 PARTA): 78–87. https://doi.org/10.1016/j.bbamem.2013.07.010.

Morales-García, J. A., C. Susín, S. Alonso-Gil, D. I. Pérez, V. Palomo, C. Pérez, S. Conde, et al. 2013. “Glycogen Synthase Kinase-3 Inhibitors as Potent Therapeutic Agents for the Treatment of Parkinson Disease.” *ACS Chemical Neuroscience* 4 (2): 350–60. https://doi.org/10.1021/cn300182g.

Moujalled, Diane, Janine L. James, Sarah J. Parker, Grace E. Lidgerwood, Clare Duncan, Jodi Meyerowitz, Takashi Nonaka, et al. 2013. “Kinase Inhibitor Screening Identifies Cyclin-Dependent Kinases and Glycogen Synthase Kinase 3 as Potential Modulators of TDP-43 Cytosolic Accumulation during Cell Stress.” *PLoS ONE* 8 (6). https://doi.org/10.1371/journal.pone.0067433.

Mukai, Fumiko, Koichi Ishiguro, Yumiko Sano, and Shinobu C. Fujita. 2002. “Aternative Splicing Isoform of Tau Protein Kinase I/Glycogen Synthase Kinase 3β.” *Journal of Neurochemistry* 81 (5): 1073–83. https://doi.org/10.1046/j.1471-4159.2002.00918.x.

Müller, Frank D., Christian W. Schink, Egbert Hoiczyk, Emöke Cserti, and Penelope I. Higgs. 2012. “Spore Formation in Myxococcus Xanthus Is Tied to Cytoskeleton Functions and Polysaccharide Spore Coat Deposition.” *Molecular Microbiology* 83 (3): 486–505. https://doi.org/10.1111/j.1365-2958.2011.07944.x.

Mullineaux, Conrad W., Anja Nenninger, Nicola Ray, and Colin Robinson. 2006. “Diffusion of Green Fluorescent Protein in Three Cell Environments in Escherichia Coli.” *Journal of Bacteriology* 188 (10): 3442–48. https://doi.org/10.1128/JB.188.10.3442-3448.2006.

Murray, Gerald L., Stephen R. Attridge, and Renato Morona. 2006. “Altering the Length of the Lipopolysaccharide O Antigen Has an Impact on the Interaction of Salmonella Enterica Serovar Typhimurium with Macrophages and Complement.” *Journal of Bacteriology* 188 (7): 2735–39. https://doi.org/10.1128/JB.188.7.2735-2739.2006.

Neill, Jim O ’. 2014. “Antimicrobial Resistance: Tackling a Crisis for the Health and Wealth of Nations The Review on Antimicrobial Resistance Chaired,” no. December.

Neuhaus, Francis C, and James Baddiley. 2003. “A Continuum of Anionic Charge: Structures and Functions Of.” *Microbiology* 67 (4): 686–723. https://doi.org/10.1128/MMBR.67.4.686.

Nikaido, Hiroshi. 2003. “Outer Membrane. In: Neidhardt F C, Curtiss III R, Ingraham J L, Lin E C C, Low K B Jr, Magasanik B, Reznikoff W S, Riley M, Schaechter M, Umbarger H E, Editors. Escherichia Coli and Salmonella: Cellular and Molecular Biology. 2nd Ed. Washington, D.C: Amer.” *Microbiology and Molecular Biology Reviews* 67 (4): 29–47. https://doi.org/10.1128/MMBR.67.4.593.

Noble, Martin E M, Jane A Endicott, and Louise N Johnson. 2004. “Protein Kinase Inhibitors : Insights into Drug Design from Structure” 303 (March): 1800–1806.

Nogales, Eva. 2016. “The Development of Cryo-EM into a Mainstream Structural Biology Technique” 13 (1): 24–27.

Noh, M-Y, S-H Koh, Y Kim, H. K. Kim, G. W. Cho, and S. H. Kim. 2009. “Neuroprotective Effect of Donepezil through Inhibition of GSK-3 Activity in Amyloid-B-Induced Neuronal Cell

Death," 1116–25. https://doi.org/10.1111/j.1471-4159.2008.05837.x.
Obritsch, Marilee D., Douglas N. Fish, Robert MacLaren, and Rose Jung. 2005. "Nosocomial Infections Due to Multidrug-Resistant Pseudomonas Aeruginosa: Epidemiology and Treatment Options." *Pharmacotherapy* 25 (10 I): 1353–64. https://doi.org/10.1592/phco.2005.25.10.1353.
Ohi, Melanie, Ying Li, Yifan Cheng, and Thomas Walz. 2004. "Negative Staining and Image Classification - Powerful Tools in Modern Electron Microscopy." *Biological Procedures Online* 6 (1): 23–34. https://doi.org/10.1251/bpo70.
Okochi, Masayasu, Jochen Walter, Akihiko Koyama, Shigeo Nakajo, Minami Baba, Takeshi Iwatsubo, Laurent Meijer, Philipp J. Kahle, and Christian Haass. 2000. "Constitutive Phosphorylation of the Parkinson's Disease Associated α- Synuclein." *Journal of Biological Chemistry* 275 (1): 390–97. https://doi.org/10.1074/jbc.275.1.390.
Oladepo, Sulayman A., Kan Xiong, Zhenmin Hong, Sanford A. Asher, Joseph Handen, and Igor K. Lednev. 2012. "UV Resonance Raman Investigations of Peptide and Protein Structure and Dynamics." *Chemical Reviews* 112 (5): 2604–28. https://doi.org/10.1021/cr200198a.
Oren, Moshe. 2003. "Decision Making by P53: Life, Death and Cancer." *Cell Death and Differentiation* 10 (4): 431–42. https://doi.org/10.1038/sj.cdd.4401183.
Overington, John P., Bissan Al-Lazikani, and Andrew L. Hopkins. 2006. "How Many Drug Targets Are There?" *Nature Reviews Drug Discovery* 5 (12): 993–96. https://doi.org/10.1038/nrd2199.
Pan, Y., C. B. Bai, A. L. Joyner, and B. Wang. 2006. "Sonic Hedgehog Signaling Regulates Gli2 Transcriptional Activity by Suppressing Its Processing and Degradation." *Molecular and Cellular Biology* 26 (9): 3365–77. https://doi.org/10.1128/mcb.26.9.3365-3377.2006.
Pandey, Mukesh K, and Timothy R Degrado. 2016. "Glycogen Synthase Kinase-3 (GSK-3)– Targeted Therapy and Imaging" 6 (4). https://doi.org/10.7150/thno.14334.
Pantoliano, MW, E.C. Petrella, J.D. Kwasnoski, V.S. Lobanov, J Myslik, E Graf, T Carver, et al. 2001. "High-Density Miniaturized Thermal Shift Assays as a General Strategy for Drug Discovery."
Park, Eunyong, and Tom A. Rapoport. 2012. "Mechanisms of Sec61/SecY-Mediated Protein Translocation Across Membranes." *Annual Review of Biophysics* 41 (1): 21–40. https://doi.org/10.1146/annurev-biophys-050511-102312.
Park, Kyong Su, Jaewook Lee, Su Chul Jang, Sae Rom Kim, Myoung Ho Jang, Jan Lötvall, Yoon Keun Kim, and Yong Song Gho. 2013. "Pulmonary Inflammation Induced by Bacteria-Free Outer Membrane Vesicles from Pseudomonas Aeruginosa." *American Journal of Respiratory Cell and Molecular Biology* 49 (4): 637–45. https://doi.org/10.1165/rcmb.2012-0370OC.
Parker, M. W. 2003. "Protein Structure from X-Ray Diffraction." *Journal of Biological Physics* 29 (4): 341–62. https://doi.org/10.1023/A:1027310719146.
Pelikan, Martin, Greg L. Hura, and Michal Hammel. 2009. "Structure and Flexibility within Proteins as Identified through Small Angle X-Ray Scattering." *General Physiology and Biophysics* 28 (2): 174–89. https://doi.org/10.4149/gpb_2009_02_174.
Perez, Ruth G, Jack C Waymire, Eva Lin, Jen J Liu, Fengli Guo, and Michael J Zigmond. 2002. "A Role for ⎵ -Synuclein in the Regulation of Dopamine Biosynthesis" 22 (8): 3090–99.
Petit-Paitel*, Agnes, Frederic Brau, Julie Cazareth, and Joelle Chabry. 2009. "Involvment of Cytosolic and Mitochondrial GSK-3 b in Mitochondrial Dysfunction and Neuronal Cell Death of MPTP / MPP + -Treated Neurons" 4 (5). https://doi.org/10.1371/journal.pone.0005491.
Pluquet, O., L.-K. Qu, D. Baltzis, and A. E. Koromilas. 2005. "Endoplasmic Reticulum Stress Accelerates P53 Degradation by the Cooperative Actions of Hdm2 and Glycogen Synthase Kinase 3 ." *Molecular and Cellular Biology* 25 (21): 9392–9405. https://doi.org/10.1128/mcb.25.21.9392-9405.2005.
Polakis, Paul. 2000. "Wnt Signaling and Cancer." *Kaibogaku Zasshi. Journal of Anatomy* 84 (4): 111–12. https://doi.org/10.1101/gad.14.15.1837.
Prati, Federica, Angela De Simone, Paola Bisignano, Andrea Armirotti, Maria Summa, Daniela

Pizzirani, Rita Scarpelli, et al. 2015. “Multitarget Drug Discovery for Alzheimer’s Disease: Triazinones as BACE-1 and GSK-3β Inhibitors.” *Angewandte Chemie - International Edition* 54 (5): 1578–82. https://doi.org/10.1002/anie.201410456.

Price, Mary Ann, and Daniel Kalderon. 2002. “Proteolysis of the Hedgehog Signaling Effector Cubitus Interruptus Requires Phosphorylation by Glycogen Synthase Kinase 3 and Casein Kinase 1” 108: 823–35.

Privé, Gilbert G. 2007. “Detergents for the Stabilization and Crystallization of Membrane Proteins.” *Methods* 41 (4): 388–97. https://doi.org/10.1016/j.ymeth.2007.01.007.

Raetz, Christian R. H., and Chris Whitfield. 2002. “Lipopolysaccharide Endotoxins.” *Annual Review of Biochemistry* 71 (1): 635–700. https://doi.org/10.1146/annurev.biochem.71.110601.135414.

Raetz, Christian R.H., C. Michael Reynolds, M. Stephen Trent, and Russell E. Bishop. 2007. “Lipid A Modification Systems in Gram-Negative Bacteria.” *Annual Review of Biochemistry* 76 (1): 295–329. https://doi.org/10.1146/annurev.biochem.76.010307.145803.

Rahman, Moazur, Fouzia Ismat, Michael J.J. McPherson, and Stephen A. Baldwin. 2007. “Topology-Informed Strategies for the Overexpression and Purification of Membrane Proteins.” *Molecular Membrane Biology* 24 (5–6): 407–18. https://doi.org/10.1080/09687860701243998.

Ramesh, Geeta, Andrew G. Maclean, and Mario T. Philipp. 2013. “Cytokines and Chemokines at the Crossroads of Neuroinflammation, Neurodegeneration, and Neuropathic Pain.” *Mediators of Inflammation* 2013. https://doi.org/10.1155/2013/480739.

Raymond, Christopher K., Elizabeth H. Sims, Arnold Kas, David H. Spencer, Tanya V. Kutyavin, Richard G. Ivey, Yang Zhou, Rajinder Kaul, James B. Clendenning, and Maynard V. Olson. 2002. “Genetic Variation at the O-Antigen Biosynthetic Locus in Pseudomonas Aeruginosa.” *Journal of Bacteriology* 184 (13): 3614–22. https://doi.org/10.1128/JB.184.13.3614-3622.2002.

Redenti, S., I. Marcovich, T. De Vita, C. Pérez, R. De Zorzi, N. Demitri, D.I. Perez, et al. 2019. “A Triazolotriazine-Based Dual GSK-3β/CK-1δ Ligand as a Potential Neuroprotective Agent Presenting Two Different Mechanisms of Enzymatic Inhibition.” *ChemMedChem* 14 (3). https://doi.org/10.1002/cmdc.201800778.

Reinhard, Linda, Hubert Mayerhofer, Arie Geerlof, Jochen Mueller-Dieckmann, and Manfred S. Weiss. 2013. “Optimization of Protein Buffer Cocktails Using Thermofluor.” *Acta Crystallographica Section F: Structural Biology and Crystallization Communications* 69 (2): 209–14. https://doi.org/10.1107/S1744309112051858.

Reyrat, Jean-marc, Vladimir Pelicic, Brigitte Gicquel, and Rino Rappuoli. 1998. “Counterselectable Markers: Untapped Tools for Bacterial Genetics and Pathogenesis” 66 (9): 4011–17.

Rick, P. D., S. Wolski, K. Barr, S. Ward, and L. Ramsay-Sharer. 1988. “Accumulation of a Lipid-Linked Intermediate Involved in Enterobacterial Common Antigen Synthesis in Salmonella Typhimurium Mutants Lacking DTDP-Glucose Pyrophosphorylase.” *Journal of Bacteriology* 170 (9): 4008–14. https://doi.org/10.1128/jb.170.9.4008-4014.1988.

Rick, Paul D., Gail L. Hubbard, Masahiro Kitaoka, Hidemi Nagaki, Takeshi Kinoshita, Susan Dowd, Virgil Simplaceanu, and Chien Ho. 1998. “Characterization of the Lipid-Carrier Involved in the Synthesis of Enterobacterial Common Antigen (ECA) and Identification of a Novel Phosphoglyceride in a Mutant of Salmonella Typhimurium Defective in ECA Synthesis.” *Glycobiology* 8 (6): 557–67. https://doi.org/10.1093/glycob/8.6.557.

Ricklin, Daniel, George Hajishengallis, Kun Yang, and John D. Lambris. 2010. “Complement: A Key System for Immune Surveillance and Homeostasis.” *Nature Immunology* 11 (9): 785–97. https://doi.org/10.1038/ni.1923.

Robbins, P. W., D. Bray, M. Dankert, and A. Wright. 1967. “Direction of Chain Growth in Polysaccharide Synthesis.” *Science* 158 (3808): 1536–42. https://doi.org/10.1126/science.158.3808.1536.

Rocchetta, Heather L., and Joseph S. Lam. 1997. “Identification and Functional Characterization of an ABC Transport System Involved in Polysaccharide Export of A-Band Lipopolysaccharide in Pseudomonas Aeruginosa.” *Journal of Bacteriology* 179 (15): 4713–24. https://doi.org/10.1128/jb.179.15.4713-4724.1997.

Rohrer, Susanne, and Brigitte Berger-Bächi. 2003. “Application of a Bacterial Two-Hybrid System for the Analysis of Protein-Protein Interactions between FemABX Family Proteins.” *Microbiology* 149 (10): 2733–38. https://doi.org/10.1099/mic.0.26315-0.

Roskoski, Robert. 2014a. “ErbB/HER Protein-Tyrosine Kinases: Structures and Small Molecule Inhibitors.” *Pharmacological Research* 87: 42–59. https://doi.org/10.1016/j.phrs.2014.06.001.

Roskoski, Robert. 2014b. “The ErbB/HER Family of Protein-Tyrosine Kinases and Cancer.” *Pharmacological Research* 79: 34–74. https://doi.org/10.1016/j.phrs.2013.11.002.

Roskoski, Robert. 2016. “Classification of Small Molecule Protein Kinase Inhibitors Based upon the Structures of Their Drug-Enzyme Complexes.” *Pharmacological Research* 103: 26–48. https://doi.org/10.1016/j.phrs.2015.10.021.

Roskoski, Robert Jr. 2015. “A Historical Overview of Protein Kinases and Their Targeted Small Molecule Inhibitors.” *Pharmacological Research* 100: 1–23. https://doi.org/10.1016/j.phrs.2015.07.010.

Rowles, Joie, Clive Slaughter, Carolyn Moomaw, Joan Hsu, and Melanie H. Cobb. 1991. “Purification of Casein Kinase I and Isolation of CDNAs Encoding Multiple Casein Kinase I-like Enzymes.” *Proceedings of the National Academy of Sciences of the United States of America* 88 (21): 9548–52. https://doi.org/10.1073/pnas.88.21.9548.

Ruan, Xiang, David E. Loyola, Cristina L. Marolda, José M. Perez-Donoso, and Miguel A. Valvano. 2012. “The WaaL O-Antigen Lipopolysaccharide Ligase Has Features in Common with Metal Ion-Independent Inverting Glycosyltransferases.” *Glycobiology* 22 (2): 288–99. https://doi.org/10.1093/glycob/cwr150.

Ryback, Ralph. 2001. “Bioelectrical Modulators and the Cell Membrane in Psychiatric Medicine” 35 (4): 5–45.

Rygula, A., K. Majzner, K. M. Marzec, A. Kaczor, M. Pilarczyk, and M. Baranska. 2013. “Raman Spectroscopy of Proteins: A Review.” *Journal of Raman Spectroscopy* 44 (8): 1061–76. https://doi.org/10.1002/jrs.4335.

Sacha, Paweł, Piotr Wieczorek, Tomasz Hauschild, Marcin Zórawski, Dorota Olszańska, and Elzbieta Tryniszewska. 2008. “Metallo-β-Lactamases of Pseudomonas Aeruginosa - A Novel Mechanism Resistance to β-Lactam Antibiotics.” *Folia Histochemica et Cytobiologica* 46 (2): 137–42. https://doi.org/10.2478/v10042-008-0020-9.

Sadovskaya, Irina, Jean Robert Brisson, Pierre Thibault, James C. Richards, Joseph S. Lam, and Eleonora Altman. 2000. “Structural Characterization of the Outer Core and the O-Chain Linkage Region of Lipopolysaccharide from Pseudomonas Aeruginosa Serotype O5.” *European Journal of Biochemistry* 267 (6): 1640–50. https://doi.org/10.1046/j.1432-1327.2000.01156.x.

Saldías, M. Soledad, Ximena Ortega, and Miguel A. Valvano. 2009. “Burkholderia Cenocepacia O Antigen Lipopolysaccharide Prevents Phagocytosis by Macrophages and Adhesion to Epithelial Cells.” *Journal of Medical Microbiology* 58 (12): 1542–48. https://doi.org/10.1099/jmm.0.013235-0.

Sankaran, Krishnan, and Henry C Wus. 1994. “Lipid Modification of Bacterial Prolipoprotein.” *The Journal of Biological Chemistry* 269 (31): 19701–6. http://www.jbc.org/content/269/31/19701.full.pdf.

Sarno, Patrizia De, Gautam N. Bijur, Anna A. Zmijewska, Xiaohua Li, and Richard S. Jope. 2006. “In Vivo Regulation of GSK3 Phosphorylation by Cholinergic and NMDA Receptors Patrizia” 27 (3): 413–22.

Sarti, Edoardo, Antoniya A. Aleksandrova, Srujan K. Ganta, Amarendra S. Yavatkar, and Lucy R. Forrest. 2019. “EncoMPASS: An Online Database for Analyzing Structure and Symmetry in

Membrane Proteins." *Nucleic Acids Research* 47 (D1): D315–21. https://doi.org/10.1093/nar/gky952.

Sato, H., K. Okinaga, and H. Saito. 1988. "Role of Pili in the Pathogenesis of Pseudomonas Aeruginosa Burn Infection of Pseudomonas Aeruginosa Indicates That the Presence of Pili Enhances the Virulence of the Organisms in Experimental P . Aeruginosa Was at Least 105 Times Higher than Those Inocula" 32 (2): 131–39.

Sauvage, Eric, Ailsa J. Powell, Jason Heilemann, Helen R. Josephine, Paulette Charlier, Christopher Davies, and R. F. Pratt. 2008. "Crystal Structures of Complexes of Bacterial Dd-Peptidases with Peptidoglycan-Mimetic Ligands: The Substrate Specificity Puzzle." *Journal of Molecular Biology* 381 (2): 383–93. https://doi.org/10.1016/j.jmb.2008.06.012.

Scales, Suzie J., and Frederic J. de Sauvage. 2009. "Mechanisms of Hedgehog Pathway Activation in Cancer and Implications for Therapy." *Trends in Pharmacological Sciences* 30 (6): 303–12. https://doi.org/10.1016/j.tips.2009.03.007.

Schroeder, Torsten H., Nina Reiniger, Gloria Meluleni, Martha Grout, Fadie T. Coleman, and Gerald B. Pier. 2001. " Transgenic Cystic Fibrosis Mice Exhibit Reduced Early Clearance of Pseudomonas Aeruginosa from the Respiratory Tract ." *The Journal of Immunology* 166 (12): 7410–18. https://doi.org/10.4049/jimmunol.166.12.7410.

Schwab, Claudia, Anthony J. Demaggio, Nupur Ghoshal, Lester I. Binder, Jeff Kuret, and Patrick L. McGeer. 2000. "Casein Kinase 1 Delta Is Associated with Pathological Accumulation of Tau in Several Neurodegenerative Diseases." *Neurobiology of Aging* 21 (4): 503–10. https://doi.org/10.1016/S0197-4580(00)00110-X.

Schwartz, Phillip A, and Brion W Murray. 2011. "Protein Kinase Biochemistry and Drug Discovery." *Bioorganic Chemistry* 39: 192–210. https://doi.org/10.1016/j.bioorg.2011.07.004.

Seddon, Annela M., Paul Curnow, and Paula J. Booth. 2004. "Membrane Proteins, Lipids and Detergents: Not Just a Soap Opera." *Biochimica et Biophysica Acta - Biomembranes* 1666 (1–2): 105–17. https://doi.org/10.1016/j.bbamem.2004.04.011.

Ser, Teodoro Del, Klaus C. Steinwachs, Hermann J. Gertz, María V. Andrés, Belén Gómez-Carrillo, Migue Medina, Joan A. Vericat, Pilar Redondo, David Fleet, and Teresa León. 2013. "Treatment of Alzheimer's Disease with the GSK-3 Inhibitor Tideglusib: A Pilot Study." *Journal of Alzheimer's Disease* 33 (1): 205–15. https://doi.org/10.3233/JAD-2012-120805.

Serenó, L, M Coma, M Rodríguez, P Sánchez-ferrer, M B Sánchez, I Gich, J M Agulló, and M Pérez. 2009. "Neurobiology of Disease A Novel GSK-3 β Inhibitor Reduces Alzheimer ' s Pathology and Rescues Neuronal Loss in Vivo." *Neurobiology of Disease* 35 (3): 359–67. https://doi.org/10.1016/j.nbd.2009.05.025.

Shi, Dan, Brent L. Nannenga, Matthew G. Iadanza, and Tamir Gonen. 2013. "Three-Dimensional Electron Crystallography of Protein Microcrystals." *ELife* 2013 (2): 1–17. https://doi.org/10.7554/eLife.01345.001.

Silhavy, Thomas J., Daniel Kahne, and Suzanne Walker. 2010. "The Bacterial Cell Envelope." *Cold Spring Harbor Perspectives in Biology*. https://doi.org/10.1101/cshperspect.a000414.

Silva, Tiago, Joana Reis, José Teixeira, and Fernanda Borges. 2014. "Alzheimer ' s Disease , Enzyme Targets and Drug Discovery Struggles : From Natural Products to Drug Prototypes." *Ageing Research Reviews* 15: 116–45. https://doi.org/10.1016/j.arr.2014.03.008.

Simpson, Brent W., Janine M. May, David J. Sherman, Daniel Kahne, and Natividad Ruiz. 2015. "Lipopolysaccharide Transport to the Cell Surface: Periplasmic Transport and Assembly into the Outer Membrane." *Philosophical Transactions of the Royal Society B: Biological Sciences* 370 (1679). https://doi.org/10.1098/rstb.2015.0029.

Singh, Toolsee J., Niloufar Haque, Inge Grundke-Iqbal, and Khalid Iqbal. 1995. "Rapid Alzheimer-like Phosphorylation of Tau by the Synergistic Actions of Non-Proline-Dependent Protein Kinases and GSK-3." *FEBS Letters* 358 (3): 267–72. https://doi.org/10.1016/0014-5793(94)01445-7.

Smith, P. K., R. I. Krohn, G. T. Hermanson, A. K. Mallia, F. H. Gartner, M. D. Provenzano, E. K.

Fujimoto, N. M. Goeke, B. J. Olson, and D. C. Klenk. 1985. “Measurement of Protein Using Bicinchoninic Acid.” *Analytical Biochemistry* 150 (1): 76–85. https://doi.org/10.1016/0003-2697(85)90442-7.

Smyth, Lynette A., and Ian Collins. 2009. “Measuring and Interpreting the Selectivity of Protein Kinase Inhibitors.” *Journal of Chemical Biology* 2 (3): 131–51. https://doi.org/10.1007/s12154-009-0023-9.

Snijder, H. J., I. Ubarretxena-Belandia, M. Blaauw, K. H. Kalk, H. M. Verheij, M. R. Egmond, N. Dekker, and B. W. Dijkstra. 1999. “Structural Evidence for Dimerization-Regulated Activation of an Integral Membrane Phospholipase.” *Nature* 401 (6754): 717–21. https://doi.org/10.1038/44890.

Soldo, Blazenka, Vladimir Lazarevic, Marco Pagni, and Dimitri Karamata. 1999. “Teichuronic Acid Operon of Bacillus Subtilis 168.” *Molecular Microbiology* 31 (3): 795–805. https://doi.org/10.1046/j.1365-2958.1999.01218.x.

Song, Ling, Patrizia De Sarno, and Richard S Jope. 2002. “Central Role of Glycogen Synthase Kinase-3 ␣ in Endoplasmic Reticulum Stress-Induced Caspase-3 Activation *” 277 (47): 44701–8. https://doi.org/10.1074/jbc.M206047200.

Stacey, Glyn, and John Davis. 2007. *Medicines from Animal Cell Culture*. *Medicines from Animal Cell Culture*. https://doi.org/10.1002/9780470723791.

Steichen, Jon M., Ganesh H. Iyer, Sheng Li, Adrian Saldanha, Michael S. Deal, Virgil L. Woods, and Susan S. Taylor. 2010. “Global Consequences of Activation Loop Phosphorylation on Protein Kinase A.” *Journal of Biological Chemistry* 285 (6): 3825–32. https://doi.org/10.1074/jbc.M109.061820.

Steinbrecher, Kris A, Willie Wilson, C Patricia, Nf- B-dependent Transcription, Willie Wilson Iii, Patricia C Cogswell, and Albert S Baldwin. 2005. “Glycogen Synthase Kinase 3 { Beta } Functions To Specify Gene-Specific , Transcription Glycogen Synthase Kinase 3 ␣ Functions To Specify Gene-Specific ,” 25 (19): 8444–55. https://doi.org/10.1128/MCB.25.19.8444.

Streit, Wolfgang J., Robert E. Mrak, and W. Sue T Griffin. 2004. “Microglia and Neuroinflammation: A Pathological Perspective.” *Journal of Neuroinflammation* 1: 1–4. https://doi.org/10.1186/1742-2094-1-14.

Sundara, Siva, Kumar Durairajan, Liang-feng Liu, Jia-hong Lu, Lei-lei Chen, Qiuju Yuan, Sookja K Chung, et al. 2012. “Berberine Ameliorates ␣ -Amyloid Pathology , Gliosis , and Cognitive Impairment in an Alzheimer ’ s Disease Transgenic Mouse Model” 33: 2903–19. https://doi.org/10.1016/j.neurobiolaging.2012.02.016.

Tajes, Marta, Javier Gutierrez-cuesta, Jaume Folch, Isidre Ferrer, Beatriz Caballero, Mark A Smith, Gemma Casadesus, and Antoni Camins. 2008. “Lithium Treatment Decreases Activities of Tau Kinases in a Murine Model of Senescence” 67 (6): 612–23.

Tan, Sandra, Tong Tan Hwee, and Maxey C.M. Chung. 2008. “Membrane Proteins and Membrane Proteomics.” *Proteomics* 8 (19): 3924–32. https://doi.org/10.1002/pmic.200800597.

Tayeb, Haythum O, Hyun Duk, Bruce H Price, and Frank I Tarazi. 2012. “Pharmacology & Therapeutics Pharmacotherapies for Alzheimer ’ s Disease : Beyond Cholinesterase Inhibitors.” *Pharmacology and Therapeutics* 134 (1): 8–25. https://doi.org/10.1016/j.pharmthera.2011.12.002.

Taylor, Susan S, and Alexandr P Kornev. 2011. “Protein Kinases : Evolution of Dynamic Regulatory Proteins” 36 (2). https://doi.org/10.1016/j.tibs.2010.09.006.

Thorsen, Thor Seneca, Rachel Matt, William I Weis, Brian Kobilka, Cellular Physiology, Campus Drive, Campus Drive, and Cellular Physiology. 2014. “Modified T4 Lysozyme Fusion Proteins Facilitate G Protein- Coupled Receptor Crystallogenesis” 22 (11): 1657–64. https://doi.org/10.1016/j.str.2014.08.022.Modified.

Toh, Evelyn, Harry D. Kurtz, and Yves V. Brun. 2008. “Characterization of the Caulobacter Crescentus Holdfast Polysaccharide Biosynthesis Pathway Reveals Significant Redundancy in the Initiating Glycosyltransferase and Polymerase Steps.” *Journal of Bacteriology* 190 (21):

7219–31. https://doi.org/10.1128/JB.01003-08.
Tolman, J. R., J. M. Flanagan, M. A. Kennedy, and J. H. Prestegard. 1998. “Nuclear Magnetic Dipole Interactions in Field-Oriented Proteins: Information for Structure Determination in Solution.” *Chemtracts* 11 (12): 918–22.
Traxler, Peter, and Pascal Furet. 1999. “Strategies toward the Design of Novel and Selective Protein Tyrosine Kinase Inhibitors” 82 (98): 195–206.
Tuma, Roman. 2005. “Raman Spectroscopy of Proteins: From Peptides to Large Assemblies.” *Journal of Raman Spectroscopy* 36 (4): 307–19. https://doi.org/10.1002/jrs.1323.
Turner, R Scott, Ronald G Thomas, Suzanne Craft, Christopher H Van Dyck, Jacobo Mintzer, Brigid A Reynolds, James B Brewer, Robert A Rissman, and Paul S Aisen. 2015. “Placebo-Controlled Trial of Resveratrol for Alzheimer Disease” 0: 1383–91.
Typas, Athanasios, Manuel Banzhaf, Carol A. Gross, and Waldemar Vollmer. 2017. “From the Regulation of Peptidoglycan Synthesis to Bacterial Growth and Morphology.” *Physiology & Behavior* 176 (10): 139–48. https://doi.org/10.1016/j.physbeh.2017.03.040.
Üstün-Aytekin, Özlem, Ismet Deliloğlu Gürhan, Kayoko Ohura, Teruko Imai, and Gaye Öngen. 2014. “Monitoring of the Effects of Transfection with Baculovirus on Sf9 Cell Line and Expression of Human Dipeptidyl Peptidase IV.” *Cytotechnology* 66 (1): 159–68. https://doi.org/10.1007/s10616-013-9549-3.
Vagin, Alexei A., and Michail N. Isupov. 2001. “Spherically Averaged Phased Translation Function and Its Application to the Search for Molecules and Fragments in Electron-Density Maps.” *Acta Crystallographica - Section D Biological Crystallography* 57 (10): 1451–56. https://doi.org/10.1107/S0907444901012409.
Vandeputte-Rutten, Lucy, R. Arjen Kramer, Jan Kroon, Niek Dekker, Maarten R. Egmond, and Piet Gros. 2001. “Crystal Structure of the Outer Membrane Protease Ompt from Escherichia Coli Suggests a Novel Catalytic Site.” *EMBO Journal* 20 (18): 5033–39. https://doi.org/10.1093/emboj/20.18.5033.
Venyaminov, S. Yu, I. A. BaikalovI, Z. M. Shen, C.S.C. Wu, and J.T. Yang. 1993. “Circular Dichroic Analysis of Denatured Proteins in the Reference Set.”
Vollmer, Waldemar, Didier Blanot, and Miguel A. De Pedro. 2008. “Peptidoglycan Structure and Architecture.” *FEMS Microbiology Reviews* 32 (2): 149–67. https://doi.org/10.1111/j.1574-6976.2007.00094.x.
Wagner, Samuel, Mirjam M. Klepsch, Susan Schlegel, Ansgar Appel, Roger Draheim, Michael Tarry, Martin Högbom, et al. 2008. “Tuning Escherichia Coli for Membrane Protein Overexpression.” *Proceedings of the National Academy of Sciences of the United States of America* 105 (38): 14371–76. https://doi.org/10.1073/pnas.0804090105.
Wallin, Erik, and Gunnar Von Heijne. 1998. “Genome-Wide Analysis of Integral Membrane Proteins from Eubacterial, Archaean, and Eukaryotic Organisms.” *Protein Science* 7 (4): 1029–38. https://doi.org/10.1002/pro.5560070420.
Walsh, Christopher. 2000. “Molecular Mechanisms That Confer Antibacterial Drug Resistance.” *Nature* 406 (6797): 775–81. https://doi.org/10.1038/35021219.
Walsh, Nathan P., Benjamin M. Alba, Baundauna Bose, Carol A. Gross, and Robert T. Sauer. 2003. “OMP Peptide Signals Initiate the Envelope-Stress Response by Activating DegS Protease via Relief of Inhibition Mediated by Its PDZ Domain.” *Cell* 113 (1): 61–71. https://doi.org/10.1016/S0092-8674(03)00203-4.
Wang, Baolin, and Yanyun Li. 2006. “Evidence for the Direct Involvement of BTrCP in Gli3 Protein Processing.” *Proceedings of the National Academy of Sciences of the United States of America* 103 (1): 33–38. https://doi.org/10.1073/pnas.0509927103.
Wang, Q. May, Carol J. Fiol, Anna A. DePaoli-Roach, and Peter J. Roach. 1994. “Glycogen Synthase Kinase-3beta Is a Dual Specificity Kinase Differentially Regulated by Tyrosine and Serine/Threonine Phosphorylation.” *Journal of Biological Chemistry* 269 (20): 14566–74.
Wang, Xiaolei, Fan Yang, and Susanne B. von Bodman. 2012. “The Genetic and Structural Basis of

Two Distinct Terminal Side Branch Residues in Stewartan and Amylovoran Exopolysaccharides and Their Potential Role in Host Adaptation." *Molecular Microbiology* 83 (1): 195–207. https://doi.org/10.1111/j.1365-2958.2011.07926.x.

Watcharasit, Piyajit, Gautam N. Bijur, Ling Song, Jianhui Zhu, Xinbin Chen, and Richard S. Jope. 2003. "Glycogen Synthase Kinase-3β (GSK3β) Binds to and Promotes the Actions of P53." *Bone* 23 (1): 1–7. https://doi.org/10.1038/jid.2014.371.

Watcharasit, Piyajit, Gautam N. Bijur, Jaroslaw W. Zmijewski, Ling Song, Anna Zmijewska, Xinbin Chen, Gail V.W. Johnson, and Richard S. Jope. 2002. "Direct, Activating Interaction between Glycogen Synthase Kinase-3β and P53 after DNA Damage." *Proceedings of the National Academy of Sciences of the United States of America* 99 (12): 7951–55. https://doi.org/10.1073/pnas.122062299.

West, Nicholas P., Philippe Sansonetti, Joëlle Mounier, Rachel M. Exley, Claude Parsot, Stéphanie Guadagnini, Marie Christine Prévost, et al. 2005. "Optimization of Virulence Functions through Glucosylation of Shigella LPS." *Science* 307 (5713): 1313–17. https://doi.org/10.1126/science.1108472.

Westheimer, F H. 1987. "Nature Chose Phosphates The Role of Phosphates The Importance of Being Ionized." *Science (New York, N.Y.)* 235 (1): 1173–78.

Whitfield, C. 1995. "Biosynthesis of Lipopolysaccharide O Antigens." *Trends in Microbiology* 3 (5): 178–85. https://doi.org/10.1016/S0966-842X(00)88917-9.

Whitfield, Chris. 2006. " Biosynthesis and Assembly of Capsular Polysaccharides in Escherichia Coli ." *Annual Review of Biochemistry* 75 (1): 39–68. https://doi.org/10.1146/annurev.biochem.75.103004.142545.

Whitfield, Chris, and M. Stephen Trent. 2014. "Biosynthesis and Export of Bacterial Lipopolysaccharides." *Annual Review of Biochemistry* 83 (1): 99–128. https://doi.org/10.1146/annurev-biochem-060713-035600.

Wiseman, Benjamin, Arnaud Kilburg, Vincent Chaptal, Gina Catalina Reyes-Mejia, Jonathan Sarwan, Pierre Falson, and Jean Michel Jault. 2014. "Stubborn Contaminants: Influence of Detergents on the Purity of the Multidrug ABC Transporter BmrA." *PLoS ONE* 9 (12). https://doi.org/10.1371/journal.pone.0114864.

Woodward, Robert, Wen Yi, Lei Li, Guohui Zhao, Hironobu Eguchi, Perali Ramu Sridhar, Hongjie Guo, et al. 2010. "In Vitro Bacterial Polysaccharide Biosynthesis: Defining the Functions of Wzy and Wzz." *Nature Chemical Biology* 6 (6): 418–23. https://doi.org/10.1038/nchembio.351.

Wüthrich, Kurt. 1989. "The Development of Nuclear Magnetic Resonance Spectroscopy as a Technique for Protein Structure Determination." *Accounts of Chemical Research* 22 (1): 36–44. https://doi.org/10.1021/ar00157a006.

Xu, R.M., G. Carmel, R.M. Sweet, J. Kuret, and X. Cheng. 1995. "Crystal Structure of Casein Kinase-1, a Phosphate-Directed Protein Kinase." *The EMBO Journal* 14 (5): 1015–23. https://doi.org/10.1002/j.1460-2075.1995.tb07082.x.

Yuasa, Ryosyke, Mark Levinthal, and Hiroshi Nikaido. 1969. "Biosynthesis of Cell Wall Lipopolysaccharide in Mutants of Salmonella" 100 (I): 433–44.

Zeng, Fanli, Zhimin Hao, Pan Li, Yanan Meng, Jingao Dong, and Yibin Lin. 2017. "A Restriction-Free Method for Gene Reconstitution Using Two Single-Primer PCRs in Parallel to Generate Compatible Cohesive Ends." *BMC Biotechnology* 17 (1): 1–7. https://doi.org/10.1186/s12896-017-0346-5.

Zhang, G.; Meredith, T. C.; Kahne, D. 2014. "On the Essentiality of Lipopolysaccharide to Gram-Negative Bacteria." *Curr Opin Microbiol* 16 (6): 779–85. https://doi.org/10.1016/j.mib.2013.09.007.On.

Zhang, Jianming, Priscilla L. Yang, and Nathanael S. Gray. 2009. "Targeting Cancer with Small Molecule Kinase Inhibitors." *Nature Reviews Cancer* 9 (1): 28–39. https://doi.org/10.1038/nrc2559.

Zhang, Zhao-xu, Rui-ping Zhao, De-sheng Wang, and An-ning Wang. 2016. “Fuzhisan Ameliorates A β Production and Tau Phosphorylation in Hippocampal of 11 Month Old APP / PS1 Transgenic Mice : A Western Blot Study.” *EXG* 84: 88–95. https://doi.org/10.1016/j.exger.2016.09.003.

Zhao, Guohui, Baolin Wu, Lei Li, and Peng George Wang. 2014. “O-Antigen Polymerase Adopts a Distributive Mechanism for Lipopolysaccharide Biosynthesis.” *Applied Microbiology and Biotechnology* 98 (9): 4075–81. https://doi.org/10.1007/s00253-014-5552-7.

Zhou, Guo Ping, and Frederic A. Troy. 2005. “NMR Study of the Preferred Membrane Orientation of Polyisoprenols (Dolichol) and the Impact of Their Complex with Polyisoprenyl Recognition Sequence Peptides on Membrane Structure.” *Glycobiology* 15 (4): 347–59. https://doi.org/10.1093/glycob/cwi016.

Zuccotto, Fabio, Elena Ardini, Elena Casale, and Mauro Angiolini. 2010. “Through the ‘Gatekeeper Door’: Exploiting the Active Kinase Conformation.” *Journal of Medicinal Chemistry* 53 (7): 2681–94. https://doi.org/10.1021/jm901443h.